2016-10

Development of Holographic Sensors for Monitoring Relative Humidity and Temperature

Tatsiana Mikulchyk
Technological University Dublin, t.mikulchyk@gmail.com

DEVELOPMENT OF HOLOGRAPHIC SENSORS FOR MONITORING RELATIVE HUMIDITY AND TEMPERATURE

Tatsiana Mikulchyk, B.Sc.

A thesis submitted for the degree of Doctor of Philosophy to the Dublin Institute of Technology

Supervisors:

Dr. Izabela Naydenova and Dr. Suzanne Martin

Centre for Industrial and Engineering Optics,

School of Physics and Clinical & Optometric Sciences

College of Science and Health

Dublin Institute of Technology

October 2016

ABSTRACT

Photonic structures capable of responding to an analyte with an easily identifiable change in their optical properties have generated wide interest due to their possible application as holographic sensors. Holographic sensors are considered a low-cost, lightweight and disposable technology, and have potential for application in different areas ranging from medical diagnostics to environmental sensing including the monitoring of environmental temperature and relative humidity. In spite of the existing wide range of temperature and humidity sensors, holographic sensors are of special interest as they can provide fast, real-time, reversible or irreversible, visual colorimetric or electronic readouts.

The main objective of this project was the development of holographic sensors with response to relative humidity and/or temperature. Holographic humidity sensors were fabricated by holographic recording of volume phase transmission gratings in acrylamide /diacetone acrylamide-based photopolymers containing polyvinyl alcohol as a binder. The diffraction efficiency and the Bragg angle were found to be humidity dependent in the relative humidity range 20 - 90 %. It was shown that reversibility of the response, sensitivity and operation range of the sensor can be tuned by varying the photopolymer composition. Best sensitivity up to 3%DE/%RH was observed for diacetone acrylamide-based gratings in the relative humidity range 70 - 90 %.

A novel thermosensitive photopolymer containing *N*-isopropylacrylamide as the main monomer was developed. The diffraction efficiency up to 80 % in transmission mode and 20 % in reflection mode was achieved. It was demonstrated that the temperature switchable swelling/shrinking of the novel *N*-isopropylacrylamide-based photopolymer can be implemented in the development of holographic temperature sensors, temperature visual indicators and holographic optical elements with temperature controlled direction of the diffracted light and diffraction efficiency. Best sensitivity up to 2%DE/^{o}C and 4.3nm/^{o}C was obtained for sensors based on volume phase transmission and reflection gratings, respectively.

For the first time, an optical sensor based on the surface relief structure with reversible response to relative humidity in the range 35 - 97 % was developed. The device comprises the Aztec grating as a substrate and a coating thin polymer film as a sensing medium. It was demonstrated that alteration of the coating layer composition allows tuning the operation range and sensitivity of the device.

DECLARATION

I certify that this thesis which I now submit for examination for the award of Doctor of Philosophy, is entirely my own work and has not been taken from the work from others, save and to the extent that such work has been cited and acknowledged within the text of my work.

This thesis was prepared according to the regulations for postgraduate study by research of the Dublin Institute of Technology and has not been submitted in whole or in part for another award in any other third level institution.

The work reported on in this thesis conforms to the principles and requirements of the DIT's guidelines for ethics in research.

DIT has permission to keep, lend or copy this thesis in whole or part, on condition that any such use of the material of the thesis is duly acknowledged.

Signature_____Date_____

Candidate: Tatsiana Mikulchyk

ACKNOWLEDGEMENTS

First and foremost, I would like to express my gratitude to my supervisors Dr. Izabela Naydenova and Dr. Suzanne Martin for their guidance, valuable suggestions, encouragement all through my project and example on how to develop science in innovative and competitive world.

Many thanks to my research colleagues and friends from the Centre for Industrial and Engineering Optics: Prof. Vincent Toal, Dr. Emilia Mihaylova, Dr. Lina Persechini, Dr. Jacinta Browne, Dr. Dervil Cody, Dr. Hoda Akbari, Dr. Mohesh Moothanchery, Dr. Monika Zawadzka, Dr. Subhash Chandra, Dr. Kevin Murphy, Ms. Sabad-e-Gul, Ms. Amanda Creane, Mr. Sanjay Kumar Keshri, Dr. Aritra Ghosh, Ms. Andrea Doyle and Mr. Andrew Malone for the discussions, valuable comments and assistance.

I'm very grateful to all staff and researchers in the FOCAS Research Institute who have always been extremely helpful. In particular, I would like to thank Dr. Swarna Jaiswal, Dr. Brendan Duffy and Dr. Alan Casey. I would like to thank Prof. Svetlana Mintova and all her colleagues at the Laboratoire Catalyse & Spectrochimie for our collaborative work. I would also like to thank Dr. A. K. Yetisen from Harvard Medical School and the Wellman Centre for Photomedicine, Massachusetts General Hospital, Cambridge, USA for providing the Aztec structures and his valuable suggestions.

I would like to acknowledge the Irish Research Council and Enterprise Ireland for financial support and also thank the Ulysses Research Programme for funding my research visit to the Laboratoire Catalyse & Spectrochimie in Caen, France. I would like to acknowledge the FOCAS Research Institute for providing the research facilities.

I would like to say a big thank you to my family for their encouragement and support.

ACRONYMS AND SYMBOLS

AA	Acrylamide
AH	Absolute humidity
CTA	Chain transfer agent
d	Grating thickness
DA	Diacetone acrylamide
Δd	Grating thickness change
$\Delta\lambda$	Wavelength shift
$\Delta n'$	Refractive index modulation change
$\Delta\eta$	Diffraction efficiency alteration
$\Delta\theta$	Bragg angle shift (inside the medium)
DSC	Differential scanning calorimetry
φ	Slant angle
h	Step height of the nanostepped structure
I_0	Intensity of the transmitted beam
I_d	Intensity of the diffracted beam
I_{in}	Intensity of the incident beam
I_{refl}	Intensity of the reflected beam
$\overrightarrow{K}$	Grating wave vector
λ	Wavelength of light
Λ	Fringe spacing of a holographic grating
LCST	Lower critical solution temperature
m_w	Mass of water vapour
n	Average refractive index of the medium
n'	Refractive index modulation
η	Diffraction efficiency of a holographic grating
NIPA	*N*-isopropylacrylamide
NPG	*N*-phenylglycine
NPG-sample	Grating recorded in the AA-based photopolymer layer containing NPG

PVA	Polyvinyl alcohol
PNIPA	Poly(*N*-isopropylacrylamide)
p_w	Partial pressure of water vapour
p_{ws}	Saturated vapour pressure of water
ψ	Tilt angle of grating planes
RH	Relative humidity
T	Temperature
θ	Bragg angle inside the medium
θ'	Bragg angle outside the medium
TEA	Triethanolamine
TEA-sample	Grating recorded in the AA-based photopolymer layer containing TEA
V	Volume of gas

TABLE OF CONTENTS

10. CONCLUSIONS AND FUTURE WORK

LIST OF FIGURES

LIST OF TABLES

1. THE NEED FOR RELATIVE HUMIDITY AND TEMPERATURE MONITORING

Temperature and humidity have a big impact on our life and they are the most frequently measured physical quantities, as all processes in nature and in industry depend on temperature and humidity. Their accurate measurement and control are necessary in both industrial processes and domestic applications. Thus, temperature and humidity sensors have a large number of applications in textile and food processing industries, meteorological services, automotive and microelectronic industries, intelligent control of the living environment in buildings and many others. To satisfy this wide range of demands, various techniques and instrumentations are implemented depending on measurement requirements in different industrial processes. The review of currently used humidity and temperature sensors is presented in the following sections.

1.1. Humidity sensors

There are a lot of techniques for the humidity detection ranging from the simplest method of exploiting the contraction/expansion of human hair to the most sophisticated techniques utilising a miniaturised electronic chip [1-5]. These techniques are based either on probing the fundamental properties of water vapour or employing different transduction methods. Depending on the sensing material, humidity sensors can be classified into semiconductor, ceramic, electrolyte and polymer humidity sensors [6, 7]. According to the transduction techniques, humidity sensors can be categorised into mechanical, optical, gravimetric, resistive, capacitive, piezoresistive and magnetoelastic sensors [6-8]. The main interest of this project is optical humidity sensors and holographic humidity sensors, in particular.

Optical humidity sensors are based on colour changing holograms [9-13], on grating/prism couplers [14-16], optical fibres [17-29] and the chilled mirror hygrometer [30, 31]. They can be used for the determination of humidity and the dew point temperature.

The humidity measurement defines the water vapour amount present in a gas or gas mixtures, such as air. Humidity can be expressed in different terms and units. Absolute humidity (*AH*), relative humidity (*RH*) and dew/frost point are commonly used terms. Absolute humidity is the ratio of the mass of water vapour (m_w) to the volume of gas or gas mixtures (V) in which the water vapour resides. Absolute humidity is expressed in grams per cubic meter and defined as follows:

$$AH = \frac{m_w}{V}. \tag{1.1}$$

The ratio of the partial pressure (p_{w}) of water vapour present in a gas at a particular temperature and pressure to the saturation water vapour pressure (p_{ws}) at that temperature and pressure is called relative humidity. Relative humidity is determined by [32]:

$$RH = \frac{p_w}{p_{ws}} * 100\%. \tag{1.2}$$

Relative humidity is a function of temperature, and thus it is a relative measurement.

When air is cooled down significantly and it becomes saturated with water molecules (*RH* = 100 %), condensation will occur. The temperature (above 0^{o}) at which the water vapour in a gas condenses to water is called the dew point. Frost point is the temperature (below 0^{o}) at which the water vapour condenses to ice. The dew/frost point temperature is preferably used in meteorology.

According to the measurement units, there are two types of humidity sensors: Relative humidity sensors and absolute humidity (moisture) sensors. Most of the humidity sensors available on the market are relative humidity sensors.

Crucial parameters of a humidity sensor are operating range, accuracy, response time, repeatability and reversibility (for reversible sensors), size, weight, cost, ease of operation and maintenance. The requirements for humidity sensors vary according to their applications. All the techniques discussed above have their own particular advantages and disadvantages and none of them fulfils all the requirements. Due to a wide range of applications, it is obvious that there is no single measurement technique suitable for all applications.

1.2. Temperature sensors

A wide range of temperature sensors is available for temperature (T) measurements in both industry and laboratory [33-46]. In science, the thermodynamic definition of temperature of any bulk quantity of matter is based on the term of the average kinetic energy per classical degree of freedom of its constituent particles. Practical way of temperature measurement is associated with the use of calibrated transducers to convert a measurable physical quantity into a temperature meaning [47, 48]. So, all temperature measurements are indirect.

A primary standard system for temperature measurement is the Kelvin thermodynamic scale. In early 1800's, Kelvin established the concept of absolute zero and developed a thermodynamic scale based on the coefficient of an ideal gas expansion. His scale is a standard for modern International Temperature Scale of 1990. International Temperature Scale of 1990 applies numerous defined points based on

various thermodynamic equilibrium states of fourteen pure chemical elements and one compound such as water [49].

Depending on a heat (energy) transfer mechanism, all temperature sensors are divided into two groups, i.e. contacting and non-contacting [50-52]. In contacting temperature sensors, convection and conduction are used as a heat transfer mechanism, whereas in non-contacting temperature sensors – radiation.

There are three main approaches for non-contacting temperature measurements. In the laser-based methods, the laser beam stimulates the vibration of molecules in the body under the measurement. Then, fluorescence analysis, spectroscopy, optical refraction and tomographic thermometry are implemented. In the second approach, acoustic/ultrasound waves are used. These sensors use the dependence of the sound velocity on temperature of the medium where sound propagates. The third type is radiative heat transfer thermometers which are usually called as pyrometers or infrared thermometers. Pyrometers define the temperature of a body by the radiation which the body emits.

Contacting thermometers can be classified as non-electrical and electrical. There is a big variety of electrical thermometers depending on measureable physical quantity and sensing material. Among them are resistance temperature detectors (resistance of a metal), thermocouples (electromotive force in metal), thermistors (resistance of a ceramic semiconductor), integrated circuit sensors (voltage-current at semiconductor junction) and others.

There are diverse methods for non-electrical contacting temperature sensing (Figure 1.1) [52]. Among non-electrical thermometers based on thermal expansion are liquid-bulb thermometers (volume expansion of liquid), gas-bulb thermometers (volume expansion of gas) and bimetallic thermometers (dimensional change of metal). Other

examples of non-electrical thermometers are thermal indicators, quartz thermometers and fibre optic thermometers.

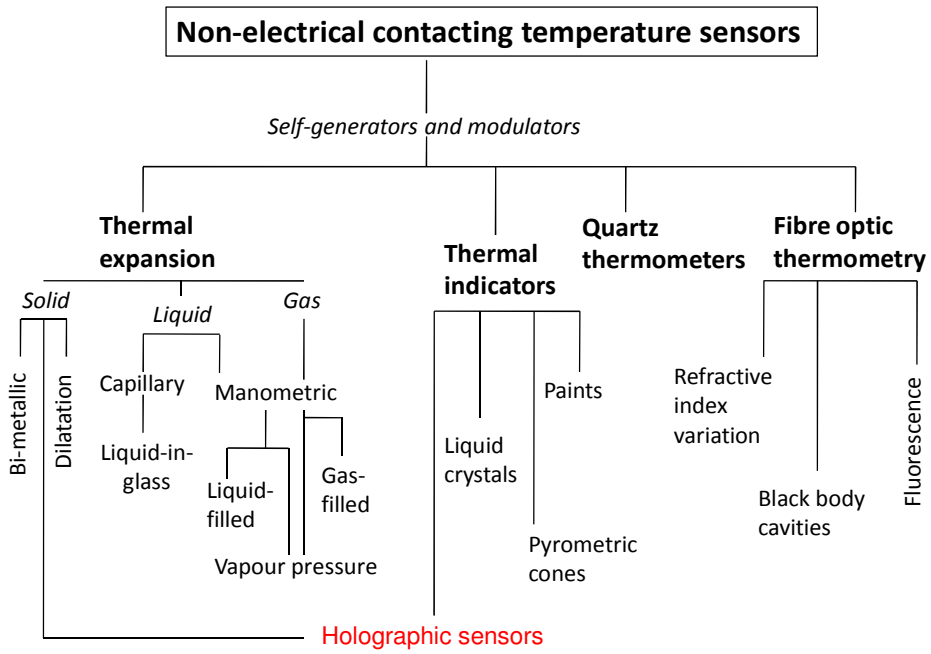

Figure 1.1. Classification of temperature measuring instruments/sensors by structure and/or energy form.

Holographic temperature sensors can be classified as the sub-category of thermal indicators and thermometers based on thermal expansion due to the following reasons. Firstly, the operation of holographic temperature sensors can be based on thermal expansion of the holographic material. Secondly, temperature changes cause a change in the reflectivity/transmittance of the holographic grating or a change in the wavelength of the diffracted light. In case a holographic sensor is based on a reflection holographic grating, it can work as a thermal indicator.

Among the big variety of sensors available for humidity and temperature monitoring, holographic sensors are of specific interest in this project due to their

advantages. Motivation for the development of holographic sensors is discussed in the following section.

1.3. Motivation for the development of holographic humidity and temperature sensors

As outlined in the previous section, there is the need for monitoring of the environmental temperature and humidity in both industrial processes and domestic applications. This project is focused on the development of humidity and temperature holographic sensors because holographic sensors offer specific advantages. A variety of holographic recording materials with potential of functionalisation allows developing holographic sensors with capability to detect both analytes in gas and liquid phase and different physical stimuli. Depending on the reversibility of the changes caused by interaction with the analyte, holographic sensors can be reversible and irreversible. Due to their compact size and light weight, holographic sensors may be incorporated into packaging. Sensors based on reflection gratings change the colour under exposure to an analyte and can be used as visual indicators as they provide visual information easily interpreted by non-specialist. Only a white light source is required to display quick analytical information provided by the holographic indicator. Such sensors do not need an additional readout panel and a power source. Another feature of holographic sensors is relatively low cost of its manufacturing which is beneficial for the disposable sensor production. Manufacturing holographic sensors can be attributed to Green Engineering [53] as it does not require many chemicals, large amount of water and energy. The capability for miniaturisation allows construction of holographic sensor arrays [54] and their integration into microfluidic devices [55, 56]. Holographic sensors have the

potential for applications in diverse areas such as security, environmental monitoring, medical diagnostics, dynamic displays and others [57].

One of the promising applications of holographic sensors is developing advanced packaging comprising intelligent component such as a holographic label. According to BCC Research, the global market for advanced packaging continuously increases [58]. It was estimated at $31.4 billion in 2011 and the overall market value for 2017 is predicted to be about $44.3 billion. For example, there is a great demand for smart packaging for pharmaceutical products which require specific storage and transportation conditions. Exposure to humidity and heat outside of tolerance levels can cause devices to operate in unusual way, compromise the sterility of the products, decrease the efficiency of reagents, reduce the shelf-life or fully destroy the products. In order to guarantee the product quality, specific storage and transportation conditions are required for many products, for instance, leather and paper production.

Significant challenges in the development of holographic sensors are functionalisation of holographic recording materials and improvement of their selectivity. These materials should be permeable to the analyte and their properties should change under exposure to the analyte. The approaches used for the development of holographic humidity and temperature sensors in the present research are described in the following section.

1.4. Approaches for the holographic sensor development

In this project three approaches were used in order to develop holographic sensors. The first approach was based on exploiting the intrinsic properties of the holographic recording material. Many holographic materials respond to changes in environmental conditions, such as temperature and humidity, either causing changes in the recorded

hologram or causing its deterioration or destruction. For example, dichromated gelatine holograms are found to change their colour at different levels of relative humidity [59]. However, in high humidity environments the lifetime of dichromated gelatine holograms is poor [60, 61]. In thermoplastic materials high temperatures are used to deliberately destroy/erase the hologram for the purposes of re-writing [62, 63]. The humidity sensitivity of acrylamide-based photopolymer films has been known for many years [64, 65]. Due to the highly hygroscopic nature of photopolymer component, such as the polyvinyl alcohol binder and the polyacrylamide produced during the recording of the hologram, the sensitivity of this photopolymer film to humidity can be significant. While this can be a problem in terms of hologram lifetime, it can also be turned to advantage in sensing applications. The humidity sensitivity of volume phase reflection gratings recorded in an acrylamide-based photopolymer has been demonstrated and characterised in the relative humidity range of 5 – 80 % [11-13]. Reversible changes in fringe spacing due to water vapour absorption have been found to cause fully reversible variations in the diffracted light wavelength. The natural ability of the acrylamide-based photopolymer layer to swell or shrink at different levels of relative humidity has been exploited for the design of a holographic humidity indicator [11].

Due to highly hygroscopic nature, acrylamide/diacetone acrylamide-based photopolymers were used as holographic recording materials in the first phase of the research. The variety of photopolymer compositions and the possibility to tune the properties of photopolymers by altering their compositions indicate the potential of these materials in holographic sensing applications. Research is needed to fully characterise the response of photopolymer-based holographic gratings to humidity changes and to better understand the nature of the changes that occur. Thus, in order to achieve the full potential of photopolymers, it is required to understand their behaviour

at different levels of relative humidity and know the moisture stability limit. Also, with better understanding of the processes occurring, the response of holographic gratings to humidity changes can be implemented for the development of holographic humidity sensors.

The aim of the first phase of the research was the investigation of changes in the properties of volume phase transmission holograms recorded in photopolymers in response to changes in the relative humidity with particular emphasis on irreversible changes. The humidity response of volume phase transmission gratings recorded in acrylamide/ diacetone acrylamide-based photopolymers was investigated. This knowledge could allow development of irreversible humidity indicators to provide warning of high humidity exposure, for example, for application in medical device and pharmaceutical packaging. Also, it may help in the development of more stable photopolymer materials for applications where an environmentally stable hologram is essential, such as holographic data storage or holographic optical elements.

The focus of the second phase of the research was the development of a holographic temperature sensor. For the development of holographic temperature sensors a material with specific properties was required. The approach was based on functionalisation of the holographic recording material, such as a photopolymer, by incorporation of a component with sensitivity to temperature.

Undoped photopolymer compositions have significant sensitivity to humidity and little temperature sensitivity in the range of the environmental temperatures. Most of the photopolymers including acrylamide derivative-based photopolymers have low glass transition temperature. In these materials, temperature exposure is known to induce grating detuning effects originating from changes in the refractive index and the dimensions of the photopolymer layers. The investigation of the temperature response

of volume phase reflection gratings recorded in an acrylamide based photopolymer was previously carried out in the temperature range of 15 - 60 ^{o}C [12]. It has been shown that the temperature response highly depends on the relative humidity level. The temperature-induced changes in properties of volume phase transmission gratings recorded in an acrylate-based photopolymer were investigated in the temperature range of 27 - 43 ^{o}C [66]. At 43 ^{o}C a shift of the Bragg angle about 0.2^{o} was observed in the grating with the slant angle of 30^{o}. The percentage thermal expansion of the medium was found to be about 1 %. Such sensitivity to temperature limits the applications of photopolymer-based gratings in data storage or as holographic optical elements. However, the observed temperature induced changes were not sufficient for the development of the temperature sensor with high sensitivity. Novel photopolymer systems with better capacity to respond to temperature changes are needed. The aim of the present research was the development of a holographic temperature sensor. The objectives were to develop the temperature sensitive photopolymer composition capable of recording both transmission and reflection volume holograms and characterise the temperature response of holographic gratings recorded in this photopolymer composition.

The focus of the third phase of the research was the development of an optical sensor responsive to changes in relative humidity. The approach was based on functionalisation of the surface photonic structure by coating it with the analyte-sensitive film. The optical sensor comprises an embossed honeycomb pyramidal grating as a substrate (the basis for a sensor) and a coating thin polymer film as a sensing medium. The embossed honeycomb pyramidal grating presents a surface-relief reflective diffractive structure which comprises a hexagonal array of circular hollow nanostepped pyramids [67, 68]. The aim of using the surface photonic structure was to

provide an optical signal, changing due to a change in the refractive index of the coating thin film while the geometrical parameters of the structure remained the same. The coating layer was utilised to functionalise the photonic nanostructure and introduce the response to an analyte. The advantage of the optical sensor based on the surface structure is unchanged spatial period of the grating under exposure to an analyte. This allows excluding the effect of grating thickness change and analysing the contribution of the refractive index change in the wavelength shift caused by exposure to an analyte. In volume gratings the response to an analyte can be caused by changes in both the spatial period change and the refractive index change which leads to more complex analysis. Another feature of the optical sensor is possibility to control the operation range and time response by using coating layers with different compositions. The aim of the research was the development of the optical humidity sensor based on the surface relief photonic structure coated with a thin polymer film.

1.5. Objectives of the PhD research

- Characterisation of changes in the properties of volume phase transmission gratings recorded in photopolymers in response to changes in the relative humidity with particular emphasis on irreversible changes.
- Investigation of capability to manipulate the humidity sensitivity of photopolymer-based gratings by variations of photopolymer compositions.
- Development and optimisation of the temperature sensitive photopolymer composition which uses a thermosensitive monomer, such as *N*-isopropylacrylamide, as the main monomer.
- Characterisation of the holographic recording ability of the thermosensitive photopolymer in both transmission and reflection modes.

- Characterisation of the temperature response of volume phase transmission and reflection holographic gratings recorded in the temperature sensitive photopolymer composition.
- Development of the temperature indicator based on the reflection grating recorded in the thermosensitive photopolymer.
- Development of an optical humidity sensor based on the surface relief photonic structure coated with a thin polymer film. The surface relief photonic structure comprises an embossed honeycomb pyramidal grating.

References

1. Kulwicki, B.M., *Humidity sensors.* Journal of the American Ceramic Society, 1991. **74**(4): p. 697-708.
2. Farahani, H., Wagiran, R. and Hamidon, M. *Humidity sensors principle, mechanism, and fabrication technologies: A comprehensive review.* Sensors, 2014. **14**(5): p. 7881-7939.
3. Chen, Z. and Lu, C., *Humidity sensors: A review of materials and mechanisms.* Sensor Letters, 2005. **3**(4): p. 274-295.
4. Yamazoe, N. and Shimizu, Y., *Humidity sensors: Principles and applications.* Sensors and Actuators, 1986. **10**(3): p. 379-398.
5. Arai, H. and Seiyama, T., *Humidity sensors*, in *Sensors set*: *A comprehensive survey*, 2008, Wiley-VCH Verlag GmbH. p. 981-1012.
6. Lee, C.-Y. and Lee, G.-B., *Humidity sensors: A review.* Sensor Letters, 2005. **3**(1): p. 1-15.
7. Rittersma, Z.M., *Recent achievements in miniaturised humidity sensors—a review of transduction techniques.* Sensors and Actuators A: Physical, 2002. **96**(2–3): p. 196-210.
8. Kolpakov, S.A., Gordon, N.T., Mou, C. and Zhou, K., *Toward a new generation of photonic humidity sensors.* Sensors, 2014. **14**(3): p. 3986-4013.
9. Naydenova, I., Raghavendra, J., Martin, S. and Toal, V., *Holographic humidity sensors*, in *Humidity sensors*, C. Okada (Ed.), Nova Science Publishers 2011.
10. Mihaylova, E., Cody, D., Naydenova, I., Raghavendra, J., Martin, S. and Toal, V., *Research on holographic sensors and novel photopolymers at the Centre for Industrial and Egnineering Optics,* in: *Holography: basic principles and contemporary applications.* E. Mihaylova (Ed.), Intech 2013.

11. Naydenova, I., Raghavendra, J., Toal, V. and Martin, S., *A visual indication of environmental humidity using a color changing hologram recorded in a self-developing photopolymer.* Applied Physics Letters, 2008. **92**(3): p. 031109.

12. Naydenova, I., Raghavendra, J., Toal, V. and Martin, S., *Characterisation of the humidity and temperature responses of a reflection hologram recorded in acrylamide-based photopolymer.* Sensors and Actuators B: Chemical, 2009. **139**(1): p. 35-38.

13. Naydenova, I., Sherif, H., Martin, S., Jallapuram, R., Toal, V., *Holographic sensor*. 2012, Patent US8535853 B2.

14. Yadav, B.C., Pandey, N. K., Amit, K. S. and Preeti, S, *Optical humidity sensors based on titania films fabricated by sol–gel and thermal evaporation methods.* Measurement Science and Technology, 2007. **18**(1): p. 260-264.

15. Fuke, M.V., Vijayan, A., Kanitkar, P., Kulkarni, M., Kale, B. B. and Aiyer, R. C., *Ag-polyaniline nanocomposite cladded planar optical waveguide based humidity sensor.* Journal of Materials Science: Materials in Electronics, 2009. **20**(8): p. 695-703.

16. Lee, K.J., Wawro, D., Priambodo, P.S. and Magnusson, R., *Agarose-gel based guided-mode resonance humidity sensor.* IEEE Sensors Journal, 2007. **7**(3): p. 409-414.

17. Glenn, S.J., Cullum, B. M., Nair, R. B., Nivens, D. A., Murphy, C. J. and Angel, S. M., *Lifetime-based fiber-optic water sensor using a luminescent complex in a lithium-treated Nafion™ membrane.* Analytica Chimica Acta, 2001. **448**(1–2): p. 1-8.

18. Zhou, Q., Shahriari, M.R., Kritz, D. and Sigel Jr G.H., *Porous fiber-optic sensor for high-sensitivity humidity measurements.* Analytical Chemistry, 1988. **60**(20): p. 2317-2320.

19. Brook, T.E., Taib, M.N. and Narayanaswamy, R., *Extending the range of a fibre-optic relative-humidity sensor.* Sensors and Actuators B: Chemical, 1997. **39**(1): p. 272-276.

20. Correia, S.F., Antunes, P., Pecoraro, E., Lima, P.P., Varum, H., Carlos, L. D., Ferreira, R. A. S. and André, P.S., *Optical fiber relative humidity sensor based on a FBG with a Di-ureasil coating.* Sensors, 2012. **12**(7): p. 8847-8860.

21. Jindal, R., Tao, S., Singh, J.P., Gaikwad, P.S., *High dynamic range fiber optic relative humidity sensor.* Optical Engineering, 2002. **41**(5): p. 1093-1096.

22. Mathew, J., *Development of novel fiber optic humidity sensors and their derived applications*. 2012 (Doctoral Thesis), Dublin Institute of Technology:Dublin.

23. Yeo, T.L., Sun, T. and Grattan, K.T.V., *Fibre-optic sensor technologies for humidity and moisture measurement.* Sensors and Actuators A: Physical, 2008. **144**(2): p. 280-295.

24. Lin, Y., Gong, Y., Wu, Y. and Wu, H., *Polyimide-coated fiber Bragg grating for relative humidity sensing.* Photonic Sensors, 2015. **5**(1): p. 60-66.

25. *Optical fiber sensors: Advanced techniques and applications*. G. Rajan (Ed.), CRC Press 2015.

26. Aneesh, R. and Khijwania, S.K., *Titanium dioxide nanoparticle based optical fiber humidity sensor with linear response and enhanced sensitivity.* Applied Optics, 2012. **51**(12): p. 2164-2171.

27. Mathew, J., Semenova, Y. and Farrell, G., *Experimental demonstration of a high-sensitivity humidity sensor based on an Agarose-coated transmission-type*

photonic crystal fiber interferometer. Applied Optics, 2013. **52**(16): p. 3884-3890.

28. Mathew, J., Semenova, Y. and Farrell, G, *Fiber optic hybrid device for simultaneous measurement of humidity and temperature.* IEEE Sensors Journal, 2013. **13**(5): p. 1632-1636.
29. Mathew, J., Semenova, Y. and Farrell, G, *Effect of coating thickness on the sensitivity of a humidity sensor based on an Agarose coated photonic crystal fiber interferometer.* Optics Express, 2013. **21**(5): p. 6313-6320.
30. Beaubien, D., *The chilled mirror hygrometer: how it works, where it works-and where it doesn't.* Sensors Online, 2005. **22**(5): p. 30-34.
31. Wiederhold, P., *The principles of chilled mirror hygrometry.* Sensors, 2000. **17**: p. 46-51.
32. Wiederhold, P., *Water vapour measurements: Methods and instrumentation.* CRC Press 1997.
33. Baker, B., *Precision temperature sensing with RTD circuits*, Microchip Technology Inc Tempe AZ USA AN687, 1998.
34. Park, R., *Manual on the use of thermocouples in temperature measurement.* 4th ed. American Society for Testing and Materials Baltimore MD USA, 1993.
35. Maiti, T.K., *A Novel Lead-Wire-Resistance Compensation Technique Using Two-Wire Resistance Temperature Detector.* IEEE Sensors Journal, 2006. **6**(6): p. 1454-1458.
36. Kim, J., Shin, Y. and Yoon, Y., *A study on the fabrication of an RTD (resistance temperature detector) by using Pt thin film.* Korean Journal of Chemical Engineering, 2001 **18**: p. 61–66.

37. McGee, T., *Principles and methods of temperature measurement.* John Wiley & Sons New York USA 1988.

38. Yang, J., *A silicon carbide wireless temperature sensing system for high temperature applications.* Sensors, 2013. **13**(2): p. 1884-1901.

39. Ross-Pinnock, D. and Maropoulos, P.G. *Review of industrial temperature measurement technologies and research priorities for the thermal characterisation of the factories of the future.* Proceedings of the Institution of Mechanical Engineers, Part B: Journal of Engineering Manufacture, 2016. **230**(5): p. 793-806.

40. Ross-Pinnock, D. and Maropoulos, P. G., *Identification of key temperature measurement technologies for the enhancement of product and equipment integrity in the light controlled factory.* Procedia CIRP, 2014. **25**: p. 114-121.

41. Chen, C.-C., Chen, C.-L. and Lin, Y., *All-digital time-domain CMOS smart temperature sensor with on-chip linearity enhancement.* Sensors, 2016. **16**(2): p. 176.

42. Krummenacher, P. and Oguey, H., *Smart temperature sensor in CMOS technology.* Sensors and Actuators A: Physical, 1990. **22**(1): p. 636-638.

43. DeWitt, N., *Theory and practice of radiation thermometry.* John Wiley & Sons New York USA 1998.

44. Claus, R.O., Gunther, M.F., Wang, A. and Murphy, K.A., *Extrinsic Fabry-Perot sensor for strain and crack opening displacement measurements from -200 to 900 degrees C.* Smart Materials and Structures, 1992. **1**(3): p. 237-242.

45. Zhang, Y., Pickrell, G.R., Qi, B., Safaai-Jazi, A. and Wang, A., *Single-crystal sapphire based optical polarimetric sensor for high temperature measurement.* Sensors, 2006. **6**(8): p. 823-834.

46. Wang, Y., Pickrell, G.R., Qi, B., Safaai-Jazi, A. and Wang, A., *A passive wireless temperature sensor for harsh environment applications.* Sensors, 2008. **8**(12): p. 7982-7995.

47. Chang, H., *Inventing temperature: Measurement and scientific progress*. Oxford University Press 2004.

48. Plumb, H., *Temperature: Its measures and control in science and industry*. in *Symposium on temperature*. National Bureau of Standards, American Institute of Physics, Instrumentation, Systems, and Automation Society, Pittsburgh, PA 1972.

49. Quinn, T.J., *The international temperature scale of 1990 (ITS-90).* Physica Scripta, 1990. **41**(5): p. 730-732.

50. Bentley, R., *Handbook of temperature measurement. V.1: Temperature and humidity measurement.* Springer; New York USA 1998.

51. Childs, P.R.N., Greenwood, J.R. and Long, C.A. *Review of temperature measurement.* Review of Scientific Instruments, 2000. **71**(8): p. 2959-2978.

52. Michalski, L., Eckersdorf, K., Kucharski, J. and McGhee, J., *Temperature measurement*. 2nd ed., John Wiley &Sons Ltd 2001.

53. Abraham, M.A. and Nguyen, N., *"Green engineering: Defining the principles"— resdts from the sandestin conference.* Environmental Progress, 2003. **22**(4): p. 233-236.

54. Lowe, C.R., Davidson, C.A.B., Blyth, J., Marshall, A.J. and James, A.P., *Holographic sensors and their production*. 2004, Patent US 7443553 B2.

55. Jakoby, B., Vellekoop, M.J., Bell, L.L., Seshia, A.A., Davidson, C.A.B. and Lowe, C.R., *Integration of holographic sensors into microfluidics for the real-*

time pH sensing of L. casei metabolism. Procedia Engineering, 2010. **5**: p. 1352-1355.

56. Marhsall, A.J. and Kew, S., *Use of holographic sensors*. WO Patent Application 2007039717 A1, April 12, 2007.

57. Yetisen, A.K., Naydenova, I., Vasconcellos, F.C., Blyth, J. and Lower, C.R., *Holographic sensors: Three-dimensional analyte-sensitive nanostructures and their applications.* Chemical Reviews, 2014. **114**(20): p. 10654-10696.

58. *Market research reports: Active, controlled, and intellegent packaging.* 2013, retrieved May 1, 2016, from: http://www.bccresearch.com/.

59. Wuest, D.R. and Lakes, R.S., *Color control in reflection holograms by humidity.* Applied Optics, 1991. **30**(17): p. 2363-2367.

60. Changkakoti, R. and Pappu, S.V., *Methylene blue sensitized dichromated gelatin holograms: a study oftheir storage life and reprocessibility.* Applied Optics, 1989. **28**(2): p. 340-344.

61. Naik, G.M., Mathur, A. and Pappu, S.V., *Dichromated gelatin holograms: an investigation of their environmental stability.* Applied Optics, 1990. **29**(35): p. 5292-5297.

62. Shi, X., Lawrence, B., Dubois, M., Boden, E.P., Erben, C., Longley, K.L. and Nielsen, M.C., *Thermoplastic media for holographic data storage*. 2005, SPIE Proceedings **5939**, 59390A.

63. Edwards, J., Aspen, F., Hegel, R. and Sandstrom, C., *Thermoplastic substrates for holographic data storage media*. 2002, Patents US 20020135829 A1.

64. Gong, Q., Wang, S., Huang, M. and Gan, F., *A humidity-resistant highly sensitive holographic photopolymerizable dry film.* Materials Letters, 2005. **59**(23): p. 2969-2972.

65. Neill, F.T.O., Lawrence, J.R. and Sheridan, J.T., *Improvement of holographic recording material using aerosol sealant.* Journal of Optics A: Pure and Applied Optics, 2001. **3**(1): p. 20-25.

66. Dhar, L., Schnoes, M.G., Wysocki, T.L., Bair, H., Schilling, M. and Boyd, C., *Temperature-induced changes in photopolymer volume holograms.* Applied Physics Letters, 1998. **73**(10): p. 1337-1339.

67. Cowan, J.J., *Surface relief volume reflective diffractive structure*. 2012, Patent US 9158046 B2.

68. Cowan, J.J., *Aztec surface-relief volume diffractive structure.* Journal of the Optical Society of America A, 1990. **7**(8): p. 1529-1544.

2. FUNDAMENTALS OF HOLOGRAPHIC SENSORS

2.1. Short history of holography

The history of holography started in 1865 when James Clerk Maxwell theoretically demonstrated that light is an electromagnetic wave and the propagation of the light through the medium is governed by electromagnetic laws. A number of great discoveries had been made before the first holographic recording was realised. In 1869 Wilhem Zenker theoretically predicted the existence of the spatial variation of the light intensity (interference pattern) produced by combination of two waves. The existence of electromagnetic waves was experimentally demonstrated by Heinrich Hertz in 1887. The first recording of an interference pattern on a photographic plate was done by Otto Wiener in 1890. The following year Gabriel Lippmann developed a method of producing colour projection of the recorded image.

In the first half of the twentieth century, a number of scientists studied the atomic structure of crystalline materials by X-ray microscopy. At that time, Denis Gabor worked on the improvement of the resolution of the electron microscope capable of resolving atomic lattices and seeing single atoms. His idea was to combine the electron wave to be recorded with another wave (reference wave) and record complete electron wavefront, including its phase, on a silver halide photographic emulsion. After emulsion processing, the recorded interference pattern was illuminated by the reference wave, and the original wave, containing its phase, was reconstructed due to diffraction process. Holography as a method of recording the complete wave field, i.e. both the phase and the amplitude of the light waves, was invented by Dennis Gabor in 1948 [1]. Dennis Gabor received the Nobel Prize 1971 in Physics for his invention and the development of the holographic method.

Interference and diffraction of light waves are the two fundamental processes involved in holography. A hologram is a two-dimensional recording of interference pattern produced by the light wave scattered from the object and a reference wave. However, the hologram produces a three-dimensional image of the object by illuminating it once again with the reference wave. The main drawback of in-line holography developed by Dennis Gabor was the presence of both virtual and real reconstructed images in the same viewing plane.

In order to be successful in holographic recording, the stability of the interference pattern, as well as mechanical and thermal stability are required. In 1960 new stage in the development of holography started due to the invention of the laser which allowed producing light with temporal and spatial coherence. The light source with temporal and spatial coherence enables the production of the interference pattern which is stable during the recording and has high contrast. High contract interference fringes were required to record efficient holograms.

Following the invention of the laser, the first transmission holograms of three-dimensional objects were recorded by Emmett Leith and Juris Upatnieks in 1962 [2]. They improved Gabor's method by introducing off-axis technique which allowed overcoming the drawback of Gabor's technique and separating the twin image. Transmission holograms which produced images with realistic depth and clarity were successfully recorded. These transmission holograms required laser light to view the holographic image. At the same time Yuri Denisyuk developed a method of recording reflection holograms which could be viewed in light of a broad spectral range [3]. Another milestone in the development of holography was the invention of Rainbow holograms by Stephen Benton in 1968 [4]. Stephen Benton introduced the embossing technique to produce transmission holograms which could be viewed in white light and

produced a rainbow image. The invention of the Rainbow holograms promoted mass production of cheap holograms which have been used in security, publishing, advertising, and banking industries. Nowadays the progress in holographic development enables the fabrication of different types of holograms with controllable optical characteristics. The classification of holograms is presented in the following section.

2.2. Types of holograms

Holograms are classified based on what property of the recording medium is modulated during the recording, thickness of the recording medium, whether the information is recorded on the surface or though the volume and recording geometry.

During the holographic recording the spatially varied recording light field is replicated as a spatial variation of the material properties. A phase hologram is recorded as a spatial variation of the refractive index and/or thickness. An amplitude hologram is recorded as a spatial variation of absorption coefficient.

Depending on the thickness of the photosensitive medium, the recorded holographic gratings can be classified as thin (plain) or thick (volume). The important parameter for the classification is the ratio of the fringe spacing (Λ) and the thickness of the photosensitive layer (d). The holographic grating is thin, if the thickness of the recording medium is small compared to the average fringe spacing. Parameter Q is used to classify holographic gratings into thin and thick. According to [5], parameter Q is defined by the relation:

$$Q = \frac{2\pi\lambda d}{n\Lambda^2} \tag{2.1}$$

where λ is the wavelength of the recording light, n is the average refractive index of the medium. Holographic gratings with values of $Q >> 1$ are thick while gratings with $Q < 1$ are considered as thin.

In some cases the spatially varied recording light field is replicated in the form of the thickness variation and a surface hologram is recorded. This project is focused on holographic sensors based on volume holograms in which the thickness of the sensitive layer does play a role. For this reason the holographic recording using different recording geometry will be considered in this type of holograms.

There are two main types of holographic gratings depending on the recording geometry. Consider the case of unslanted gratings which can be recorded by two plane waves whose wave vectors make equal but opposite angles (θ') to the surface of the photosensitive medium. The first type is a transmission grating. The transmission grating can be produced when the two interfering wavefronts (subject wave (S_{wave}) and reference wave (R_{wave})) are incident on the photosensitive medium from the same side (Figure 2.1(a)). The holographic grating recorded in this fashion is to be viewed in transmitted light (Figure 2.1(b)).

For volume transmission grating, diffraction of a beam with a specific wavelength happens at a specific angle which is called Bragg angle (θ') and is determined by the Bragg equation:

$$2\Lambda \sin \theta' = \lambda \,, \tag{2.2}$$

where λ is the wavelength of the reconstructing light.

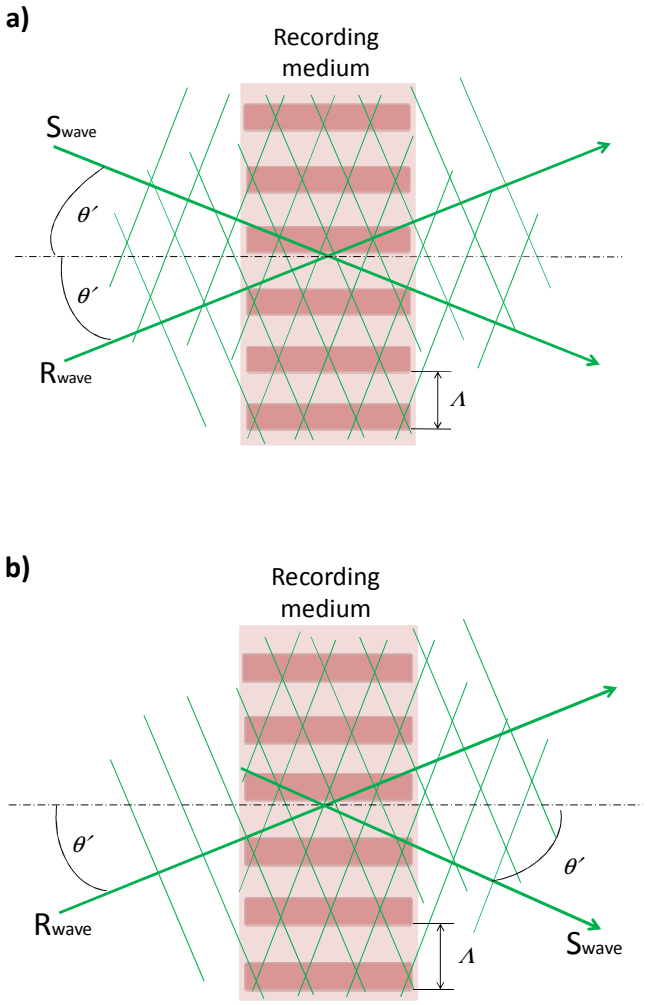

Figure 2.1. Transmission hologram recording (a) and reconstruction (b).

The second type is a reflection grating. The reflection grating is recorded if two wavefronts reach the photosensitive medium from opposite sides (Figure 2.2(a)). Gratings of this type are to be viewed in reflected light (Figure 2.2(b)). For volume reflection grating, the Bragg equation can be written as:

$$2n\Lambda \sin\theta' = \lambda . \tag{2.3}$$

The Bragg angle (θ') is defined as the angle between the incident beam and the planes of varying refractive index recorded in the material.

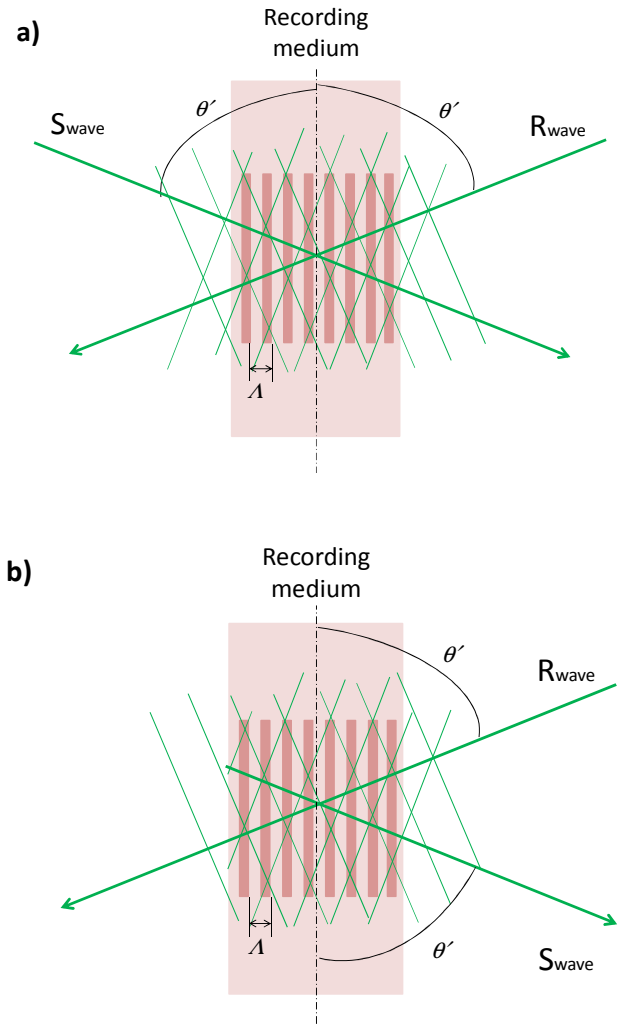

Figure 2.2. Reflection hologram recording (a) and reconstruction (b).

Diverse applications for holography have been developed. In general, these applications can be divided into two classes depending on the function of the hologram. In the first class, the hologram reconstructs an image. Possible applications for this class are data storage, imaging and security [6-13]. In the second class, the hologram functions as an optical element. Examples of applications are displays, projection screens, solar energy concentrators and sensors [14-24]. This project is focused on application of holographic gratings for the development of holographic sensors and the following section describes the fundamentals of holographic sensors.

2.3. Working principle of holographic sensors

Holographic sensors are photonic structures created by holographic patterning of a photosensitive material which is responsive to a specific analyte. Holographic sensors can systematically diffract narrow-band light in the ultraviolet to near-infrared range and provide visual colorimetric/optical readouts in real time and reversible/irreversible manner. Holographic sensors can detect analytes in gas and in liquid phase as well as different physical stimuli such as pressure and magnetic fields [17-20, 25-32]. Holographic sensors are considered a low-cost, lightweight, and disposable technology and have potential for application in different areas ranging from medical diagnostics to environmental sensing.

The sensing principle of all holographic sensors is based on the same optical phenomena regardless of the analyte which the sensor detects. To exploit the hologram's response for the development of the sensors, it is necessary to understand the way this response occurs. The base of the holographic sensor is a holographic grating. A holographic grating has all necessary components to act as a sensor. The analyte-sensitive film performs as a recognition component, selecting the analyte. The sensing mechanisms are changes in the fringe spacing of the holographic grating as well as the refractive index modulation of the photonic structure. The periodic structure is therefore a transducer and the senor signal is the change in different holographic grating characteristics such as the peak wavelength of the diffracted light, diffraction efficiency and the Bragg angle.

There are two types of holographic sensors depending on the recording geometry of the holographic grating utilised. The first type is a sensor based on a transmission diffraction grating. This sensor relies on the alterations of the diffraction efficiency and the Bragg angle shift when interaction with a target analyte occurs (Figure 2.3). The

sensor requires both a light source of a specific wavelength for its illumination and a photodetector to monitor a change in a signal level, such as a diffraction efficiency alteration or a variation of the diffracted light direction. The diffraction efficiency (η) of a volume phase transmission grating at Bragg incidence is determined by the coupled wave theory [33]:

$$\eta = \sin^2\left(\frac{\pi n' d}{\lambda \cos\theta}\right), \tag{2.4}$$

where n' is the refractive index modulation, λ is the wavelength of the reconstructing beam, θ is the Bragg angle inside the photopolymer layer. Changes in the diffraction efficiency occur due to variation of the refractive index modulation and/or thickness of the grating. Thickness changes arise through swelling or shrinkage of the bulk material leading to changes in the grating spacing, causing the Bragg angle shift.

Figure 2.3 illustrates the sensing principle of a holographic sensor based on a transmission grating. Consider the case of a volume transmission grating with the following parameters: the thickness d_1, the refractive index modulation n_1', the spatial period Λ_1 and the Bragg angle outside the layer θ_1'. Upon illumination the grating diffracts the light and the diffraction efficiency of the grating is a function of d_1, n_1', Λ_1 and θ_1'. The interaction with the analyte produces changes in optical properties of the sensitive film and in holographic grating geometry. These changes ultimately cause alterations in the direction of the diffracted light and the diffraction efficiency which is now a function of new parameters: d_2, n_2', Λ_2 and θ_2'.

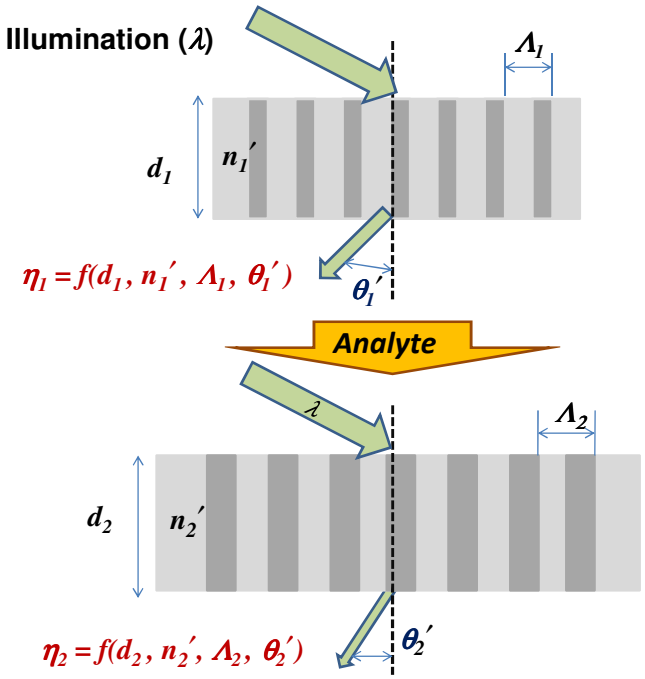

Figure 2.3. The principle of operation of a holographic transmission grating sensor.

Diffraction efficiency alterations ($\Delta\eta$) can be caused by the effect of different parameters which can be determined by the differentiation of Equation (2.4) [34]:

$$\frac{\Delta\eta}{\eta} = \frac{2}{\tan\left(\frac{\pi n' d}{\lambda \cos\theta}\right)}\left(\frac{\pi n' d}{\lambda \cos\theta}\right)\left(\frac{\Delta n'}{n'} + \frac{\Delta d}{d} - \frac{\Delta\lambda}{\lambda} + \tan\theta\Delta\theta\right), \qquad (2.5)$$

where $\Delta n'$ is the refractive index modulation change, Δd is the thickness change, $\Delta\lambda$ is the variation of probe wavelength and $\Delta\theta$ is the shift of the Bragg angle inside the medium.

The second type of the holographic sensor is a sensor based on a reflection grating. The sensor operates via changes in the wavelength (colour) of the diffracted light under exposure to an analyte. These sensors are the focus of the most of the research as they can be used as visual indicators which don't need an additional readout

device to interpret the response. The direction of the maximum intensity of the light diffracted from the periodic photonic structure created in reflection mode is determined by Bragg's law (Equation 2.3). Differentiation of Equation (2.3) allows evaluating the contribution of different parameters on the spectral response of the sensor [20]:

$$\frac{\Delta\lambda}{\lambda} = \frac{\Delta n}{n} + \frac{\Delta\Lambda}{\Lambda} + \cot\theta' \Delta\theta' . \tag{2.6}$$

Bragg angles in reflection geometry of recording are typically close to 90°. Thus, the contribution of the last term in Equation (2.6) is usually negligible. Depending on the properties of the sensitive medium, the fringe spacing variation and the change in the overall refractive index of the sensitive medium have different impact on the spectral response of the sensor. The operation principle of a holographic reflection grating sensor is shown in Figure 2.4.

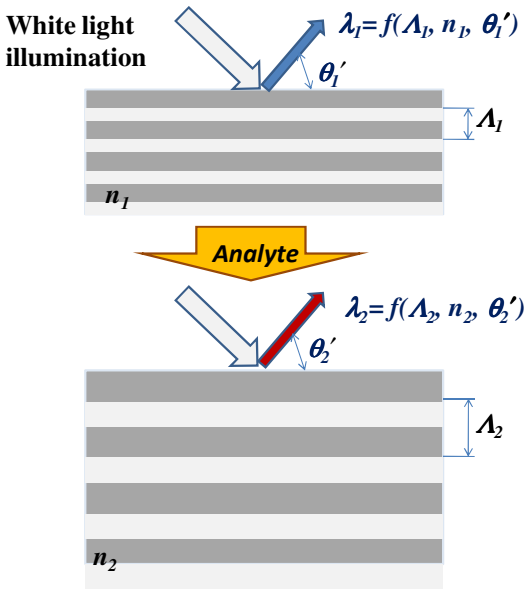

Figure 2.4. The principle of operation of a holographic reflection grating sensor.

When the reflection grating is illuminated with white light, light of a specific wavelength (colour) is diffracted. The colour of the observed light is determined by the

fringe spacing. The interaction with the analyte causes the dimensional changes of the sensitive medium due to its shrinkage or swelling. This leads to the variation in fringe spacing and, hence, the wavelength of the diffracted light alters. Thus, if the sensing material swells, the wavelength of the diffracted light will shift to longer wavelengths.

Moreover, the interaction with the analyte can have effect on the effective refractive index of the sensitive medium. The effective refractive index can be changed because of the physicochemical modification of the holographic material during exposure to the analyte. These changes ultimately cause a change in the optical path length between holographic fringes leading to the wavelength shift. Observable change in the wavelength of the diffracted light due to refractive index variation can be obtained in the case of a significant change of the refractive index.

The physicochemical properties of a holographic recording material are a key factor for the development of the holographic sensor. Holographic materials with the sensitivity to a specific analyte are good candidates for the applications in holographic sensor production. Holographic recording materials available for holographic sensing applications are discussed in the following section.

2.4. Holographic recording materials for holographic sensing

In addition to fulfilling the requirements for holographic recording, holographic materials for sensing applications should be responsive to a target analyte providing detectable changes in properties of created photonic structures in the presence of the analyte. There are three main groups of photonic materials utilised for holographic sensing which are classified by photochemical and physical processes involved in the holographic recording.

2.4.1. Photopolymers

The first type is photopolymer materials that are capable of changing their optical properties under light. A wide variety of photopolymerisable materials for holographic recording has been reported in literature [35-43]. A photopolymer system generally consists of a main monomer and, optionally, a cross-linking monomer, a photoinitiating system including a sensitising dye and an electron donor, and a polymeric binder. Chain transfer agent can be added in order to improve the spatial resolution of some materials for recording in reflection mode. The main advantages of the photopolymer materials are wide dynamic range, high sensitivity, low scattering, the ease of preparation, self-processing nature and relatively low cost. However, photopolymers suffer from the material shrinkage during the holographic recording [44, 45].

Most of the research on applications of photopolymers for holographic sensing is dealing with acrylamide/acrylamide derivative-based photopolymers. The advantage of photopolymer-based holographic sensors is the ability to achieve high diffraction efficiency. The sensitivity of the photopolymer to a specific analyte arises from the natural ability of the photopolymer to respond to the external stimuli. The natural ability of the acrylamide derivative photopolymer layer to swell or shrink at different levels of relative humidity or applied pressure was exploited for the design of a holographic humidity sensor [31] and a pressure sensor [46, 47].

The fabrication of the holographic sensor in the acrylamide derivative-based photopolymer includes two steps. Firstly, the photopolymer layers are prepared by mixing photopolymer components followed by coating the solution on a substrate and drying at ambient temperature and low relative humidity. Secondly, the photonic structure is created by holographic patterning of the photopolymer layer. Figure 2.5

shows the formation of a volume phase transmission grating during holographic recording in the photopolymer.

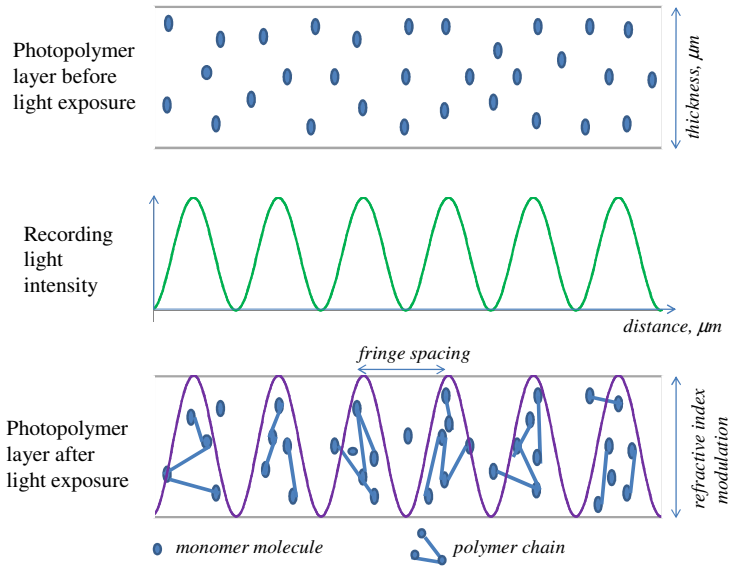

Figure 2.5. Formation of a holographic grating through photopolymer chemistry.

When the photopolymer layer is exposed to the interference pattern, a polymerisation process is initiated in the illuminated areas where monomer molecules form polymer chains leading to change in molecular polarisability and density change. The photopolymerisation is accompanied by the diffusion process. Due to the created concentration gradient, monomers diffuse from dark to bright regions and short polymer chains diffuse in opposite direction. Holographic patterning of the photopolymer leads to the spatial variation of the refractive index of the material due to photopolymerisation and diffusion of photopolymer components [48-56]. A volume phase grating is recorded as a spatial variation of the refractive index. Depending on the permeability of the polymer matrix which greatly affects the diffusion rate, the main contributor to the refractive index modulation can be either density change or molecular polarisability change [54].

The fabrication of holographic sensors through photopolymer chemistry has a great potential due to the ease of the holographic sensor preparation and its low cost. These are beneficial for the mass production of disposable sensors. Also, capability to achieve high diffraction efficiency of photopolymer-based gratings allows creating labels with a bright image.

2.4.2. Silver halides-based materials

The second class is silver halide based materials which have higher light sensitivity than photopolymers [57-60]. Silver halide emulsions consist of silver halide with a light-sensitive dye dispersed in functionalised polymer matrix. Silver bromide is the most commonly used silver halide. Polymer matrix can be composed of gelatine, poly(2-hydroxyethylmethacrylate), polyacrylamide and polyvinylalcohol. Utilisation of different synthetic dyes allows holographic recording at different wavelengths.

In contrast to photopolymer materials, the development of the sensor based on silver halide materials is a time consuming process and consists of a lot of steps. The creation of the holographic sensor through silver halide chemistry includes 1) making of the analyte-sensitive polymer matrix, 2) diffusion of silver ions into the matrix and formation of silver halides, 3) holographic patterning of the material to produce multilayer photonic structure and 4) developing and post-processing steps to fix the hologram and improve the diffraction efficiency [58, 61]. A volume phase grating developed by silver halide photochemistry represents a periodic variation of the refractive index produced by periodic distribution of silver nanoparticles in the functionalised polymer matrix (Figure 2.6). The sensitivity of the hologram to a target analyte originates from the ability of functionalised polymer matrix to alter its properties under exposure to the analyte.

A variety of holographic sensors developed through silver halide chemistry will be discussed in section 2.5. One of the main advantages of this technique is the possibility to create a holographic sensor in hydrophobic polymer to detect analytes in aqueous solutions [25, 62].

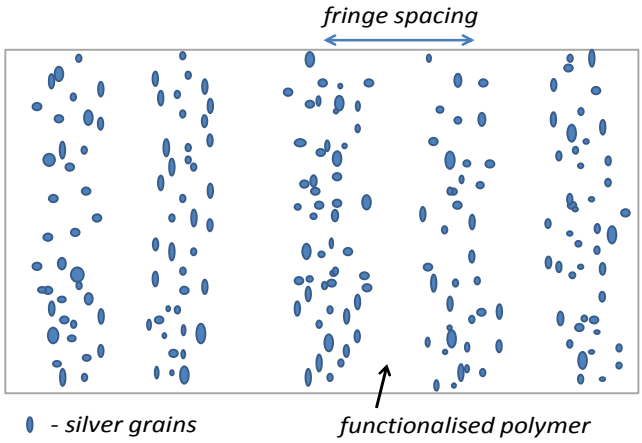

Figure 2.6. Distribution of silver grains formed by holographic patterning in functionalised polymer matrix.

2.4.3. Photopolymers doped with nanosized zeolites

The third class are photopolymers doped with nanosized zeolites. Zeolites are crystalline materials with a very regular pore structure of molecular dimensions [63-65]. There is a large variety of nanosized zeolites depending on their framework type, pore dimensions and Si/Al or Al/P ratios [66]. The incorporation of zeolites having various shapes and structures into a photopolymer medium can improve the dynamic range of the material, decrease its shrinkage and create sensitivity of the material to a specific analyte [29, 67-72].

The fabrication of a holographic sensor based on zeolite-doped photopolymers includes the steps described for undoped photopolymers in section 2.4.1 and one

additional step. Doping the photopolymer solution with the nanoparticle suspension has to be done during the mixing photopolymer components. Figure 2.7 shows the formation of a volume phase transmission grating in a nanoparticle doped photopolymer layer. During holographic recording the nanoparticles are excluded from the bright fringe area without participation in polymerisation process.

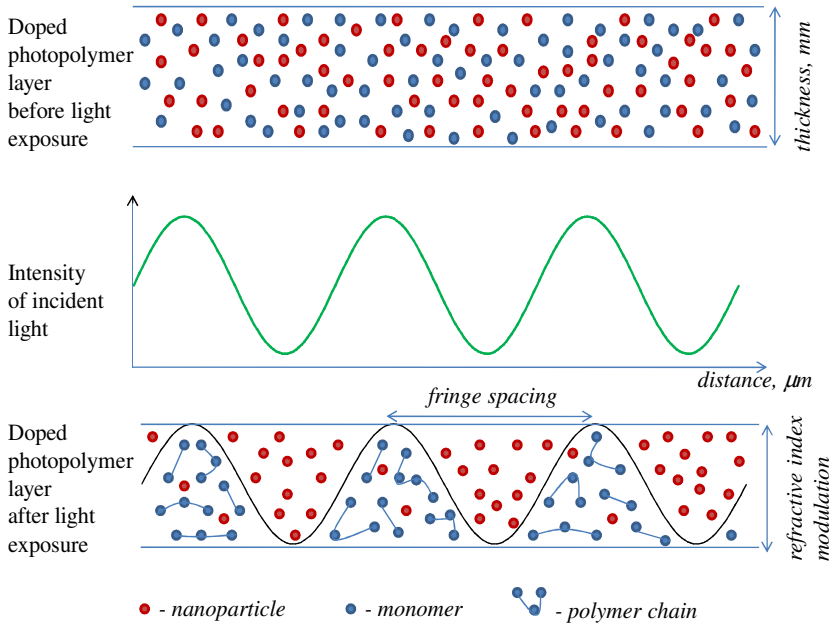

Figure 2.7. Formation of a holographic grating in a photopolymer doped with nanoparticles through light induced redistribution of nanoparticles and photopolymer chemistry.

The model based on exclusion of nanoparticles from the bright fringe area is strongly supported by the experimental data [67, 68, 70, 71, 73-80]. The materials contained nanoparticles with refractive index lower than that of the host of the material have the refractive index profile as shown in Figure 2.7. In the case of materials doped with nanoparticles having higher refractive index, a phase shift of 180^{o} between the interference pattern profile and the refractive index profile is observed. The response of

the hologram recorded in nanocomposites to a target analyte originates from the ability of nanoparticles to absorb the analyte leading to changes in the refractive index modulation of the created photonic structure. A big variety of nanoparticles with different shape and size provides possibility to manipulate the selectivity of the holographic sensors.

Despite of the advantages of nanotechnology, there are the health issues originating from the utilisation of nanocomposites [81-83]. Nanoparticle toxicology establishes the hazard of nanoparticles and their potential risk during the development, production, utilisation and discarding the nanomaterials. The toxicity of nanoparticles arises from their fine size which is smaller than cells and cellular organelles. This allows nanoparticles to penetrate basic biological structures disrupting their normal function. Harmful effects of nanoparticles on human health are known to depend on both personal factors and nanoparticle properties such as size, chemistry, shape and electromagnetic properties [84-88]. Thus, to benefit from nanotechnologies, toxicity safe design of materials and devices is required in order to minimise or prevent adverse health impacts.

2.5. Progress in holographic sensor technology

Holographic sensors fabricated using different photonic materials are summarised in this section. So far, a variety of holographic sensors with sensitivity to different analytes have been developed. Holographic gratings can be used as sensors for analytes in gas and liquid phase as well as different physical stimuli such as pressure and magnetic field. Sensors also vary in type depending on the sensing mechanism.

One of the first holographic sensors was capable of measuring water activity in hydrocarbon solvents [89]. Reflection holograms recorded in gelatine-based

holographic plates were immersed in different mixtures of water and solvent. The shift of the wavelength of the diffracted light due water activity was monitored using a spectrophotometer. Gelatine-based reflection gratings were also used for the detection of biological molecules. Holographic sensors showed the sensitivity to trypsin and chymotrypsin [90] and amylase [25]. Quantification of alcohol content was carried out by a holographic sensor developed in poly(2-hydroxyethyl methacrylate) film [62]. A variety of alcoholic beverages were tested and the accuracy of the measurements was found to be within 0.3 vol %. A holographic sensor developed through dye-based photopolymerisation was fabricated to monitor organic solvent (ethanol, methanol, propan-2-ol, dimethyl sulfoxide) concentration [91].

A number of holographic sensors have been developed for pH detection. Among them are hydrogel-based nanoparticle-doped photonic crystal sensors [19, 92] and sensors based on hydrogel containing ionisable monomers [93] or *N*-acryloyl-m-aminophenylboronic acid [28]. Holographic sensors for ions of Na^+ and K^+ have been fabricated from crown ethers incorporated into polymeric hydrogels [94]. A holographic sensor for real-time detection of divalent metal ions (Ca^{2+}, Mg^{2+}, Ni^{2+}, $Co^{2+}$and Zn^{2+}) has been created by incorporating a chelating monomer into a hydrogel matrix [95]. Holographic gratings recorded in polymer hydrogels, such as acrylate, acrylamide and vinyl alcohol, have been used for detection of glucose [26], bacterial spores [27], lactate [96, 97]. Molecularly imprinted silver-halide reflection and transmission gratings have been developed for the detection of testosterone [17, 98].

Holographic sensors are also capable of effective monitoring of levels of potentially hazardous or toxic gases. Ammonia-sensitive photonic structures have been produced in Nafion membranes [99]. Hydrocarbons and volatile organic compounds can be detected by the holographic sensor developed in silicon elastomer [30].

Holographic sensors can detect a physical influence such as magnetism or pressure. A holographic sensor with the response to magnetic field can be developed by using organic polymer which exhibits magnetic properties as a recording medium and creating a hologram in this material through silver-halide chemistry [100]. A holographic pressure sensor based on reflection holograms recorded using silver-halide chemistry in an acrylamide copolymer [100] and a pressure sensor based on reflection gratings recorded in the diacetone acrylamide-based photopolymer [47] have been developed.

Sensors based on nanocomposites have also been created. Incorporation of AlPO-18 zeolite nanoparticles to the acrylamide-based photopolymer has been found to introduce an irreversible change in the diffraction efficiency of holographic gratings under exposure to high humidity [101]. Holographic sensors based on diffraction gratings recorded in the diacetone-acrylamide-based photopolymer doped with BEA type zeolite nanoparticles have response to methanol, isopropanol, and 2-methylpropan-2-ol and allow the real-time measurements of alcohol in its gaseous form [102].

As shown above, a range of holographic sensors has been developed for different analytes. However, only few systems for humidity and temperature measurement have been reported. The aim of this project is to develop holographic sensors with response to the relative humidity changes or temperature variations. Following chapters present experimental results obtained during the research.

References

1. Gabor, D., *A New Microscopic principle.* Nature, 1948. **161**: p. 777-778.
2. Leith, E.N. and Upatnieks, J., *Reconstructed wavefronts and communication theory.* Journal of the Optical Society of America, 1962. **52**(10): p. 1123-1130.
3. Denisyuk, Y., *On the reflection of optical properties of an object in a wave field of light scattered by it.* Doklady Akademii Nauk SSSR, 1962. **144**(6): p. 1275-1278.
4. Benton, S.A., *Method for making reduced bandwidth holograms*. 1972, Patent US 3633989 A.
5. Phariseau, P., *On the diffraction of light by progressive supersonic waves.* Proceedings of the Indian Academy of Sciences - Section A, 1956. **44**(4): p. 165-170.
6. Dhar, L., *High-performance polymer recording materials for holographic data storage.* MRS Bulletin, 2006. **31**(04): p. 324-328.
7. Guo, J., Gleeson, M. and Sheridan, J., *A Review of the optimisation of photopolymer materials for holographic data storage.* Physics Research International, 2012. **2012**: p. 1-16.
8. Toal, V., *Introduction to holography*. Press Taylor and Francis Group 2011.
9. Dhar, L., Curtis, K. and Facke, T., *Holographic data storage: Coming of age.* Nature Photonics, 2008. **2**(7): p. 403-405.
10. Curtis, K., Dhar, L., Hill, A., Wilson, W. and Ayres, M., *Holographic data storage from theory to practical systems*. Wiley 2010.
11. Zhao, Q., Yetisen, A.K., Anthony, C.J., Fowler, W.R., Yun, S.H. and Butt, H., *Printable ink holograms.* Applied Physics Letters, 2015. **107**(4): p. 041115.

12. Cowan, J.J., *Aztec surface-relief volume diffractive structure.* Journal of the Optical Society of America A, 1990. **7**(8): p. 1529-1544.

13. Macko, P. and Whelan, M.P., *Fabrication of holographic diffractive optical elements for enhancing light collection from fluorescence-based biochips.* Optics Letters, 2008. **33**(22): p. 2614-2616.

14. Tay, S., Blanche, P.-A., Voorakaranam, R., Tunç, A.V., Lin, W., Rokutanda, S., Gu, T., Flores, D., Wang, P., Li, G., St. Hilaire, P., Thomas, J., Norwood, R.A., Yamamoto, M. and Peyghambarian, N., *An updatable holographic three-dimensional display.* Nature, 2008. **451**(7179): p. 694-698.

15. Smalley, D.E., Smithwick, Q.Y.J., Bove, V.M., Barabas, J. and Jolly, S., *Anisotropic leaky-mode modulator for holographic video displays.* Nature, 2013. **498**(7454): p. 313-317.

16. St. Hilaire, P., Benton, S.A. and Lucente, M., *Synthetic aperture holography: a novel approach to three-dimensional displays.* Journal of the Optical Society of America A, 1992. **9**(11): p. 1969-1977.

17. Fuchs, Y., Kunath, S., Soppera, O., Haupt, K. and Mayes, A.G., *Molecularly imprinted silver-halide reflection holograms for label-free opto-chemical sensing.* Advanced Functional Materials, 2014. **24**(5): p. 688-694.

18. Mihaylova, E., Cody, D., Naydenova, I., Raghavendra, J., Martin, S. and Toal, V., *Research on holographic sensors and novel photopolymers at the Centre for Industrial and Egnineering Optic,* in: Holography: basic principles and contemporary applications. E. Mihaylova (Ed.), Intech 2013.

19. Yetisen, A.K., Butt, H., Vasconcellos, F.C., Montelongo, Y., Davidson, C.A.B., Blyth, J., Chan, L., Carmody, B.J., Vignolini, S.,Steiner, U., et.al., *Light-directed*

writing of chemically tunable narrow-band holographic sensors. Advanced Optical Materials, 2014. **2**(3): p. 250-254.

20. Yetisen, A.K., Naydenova, I., Vasconcellos, F.C., Blyth, J. and Lower, C.R., *Holographic sensors: Three-dimensional analyte-sensitive nanostructures and their applications.* Chemical Reviews, 2014. **114**(20): p. 10654-10696.
21. Castro, J.M., Zhang, D., Myer, B. and Kostuk, R.K., *Energy collection efficiency of holographic planar solar concentrators.* Applied Optics, 2010. **49**(5): p. 858-870.
22. Bloss, W.H., Griesinger, M. and Reinhardt, E.R., *Dispersive concentrating systems based on transmission phase holograms for solar applications.* Applied Optics, 1982. **21**(20): p. 3739-3742.
23. James, P.A.B. and Bahaj, A.S., *Holographic optical elements: various principles for solar control of conservatories and sunrooms.* Solar Energy, 2005. **78**(3): p. 441-454.
24. Akbari, H., Naydenova, I. and Martin, S., *Using acrylamide-based photopolymers for fabrication of holographic optical elements in solar energy applications.* Applied Optics, 2014. **53**(7): p. 1343-1353.
25. Blyth, J., Lowe, C.R., Mayers, A.G. and Millington, R.B., *Holographic sensors and their production*. 1999, Patent WO 1999063408 A1.
26. Kabilan, S., Blyth, J., Lee, M., Marshall, A., Hussain, A., Yang, X. and Lowe, C., *Glucose-sensitive holographic sensors.* Journal of Molecular Recognition, 2004. **17**(3): p. 162-166.
27. Bhatta, D., Christie, G., Madrigal-Gonzalez, B., Blyth, J. and Lowe, C., *Holographic sensors for the detection of bacterial spores.* Biosensors and Bioelectronics, 2007. **23**(4): p. 520-527.

28. Kraiskii, A., Postnikov, V., Sultanov, T. and Khamudilin, A., *Holographic sensors for diagnostics of solution components.* Quantum Electronics, 2010. **40**(2): p. 178-182.

29. Leite, E., Naydenova, I., Mintova, S., Leclercq, L. and Toal,V., *Photopolymerizable nanocomposites for holographic recording and sensor application.* Applied Optics, 2010. **49**(19): p. 3652-3660.

30. Martínez-Hurtado, J.L., Davidson, C., Blyth, J. and Lowe, C., *Holographic detection of hydrocarbon gases and other volatile organic compounds.* Langmuir, 2010. **26**(19): p. 15694-15699.

31. Naydenova, I., Raghavendra, J., Toal, V. and Martin, S., *A visual indication of environmental humidity using a color changing hologram recorded in a self-developing photopolymer.* Applied Physics Letters, 2008. **92**(3): p. 031109.

32. Naydenova, I., Sherif, H., Martin, S., Jallapuram, R., Toal, V., *Holographic sensor*. 2012, Patent US8535853 B2.

33. Kogelnik, H., *Coupled wave theory for thick hologram gratings.* The Bell System Technical Journal, 1969. **48**(9): p. 2909-2947.

34. Naydenova, I., Raghavendra, J., Martin, S. and Toal, V., *Holographic humidity sensors*, in: *Humidity sensors*, C. Okada (Ed.), Nova Science Publishers 2011.

35. Calixto, S., *Dry polymer for holographic recording.* Applied Optics, 1987. **26**(18): p. 3904-3910.

36. Smothers, W.K., Monroe, B.M., Weber, A.M. and Keys, D.E., *Photopolymers for holography*. SPIE Proceedings, 1990. **1212**.

37. Lawrence, J.R., O'Neill, F.T. and Sheridan, J.T., *Photopolymer holographic recording material.* Optik - International Journal for Light and Electron Optics, 2001. **112**(10): p. 449-463.

38. Martin, S., Leclere, P., Renotte, Y., Toal, V. and Lion, Y., *Characterization of an acrylamide-based dry photopolymer holographic recording material.* Optical Engineering, 1994. **33**(12): p. 3942-3946.

39. Cody, D., Naydenova,I. and Mihaylova, E., *New non-toxic holographic photopolymer material.* Journal of Optics, 2012. **14**(1): p. 015601.

40. Gong, Q., Wang, S., Huang, M. and Gan, F., *A humidity-resistant highly sensitive holographic photopolymerizable dry film.* Materials Letters, 2005. **59**(23): p. 2969-2972.

41. Blaya, S., Mallavia, R., Carretero, L., Fimia, A. and Madrigal, R. F., *Highly sensitive photopolymerizable dry film for use in real time holography.* Applied Physics Letters, 1998. **73**(12): p. 1628-1630.

42. Kim, W.S., Jeong, Y-C., Park, J-K., Shin, C-W. and Nam, K., *Diffraction efficiency behavior of photopolymer based on P(MMA-co-MAA) copolymer matrix.* Optical Materials, 2007. **29**(12): p. 1736-1740.

43. Trentler, T.J., Boyd, J.E. and Colvin, V.L., *Epoxy resin−photopolymer composites for volume holography.* Chemistry of Materials, 2000. **12**(5): p. 1431-1438.

44. Moothanchery, M., Naydenova, I. and Toal, V., *Studies of shrinkage as a result of holographic recording in acrylamide-based photopolymer film.* Applied Physics A, 2011. **104**(3): p. 899-902.

45. Hosam, S., Naydenova, I., Martin, S., McGinn, C. and Toal, V., *Characterization of an acrylamide-based photopolymer for data storage utilizing holographic angular multiplexing.* Journal of Optics A: Pure and Applied Optics, 2005. **7**(5): p. 255-260.

46. Cody, D., *Low-toxicity diacetone acrylamide-based photopolymer for applications in holography*. 2014, (Doctoral Thesis), Dublin Institute of Technology: Dublin.

47. Mihaylova, E., Cody, D., Naydenova, I., Martin, S. and Toal, V., *Diacetone-acrylamide based pressure sensitive photopolymer*, 2014, Patent Application No. GB1411640.4.

48. Piazzolla, S. and Jenkins, B.K., *First-harmonic diffusion model for holographic grating formation in photopolymers.* Journal of the Optical Society of America B, 2000. **17**(7): p. 1147-1157.

49. Moreau, V., Renotte, Y. and Lion, Y., *Characterization of DuPont photopolymer: determination of kinetic parameters in a diffusion model.* Applied Optics, 2002. **41**(17): p. 3427-3435.

50. Zhao, G. and Mouroulis, P., *Diffusion model of hologram formation in dry photopolymer materials.* Journal of Modern Optics, 1994. **41**(10): p. 1929-1939.

51. Colvin, V.L., Larson, R. G., Harris, A. L. and Schilling, M. L., *Quantitative model of volume hologram formation in photopolymers.* Journal of Applied Physics, 1997. **81**(9): p. 5913-5923.

52. Lawrence, J.R., O'Neill, F.T. and Sheridan, J.T., *Adjusted intensity nonlocal diffusion model of photopolymer grating formation.* Journal of the Optical Society of America B, 2002. **19**(4): p. 621-629.

53. Babeva, T., Naydenova, I., Mackey, D., Martin, S. and Toal, V., *Two-way diffusion model for short-exposure holographic grating formation in acrylamide-based photopolymer.* Journal of the Optical Society of America B, 2010. **27**(2): p. 197-203.

54. Martin, S., Naydenova, I., Jallapuram, R., Howard, R. and Toal, V., *Two way diffusion model for the recording mechanism in a self developing dry acrylamide photopolymer*. SPIE Proceedings, 2006. **6252**, p. 37-44.

55. Kwon, J.H., Hwang, H.C. and Woo, K.C., *Analysis of temporal behavior of beams diffracted by volume gratings formed in photopolymers.* Journal of the Optical Society of America B, 1999. **16**(10): p. 1651-1657.

56. Ortuño, M., Gallego, S., García, C., Neipp, C. and Pascual, I., *Holographic characteristics of a 1-mm-thick photopolymer to be used in holographic memories.* Applied Optics, 2003. **42**(35): p. 7008-7012.

57. Bjelkhagen, H.I., Crosby, P. G., Green, D. P. M., Mirlis, E. and Phillips, N. J., *Fabrication of ultra-fine-grain silver halide recording material for color holography*. SPIE Proceedings 2008. **6912**, 09-1-14

58. Bjelkhagen, H., *Silver-halide recording materials for holography and their processing*. Springer: Heidelberg 1995.

59. Saxby, G., *Practical Holography*. Institute of Physics Publishing: London 2004.

60. Gentet, Y. and Gentet, P., *Ultimate emulsion and its applications: a laboratory-made silver halide emulsion of optimized quality for monochromatic pulsed and full-color holography*. SPIE Proceedings: Holography, 2000. **4149**: p. 56–62.

61. Blyth, J., Millington, R., Mayes, A. and Lowe, C., *A diffusion method for making silver bromide based holographic recording material.* The Imaging science journal, 1999. **47**: p. 87-91.

62. Mayes, A.G., Blyth, J., Kyröläinen-Reay, M., Millington, R.B. and Lowe, C.R., *A holographic alcohol sensor.* Analytical Chemistry, 1999. **71**(16): p. 3390-3396.

63. McCusker, L.B. and Baerlocher, C., *Zeolite structures*, in: *Studies in surface science and catalysis*, H. van Bekkum, et al., (Ed.), Elsevier. p. 37-67, 2001.

64. Baerlocher, C., Xie, D., McCusker, L.B., Hwang, S-J., Chan, I.Y., Ong, K., Burton, A.W. and Zones, S.I., *Ordered silicon vacancies in the framework structure of the zeolite catalyst SSZ-74.* Nature Materials, 2008. **7**(8): p. 631-635.

65. Jacobs, P.A., Flanigen, E.M., Jansen, J.C. and van Bekkum, H., *Introduction to zeolite science and practice*. Elsevier Science 2001.

66. Baerlocher, C. McCusker, L.B. and Olson, D.H., *Atlas of zeolite framework types*, *6th ed.*, Elsevier, Amsterdam, 2007.

67. Naydenova, I., Sherif, H., Mintova, S., Martin, S. and Toal, V., *Holographic recording in nanoparticle-doped photopolymer*. SPIE Proceedings 2006. **6252**: p.45-50.

68. Naydenova, I., Mintova, S., Martin, S. and Toal, V., *Nanocomposites for novel hologhraphic applications.* SPIE Newsroom, 2008.

69. Moothanchery, M., Naydenova, I., Mintova, S. and Toal, V., *Nanozeolites doped photopolymer layers with reduced shrinkage.* Optics Express, 2011. **19**(25): p. 25786-25791.

70. Babeva, T., Todorov, R., Mintova, S.,Yovcheva, T., Naydenova, I. and Toal, V., *Optical properties of silica MFI doped acrylamide-based photopolymer.* Journal of Optics A: Pure and Applied Optics, 2009. **11**(2): p. 024015.

71. Naydenova, I., Leite, E., Babeva, T., Pandey, N., Baron, T., Yovcheva, T., Sainov, S., Martin, S., Mintova, S. and Toal, V., *Optical properties of photopolymerizable nanocomposites containing nanosized molecular sieves.* Journal of Optics, 2011. **13**(4): p. 044019.

72. Cody, D., Mihaylova, E., O'Neill, L., Babeva, T., Awala, H., Retoux, R., Mintova, S. and Naydenova, I., *Effect of zeolite nanoparticles on the optical properties of diacetone acrylamide-based photopolymer.* Optical Materials, 2014. **37**: p. 181-187.

73. Suzuki, N., Tomita, Y., Ohmori, K., Hidaka, M. and Chikama, K., *Highly transparent ZrO2 nanoparticle-dispersed acrylate photopolymers for volume holographic recording.* Optics Express, 2006. **14**(26): p. 12712-12719.

74. Vaia, R.A., Dennis, C. L., Natarajan, L. V., Tondiglia, V. P., Tomlin, D. W., Bunning, T. J., *One-step, micrometer-scale organization of nano- and mesoparticles using holographic photopolymerization: A generic technique.* Advanced Materials, 2001. **13**(20): p. 1570-1574.

75. Tomita, Y., Suzuki, N. and Chikama, K., *Holographic manipulation of nanoparticle distribution morphology in nanoparticle-dispersed photopolymers.* Optics Letters, 2005. **30**(8): p. 839-841.

76. Tomita, Y., Chikama, K., Nohara, Y., Suzuki, N., Furushima, K. and Endoh, Y., *Two-dimensional imaging of atomic distribution morphology created by holographically induced mass transfer of monomer molecules and nanoparticles in a silica-nanoparticle-dispersed photopolymer film.* Optics Letters, 2006. **31**(10): p. 1402-1404.

77. Sakhno, O.V., Goldenberg, L. M., Stumpe, J. and Smirnova, T. N., *Surface modified ZrO 2 and TiO 2 nanoparticles embedded in organic photopolymers for highly effective and UV-stable volume holograms.* Nanotechnology, 2007. **18**(10): p. 105704.

78. Suzuki, N., Tomita, Y. and Kojima, T., *Holographic recording in TiO2 nanoparticle-dispersed methacrylate photopolymer films.* Applied Physics Letters, 2002. **81**(22): p. 4121-4123.

79. Tomita, Y., Urano, H., Fukamizu, T., Kametani, Y., Nishimura, N. and Odoi, K., *Nanoparticle-polymer composite volume holographic gratings dispersed with ultrahigh-refractive-index hyperbranched polymer as organic nanoparticles.* Optics Letters, 2016. **41**(6): p. 1281-1284.

80. Sánchez, C., Escuti, M. J., van Heesch, C., Bastiaansen, C.W.M., Broer, D.J., Loos, J. and Nussbaumer, R., *TiO2 nanoparticle–photopolymer composites for volume holographic recording.* Advanced Functional Materials, 2005. **15**(10): p. 1623-1629.

81. Donaldson, K., Stone, V., Tran, C.L., Kreyling, W. and Borm, P.J.A., *Nanotoxicology.* Occupational and Environmental Medicine, 2004. **61**(9): p. 727-728.

82. Sayes, C.M. and Warheit, D.B., *Characterization of nanomaterials for toxicity assessment.* Wiley Interdisciplinary Reviews: Nanomedicine and Nanobiotechnology, 2009. **1**(6): p. 660-670.

83. Park, H. and Grassian, V.H., *Commercially manufactured engineered nanomaterials for environmental and health studies: Important insights provided by independent characterization.* Environmental Toxicology and Chemistry, 2010. **29**(3): p. 715-721.

84. Elsaesser, A. and Howard, C.V., *Toxicology of nanoparticles.* Advanced Drug Delivery Reviews, 2012. **64**(2): p. 129-137.

85. Hansen, S.F., Michelson, E., Kamper, A., Borling, P., Stuer-Lauridsen, F. and Baun, A., *Categorization framework to aid exposure assessment of nanomaterials in consumer products.* Ecotoxicology, 2008. **17**(5): p. 438-447.

86. Carnovale, C., Bryant, G., Shukla, R. and Bansal, V., *Size, shape and surface chemistry of nano-gold dictate its cellular interactions, uptake and toxicity.* Progress in Materials Science, 2016. **83**: p. 152-190.

87. Petushkov, A., Ndiege, N., Salem, A.K. and Larsen, S.C., *Toxicity of silica nanomaterials: zeolites, mesoporous silica, and amorphous silica nanoparticles*, in: *Advances in molecular toxicology*, C.F. James (Ed.), Elsevier. p. 223-266, 2010.

88. Thomas, J.A. and Ballantyne, B., *Toxicological assessment of zeolites.* International Journal of Toxicology, 1992. **11**(3): p. 259-273.

89. Blyth, J., Millington, R.B., Mayes, A.G., Frears, E.R. and Lowe, C.R., *Holographic sensor for water in solvents.* Analytical Chemistry, 1996. **68**(7): p. 1089-1094.

90. Millington, R.B., Mayes, A.G., Blyth, J. and Lowe, C.R., *Eurosensors IXA hologram biosensor for proteases.* Sensors and Actuators B: Chemical, 1996. **33**(1): p. 55-59.

91. Yetisen, A.K., Qasim, M. M., Nosheen, S., Wilkinson, T. D. and Lowe, C.R., *Pulsed laser writing of holographic nanosensors.* Journal of Materials Chemistry C, 2014. **2**(18): p. 3569-3576.

92. Tsangarides, C.P., Yetisen, A.K., da Cruz Vasconcellos, F., Montelongo, Y., Qasim, M.M., Wilkinson, T.D., Lowe, C.R. and Butt, H., *Computational modelling and characterisation of nanoparticle-based tuneable photonic crystal sensors.* RSC Advances, 2014. **4**(21): p. 10454-10461.

93. Marshall, A.J., Blyth, J., Davidson, C.A.B. and Lowe, C.R., *pH-sensitive holographic sensors.* Analytical Chemistry, 2003. **75**(17): p. 4423-4431.

94. Mayes, A.G., Blyth, J., Millington, R.B. and Lowe, C.R., *Metal ion-sensitive holographic sensors.* Analytical Chemistry, 2002. **74**(15): p. 3649-3657.

95. Madrigal González, B., Christie, G., Davidson, C.A.B., Blyth, J. and Lowe, C.R., *Divalent metal ion-sensitive holographic sensors.* Analytica Chimica Acta, 2005. **528**(2): p. 219-228.

96. Sartain, F.K., Yang, X. and Lowe, C.R., *Holographic lactate sensor.* Analytical Chemistry, 2006. **78**(16): p. 5664-5670.

97. Sartain, F.K., Yang, X. and Lowe, C.R., *Complexation of L-lactate with boronic acids: A solution and holographic analysis.* Chemistry – A European Journal, 2008. **14**(13): p. 4060-4067.

98. Fuchs, Y., Kunath, S., Soppera, O., Haupt, K. and Mayes, A.G., *Holographic molecularly imprinted polymers for label-free chemical sensing.* Advanced Materials, 2013. **25**(4): p. 566-570.

99. Hurtado, J.L.M. and Lowe, C.R., *Ammonia-sensitive photonic structures fabricated in nafion membranes by laser ablation.* ACS Applied Materials & Interfaces, 2014. **6**(11): p. 8903-8908.

100. Lowe, C.R., Blyth, J. and James, A.P., *Interrogation of a sensor*. 2006, WO Patent Application 2006008531 A1.

101. Leite, E., Babeva, T., Ng, E.P., Toal, V., Mintova, S. and Naydenova, I., *Optical properties of photopolymer layers doped with aluminophosphate nanocrystals.* The Journal of Physical Chemistry C, 2010. **114**(39): p. 16767-16775.

102. Zawadzka, M., et al., *Photonic materials for holographic sensing*, in: *Photonic materials for sensing, biosensing and display devices*, J.M. Serpe, Y. Kang, and M.Q. Zhang, (Eds.), Springer International Publishing: Cham. p. 315-359, 2016.

3. THE EFFECT OF HUMIDITY AND TEMPERATURE ON THE PROPERTIES OF UNSLANTED TRANSMISSION GRATINGS RECORDED IN AN ACRYLAMIDE-BASED PHOTOPOLYMER

3.1. Introduction

This chapter reports the investigation of the effect of humidity and temperature on properties of unslanted volume phase transmission gratings recorded in an acrylamide-based photopolymer. The acrylamide-based photopolymer is under continuous study due to its advantages discussed in Chapter 2, section 2.4.1 and because of its possible practical applications, such as holographic interferometry [1-5], holographic optical elements [6-8], holographic data storage [9-14] and holographic sensors [15-19]. The application of photopolymer-based gratings for the holographic sensing of humidity is the focus of the research presented in this chapter.

It has been observed that in certain environmental conditions the diffraction efficiency, Bragg angle of recorded gratings, and even the layer surface can be affected by humidity. In [18] the humidity response of a volume reflection hologram recorded in an acrylamide-based photopolymer was investigated in the relative humidity range from 5 to 80 %. Humidity-induced changes in properties of the grating were found to be fully reversible after exposure to the relative humidity up to 80 %, and the hologram regained its original characteristics when the humidity returned to 20 %. The humidity response of the reflection grating was utilised for the development of a visual indicator of environmental humidity [19]. The indicator changed its colour under exposure to different levels of humidity due to the humidity-induced changes in the fringe spacing as the medium gained or lost moisture. Later, responses of a volume reflection hologram to humidity (10 – 80 % *RH*) and temperature (15 - 50 ^{o}C) were studied in

more detail [17]. Only reversible changes of holographic grating properties were observed. Research into the effects of humidity on transmission gratings is very limited and has been carried out only at 60 % *RH* [20]. After exposure to the relative humidity of 60 % the diffraction efficiency of the transmission grating is found to return to its initial value measured at low humidity of 20 %. However, high humidity can cause irreversible changes to the recorded hologram, even in transmission gratings. A systematic investigation of the behaviour of transmission gratings exposed to high humidity is of significant interest for two reasons. Firstly, the grating's sensitivity to humidity can be exploited for the development of irreversible humidity indicators. Secondly, too much sensitivity to humidity can limit the use of these materials in applications where an environmentally stable hologram is required. Research is needed to fully characterise the effect of high humidity on the properties of transmission gratings to better understand the nature of the irreversible changes and find out the moisture stability limit of the grating.

The aim of the research presented in this chapter is the investigation of the behaviour of diffraction efficiency, thickness, refractive index modulation and Bragg angle of unslanted volume phase transmission gratings recorded in acrylamide-based photopolymer layers under humidity exposure at different temperatures. Specifically the irreversible changes of the properties of transmission gratings caused by exposure to high humidity ($RH \geq 80$ %) and the role of temperature on these changes are analysed.

3.2. Theoretical background for the refractive index modulation calculation

Kogelnik's coupled wave theory provides analytic formulae for the calculation of the diffraction efficiency of the volume gratings [21]. To evaluate the applicability of the

coupled wave theory in a particular case, Q factor should be calculated using Equation (2.1). In the present research, unslanted volume phase transmission gratings with a spatial frequency of 1000 ± 27 lines/mm were recorded in the photopolymer layers with the thickness of 80 ± 5 μm. According to Equation (2.1), these parameters correspond to Q factor of about 200 and, thus, the coupled wave theory for the calculation of the diffraction efficiency/refractive index modulation can be applied. According to the coupled wave theory, refractive index modulation is determined by:

$$\Delta n = \frac{\lambda \cos\theta \sin^{-1}\left(\sqrt{\eta}\right)}{\pi d}, \tag{3.1}$$

where λ is the wavelength of the reconstructing beam, θ is the Bragg angle inside the photopolymer layer at this wavelength, η is diffraction efficiency of the recorded volume transmission grating. θ is related to the external Bragg angle (θ') by Snell's law:

$$n \sin\theta = \sin\theta' . \tag{3.2}$$

θ' is given by Bragg's law (Equation 2.2).

3.3. Experimental

3.3.1. Sample preparation

A self-processing acrylamide-based photopolymer developed at the Centre for Industrial and Engineering Optics, Dublin Institute of Technology [22-24] was used as a holographic recording material. The photosensitive solution optimised for recording in transmission mode consisted of two monomers - 0.6 g acrylamide and 0.2 g N,N'–methylenebisacrylamide, 2 ml of triethanolamine, 17.5 ml of 10 % w/v polyvinylalcohol stock solution and 4 ml of 0.11 % w/v of methylene blue stock solution. The 10% w/v polyvinyl alcohol stock solution was prepared by adding 10 g of

polyvinyl alcohol into 100 ml of deionised water. The solution was slowly heated up to T = 80 ^{o}C and stirred by using a magnetic stirrer. The 0.11 % w/v dye solution was prepared by dissolving 0.11 g of methylene blue in 100 ml of deionised water. To make the photopolymer stock solution, the components were mixed using a magnetic stirrer in a dark room. Photopolymer layers were prepared by depositing the photopolymer stock solution on the levelled glass slides (26 × 76 mm^2) and drying for 24 hours in a dark room at T = 21 ± 2 ^{o}C and RH = 35 ± 5 %.

3.3.2. Holographic recording

Unslanted transmission volume phase gratings with a spatial frequency of 1000 ± 27 lines/mm were recorded using a two-beam set-up (Figure 3.1) with an angle of 37^{o} between the beams.

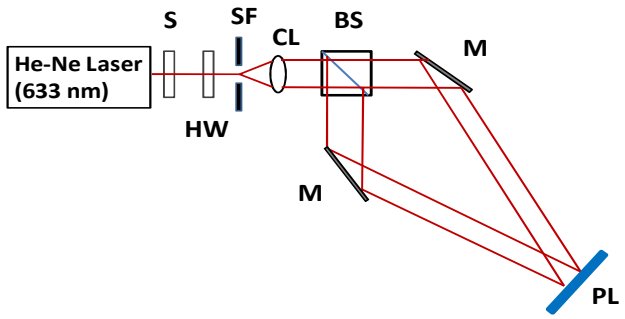

Figure 3.1. Recording set-up: S -electronic shutter; HW – half-wave plate; SF – spatial filter; CL – collimator; BS – beam splitter; M – mirror; PL – photopolymer layer.

The photopolymer layers were exposed to two 633 nm beams obtained by splitting He-Ne laser beam. The total recording intensity was 5 mW/cm^2 and the recording time was 10 sec. Recording time of 10 sec was used in order to achieve the diffraction efficiency of gratings in the range of 35 - 40 %. Immediately after the recording the gratings were

UV-cured with the exposure of 9 J/cm^2 using a UV Exposure unit (Mega Electronics, model 5503-11) in order to polymerise all residual monomers. After UV-curing, the absorption of the photopolymer layer at 633 nm was negligible, so 633 nm beam from He-Ne laser was employed as a probe beam for the Bragg selectivity curve measurements.

3.3.3. Bragg selectivity curve recording and thickness measurement

Each grating was characterised by measuring its diffraction efficiency at different incident angles and its Bragg selectivity curve was recorded by a computer controlled system. The set-up for the Bragg selectivity curve recording is shown in Figure 3.2.

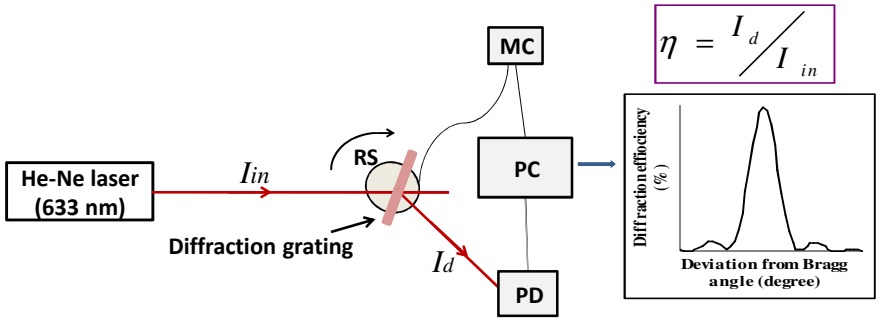

Figure 3.2. Set-up for the Bragg selectivity curve recording: RS – rotation stage; MC – motion controller; PC – computer; PD – photodetector.

To measure the Bragg selectivity curve, the sample was mounted on a rotation stage which was computer controlled *via* a motion controller (model Newport ESP300 with angular resolution of 0.1^o). A 633 nm beam from He-Ne laser was employed as a probe beam during the Bragg curve measurements. The Bragg selectivity curve measurement was performed by monitoring the first-order diffracted beam intensity (I_d) using an

optical power meter (Newport Model 840) while the sample was rotated. LabVIEW software was used to plot the data of the diffraction efficiency in real time as the incident angle of the probe beam was varied ± 2° from the Bragg angle. The diffraction efficiency was defined as the ratio of the diffracted beam intensity and the intensity of the incident beam (I_{in}).

The Bragg selectivity curve and thickness measurements had been carried out before and after humidity exposure. After humidity exposure, all the samples had been dried for 24 hours at T = 18 ± 2 °C and RH = 35 ± 5 %. The diffraction efficiency of the grating was estimated from the maximum of Bragg selectivity curve. The thickness of the dry layers was measured with a white light interferometric surface profiler MicroXAM S/N 8038.

3.3.4. Testing the humidity and temperature responses of holograms

The experimental set-up for the testing the humidity response of transmission gratings is presented in Figure 3.3. A controlled environment chamber with humidity and temperature control system (Electro-tech system, model 5503-11) was utilised to obtain different environmental conditions. The chamber is equipped with ETS Series 5000 Microprocessor Controller which is used to precisely control the temperature and humidity, to provide an accurate measurement and to monitor the chamber environment. The humidity level in the chamber can be reduced down to 10 % *RH* by the desiccant/pump dehumidification system. An ultrasonic humidification system allows the relative humidity to be increased up to 100 %. The heating system can increase the temperature from ambient temperature to 55 °C. The chamber was able to maintain the relative humidity and temperature with accuracy of ± 1 % and ± 1 °C, respectively.

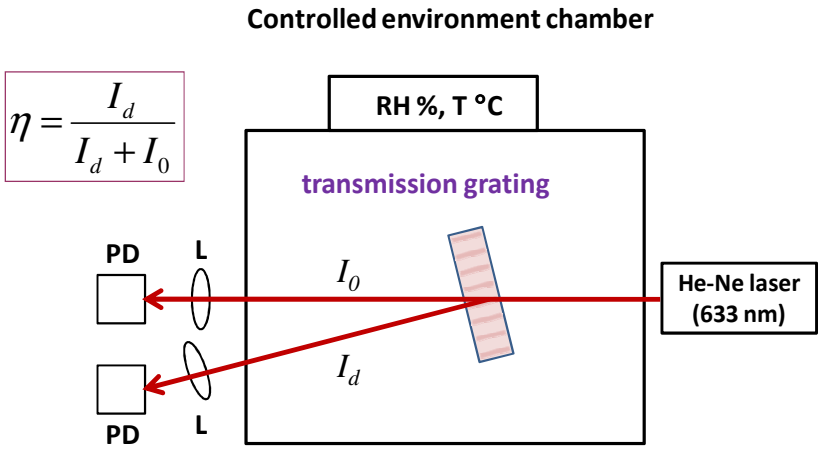

Figure 3.3. Schematic representation of the set-up for the testing the humidity response of the transmission grating during the humidity exposure. PD – photodetector, L - lens.

To minimise the inaccuracy caused by beam scattering due to water condensation on the photopolymer layer surface, intensities of transmitted (I_0) and diffracted (I_d) beams were monitored during humidity exposure. The readings were taken after 30 min of humidity exposure to allow the samples to equilibrate with the surrounding conditions and the diffraction efficiency in this particular experiment was defined as $I_d/(I_d+I_0)$.

3.4. Results and Discussion

3.4.1. Diffraction efficiency change due to variation of relative humidity

In order to characterise the influence of relative humidity on the diffraction efficiency, the gratings were placed in the humidity chamber and the diffraction efficiency was measured. For ease of comparison, normalised diffraction efficiency was used. The normalised diffraction efficiency was defined as the ratio of the diffraction efficiency at the current relative humidity and the diffraction efficiency at the start of the experiment, measured at the relative humidity of 20 %. Figure 3.4 shows the dependence of

normalised diffraction efficiency on relative humidity during humidity exposure at different temperatures.

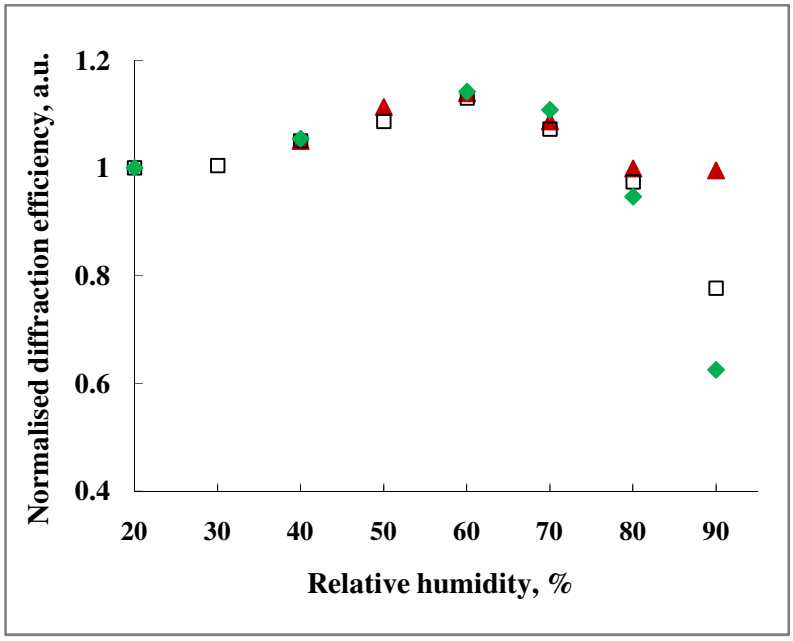

Figure 3.4. Normalised diffraction efficiency *versus* relative humidity at different temperatures: (▲) - 8 ± 1 °C; (□) - 16 ± 1 °C; (♦) - 21 ± 1 °C.

As can be seen from Figure 3.4, at 20 % ≤ *RH* ≤ 70 % the change in diffraction efficiency during humidity exposure does not depend on the temperature and follows the same trend for all three temperatures. However, at *RH* = 80 % and 90 % the normalised diffraction efficiency is different for different temperatures. As the temperature increases, the normalised diffraction efficiency drops further at the higher humidity.

It can also be observed in Figure 3.4 that for all three temperatures the normalised diffraction efficiency slightly increases in the relative humidity range 20 – 60 %. This is most probably due to swelling of the photopolymer layer as a result of absorption of moisture from the environment. The swelling is initially only in

direction perpendicular to the glass substrate, as the good adhesion of the photopolymer layer to the glass substrate prevents dimensional change in direction along the surface. Thus effectively the thickness of the hologram is increased and the diffraction efficiency increases as well. Similar swelling/shrinkage occurring only in the vertical direction was previously observed in reflection gratings [17, 18].

In addition it has been previously shown [17, 18], that the changes in diffraction efficiency of reflection gratings, recorded in acrylamide-based photopolymer layers, after exposure to $RH \leq 80$ % are reversible. Since we aim to investigate irreversible changes, we focused our attention on high humidity ($RH = 80$ % and 90 %).

3.4.2. Diffraction efficiency change after exposure to RH = 80 % and 90 %

To investigate the reversibility of the diffraction efficiency changes observed during the exposure to high humidity, samples were exposed to high humidity at different temperatures for 60 min and left to recover for 24 hours at $T = 18 \pm 2$ ^{o}C and $RH = 35 \pm 5$ %. Normalised diffraction efficiency, calculated as the ratio of the diffraction efficiency after humidity exposure followed by drying and the diffraction efficiency at the start of the experiment (before humidity exposure), is presented in Figure 3.5. As seen from the graph, except for the lowest temperature of 8 ± 1 ^{o}C, exposure to high humidity does result in an irreversible decrease of the diffraction efficiency. The magnitude of the irreversible decrease also depends on temperature during humidity exposure and it is greatest at $T = 21 \pm 1$ ^{o}C and $RH = 90$ %, dropping to approximately half the initial value.

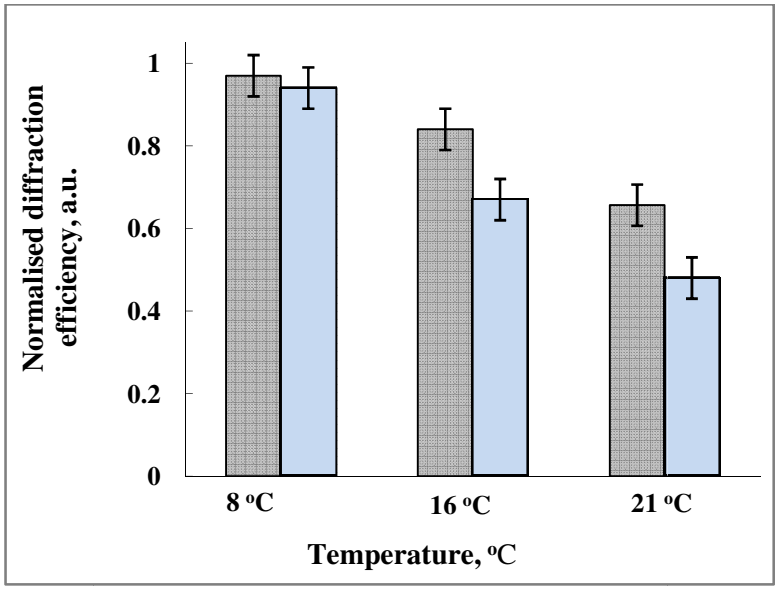

Figure 3.5. Normalised diffraction efficiency after exposure to high humidity and drying: *RH* = 80 % (■) and 90 % (■) at different temperatures.

3.4.3. Diffraction efficiency change after exposure to RH = 90%: dependence on time of exposure

In this section we investigate the effect of the duration of the humidity exposure on the observed change in diffraction efficiency. The time for which the grating has been exposed is found to have a significant effect on the diffraction efficiency after exposure. Figure 3.6 shows the normalised diffraction efficiency measured after exposure to high humidity for a set period of time at three different temperatures: 8 ± 1 ^{o}C, 16 ± 1 ^{o}C and 21 ± 1 ^{o}C. These samples were exposed to *RH* = 90 % for the specified amount of time and then were returned to normal humidity (*RH* = 30 - 40 %) before the measurement was taken. At *T* = 8 ± 1 ^{o}C a few percent reduction in diffraction efficiency is observed for samples exposed to up to 2 hours at high humidity. At *T* = 16 ± 1 ^{o}C and 21 ± 1 ^{o}C normalised diffraction efficiency significantly declines during the first 40 min of exposure and then is almost constant. Fitting the experimental curves by single

exponential decay, time constants were found to equal to 31 min, 22 min and 18 min at 8 ± 1 °C, 16 ± 1 °C and 21 ± 1 °C, respectively. Hence, the time constant is shorter, i.e. the process is faster, at higher temperature. From this result we can conclude that the magnitude of the irreversible decrease of the diffraction efficiency depends on both humidity exposure time and temperature during humidity exposure.

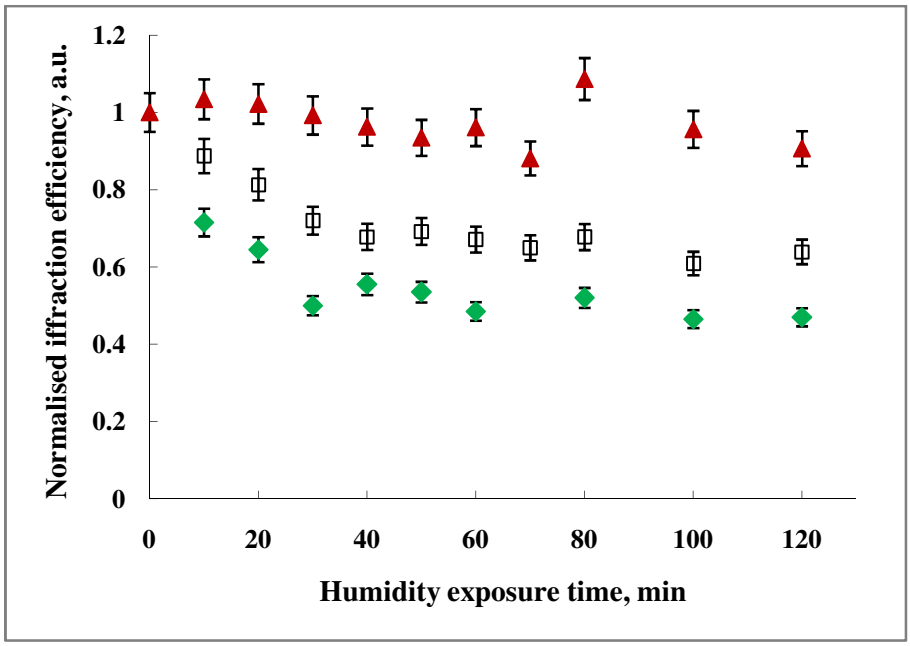

Figure 3.6. Normalised diffraction efficiency after exposure to *RH* = 90 % at *T* = 8 ± 1 °C (▲), 16 ± 1 °C (□), 21 ± 1 °C (♦) *versus* humidity exposure time.

3.4.4. Diffraction efficiency change after exposure to RH = 90 %: dependence on temperature

The temperature dependence of irreversible decrease of the diffraction efficiency after exposure to *RH* = 90 % has been investigated in more detail. The results are presented in Figure 3.7. Humidity exposure time was 60 min for this graph, as after this period of time saturation of humidity induced changes was observed (Figure 3.6).

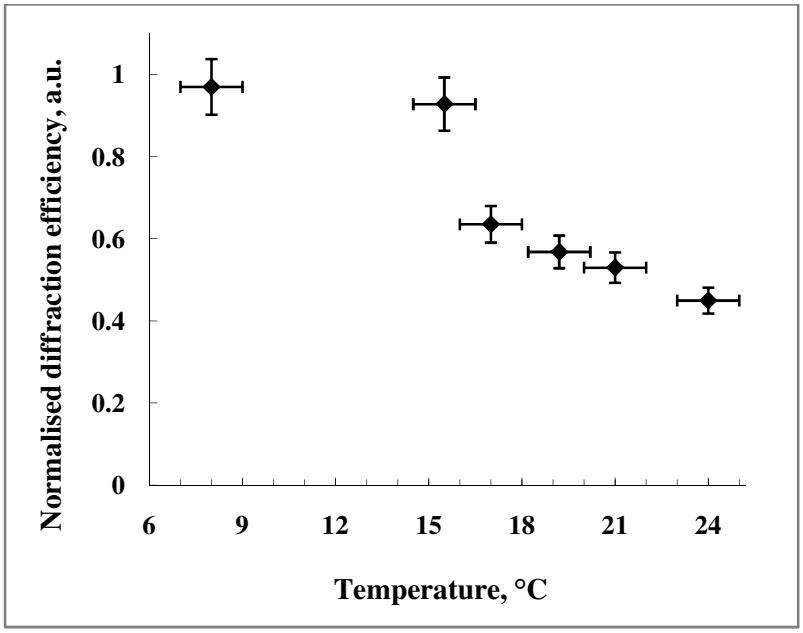

Figure 3.7. Temperature dependence of normalised diffraction efficiency after exposure to *RH* = 90 % for 60 min.

It can be seen that changes in normalised diffraction efficiency induced by exposure to *RH* = 90 % are fully reversible, when the temperature during the humidity exposure is kept below 9 ^{o}C. At 9 < *T* < 16 ^{o}C decrease of normalised diffraction efficiency is about few percents. In case the temperature exceeds 16 ^{o}C the changes become irreversible. Moreover, exposure to *RH* = 90 % at higher temperature leads to a larger drop in normalised diffraction efficiency. These results suggest that it might be that the structure changes in the holographic grating under the combined influence of high humidity and elevated temperature. Changes in structure are supposed to be attributed to one of the ingredients of the photopolymer – triethanolamine. The content of triethanolamine is about 47 % of total weight. It is well known that the freezing/melting temperature range of triethanolamine is in the range of 17.9 - 21 ^{o}C [25]. Below this temperature range the created photonic structure is likely to be more stable and, consequently, the diffraction efficiency changes are reversible.

3.4.5. Change in grating thickness, Bragg angle and refractive index modulation

3.4.5.1. Change in grating thickness

According to the coupled wave theory [21], the change in diffraction efficiency of unslanted transmission gratings implies a change in thickness and/or refractive index modulation in the recorded gratings, assuming the value is measured at the Bragg angle. To better understand the processes behind the observed diffraction efficiency decrease, the change in thickness after exposure to *RH* = 90 % for different amount of time has been measured (Figure 3.8).

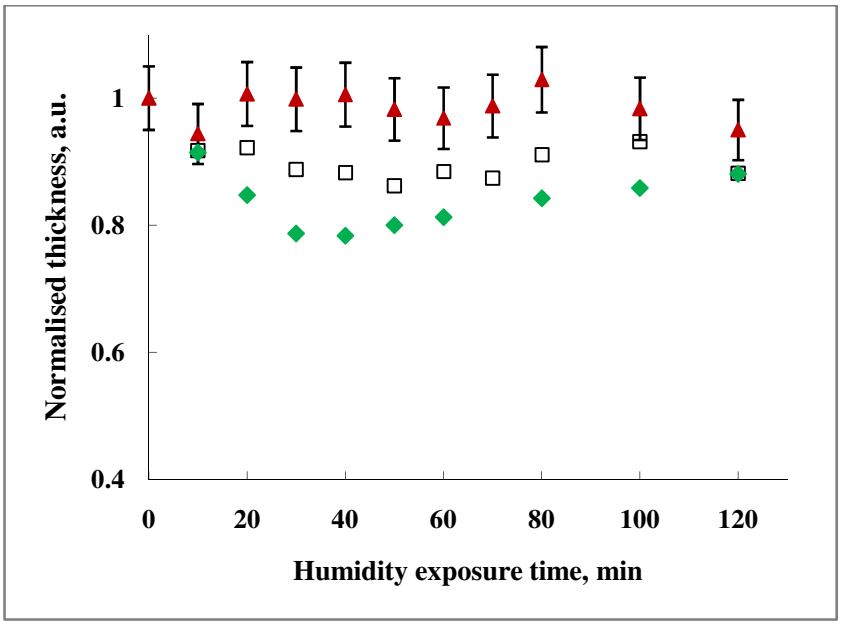

Figure 3.8. Normalised thickness after exposure to *RH* = 90 % at *T* = 8 ± 1 °C (▲), 16 ± 1 °C (□), 21 ± 1 °C (♦) *versus* humidity exposure time.

The graph shows normalised thickness as a function of time of exposure to high humidity. Normalised thickness was calculated as the ratio of the thickness measured after exposure to humidity followed by drying and the thickness measured before

exposure to humidity. Irreversible decrease in thickness indeed takes place and it is larger when the temperature is higher (Figure 3.8). It has also been visually observed that there is lateral dimensional change of the photopolymer layer as illustrated in Figure 3.9.

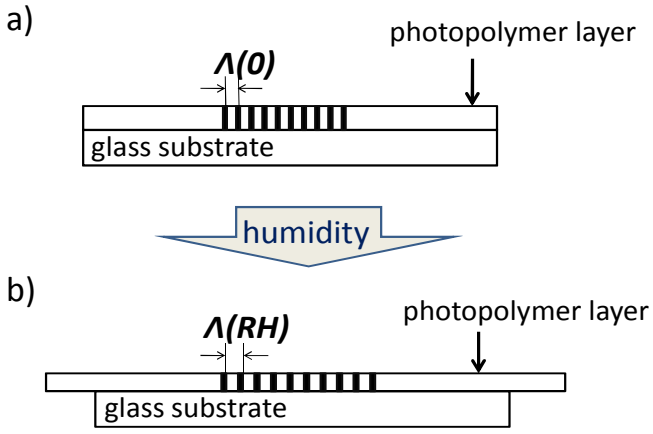

Figure 3.9. Schematic representation of the photopolymer layer before (a) and after (b) exposure to $RH = 90$ % at $T > 15$ °C. $\Lambda(0)$ and $\Lambda(RH)$ is the fringe spacing before and after humidity exposure, respectively.

The thickness decrease and lateral stretch observed can be explained as follows. Upon exposure to humidity the layer swells in all directions increasing the thickness and both lateral dimensions. Because the layer is centimetres long in the two lateral dimensions and only around 80 μm in the thickness dimension, the effect is much more noticeable in the layer width and length, which are observed to visibly increase and overhang the edge of the substrate by a few millimetres. In moderate humidity and/or lower temperatures the layer will recover its original dimensions fully when returned to the original conditions, but above certain temperatures and humidity levels, the layer is stretched beyond its capacity to recover and collapses to a lower thickness while remaining 'stretched' in the lateral dimensions.

Because of this lateral stretch the fringe spacing also changes irreversibly and Bragg's law (Equation (2.2)) predicts a change in the Bragg angle. Experimentally this can be observed as a shift in the Bragg angular selectivity curve and it will be discussed in section 3.4.5.2.

3.4.5.2. Shift in Bragg selectivity curve

Figure 3.10 illustrates the Bragg selectivity curve of a typical phase volume transmission grating measured before and after exposure to RH = 90 % at T = 16 ± 1 °C for 60 min.

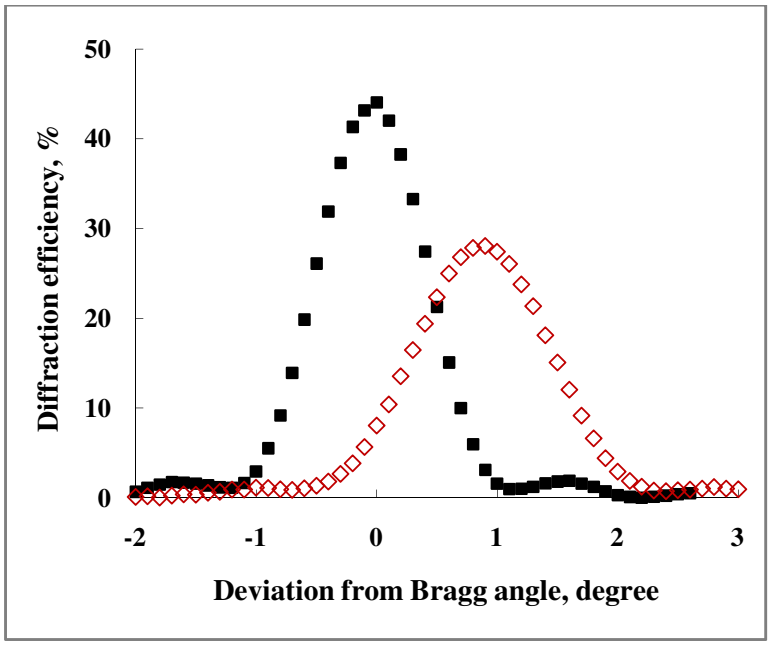

Figure 3.10. Bragg selectivity curve before (■) and after (◊) exposure to RH = 90 % at T = 16 ± 1 °C for 60 min.

By measuring the change in thickness it is possible to predict the change in the fringe spacing and thus calculate the expected Bragg angle shift using Equation (2.2). The experimentally observed shift in Bragg angle is in a good agreement with Bragg angle

shift calculated by Equation (2.2) taking into account the change in thickness of the grating after humidity exposure as discussed above. The experimentally observed shift in Bragg angle confirms that an irreversible change in fringe spacing of the transmission grating occurs which is in line with the observed irreversible layer expansion in the horizontal direction caused by exposure to high humidity. This irreversible expansion is most probably due to stretching of the layer beyond the point of elastic deformation. As the photopolymer is a viscoelastic material, the irreversible layer expansion can be explained by decreasing layer viscosity due to water absorption and, hence, by decreasing its elasticity.

The shift in Bragg angle has been analysed for different exposure times at different temperatures (Figure 3.11).

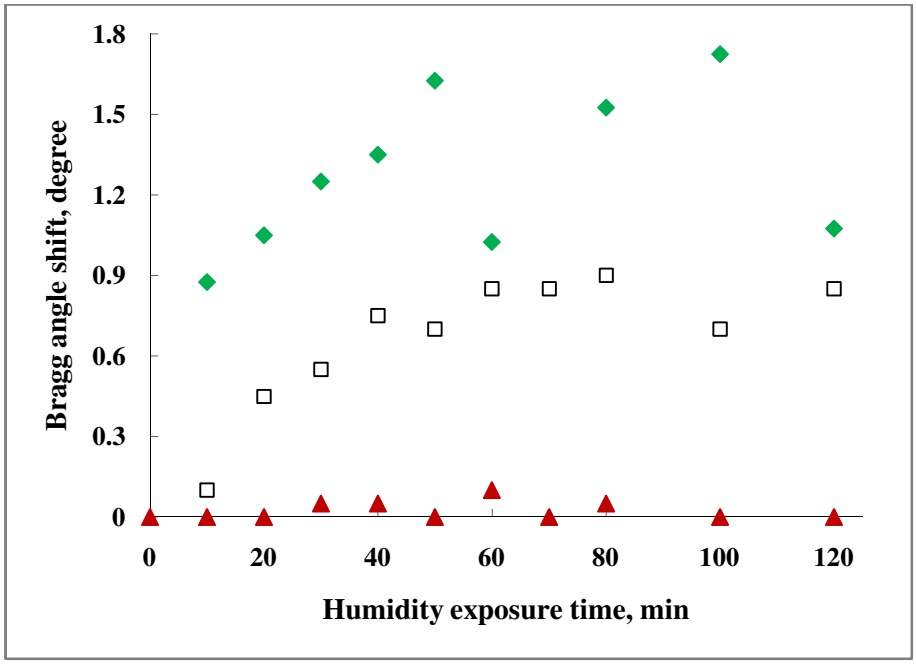

Figure 3.11. Bragg angle shift after exposure to *RH* = 90 % at *T* = 8 ± 1 °C (▲), 16 ± 1 °C (□), 21 ± 1 °C (♦) *versus* humidity exposure time.

It is clearly seen that the magnitude of the Bragg angle shift (Figure 3.11) follows the same trend as the thickness change (Figure 3.8). At $T = 8 \pm 1$ ^{o}C unchanged thickness is accompanied by a zero shift in Bragg angle. At higher temperatures shift in Bragg angle is bigger because of the bigger layer expansion. It is worth emphasising again that the Bragg selectivity curve shift that would be expected due to thickness change is in a good agreement with the measured value. So, for example, after exposure to 90 % *RH* for 100 min, the observed and calculated from the change in layer's dimensions shifts in Bragg angle for the three different temperatures are shown in Table 3.1.

Table 3.1. Comparison of the experimentally measured and calculated from the layer's thickness change Bragg angle shift at different temperatures.

Temperature, ^{o}C	**Measured Bragg angle shift, degree**	**Calculated Bragg angle shift, degree**
8 ± 1	0	0
16 ± 1	0.7	0.7
21 ± 1	1.8	1.5

Calculations have been done assuming that the volume of the layer remains approximately constant. For example, the 7 % drop in thickness observed for the sample exposed at $T = 16$ ^{o}C (Figure 3.8) is estimated to be accompanied by 3.5 % increase in length leading to the spatial period increase from 1 μm to 1.035 μm. Taking into account the spatial period increase, the Bragg angle shift of 0.7^{o} has been calculated using Equation (2.2). Small discrepancy between observed and calculated shift in Bragg angle at 21 ± 1 ^{o}C can be caused by thickness measurement error.

3.4.5.3. Refractive index modulation

Given the significant irreversible diffraction efficiency change that accompanies the above dimensional changes, it is important to understand whether there are other

irreversible changes taking place in the grating in addition to the dimensional deformation of the photopolymer layer. Dimensional changes alone would be unlikely to cause such a significant drop. Such changes could be mass transport between the areas illuminated by dark and bright fringes during the exposure to high humidity. Since the density and the refractive index of the photopolymer is higher in the bright fringe areas, the decrease in the diffraction efficiency due to exposure to high humidity could be caused by effective decrease of the refractive index in the bright areas and/or effective increase of the refractive index in the dark fringe areas. A mass transport from bright to dark fringe areas could be the process causing the changes described above. Another explanation could be the different porosity of the grating's fringes (created during exposure to the bright and dark fringes of the recording interference pattern) and their different ability to retain water.

Using the thickness data and taking into account the shift in Bragg angle, we have estimated the refractive index modulation by Equation (3.1). It has been found that the diffraction efficiency drop cannot be explained only by the thickness change and shift in Bragg angle. A small change in the refractive index modulation has also occurred.

Normalised refractive index modulation, defined as the ratio of refractive index modulation after exposure to humidity followed by drying and refractive index modulation before humidity exposure, is used to analyse the change in refractive index modulation (Figure 3.12). As can be seen from Figure 3.12, there is no change in normalised refractive index modulation caused by exposure to RH = 90 % at $T = 8 \pm 1\ ^{o}C$. This result is in a good agreement with unchanged normalised diffraction efficiency (Figure 3.6). Exposure to high humidity at $T = 16 \pm 1\ ^{o}C$ and $21 \pm 1\ ^{o}C$ leads

to the decrease of refractive index modulation and, consequently, normalised diffraction efficiency is also reduced (Figure 3.6).

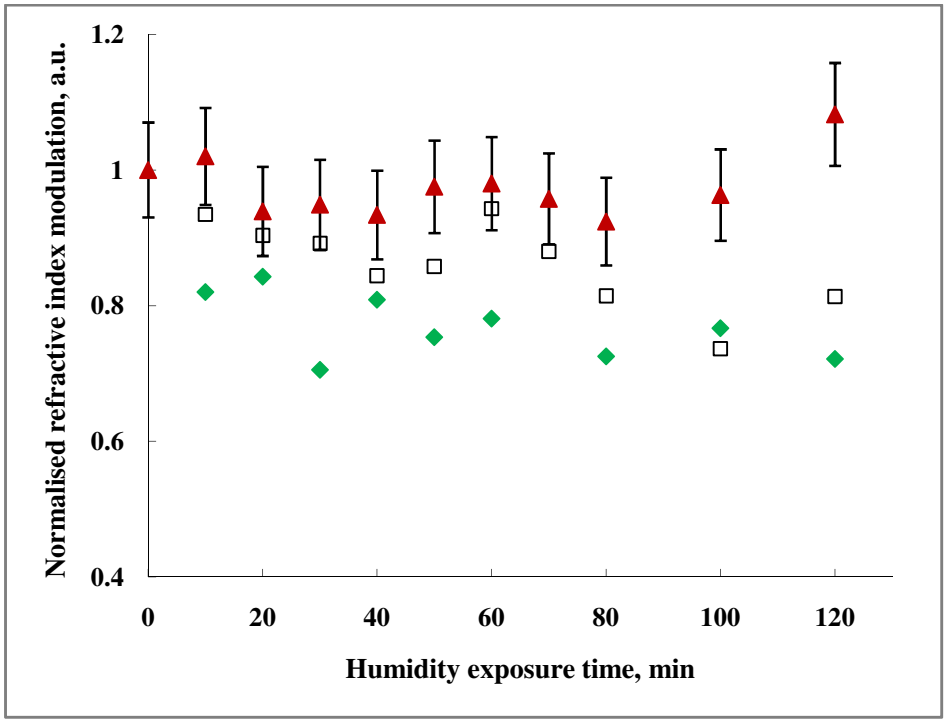

Figure 3.12. Normalised refractive index modulation after exposure to *RH* = 90 % at *T* = 8 ± 1 °C (▲), 16 ± 1 °C (□), 21 ± 1 °C (♦) *versus* humidity exposure time.

3.5. Conclusions

The investigation of the volume transmission grating properties after exposure to high humidity has been carried out. Both the diffraction efficiency and the Bragg angle are observed to change irreversibly at higher temperature, and full reversibility was confirmed for lower temperatures. When gratings were subjected to relative humidity of 80 % and 90 % at a temperature of 8 °C the observed changes were fully reversible. However, irreversible changes in diffraction efficiency, thickness, refractive index

modulation and Bragg angle were observed when the temperature during the humidity exposure was higher than 16 ^{o}C.

The shift in Bragg selectivity curve can be explained by the irreversible dimensional change in layers. Irreversible changes in diffraction efficiency, however, are caused by this change in thickness and a change in the refractive index modulation implying some diffusion processes occur more freely as the layer takes on moisture. The magnitude of the irreversible change highly depends on humidity level, temperature during the humidity exposure and on humidity exposure time.

This sensitivity of transmission gratings, recorded in acrylamide-based photopolymer layers, to high humidity ($RH \geq 80$ %) can be utilised for the development of irreversible humidity holographic sensors, but also can limit the application of this material when non-sensitive to the environment material is needed. The fuller understanding the processes induced by high humidity, knowing limits past which irreversible changes occur and quantification of those changes help in the design of sensors and also in the identification of the acrylamide based photopolymer version which is less sensitive to humidity. Further research in this direction will be discussed in Chapter 4.

References

1. Guntaka, S.R., Toal, V. and Martin, S., *Holographically recorded photopolymer diffractive optical element for holographic and electronic speckle-pattern interferometry.* Applied Optics, 2002. **41**(35): p. 7475-7479.
2. Guo, X., Zhu, J., Xia, C., Li, J. and Chen, L., *Characterization of a real-time high-sensitivity photopolymer for holographic display and holographic interferometry*. SPIE Proceedings, 2005. **5636**: p. 528-537.
3. Zhu, J., Wang, G., Hao, Y., Xie, B. and Cheng, A., *Highly sensitive and spatially resolved polyvinyl alcohol/acrylamide photopolymer for real-time holographic applications.* Optics Express, 2010. **18**(17): p. 18106-18112.
4. Bavigadda, V., Jallapuram, R., Emilia Mihaylova, E. and Toal, V., *Electronic speckle-pattern interferometer using holographic optical elements for vibration measurements.* Optics Letters, 2010. **35**(19): p. 3273-3275.
5. Gallego, S., Márquez, A., Mendez, D. and Belendez, A., *Analysis of PVA/AA based photopolymers at the zero spatial frequency limit using interferometric methods.* Applied Optics, 2008. **47**(14): p. 2557-2563.
6. O'Neill, F.T., Carr, A.J., Daniels, S.M., Gleeson, M.R., Kelly, J.V., Lawrence, J.R. and Sheridan, J.T., *Refractive elements produced in photopolymer layers.* Journal of Materials Science, 2005. **40**(15): p. 4129-4132.
7. Márquez, A., Gallego, S., Ortuño, M., Fernández, E., Álvarez, M. L., Beléndez, A. and Pascual, I., *Generation of diffractive optical elements onto a photopolymer using a liquid crystal display.* SPIE, 2010. http://dx.doi.org/10.1117/12.854786.

8. Akbari, H., Naydenova, I. and Martin, S., *Using acrylamide-based photopolymers for fabrication of holographic optical elements in solar energy applications.* Applied Optics, 2014. **53**(7): p. 1343-1353.

9. Sherif, H., Naydenova, I., Martin, S., McGinn, C. and Toal, V., *Characterization of an acrylamide-based photopolymer for data storage utilizing holographic angular multiplexing.* Journal of Optics A: Pure and Applied Optics, 2005. **7**(5): p. 255-260.

10. Ashley, J., Bernal, M.P, Burr, G.W., Jefferson, C.M., Marcus, B. et al., *Holographic data storage technology.* IBM Journal of Research and Development, 2000. **44**(3): p. 341-368.

11. Yao, H., Huang, M., Chen, Z., Hou, L. and Gan, F., *Optimization of two-monomer-based photopolymer used for holographic recording.* Materials Letters, 2002. **56**(1–2): p. 3-8.

12. Fernández, E., García, C., Pascual, I., Ortuño, M., Gallego, S. and Beléndez, A., *Optimization of a thick polyvinyl alcohol-acrylamide photopolymer for data storage using a combination of angular and peristrophic holographic multiplexing.* Applied Optics, 2006. **45**(29): p. 7661-7666.

13. Gallego, S., Márquez, A., Marini, S., Fernández, E., Ortuño, M., Pascual, I., *In dark analysis of PVA/AA materials at very low spatial frequencies: phase modulation evolution and diffusion estimation.* Optics Express, 2009. **17**(20): p. 18279-18291.

14. Castagna, R., Vita, F., Lucchetta, D.E., Criante, L., Simoni, F., *Superior-performance polymeric composite materials for high-density optical data storage.* Advanced Materials, 2009. **21**(5): p. 589-592.

15. Naydenova, I., Raghavendra, J., Martin, S. and Toal, V., *Holographic humidity sensors*, in: *Humidity Sensors*, C. Okada, (Ed.), Nova Science Publishers 2011.

16. Mihaylova, E., Cody, D., Naydenova, I., Martin, S. and Toal, V., *Research on holographic sensors and novel photopolymers at the Centre for Industrial and Egnineering Optic,* in: *Holography: basic principles and contemporary applications.* E. Mihaylova (Ed.), Intech 2013.

17. Naydenova, I., Raghavendra, J., Toal, V. and Martin, S., *Characterisation of the humidity and temperature responses of a reflection hologram recorded in acrylamide-based photopolymer.* Sensors and Actuators B: Chemical, 2009. **139**(1): p. 35-38.

18. Naydenova, I., Raghavendra, J., Toal, V. and Martin, S., *A visual indication of environmental humidity using a color changing hologram recorded in a self-developing photopolymer.* Applied Physics Letters, 2008. **92**(3): p. 031109.

19. Naydenova, I., Sherif, H., Martin, S., Jallapuram, R., Toal, V., *Holographic sensor*. 2012, Patent US8535853 B2.

20. Leite, E., Babeva, T., Ng, E.P., Toal, V., Mintova, S. and Naydenova, I., *Optical properties of photopolymer layers doped with aluminophosphate nanocrystals.* The Journal of Physical Chemistry C, 2010. **114**(39): p. 16767-16775.

21. Kogelnik, H., *Coupled wave theory for thick hologram gratings.* The Bell System Technical Journal, 1969. **48**(9): p. 2909-2947.

22. Martin, S., Feely, C.A. and Toal, V., *Holographic recording characteristics of an acrylamide-based photopolymer.* Applied Optics, 1997. **36**(23): p. 5757-5768.

23. Martin, S., Leclere, P., Renotte, Y., Toal, V. and Lion, Y., *Characterization of an acrylamide-based dry photopolymer holographic recording material.* Optical Engineering, 1994. **33**(12): p. 3942-3946.

24. Naydenova, I., Jallapuram, R., Howard, R., Martin, S. and Toal, V., *Investigation of the diffusion processes in a self-processing acrylamide-based photopolymer system.* Applied Optics, 2004. **43**(14): p. 2900-2905.

25. *Material Safety Data Sheets - T1377*; Retrieved March 1, 2013, from: http://www.sigma-aldrich.com/.

4. INVESTIGATION OF THE SENSITIVITY TO HUMIDITY OF UNSLANTED TRANSMISSION GRATINGS RECORDED IN AN ACRYLAMIDE-BASED PHOTOPOLYMER CONTAINING *N*-PHENYLGLYCINE AS A PHOTOINITIATOR

4.1. Introduction

In Chapter 3 it has been demonstrated that properties of transmission gratings recorded in an acrylamide-based photopolymer are humidity-sensitive. In analysing this sensitivity to humidity, it is important to distinguish between reversible change, irreversible change and damage. Stable holograms that exhibit repeatable, reversible changes in diffraction efficiency can make useful reversible sensors. Holograms that undergo irreversible change that is repeatable and easy to recognise visually can function as indicators, demonstrating visibly that threshold humidity has been reached. However, deterioration of diffraction efficiency and changes in fringe spacing are unacceptable in many applications such as holographic optical elements [1] and holographic data storage [2, 3]. Also, both surface damage and delamination of the photopolymer layer from the substrate are never desirable. Thus there is a demand for holographic recording materials with little or no sensitivity to humidity.

Attempts have been made to improve the environmental stability of acrylamide-based photopolymer layers, using an aerosol sealant as a protective layer [4]. It was found that the sealant increased the humidity stability of the material. However, this sealant created a layer with increased scattering and produced some deterioration in the optical quality of the resulting holographic optical elements. The use of high optical quality glass cover slide is another sealing approach which can be used to decrease the

humidity sensitivity of holographic devices. But this is not convenient for every application and adds cost and complexity to the production process.

In Chapter 3 it has been established that a photoinitiator such as triethanolamine (TEA) can affect the stability of the recorded photonic structure at temperature around or above the freezing/melting temperature of TEA. It should be noted that TEA is a commonly used photoiniator in acrylamide-based photopolymers [5-8]. The poor stability of acrylamide-based photopolymer films containing TEA at 80 % *RH* and 25 ^{o}C has also been reported in [9]. To decrease the sensitivity to humidity the authors proposed to modify the photopolymer composition by replacing traditionally used electron donor such as TEA with *N*-phenylglycine (NPG). When TEA was substituted by NPG [9], an improved surface quality was reported under humid conditions. It was shown that the NPG photopolymer layer appeared unaffected by its exposure to 80 % *RH* at 25 ^{o}C, while the TEA photopolymer layer was visibly damaged. However, no quantitative investigation of the effect of humidity on the properties of holographic optical elements recorded in the NPG material was carried out at that time.

The aim of this research is to investigate the effect of humidity on the diffraction efficiency of unslanted phase volume transmission gratings recorded in an acrylamide-based photopolymer containing NPG as a photoinitiator (NPG-sample). Experimental data of NPG-samples are compared with the experimental data of an acrylamide-based photopolymer containing photoinitiator of TEA (TEA-sample) so as to quantitatively compare the humidity sensitivity of the two materials. The humidity response of unslanted phase volume transmission gratings recorded in a photopolymer composition containing both initiators is also discussed.

4.2. Experimental

4.2.1. Sample preparation

Two types of acrylamide-based photopolymers containing different photoinitiating systems have been used as a holographic recording material. The first type is a version of the acrylamide-based photopolymer that uses NPG as the electron donor, developed in Shanghai Institute of Optics and Fine Mechanics [9, 10]. In this formulation, NPG and a red-light sensitive dye (methylene blue) is used as a photoinitiating system. The layers prepared with this formulation were reported as having an improved resistance to humidity and so it is of interest as a method of controlling humidity sensitivity. The composition of the material is presented in Table 4.1 (NPG-sample).

Table 4.1. Photopolymer compositions

Chemical reagent	**NPG-sample**	**TEA-sample**
Polyvinyl alcohol (PVA)	9.41 % w/v	7.57 % w/v
Acrylamide (AA)	0.33 M	0.64 M
N,N´- methylene bisacrylamide (BA)	0.03 M	0.054 M
Methylene blue (MB)	2.5×10^{-4}	6×10^{-4} M
Triethanolamine (TEA)	---	0.53 M
N-phenylglycine (NPG)	0.088 M	---

The second type is an acrylamide-based photopolymer composition developed at the Centre for Industrial and Engineering Optics, Dublin Institute of Technology [6, 11, 12]. In this formulation the photoinitiating system is TEA and methylene blue. In present research the standard composition of an acrylamide-based photopolymer containing TEA for recording in transmission mode was modified by increasing the amount of monomers. It was done in order to have the same monomer concentration in both types of dry layers (Figure 4.1). The reason for aiming at the same monomer concentration in both compositions is to assure that at the end of holographic recording

the amount of polyacrylamide is the same in both types of layers. Thus, any variation in their response to humidity cannot be directly attributed to the difference in polyacrylamide content which is known to be a hydroscopic material [13]. The composition of the material is presented in Table 4.1 (TEA-sample). Percentage by mass of the photopolymer components in both types of dry layers is shown in Figure 4.1.

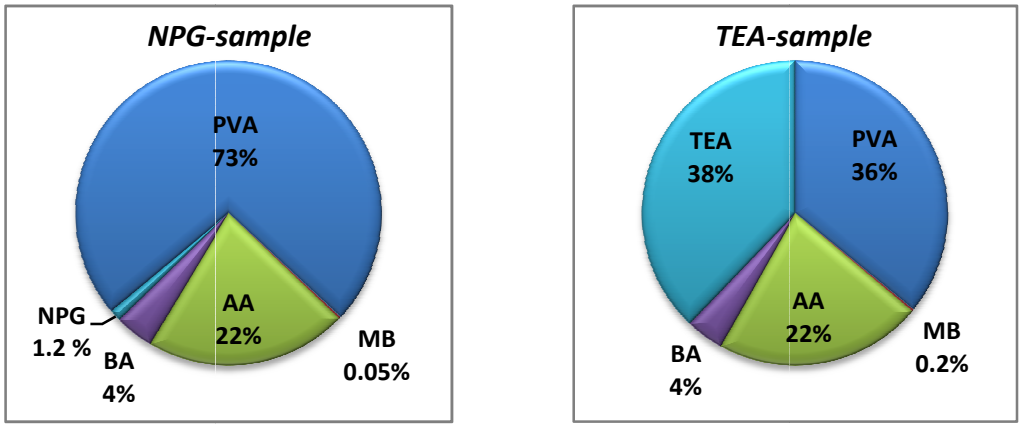

Figure 4.1. Percentage by mass of the photopolymer components in dry layers.

The 20 % w/v polyvinyl alcohol stock solution was prepared by adding 20 grams of polyvinyl alcohol into 100 ml of deionised water. The solution was slowly heated up to T = 80 ^{o}C and stirred by using a magnetic stirrer. The 0.11 % w/v dye solution was prepared as described in Chapter 3, section 3.3.1. To make the photopolymer stock solution, the components shown in Table 4.1 were mixed using a magnetic stirrer in a dark room. The layers were prepared by casting the photopolymer solution over the levelled glass slide (26 × 76 mm^2) and dried for 24 hours in a dark room at T = 21 ± 2 ^{o}C and RH = 35 ± 5 %. The amount of deposited photopolymer solutions containing NPG and TEA was 0.8 ml and 0.3 ml, respectively. The thickness of the layers was in the range of 50 - 60 μm.

The recordings of unslanted transmission volume phase gratings were carried out by using a setup presented in Figure 3.1 (Chapter 3, section 3.3.2). Transmission gratings with a spatial frequency of 1000 ± 27 lines/mm and diffraction efficiency of 35 – 40 % were recorded. The total recording intensity was 5 mW/cm^2 and the recording times for TEA-sample and NPG-sample were 10 sec and 25 sec, respectively. These conditions were chosen in order to achieve similar starting diffraction efficiency in the two types of the layers.

4.2.2. Characterisation of holographic diffraction gratings

Each holographic diffraction grating was characterised by measuring its diffraction efficiency at different incident angles. The Bragg selectivity curve was then recorded by a computer controlled system presented in Figure 3.2 (Chapter 3, section 3.3.3). An unexpanded 532 nm beam from Nd:YVO_4 laser was employed as a probe beam during the Bragg curve measurements in this study. This wavelength was chosen in order to avoid undesired absorption by samples that were still photosensitive to red wavelength (prior to UV-postexposure). Depending on the goal of the experiment, the Bragg curve measurements were carried out before and after UV-postexposure and/or before and after exposure to humidity followed by drying.

In order to investigate the effect of UV-postexposure on diffraction efficiency of samples and their humidity sensitivity, the samples were exposed to UV-light with the intensity of 2.5 mW/cm^2 for different amounts of time using a UV Exposure unit (Mega Electronics model LV 202-E). To investigate the effect of humidity on diffraction efficiency of gratings, different environmental conditions were obtained by a controlled environment chamber with humidity and temperature control system (Electro-tech system, model 5503-11) described in Chapter 3, section 3.3.4. The experimental set-up

for the testing the humidity response of transmission gratings is presented in Figure 3.3. After exposure to high humidity the samples were dried for 24 hours at $T = 18 \pm 2$ ^{o}C and $RH = 35 \pm 5$ %. Then Bragg selectivity curve measurements were carried out again.

4.3. Results and Discussion

4.3.1. Dependence of diffraction efficiency on relative humidity levels

The effect of humidity on the properties of gratings was investigated by exposing the gratings to a range of humidity levels at constant temperature ($T = 21 \pm 1$ ^{o}C). This temperature had been chosen because, as discussed in Chapter 3, section 3.4.2-3.4.4, a significant irreversible decrease of the diffraction efficiency was observed at $T = 21 \pm 1$ ^{o}C and $RH = 90$ % in TEA-samples.

In order to characterise and compare the diffraction efficiency changes for different samples under humidity exposure, normalised diffraction efficiency was calculated. For every level of relative humidity at which a diffraction efficiency measurement was carried out, the sample was remained at that level for 30 min in order to allow it to equilibrate with the environment. Both the first-order diffracted beam intensity and the transmitted beam intensity were monitored. In order to account for scattering losses due to condensation of moisture on the photopolymer surface, in this experiment the diffraction efficiency was calculated as the ratio of the first-order diffracted beam intensity and the sum of the first-order diffracted beam and transmitted beam intensities. Then the normalised diffraction efficiency was defined as the ratio of diffraction efficiency at given humidity level and the diffraction efficiency measured at the start of the experiment at 20 % *RH*.

Figure 4.2 shows the normalised diffraction efficiency of TEA-sample and NPG-sample *versus* relative humidity.

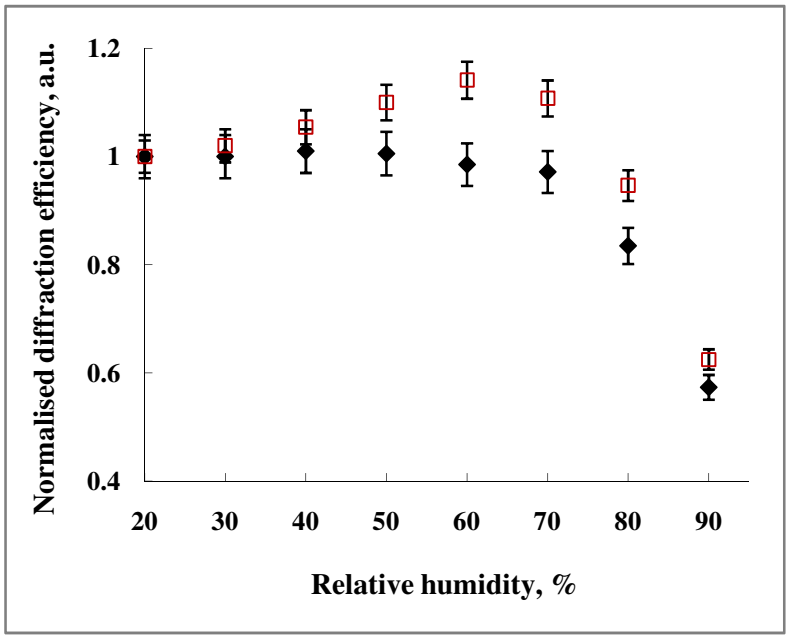

Figure 4.2. Normalised diffraction efficiency *versus* relative humidity: (♦) - NPG-sample and (□) - TEA-sample.

As can be seen from Figure 4.2, in the range of *RH* = 20 - 70 % the normalised diffraction efficiency of NPG-sample is constant, whereas the normalised diffraction efficiency of TEA-sample slightly increases. As discussed in Chapter 3, section 3.4.1, this increase can be explained by swelling of the TEA-layer in direction perpendicular to the glass slide due to water absorption. It results in the increase of thickness and, hence, the normalised diffraction efficiency increases. Since the normalised diffraction efficiency of NPG-sample remains constant, the NPG-layer absorption of moisture from the environment is either very limited and/or it doesn't cause a detectable swelling, thus, these layers are non-sensitive to humidity changes in this relative humidity range.

Different behaviour of normalised diffraction efficiency of TEA-sample and NPG-sample in the range of *RH* = 20 - 70 % can be explained in terms of different ability of these materials to absorb moisture from the environment because of their

different compositions. As can be seen from Figure 4.1, NPG-sample mainly contains polyvinyl alcohol and acrylamide which are solid materials [14, 15] whereas TEA-sample in addition to polyvinyl alcohol and acrylamide contains a significant amount of triethanolamine which is a viscous liquid [16]. Triethanolamine due to its liquid nature makes the layer less dense. The density of the layers was calculated using the mass of the deposited amount of solution and the thickness of the layer. It was found that the density of the TEA-sample and the NPG-sample is approximately 1.04 g/cm^3 and 1.75 g/cm^3, respectively. Thus, the photopolymer layer containing NPG is the denser and less porous material than the photopolymer layer containing TEA. The permeability of NPG-sample is also lower than that of TEA-sample.

At $RH > 70$ % the normalised diffraction efficiency of NPG-sample and TEA-sample drops. As shown in Chapter 3, section 3.4.2, the decrease of normalised diffraction efficiency of TEA-sample is irreversible. The change in normalised diffraction efficiency of NPG-sample at high humidity, however, was found to be completely reversible and was studied further in greater detail.

4.3.2. Diffraction efficiency dependence on the duration of humidity exposure to RH = 90 %

To investigate the effect of humidity exposure time, changes in normalised diffraction efficiency caused by exposure to $RH = 90$ % at $T = 21 \pm 1$ ^{o}C for a set of exposure times have been analysed. In this experiment the diffraction efficiency was initially measured at $RH = 30$ %, then the samples were exposed to $RH = 90$ % for different amounts of time. After exposure to high humidity the samples were left for 24 hours at $RH = 30$ % and the diffraction efficiency was measured again at $RH = 30$ %. The normalised diffraction efficiency was calculated as the ratio of the diffraction efficiency after and

before exposure to high humidity. Figure 4.3 shows the normalised diffraction efficiency of NPG-sample and TEA-sample for different humidity exposure times.

It can be observed from Figure 4.3 that normalised diffraction efficiency of NPG-sample does not decrease after exposure to *RH* = 90 % for 30 min. Therefore, the decrease of normalised diffraction efficiency of NPG-sample observed during the humidity exposure at *RH* = 80 - 90 % for 30 min (Figure 4.2) is reversible. The original diffraction efficiency of NPG-sample is fully recovered after exposure to *RH* = 90 % for 30 min. It can also be observed that the diffraction efficiency of NPG-sample does not decrease after 60 minutes exposure to *RH* = 90 %. For longer humidity exposure times the fall off in diffraction efficiency is much smaller for NPG-samples than for TEA-samples, confirming a significant resistance to grating deterioration in very high relative humidity.

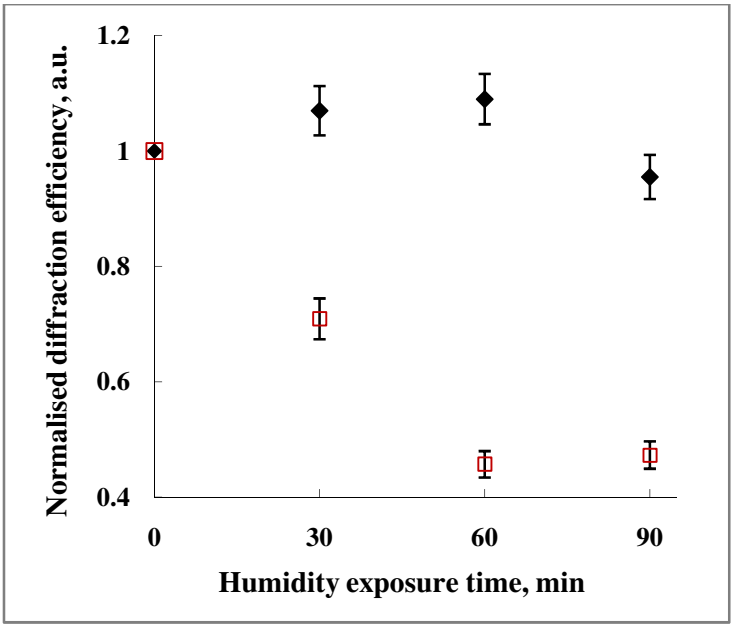

Figure 4.3. Normalised diffraction efficiency *versus* humidity exposure time: (♦) – NPG-sample and (□) - TEA-sample.

4.3.3. Effect of exposure to UV-light on the diffraction efficiency

To better understand the processes behind the observed different dynamics of the diffraction efficiency of NPG-sample and TEA-sample under exposure to humidity, the effect of UV-postexposure on TEA-sample and NPG-sample was analysed. For this purpose, after the recordings TEA-samples and NPG-samples were exposed to UV-light for a set period of time. This is normally carried out in order to remove any residual sensitivity of the layers to light. In TEA-samples TEA plays the role of both photoinitiator and plasticiser. The light absorbing dye is highly mobile over the short fringe distances (in order of 1 μm) and bleaching with UV-light has a uniform effect on bright and dark fringes. For longer exposures this means that the diffraction efficiency remains stable under UV-exposure. However, some increase of diffraction efficiency is observed for partially polymerised TEA-layers (gratings recorded during short exposure times).

The dependence of normalised diffraction efficiency on UV-postexposure time is presented in Figure 4.4 for both formulations. In this experiment the normalised diffraction efficiency has been defined as the ratio of diffraction efficiency measured after certain UV-postexposure time and the diffraction efficiency measured before UV-postexposure.

As can be seen from Figure 4.4, UV-postexposure for 30 min causes increase of normalised diffraction efficiency of TEA-sample by 60 %, whereas the normalised diffraction efficiency of NPG-sample is decreased by 60 %. The normalised diffraction efficiency of TEA-sample reaches saturation after 15 min UV-postexposure, while the normalised diffraction efficiency of NPG-sample still decreases after 15 min.

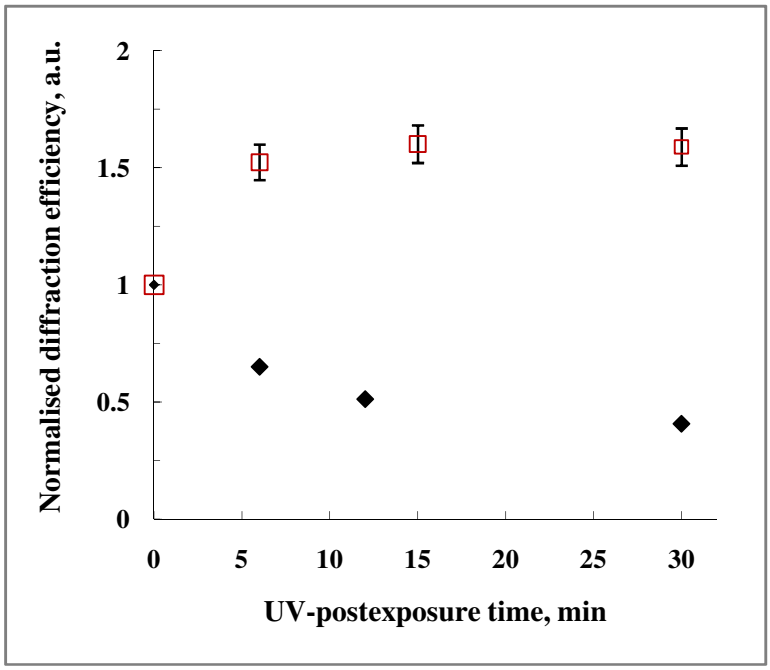

Figure 4.4. Normalised diffraction efficiency *versus* UV-postexposure time: (♦) - NPG-sample and (□) - TEA-sample.

The different dynamics of normalised diffraction efficiency of NPG-sample and TEA-sample under UV-postexposure can be explained in terms of monomer diffusion rates inside these materials. It has been observed previously that TEA affects the diffusion rates of the photopolymer components [17]. Since TEA plays the role of a plastisizer, it increases the diffusion rates. During holographic recording the monomers diffuse from dark to bright fringes where they are polymerised. Under UV-light exposure, which is uniform and has no fringe pattern, all remaining monomers are polymerised, including those remaining in the dark fringe regions. The increase of the diffraction efficiency in the case of TEA-sample implies that the refractive index modulation increases under UV-postexposure. However, UV-light exposure causes an overall deacrease in the diffraction efficiency of NPG-sample. This could be attributed to the very slow monomer diffusion rate in the NPG-sample The restricted diffusion during the recording process may lead to the gratings having the opposite refractive

index distribution to the one in the TEA-sample, causing UV polymerisation to have the opposite effect on the diffraction efficiency. This is further discussed in section 4.3.5 where two scenarios assuming fast and slow monomer diffusion are considered for the explanation of both UV-postexposure results and the influence of high humidity on the diffraction efficiency of TEA-sample and NPG-sample, respectively.

4.3.4. Humidity sensitivity of UV-stabilised samples

The humidity sensitivity of NPG-samples after UV-postexposure for 30 min has been further investigated. Changes in normalised diffraction efficiency caused by exposure to RH = 90 % at T = 21 ± 1 ^{o}C for a set period of time have been analysed. In this experiment the normalised diffraction efficiency was defined as described in section 4.3.2. Figure 4.5 shows the normalised diffraction efficiency of samples with UV-postexposure for different humidity exposure times.

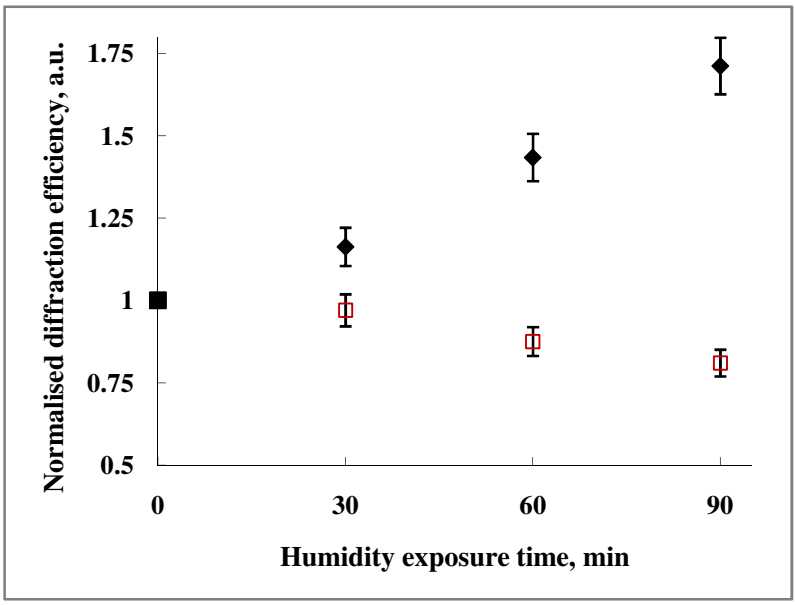

Figure 4.5. Normalised diffraction efficiency of samples with UV-postexposure *versus* humidity exposure time: (♦) - NPG-sample and (□) - TEA-sample.

As shown in Figure 4.5, the effect of duration of humidity exposure on normalised diffraction efficiency of NPG-samples and TEA-samples is significantly different. There is a 20 % decrease of normalised diffraction efficiency of TEA-sample due to exposure to RH = 90 % for 90 min. In the case of NPG-sample the normalised diffraction efficiency significantly increases with the exposure time. Thus, exposure to RH = 90 % leads to close to linear increase of the normalised diffraction efficiency reaching 70 % for 90 min exposure. To check if the increase is irreversible the diffraction efficiency measurements have been carried out again 4 days after exposure to high humidity and it was observed that this increase of diffraction efficiency was permanent. Following section presents possible explanation for humidity induced changes in the diffraction efficiency of TEA-sample and NPG-sample based on the mechanism of obtaining refractive index modulation in photopolymers.

4.3.5. Mechanism of obtaining refractive index modulation in photopolymers

According to the coupled wave theory [18], the diffraction efficiency of a volume phase holographic grating depends on the refractive index modulation of the medium where this holographic grating was recorded. The formation of the refractive index change in the photopolymer containing TEA as a photoinitiator has been investigated previously [19, 20]. Based on a model published in [21] it has been proposed that changes in density and molar refraction are the main contributors to the refractive index change created during holographic recording. Exposure to light induces the polymerisation process in the bright regions, and the polymer regions with higher density are formed. The dark regions contain monomers and have lower density. Thus, we have a periodic structure of bright and dark regions with different density. At the same time, these regions have different molar refraction. On polymerisation in each monomer unit a

carbon-carbon double bond having higher molar refraction is replaced by two carbon-carbon single bonds having lower molar refraction. The periodic conversion of double to single bonds also causes refractive index modulation which is shifted with respect to the modulation due to density variation by 180 degrees (Figure 4.6).

Figure 4.6 shows the two processes contributing to the final refractive index modulation – change in molecular refraction and change in density. Figure 4.6a presents the two processes and the resulting refractive index modulation in the TEA-sample. It is assumed that the recording is carried out in a regime when most of the monomer molecules manage to move from dark to bright fringe regions (fast diffusion regime). In the fast diffusion regime, mass transport of material from dark to bright fringe areas is the main contributor to the refractive index change [19, 20, 22]. During the holographic recording, a periodic structure of bright and dark regions with different density and molar refraction is created. The periodic variation of density is shifted by 180 degrees in respect of the periodic variation of molar refraction. The density changes outweigh the changes in molar refraction and the bright fringe areas have higher refractive index. This is supported by the experimental data on the effect of UV-light on the diffraction efficiency (Figure 4.4).

As can be seen from Figure 4.4, exposure to UV-light after holographic recording causes increase of the diffraction efficiency of TEA-sample. The diffraction efficiency increase can be explained by overall increase of the refractive index modulation due to “erasing” bond conversion variation.

Figure 4.6b shows the mechanism of obtaining refractive index modulation in NPG-sample. It is assumed that the monomer molecules diffuse slowly and only a small fraction of them reach the bright fringe area (slow diffusion regime).

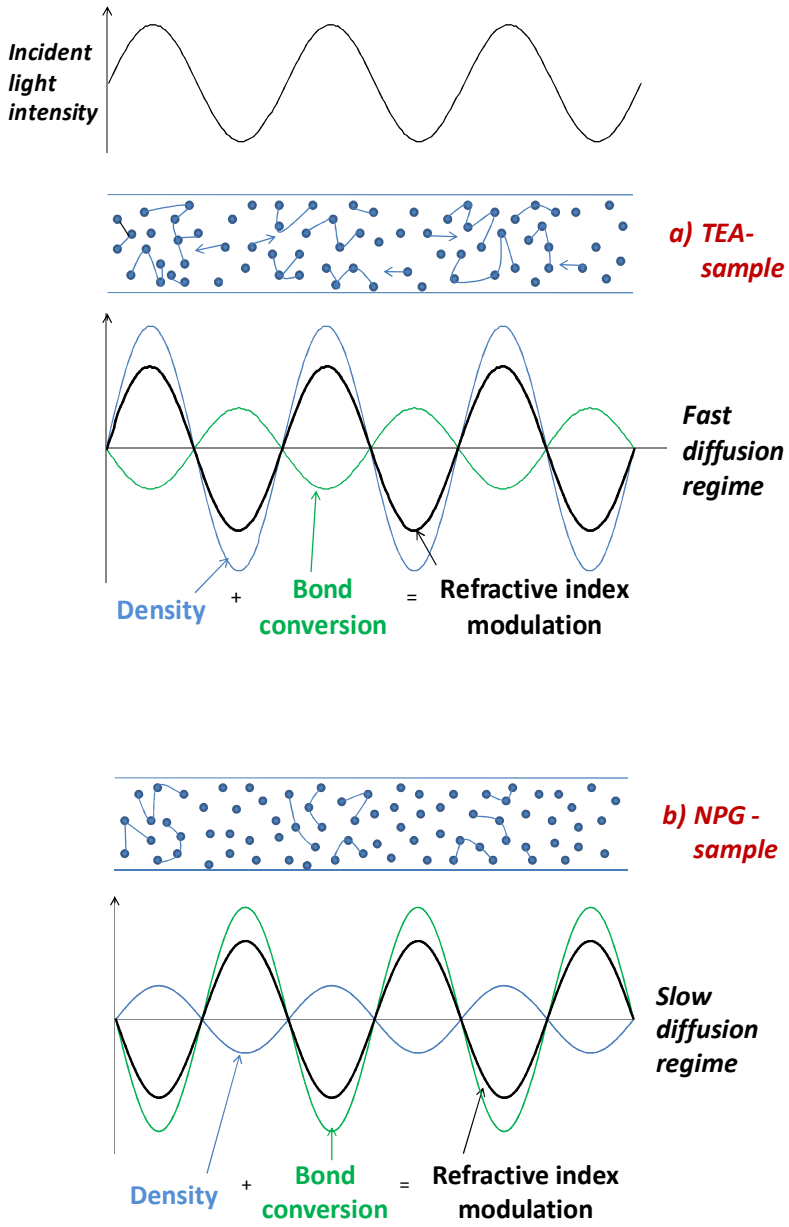

Figure 4.6. Mechanism of obtaining refractive index modulation in a) TEA-sample and b) NPG-sample.

Based on the experimental results discussed in section 4.3.2 - 4.3.4, it can be supposed that in the case of NPG-sample (slow diffusion regime), structural changes in the monomer molecule play a major role in the formation of refractive index modulation. Changes in molecular refraction outweigh the density changes and, thus, bright fringe areas have lower refractive index in NPG-sample. Exposure to UV-light

after holographic recording causes changes in the refractive index modulation due to bond conversion and, thus, leads to the decrease of the refractive index modulation in NPG-sample. Exposure to high humidity which allows the polymer chains to move from bright to dark fringe areas can then lead to a decrease in the refractive index in the bright fringe areas and, hence, decrease in diffraction efficiency of TEA-sample. In case of NPG-sample, exposure to high humidity leads to increase in refractive index in dark fringe areas and increase in diffraction efficiency (as observed in Figure 4.5).

4.3.6. Influence of triethanolamine on humidity sensitivity of photopolymer layers

To investigate the effect of TEA on humidity sensitivity of the layers, normalised diffraction efficiency of NPG-samples and TEA-samples with different content of TEA was analysed. In this experiment, two additional types of samples were prepared. The first type was an NPG-sample in which the content of TEA in the dry layer was 9 wt %. It was made by adding one-tenth of the proposed in [6] amount of TEA to the NPG-sample stock solution. The second type of the layer was the TEA-sample containing the half of the amount of TEA proposed in [6]. So, the content of TEA in this TEA-sample was 23 wt %. After the recording, all samples were exposed to UV-light for 30 min and placed into the humidity chamber at RH = 90 % for 60 min. Normalised diffraction efficiency calculated as in section 4.3.2 *versus* content of TEA is shown in Figure 4.7. As seen from Figure 4.7, the normalised diffraction efficiency of NPG-sample containing 9 wt % of TEA is significantly less than the normalised diffraction efficiency of the pure NPG-sample. The increase in normalised diffraction efficiency caused by humidity exposure is only few percent, while in the pure NPG-sample the increase is above 40 %. The normalised diffraction efficiency of TEA-samples with 23 wt % and 38 wt % of TEA is very similar. These results reveal that changes in diffraction

efficiency caused by exposure to high humidity depend on the content of TEA in photopolymer layers. The higher the content of TEA, the lower the normalised diffraction efficiency and the higher the humidity sensitivity of photopolymer layers. Thereby, it is possible to alter the humidity sensitivity of the photopolymer varying the content of TEA.

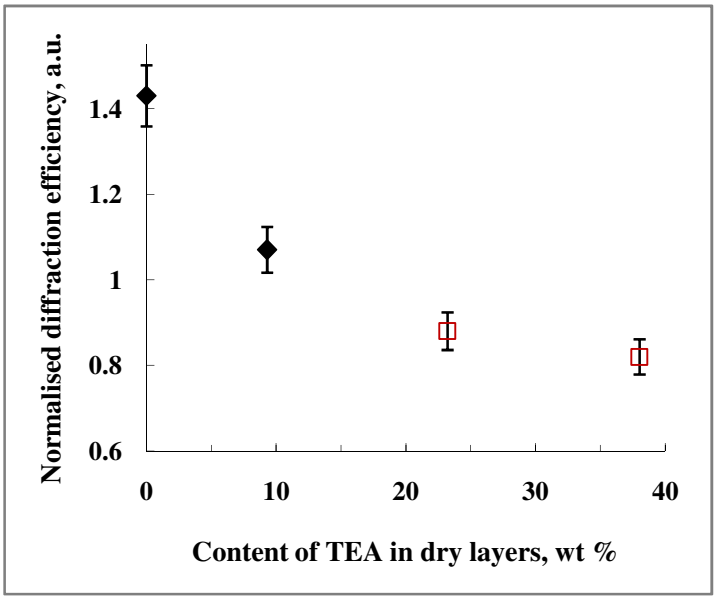

Figure 4.7. Normalised diffraction efficiency *versus* content of TEA in the dry layers: (♦) – NPG-samples and (□) – TEA-samples.

4.4. Conclusions

The investigation of the humidity sensitivity of the acrylamide-based photopolymer containing NPG as a photoinitiator has been carried out in a wide range of relative humidity *RH* = 20 – 90 %. In the relative humidity range *RH* = 20 – 70 % NPG-sample is not sensitive to humidity change and the normalised diffraction efficiency of NPG-samples is found to be constant. In the range *RH* = 80 – 90 % the normalised diffraction efficiency of NPG-sample decreases. It has been found that the normalised diffraction

efficiency of NPG-samples is recovered after exposure to 90 % *RH* for 30 min. Thus, the decrease of normalised diffraction efficiency observed at *RH* = 80 – 90 % is fully reversible. The low humidity sensitivity of the acrylamide-based photopolymer containing NPG is encouraging for applications where non-sensitive to humidity material is needed. The main disadvantage of the acrylamide-based photopolymer containing NPG is its lower exposure sensitivity as the material has lower permeability and slower diffusion rate of monomers in comparison to the acrylamide-based photopolymer containing TEA.

Based on the influence of UV-postexposure and exposure to 90 % *RH* on diffraction efficiency of gratings recorded in TEA-samples and NPG-samples the following model for the refractive index modulation can be proposed. The TEA-sample records the pattern in a regime of fast monomer diffusion, the main contributor to the refractive index modulation is the density change, and the refractive index modulation has its maxima in the bright fringe regions. The NPG-sample records in a regime of slow monomer diffusion, the main contributor to the refractive index modulation is the change in molar refraction, and the refractive index modulation has its maxima in the dark regions. Also, it has been shown that it is possible to alter the humidity sensitivity of the photopolymer by variation of the content of TEA. The obtained results are summarised in Table 4.2

Table 4.2. Characteristics of NPG-sample and TEA-sample.

	Characteristics of the material	**NPG-sample**	**TEA-sample**
Holographic performance	*Exposure sensitivity, cm^2/mJ*	0.0047	0.012
	Diffusion regime	Slow monomer diffusion	Fast monomer diffusion
	Main contributor to the refractive index modulation	Molar refraction	Density change
Sensitivity to humidity	*Relative humidity range*	*RH* > 70 %	*RH* = 20 – 90 %
	Reversibility after exposure to 90 % RH	yes	no
Effect of UV-postexposure	*Diffraction efficiency under UV-curing*	decreases	increases
	Diffraction efficiency after exposure to 90 % RH	increases	decreases

References

1. Kowalski, B.A. and McLeod, R.R., *Design concepts for diffusive holographic photopolymers.* Journal of Polymer Science Part B: Polymer Physics, 2016. **54**(11): p. 1021-1035.
2. Dhar, L., Curtis, K. and Facke, T., *Holographic data storage: Coming of age.* Nature Photonics, 2008. **2**(7): p. 403-405.
3. Hsieh, M.-L. and Hsu, K.Y., *Grating detuning effect on holographic memory in photopolymers.* Optical Engineering, 2001. **40**(10): p. 2125-2133.
4. Neill, F.T.O., Lawrence, J.R. and Sheridan, J.T., *Improvement of holographic recording material using aerosol sealant.* Journal of Optics A: Pure and Applied Optics, 2001. **3**(1): p. 20-25.
5. Boiko, Y.B., Solovjev, V.S., Calixto, S. and Lougnot D.J., *Dry photopolymer films for computer-generated infrared radiation focusing elements.* Applied Optics, 1994. **33**(5): p. 787-793.
6. Martin, S., Leclere, P., Renotte, Y., Toal, V. and Lion, Y., *Characterization of an acrylamide-based dry photopolymer holographic recording material.* Optical Engineering, 1994. **33**(12): p. 3942-3946.
7. Blaya, S., Carretero, L., Madrigal, R.F. and Fimia, A., *Optimization of a photopolymerizable holographic recording material based on polyvinylalcohol using angular responses.* Optical Materials, 2003. **23**(3–4): p. 529-538.
8. Hai, L., Ruo-Ping, L., Cai-Xia, S. and Yong, X., *Holographic property of photopolymers with different amine photoinitiators.* Chinese Physics B, 2010. **19**(2): p. 024212.

9. Gong, Q., Wang, S., Huang, M. and Gan, F., *A humidity-resistant highly sensitive holographic photopolymerizable dry film.* Materials Letters, 2005. **59**(23): p. 2969-2972.

10. Gong, Q., Sulian, W., Mingju, H., Yong, D. and Fuxi, G., *Effects of dyes and initiators on the holographic data storage properties of photopolymer*. SPIE Procedings, 2005. **5966**: p. 59660P.

11. Martin, S., Feely, C.A. and Toal, V., *Holographic recording characteristics of an acrylamide-based photopolymer.* Applied Optics, 1997. **36**(23): p. 5757-5768.

12. Naydenova, I., Jallapuram, R., Howard, R., Martin, S. and Toal, V., *Investigation of the diffusion processes in a self-processing acrylamide-based photopolymer system.* Applied Optics, 2004. **43**(14): p. 2900-2905.

13. Ahmed, E.M., *Hydrogel: Preparation, characterization, and applications: A review*. Journal of Advanced Research, 2015. **6**(2): p. 105-121.

14. *Material Safety Data Sheet - 341584*. Retrived January 20, 2014, from: http://www.sigmaaldrich.com/.

15. *Material Safety Data Sheet - A3553*. Retrived January 20, 2014, from: http://www.sigmaaldrich.com/.

16. *Material Safety Data Sheet-T58300*. Retrived January 20, 2014, from: http://www.sigmaaldrich.com/.

17. Feely, C., *The development and characterization of a red-sensitized photopolymer holographic recording material,* (Doctoral Thesis) 1998, Dublin Institute of Technology.

18. Kogelnik, H., *Coupled wave theory for thick hologram gratings.* The Bell System Technical Journal, 1969. **48**(9): p. 2909-2947.

19. Martin, S., *A new photopolymer recording material for holographic applications: photochemical and holographic studies towards an optimized system* (Doctoral Thesis) 1995, Dublin Institute of Technology.

20. Martin, S., Naydenova, I., Jallapuram, R., Howard, R. and Toal, V. *Two way diffusion model for the recording mechanism in a self developing dry acrylamide photopolymer*, SPIE Procedings, 2006. **6252**: p. 625205

21. Tomlinson, W. and Chandross, E., *Organic photochemical refractive index image recording systems*, in: *Advanced Photochemistry*, T.N. Pitts, et al., (Eds.), John Wiley Interscience p. 201-280, 1980.

22. Babeva, T., Naydenova, I., Mackey, D., Martin, S. and Toal, V., *Two-way diffusion model for short-exposure holographic grating formation in acrylamide-based photopolymer.* Journal of the Optical Society of America B, 2010. **27**(2): p. 197-203.

5. HUMIDITY AND TEMPERATURE INDUCED CHANGES IN PROPERTIES OF SLANTED PHOTOPOLYMER-BASED HOLOGRAPHIC GRATINGS

5.1. Introduction

The intrinsic properties of some photopolymers, such as their hygroscopic nature and thermal expansion, are beneficial for the development of humidity and temperature photopolymer-based holographic sensors. As discussed in Chapter 3, the hygroscopic nature of the acrylamide-based photopolymer can be used for the development of irreversible humidity sensors based on unslanted transmission gratings. Humidity-induced changes in the properties of unslanted transmission gratings are found to be dependent on the environmental temperature. In Chapter 4 it has been shown that humidity sensitivity of unslanted transmission gratings holographically recorded in acrylamide-based photopolymers can be adjusted by changing the photoinitiating system in the photopolymer composition.

In this chapter slanted gratings recorded in photopolymer materials are the focus of the research. In slanted gratings any dimensional changes of the material in direction perpendicular to the grating surface, such as shrinkage or swelling, lead to the Bragg angle shift due to changes in the tilt angle of the grating fringes (Figure 5.1). Figure 5.1 shows the schematic diagram of diffraction in a grating with slanted fringes. Before exposure to an analyte, the grating has a thickness d_1 and the grating planes are tilted with the angle ψ_1. The maximum diffraction efficiency is observed at angle θ_1'. If the interaction with the analyte causes shrinkage of the holographic recording material, both the thickness decrease (d_2) and the increase of the tilt angle (ψ_2) are induced. Dimensional changes of the grating cause alteration of the Bragg angle. The maximum

diffraction efficiency is now observed at angle θ_2'. Such behaviour of the slanted grating will be discussed in more details in section 5.4.4.

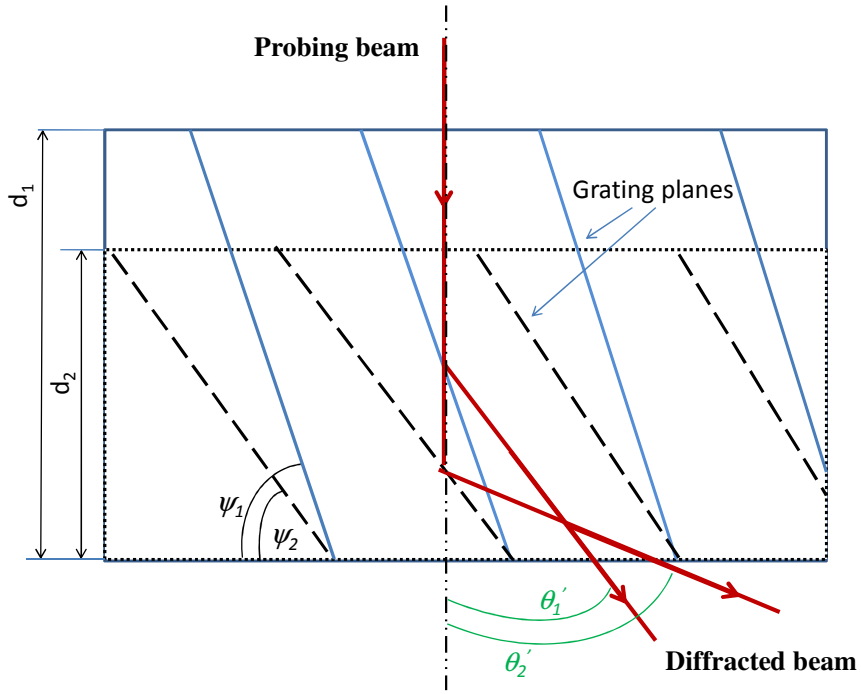

Figure 5.1. Schematic diagram showing the change in diffraction in a grating with slanted fringes as the layer shrinks.

Figure 5.2 shows the example of Bragg selectivity curves measured before and after exposure to an analyte. A sensor based on a slanted grating can operate in the following ways. Firstly, the diffraction efficiency can be monitored at Bragg incidence. This can be done by adjusting the angle of probing beam before and after exposure until the diffraction efficiency is maximised. The response of the sensor can be evaluated as the diffraction efficiency change ($\Delta\eta_2$). Secondly, the diffraction efficiency can be measured at a constant angle of the probing beam. This method provides higher sensitivity of the sensor as the shift in Bragg selectivity curve causes a bigger change in the measured diffraction efficiency ($\Delta\eta_1$) at that specific angle (Figure 5.2). The third way is to monitor the actual angular shift in the Bragg angle by Bragg selectivity curve

measurements. Thus in the case of a holographic sensor based on a transmission grating with slanted fringes, both the diffraction efficiency change and the shift in the Bragg angle can be used as a signal.

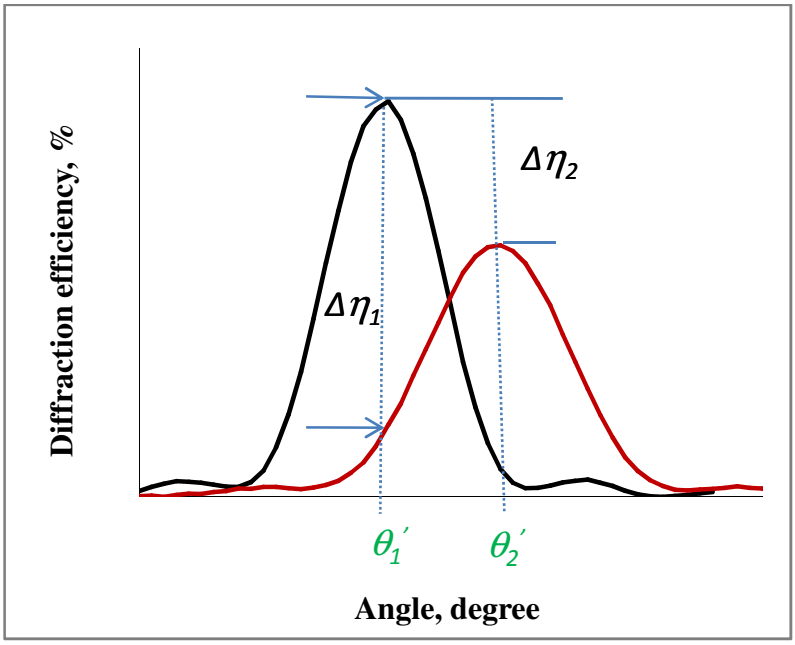

Figure 5.2. Changes in Bragg selectivity curve of the slanted grating due to shrinkage caused by exposure to an analyte.

In the present chapter the humidity and temperature response of volume phase slanted gratings recorded in photopolymers with varied chemical composition is investigated. A series of experiments has been carried out in order to characterise the humidity and temperature response of photopolymer-based gratings. The first set of experiments tests the humidity induced changes in photopolymer-based gratings at different levels of relative humidity and constant temperature. The capability to tune the response of a holographic grating to relative humidity by compositional changes in the photopolymer layer has been further explored. Previously (Chapter 4), the effect of alternate electron donors in reducing the humidity sensitivity was explored. Here, the capability to increase the response of a holographic grating to relative humidity by using

alternate monomer/polymer systems in the photopolymer layer has been investigated. The approach is based on replacing acrylamide (AA) with diacetone acrylamide (DA). The two monomers were chosen because it was previously observed that gratings recorded in photopolymer layers containing AA and DA have very different holographic and mechanical properties [1] which can influence on humidity and temperature sensitivity of the material. DA-based photopolymer composition used in the present research is a new non-toxic and environmentally-compatible photopolymer material developed at the Centre for Industrial and Engineering Optics, Dublin Institute of Technology [2-4]. In this photopolymer formulation low-toxic diacetone acrylamide is used as the main monomer. This composition is capable of holographic recording at a spatial frequency ranging from 100 to 5600 lines/mm and achieves diffraction efficiency and refractive index modulation comparable to AA-based photopolymer composition [1]. This composition is a good alternative to AA-based photopolymers for many holographic applications including holographic sensors. Holographic pressure sensor based on a reflection grating recorded in the DA-based photopolymer has been recently demonstrated [5]. Reversible changes in the spatial period under applied pressure are explained by means of high elasticity of the DA-based photopolymer layer.

The aim of the first set of experiments is to study the humidity sensitivity of volume phase slanted gratings recorded in a photopolymer containing DA as the main monomer and TEA as a photoinitiator. Comparative analysis of the humidity response of DA-based gratings and AA-based gratings has been carried out. Application of the DA-based photopolymer as a humidity-responsive material for the development of holographic humidity sensors is also discussed.

The second set of experiments examines the response of photopolymer-based grating to temperature variations at constant relative humidity. Photopolymers used as

holographic recording materials in general have a low glass transition temperature ($Tg < 80\ ^{o}C$) and a relatively large coefficient of thermal expansion (~100 ppm/^{o}C) [6–8]. Temperature variation induces grating detuning effects *via* changes in refractive index and the physical dimensions of the photopolymer layers [7, 8]. Photopolymers that exhibit this mechanical response to temperature change are required for holographic temperature sensor development. Volume changes with temperature may be implemented as a sensing mechanism in holographic temperature sensors. However, previous explorations of the temperature response of AA-based photopolymers are limited. The investigation of the reflection grating response to temperature in the range of 15 - 60 ^{o}C revealed that although there is a temperature response it depends highly on the relative humidity level [9].

The temperature response of volume phase slanted gratings recorded in photopolymers containing two types of monomers (AA and DA) and two types of initiators (TEA and NPG) is explored here. The two monomers were chosen for the reasons discussed above. The two initiators were chosen because as shown in Chapter 4, section 4.3.1 photopolymer layers containing TEA and photopolymer layers containing NPG have different density which can have an effect on the thermal expansion of the material. As a result the gratings recorded in photopolymers with various compositions can have different response to temperature variation.

The aim of the second set of experiments is to investigate the temperature sensitivity of volume phase slanted gratings recorded in a photopolymer containing either AA or DA as monomer and either TEA or NPG as an initiator. The potential application of photopolymers as a thermo-responsive material for the development of holographic temperature sensors is discussed.

5.2. Theoretical background for slanted gratings

Slanted gratings can be recorded in transmission mode when the angles of two incident beams are not symmetric with respect to the normal to the surface of the recording material: $\theta_1' \neq \theta_2'$ (Figure 5.3).

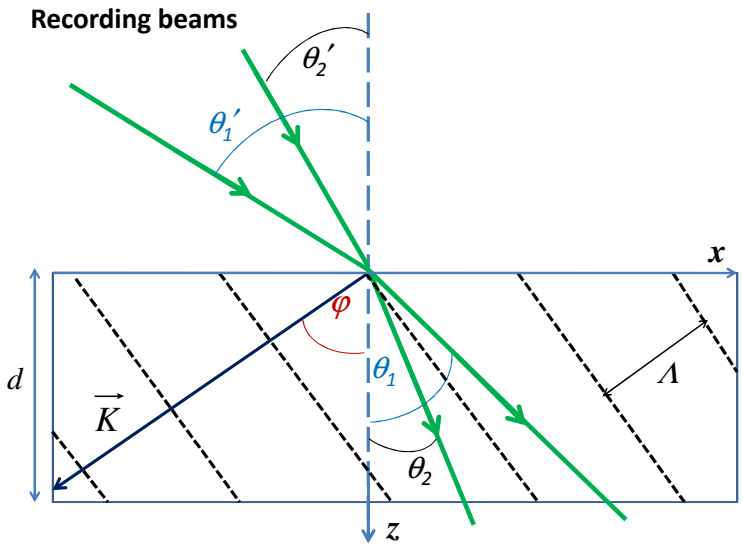

Figure 5.3. Schematic presentation of the slanted grating recorded in transmission mode. $\theta_{1,2}$ and $\theta_{1,2}'$ are the angles of recording beams inside and outside the recording medium, respectively; φ is the slant angle; Λ is the spatial period; $\vec{K}$ is the grating vector, d is the grating thickness.

In a slanted transmission grating the plane of fringes makes an angle with the normal to the surface of the recording material. The slant angle (φ) is defined as the angle between the grating wave vector $\vec{K}$ and the normal to the layer's surface (Figure 5.3). The magnitude of the grating wave vector is determined as $2\pi/\Lambda$. The slant angle can be calculated as follows:

$$\varphi = \frac{\pi - (\theta_1 + \theta_2)}{2}, \tag{5.1}$$

where θ_1 and θ_2 are the angles of recording beams inside the holographic recording material. The incident angles of the two beams inside the medium (θ_1 and θ_2) are related to the external incident angles ($\theta_1'$and θ_2') by Snell's law (Equation 3.2).

The fringe spacing (Λ) of the slanted grating is determined as:

$$\Lambda = \frac{\lambda}{2n\sin\left(\frac{\theta_1 - \theta_2}{2}\right)}, \tag{5.2}$$

where λ is the wavelength of recording light, n is the average refractive index of the material.

In accordance with the coupled wave theory [10], the diffraction efficiency (η) of a volume phase transmission grating with slanted fringes is determined:

$$\eta = \frac{\sin^2\sqrt{\left(\xi^2 + \nu^2\right)}}{1 + \xi^2/\nu^2}. \tag{5.3}$$

The parameter ν defines the maximum diffraction efficiency at Bragg incidence, whereas the parameter ξ describes deviation from the Bragg condition due to the angular and wavelength deviations. At Bragg incidence ξ = 0 and the maximum diffraction efficiency is determined:

$$\eta = \sin^2\nu. \tag{5.4}$$

The parameter ν can be written as:

$$\nu = \frac{\pi n' d}{\lambda\left(c_R c_S\right)^{1/2}}, \tag{5.5}$$

where n' is the refractive index modulation, λ is the wavelength of the reconstructing beam. Parameters c_R and c_S are defined as follows:

$$c_R = \cos\theta \ , \tag{5.6}$$

$$c_S = \cos\theta \ - \frac{\lambda}{n\Lambda}\cos\varphi, \tag{5.7}$$

where θ is the Bragg angle inside the medium. Taking into account Equations (5.5)-(5.7), the diffraction efficiency of slanted grating at Bragg incidence can be defined as follows:

$$\eta = \sin^2\left(\frac{\pi n' d}{\lambda\left[\cos\theta\left(\cos\theta - \frac{\lambda}{n\Lambda}\cos\varphi\right)\right]^{1/2}} \right). \tag{5.8}$$

In the present research slanted gratings with the slant angle of 77 ± 1^o and the spatial frequency of 960 ± 50 lines/mm are under study. Our estimations show that in this case the second term in the round brackets in Equation (5.8) is 10 times smaller than the first term. Thus, the second term can be neglected and Equation (5.8) takes the form of Equation (2.4). The diffraction efficiency changes ($\Delta\eta$) caused by the effect of different parameters can be determined by Equation (2.5).

Equation (5.4) indicates that the diffraction efficiency at Bragg incidence can have magnitude from 0 to 1 depending on the value of parameter ν. Figure 5.4 shows modelling of the diffraction efficiency as a function of deviation from the Bragg angle for different values of parameter ν. As can be seen from Figure 5.4, the diffraction efficiency at Bragg angle ($\xi = 0$) increases from 0 to 1 when parameter ν varies from 0 to $\pi/2$ and from π to $3\pi/2$. The decrease of the diffraction efficiency from 1 to 0 can be observed when parameter ν varies from $\pi/2$ to π and from $3\pi/2$ to 2π. According to Equation (5.5), during holographic recording of a grating with defined thickness and spatial period parameter ν is determined by the refractive index modulation achieved.

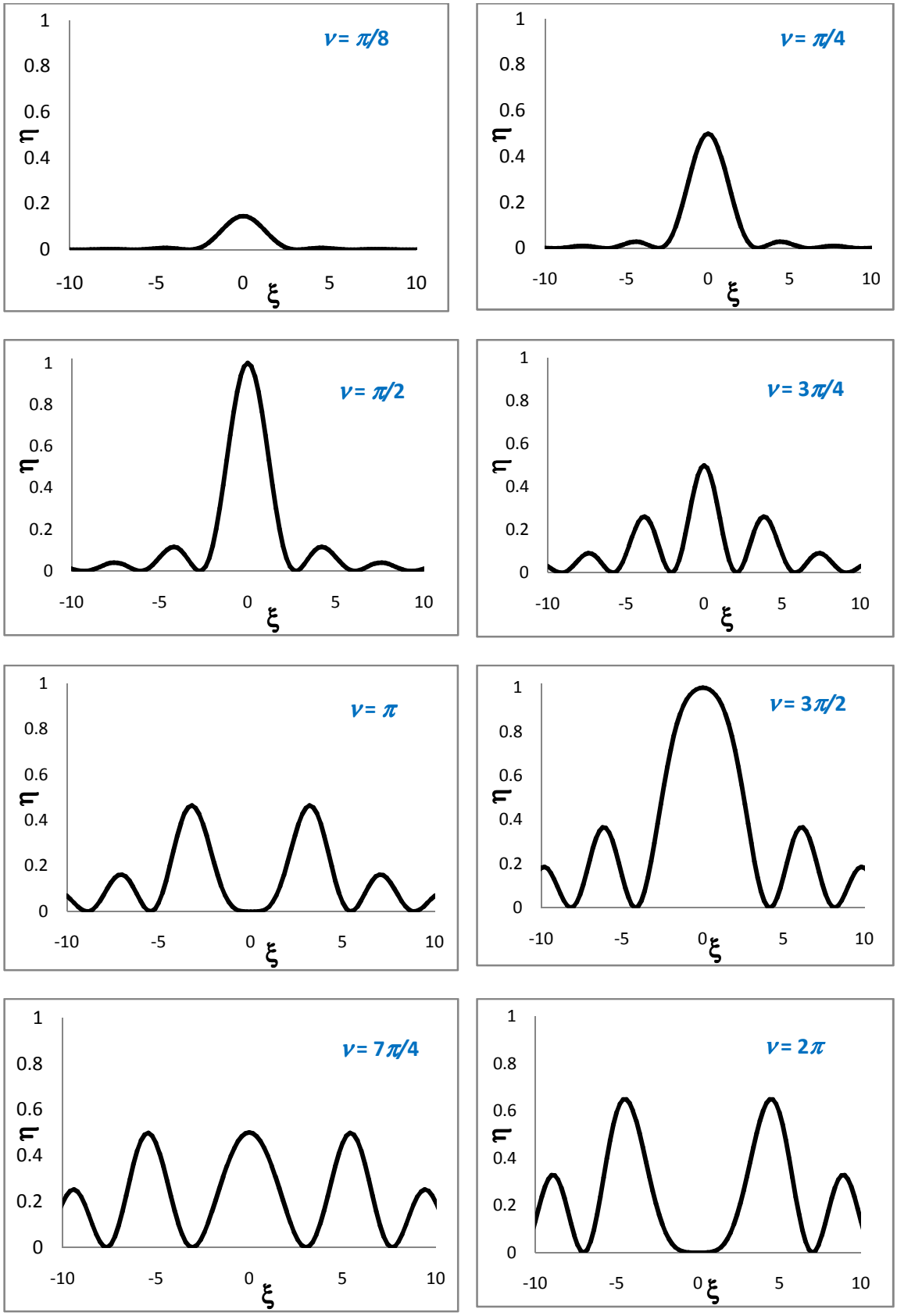

Figure 5.4. Diffraction efficiency of transmission grating *versus* parameter ξ for different values of parameter ν.

At a certain point obtained refractive index modulation gives $\nu = \pi/2$ and the diffraction efficiency at Bragg incidence reaches its maximum value of 1 (Figure 5.4). Further increase of the refractive index modulation leads to the increase of parameter ν and the decrease of the diffraction efficiency. The behaviour of the diffraction efficiency when $\nu > \pi/2$ is determined as an overmodulation regime. The diffraction efficiency at Bragg incidence *versus* parameter ν is presented in Figure 5.5. The inserts show the Bragg selectivity curves at particular value of parameter ν.

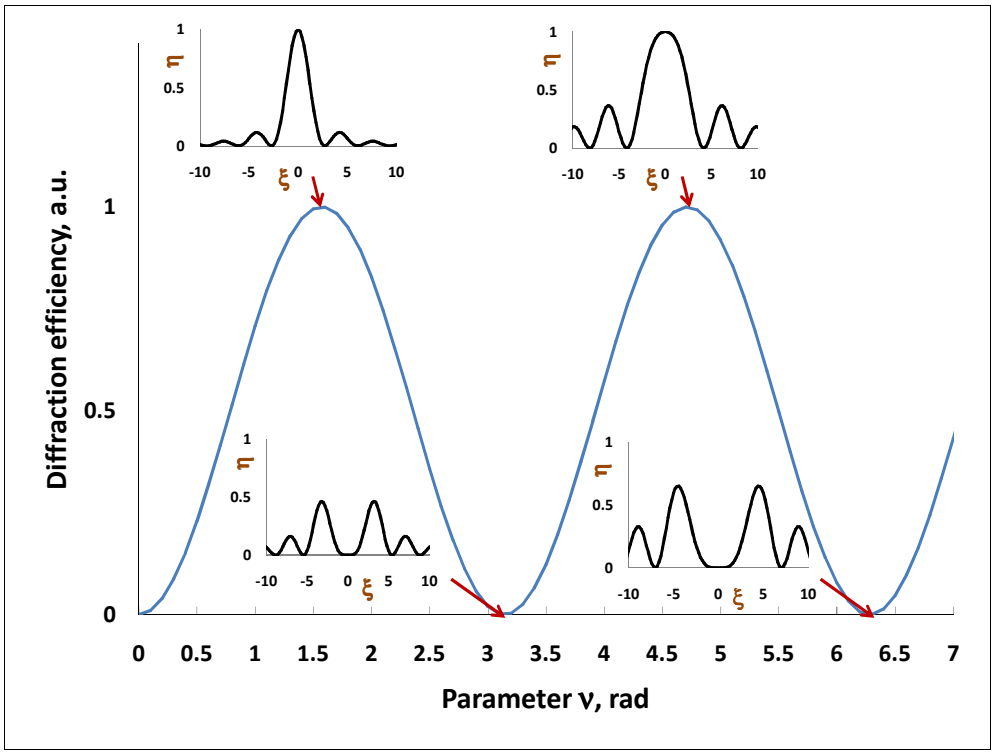

Figure 5.5. Diffraction efficiency at Bragg incidence *versus* parameter ν.

During our experiments a significant increase of the diffraction efficiency followed by its decrease was observed in DA-based gratings under exposure to humidity. The behaviour of the diffraction efficiency was attributed to the transition to overmodulation regime. Further details are presented in section 5.4.1.

5.3. Experimental

5.3.1. Layer preparation

Three types of photopolymer layers containing different main monomers and photoinitiating systems have been used as a holographic recording material (Table 5.1). The first type (photopolymer A) is an AA-based photopolymer containing TEA as a photoinitiator. Optimised composition for the recording in transmission mode [11] is presented in Table 5.1.

Table 5.1. Photopolymer compositions

Chemical reagent	**Photopolymer A**	**Photopolymer B**	**Photopolymer C**
Polyvinyl alcohol	7.45 % w/v	8.89 % w/v	7.4 % w/v
Acrylamide	0.36 M	0.37 M	---
Diacetone acrylamide	---	---	0.22 M
N,N'-methylene bisacrylamide	0.055 M	0.034 M	0.048 M
Erythrosin B	2.13×10^{-4} M	1.39×10^{-4} M	1.85×10^{-4} M
Triethanolamine	0.64 M	---	0.56 M
N-phenylglycine	---	9.81×10^{-3} M	---
Glycerol	---	---	0.51 M

The second type (photopolymer B) is a version of the AA-based photopolymer that uses NPG as a photoinitiator [12]. As shown in Chapter 4, section 4.3.1 - 4.3.2, replacing TEA with NPG enables the development of robust photopolymer layers with higher density.

The third type (photopolymer C) is a DA-based photopolymer containing TEA as a photoinitiator, and has previously been optimised for transmission mode of recording [2, 3]. In addition to the components used in photopolymer A and photopolymer B, photopolymer C contains glycerol as a plasticiser. The addition of glycerol promotes diffusion of the relatively large DA monomer molecules during

holographic recording, resulting in higher diffraction efficiency than when glycerol is excluded. The addition of glycerol also improves the stability of the solid photopolymer layer [3].

Photopolymer layers with the thickness of 60 ± 5 μm were prepared by deposition of photosensitive solutions on the levelled glass slides (26 × 76 mm^2) and dried for 24 hours in a dark room at T = 21 ± 2 °C and RH = 30 ± 5 %. The amount of solution deposited on the glass slide was 0.7 ml, 2 ml and 0.6 ml for photopolymer A, B and C, respectively. The thickness of the dry layers was measured with a white light interferometric surface profiler MicroXAM S/N 8038.

5.3.2. Holographic recording set-up

Volume phase slanted gratings were recorded using a Nd:YVO_4 laser (532 nm). The holographic optical set-up used for recording in transmission mode is presented in Figure 5.6.

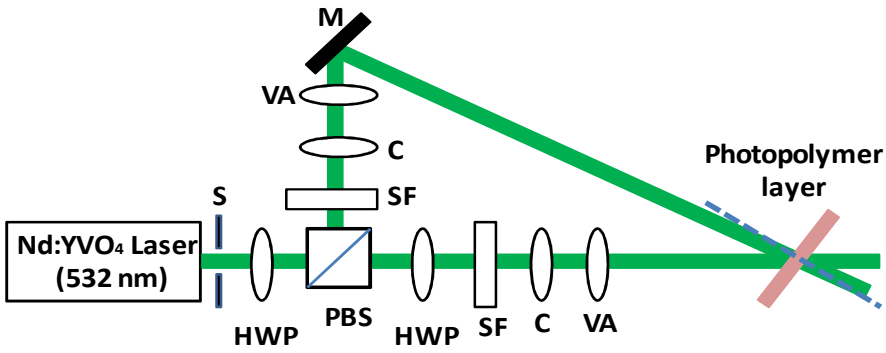

Figure 5.6. Experimental set-up for the recording of a slanted grating in transmission mode: S - electronic shutter; HWP – half-wave plate; PBS – polarising beam splitter; SF – spatial filter; C – collimator; VA-variable aperture; M – mirror.

A two-beam set-up with the incident angles of the recording beams of 4 ± 0.5^{o} and 36 ± 0.5^{o} (outside the layer), respectively to the normal to the layer surface, was utilised to record slanted gratings with a slant angle of 77.1 ± 0.2^{o} and a spatial frequency of 998 ± 60 lines/mm. The total recording intensity was 5.5 mW/cm^{2} and the recording time was 8 sec for photopolymers A and C and 22 sec for photopolymer B. These conditions were chosen in order to achieve similar starting diffraction efficiency in all three types of layers. The initial diffraction efficiency of the gratings was 37 ± 3 %. For testing the humidity response of the DA-based photopolymer the gratings with lower/higher diffraction efficiency were also recorded. Details are provided in section 5.4.1.

In order to measure the diffraction efficiency of gratings, the diffracted beam intensity was monitored at the Bragg angle using a 633 nm He-Ne laser. The diffraction efficiency of gratings was calculated as the ratio of the intensity of the diffracted beam and the intensity of the incident beam. After the recording, the gratings were exposed to UV-light with the intensity 2.5 mW/cm^{2} for 18 min in order to polymerise all residual monomers using a UV Exposure unit (Mega Electronics, model 5503-11).

5.3.3. Humidity response testing

The humidity response of slanted gratings was investigated by measuring the diffraction efficiency of gratings at different levels of relative humidity and at temperature of 21 ± 1 ^{o}C. The set-up for humidity response testing is presented in Figure 3.3.

5.3.4. Temperature response testing

The temperature response of slanted gratings was investigated by recording Bragg selectivity curves at different temperatures by a computer controlled system presented in Figure 5.7. The relative humidity during the experiment was 45 ± 5 %.

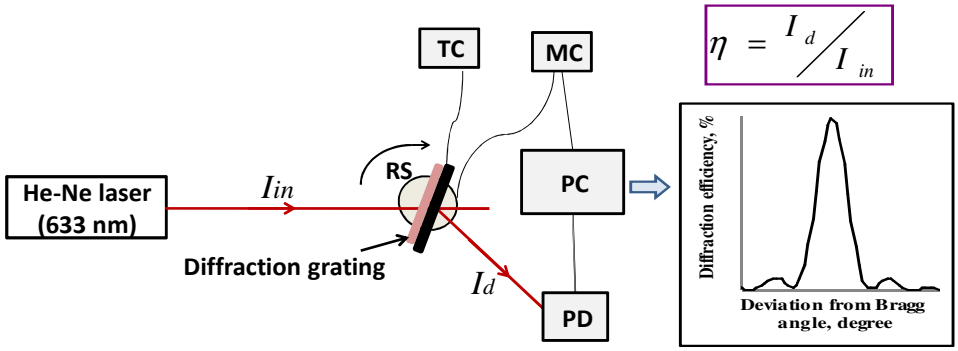

Figure 5.7. Set-up for the Bragg selectivity curve recording: RS - rotation stage; TC – temperature controller; MC – motion controller; PC – computer; PD – photodetector.

Different temperatures were maintained by a temperature controlled plate (model MS100 with a 6 mm aperture, Linkam Instruments). The temperature controlled plate was able to hold a specified temperature to ± 0.1 ^{o}C from room temperature to 60 ^{o}C. A 633 nm beam from a He-Ne laser was employed as a probe beam during the Bragg curve measurements. In order to record the Bragg curve, the grating was fixed on the temperature controlled plate and was placed on a rotation stage which was computer controlled *via* a motion controller (model Newport ESP300 with angular resolution of 0.001^{o}). The intensity of the first-order diffracted beam was monitored by an optical power meter (Newport Model 840). LabVIEW software was used to plot the data of the diffraction efficiency in real time as the incident angle of the probe beam was varied ± 3^{o} from the Bragg angle. The diffraction efficiency was defined as the ratio of the

diffracted beam intensity (I_d) and the incident beam intensity (I_{in}). The diffraction efficiency of the grating was estimated from the maximum of the Bragg selectivity curve. The Bragg curve recordings were done 5 min after the certain temperature was reached. This period of time was based on the time required to obtain equilibrium of the sample temperature with the hot plate temperature. It was observed that after this period of time saturation of the change in the measured response was achieved.

5.3.5. Differential scanning calorimetry

In order to analyse the amount of moisture desorbed from the photopolymer layers under heating, differential scanning calorimetry (DSC) was utilised. DSC measurements were performed using DSC-60 (Shimadzu). The measurements were conducted in aluminium pans by heating the samples at a rate of 2 ^{o}C/min from 17 to 100 ^{o}C. Prior to the DSC measurements, the samples were exposed to RH = 70 % at T = 21 ± 1 ^{o}C for an hour in the controlled environment chamber in order to saturate the photopolymer layers with the moisture.

5.4. Results and Discussion

5.4.1. Humidity response of slanted transmission gratings recorded in photopolymer C

The humidity response of slanted transmission gratings recorded in photopolymer C was investigated by measuring the diffraction efficiency of the gratings at Bragg incidence in the relative humidity range of 20 – 90 %. During the experiment the temperature was kept at 21 ± 1 ^{o}C. For this particular experiment the gratings with the diffraction efficiency of 26 %, 57 % and 75 % measured at 20 % RH were recorded.

Figure 5.8 shows normalised diffraction efficiency of gratings with different initial diffraction efficiency *versus* relative humidity.

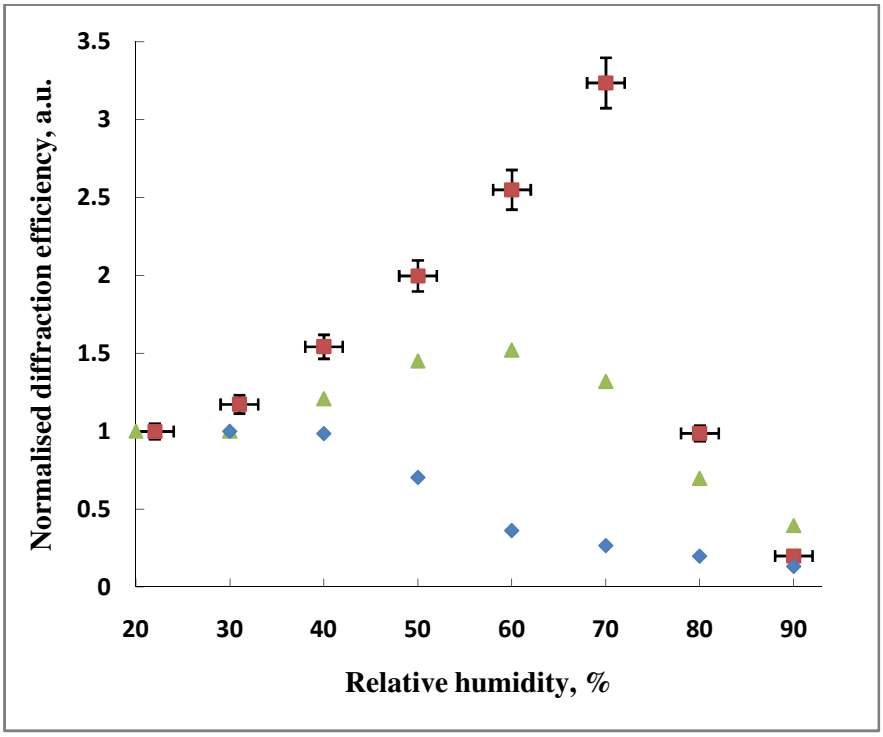

Figure 5.8. Normalised diffraction efficiency of slanted transmission gratings recorded in photopolymer C *versus* relative humidity. The initial diffraction efficiency of gratings was 26 % (■), 57 % (▲) and 75 % (♦).

The initial diffraction efficiency is defined as diffraction efficiency measured at the start of the experiment at RH = 20 %. Normalised diffraction efficiency was calculated as the ratio of the diffraction efficiency measured at certain relative humidity and the diffraction efficiency measured at RH = 20 %.

As seen from Figure 5.8, the behaviour of the diffraction efficiency under humidity exposure depends on the initial diffraction efficiency of the grating. One possible explanation is as follows. Under exposure to humidity the thickness of the grating and refractive index modulation increase due to water absorption. According to Equation (5.5), this leads to the increase of parameter ν which can cause either increase

or decrease of the diffraction efficiency depending on its value (Figure 5.4). In the case of the grating with the high diffraction efficiency, a further increase of parameter ν will lead to overmodulation and, hence, although the refractive index modulation or the thickness of the layer increases, a decrease of the diffraction efficiency at Bragg incidence is observed. This is supported by the Bragg selectivity curve of the sample with the initial diffraction efficiency of 75 % measured before exposure to humidity (the relative humidity during the measurement was 43 %) and immediately after exposure to 60 % *RH* for 30 min (Figure 5.9). As seen from Figure 5.9, the increase of the side lobes and the decrease of the main lobe are observed indicating the overmodulation regime.

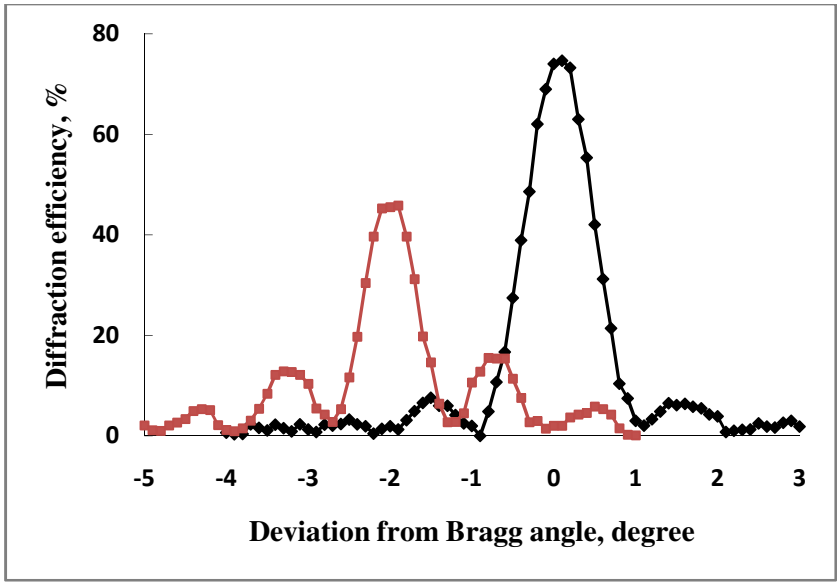

Figure 5.9. Bragg selectivity curve of the slanted transmission grating before exposure to humidity (-♦-) and immediately after exposure to 60 % *RH* for 30 min (-■-).

The decrease of the diffraction efficiency of the grating with the initial diffraction efficiency of 75 % happens at lower level of the relative humidity than in gratings with the initial diffraction efficiency of 26 % and 57 % due to the fact that to reach the overmodulation regime, a smaller change in the parameter ν is required. In the

case of the grating with low initial diffraction efficiency (low value of parameter ν), significant increase of the thickness and refractive index modulation should be reached in order to get the overmodulation regime. As can be seen from Figure 5.8, for gratings with the initial diffraction efficiency of 26 % and 57 % the diffraction efficiency reaches its maximum values of 91 % and 86 %, respectively, at 70 % *RH* and 60 % *RH*, correspondingly. After reaching the maximum value the diffraction efficiency starts to decrease due to reaching the overmodulation regime.

These results demonstrate that the initial diffraction efficiency of the grating recorded in photopolymer C should be taken into account during the development of holographic humidity sensors. Estimation of the effect of the thickness change and refractive index modulation alteration on the diffraction efficiency variation under exposure to humidity is presented in section 5.4.2.

5.4.2. Diffraction efficiency of slanted gratings recorded in photopolymer C versus relative humidity

The diffraction efficiency of slanted gratings recorded in photopolymer C was investigated in the relative humidity range of 20 – 90 %. During the experiment the temperature was kept constant at 21 ± 1 ^{o}C. For this particular experiment a slanted grating with the initial diffraction efficiency of 6 % was recorded in photopolymer C. This starting diffraction efficiency was selected in order to avoid the transfer to the overmodulation regime caused by exposure to humidity as discussed in section 5.4.1. Figure 5.10 shows the relative change in the diffraction efficiency of gratings *versus* relative humidity. The experimental data for photopolymer C is compared with the experimental data for the AA-based photopolymers (photopolymer A and photopolymer B). The relative change in the diffraction efficiency was calculated as follows. The

difference of the diffraction efficiency measured at certain relative humidity and the diffraction efficiency measured at RH = 20 % ($\Delta\eta$) was normalised to the diffraction efficiency measured at RH = 20 % (η_{20}). As can be seen from Figure 5.10, changes in diffraction efficiency of photopolymer C caused by exposure to humidity were very significant (up to 14 times), i.e. increase of the diffraction efficiency from 6 to 84 % was observed when the relative humidity changes from 20 to 90 %. The diffraction efficiency of slanted transmission gratings recorded in photopolymer A and B was relatively unchanged up to 70 % *RH* and it decreased for few percent above 70 % *RH*.

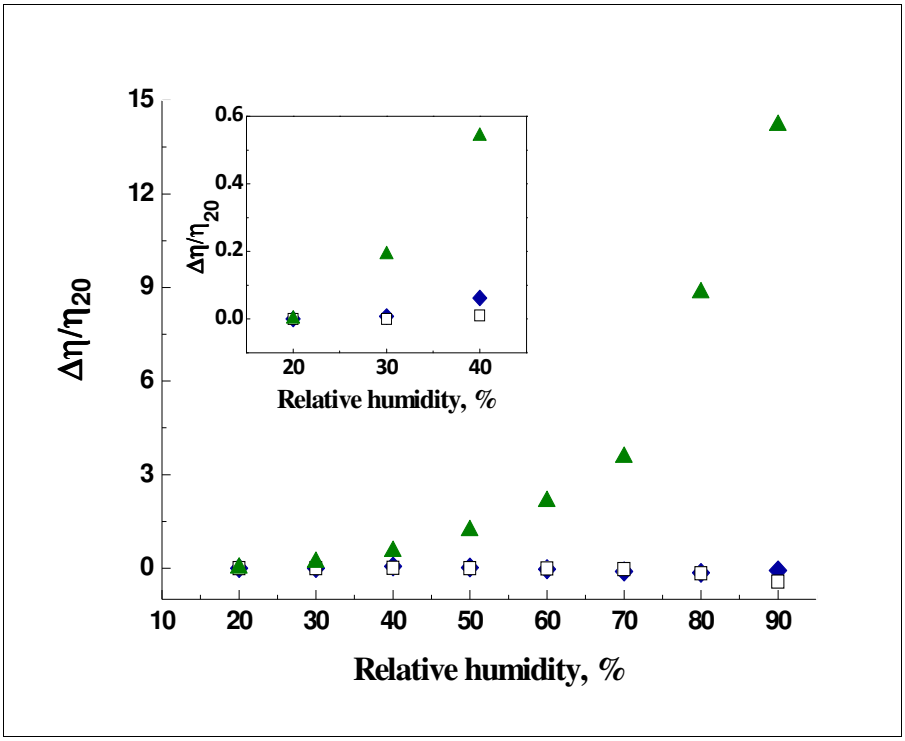

Figure 5.10. Relative changes in the on-Bragg diffraction efficiency of slanted transmission gratings recorded in photopolymer A (♦), photopolymer B (□) and photopolymer C (▲) *versus* relative humidity.

According to Equation (2.5), the significant increase of the diffraction efficiency of the transmission grating recorded in photopolymer C under humidity exposure can be

caused by changes in several parameters. In order to fully understand the mechanism behind the observed change in diffraction efficiency, the effect of variation of each parameter must be considered. To estimate the effect of different parameters, the following experiment was carried out. Transmission gratings were exposed to relative humidity of 30 % and 60 %. The diffraction efficiency at Bragg incidence, the Bragg angle and the thickness of the grating were monitored at 30 % and 60 % *RH*. The estimated contribution of different parameters is presented in Table 5.2.

Table 5.2. Effect of different parameters on the diffraction efficiency change.

Factor	**Formula**	**Estimated contribution**	**Physical process responsible to this change**	**Significance in the current experimental conditions**
Probe beam incident angle variation	$tan\theta\Delta\theta$	0.006	Spatial period increase due to swelling	Minor
Variation of probe wavelength	$\Delta\lambda/\lambda$	0	Probe beam wavelength was kept constant in this study	NA
Thickness variation	$\Delta d/d$	0.1	Swelling of the layer	High
Change in the refractive index modulation	$\Delta n'/n'$	0.1	Decrease of density in dark regions	High

The first parameter is the Bragg angle shift. Our experimental results show that change in relative humidity from 30 to 60 % causes Bragg angle shift of 2^{o}. The term describing the contribution of the Bragg angle shift is of order 0.006. The second parameter is the variation of probe wavelength. Since the probe wavelength used in this experiment was not varied the contribution of this term is zero. The third parameter is the thickness variation caused by humidity exposure. A thickness variation of 10 to 15 % was found and this resulted in a thickness change term of order 0.1. The fourth

parameter is the change in the refractive index modulation. The refractive index modulation was calculated at 30 % and 60 % *RH* using Equation (5.8). The refractive index modulation change was found to be approximately 2×10^{-4} and the term describing the contribution of the refractive index modulation alteration was of order 0.1. Thus, it can be deduced that the main contributors to the diffraction efficiency alteration of transmission gratings recorded in photopolymer C are thickness and refractive index modulation changes. This means that the diffraction efficiency increase observed in gratings recorded in photopolymer C due to humidity exposure is caused by increases in both the grating thickness and the refractive index modulation. An increase of the grating thickness under humidity exposure can be explained by the photopolymer layer swelling due to water absorption. The refractive index modulation increase under humidity exposure may be due to the different ability of dark (i.e. unpolymerised) and bright (polymerised) regions to absorb water molecules due to its different porosity. One possible explanation is that the dark regions have higher porosity and lower density and as a result water molecules are mainly absorbed in these regions. Since the average refractive index of the photopolymer is 1.5 and the refractive index of water is 1.33, absorption leads to a decrease of the average refractive index in dark regions resulting in an overall increase of the refractive index modulation and, hence, the diffraction efficiency increases.

The experimental results reveal that photopolymer C has high sensitivity to humidity even at low relative humidity of $20 - 40$ % (Figure 5.10). As seen from Figure 5.10, a 54 % increase of the diffraction efficiency of photopolymer C was observed in this range, whereas the diffraction efficiency of photopolymer A and B was increased by few percent only. As discussed in section 5.3.1, photopolymer C contains diacetone acrylamide as well as small amounts of glycerol, both of which are known

hygroscopic chemicals which readily absorb water [13, 14]. Increased water absorption would account for the observed large increase in grating diffraction efficiency due to greater changes in grating thickness and refractive index modulation.

Thus, due to its high sensitivity to humidity, the DA-based photopolymer can be utilised for the development of sensors for humidity monitoring in the relative humidity range from 20 to 90 % and at constant temperature. It should be noted that during humidity monitoring it is necessary to keep the temperature unchanged as photopolymer C is also sensitive to temperature variation (section 5.4.4). The reversibility of the observed changes in photopolymer C was confirmed at $RH \leq 60$ % and is further discussed in section 5.4.3.

5.4.3. Reversibility of the humidity induced changes in properties of gratings recorded in photopolymer C

The reversibility of the effect of elevated humidity on gratings recorded in photopolymer C has been characterised. Investigation of the reversibility of humidity induced changes in photopolymer A and photopolymer B was carried out in Chapter 3, section 3.4.2 - 3.4.4 and Chapter 4, section 4.3.2, respectively. The reversibility for photopolymer A and photopolymer B was confirmed after exposure to $RH \leq 70$ % and $RH \leq 90$ %, accordingly, for 60 min at $T = 21 \pm 1$ ^{o}C. Exposure to high humidity ($RH = 80$ - 90 %) of photopolymer A for 60 min at $T = 21 \pm 1$ ^{o}C caused irreversible decrease of the diffraction efficiency and dimensional changes in the layer.

In order to investigate the reversibility of the observed changes in the diffraction efficiency of photopolymer C during exposure to humidity (Figure 5.8 and 5.10), transmission gratings were exposed to 60 %, 70 %, 80 % and 90 % *RH* at $T = 21 \pm 1$ ^{o}C for 30 min and left to recover at $T = 21 \pm 1$ ^{o}C and $RH = 40 - 45$ % for 24 hours. Each

grating was characterised by measuring its diffraction efficiency before exposure and after exposure to humidity followed by drying. The relative humidity during these measurements was in the range of 40 – 45 %. Bragg selectivity curves of the grating before, during and 24 hours after exposure to *RH* = 60 % are presented on Figure 5.11.

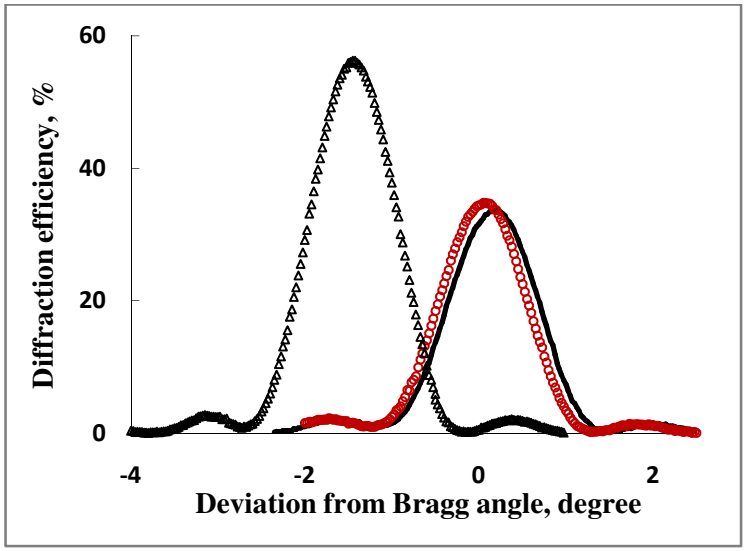

Figure 5.11. Bragg selectivity curve before (solid line), during (Δ) and 24 hours after (o) exposure to *RH* = 60 % at *T* = 21 ± 1 °C for 30 min.

As seen from Figure 5.11, the diffraction efficiency of gratings under exposure to 60 % *RH* increases from 33 to 56 % and the observed increase is in good agreement with the experimental data presented in Figure 5.10. After relaxation at 40 % *RH* the diffraction efficiency was found to be reversible within 1.5 %. Peak of the diffraction efficiency was reversible within 0.1° with respect to its original position. The thickness of the photopolymer layer before and 24 hours after exposure to *RH* = 60 % was unchanged. Thus, the increase of the diffraction efficiency observed during the exposure to humidity of 60 % *RH* is reversible.

Experimental data for the gratings exposed to 70 %, 80 % and 90 % *RH* for different amount of time are presented in Figure 5.12. To describe humidity induced changes, normalised diffraction efficiency was calculated as the ratio of the diffraction efficiency measured after exposure to humidity followed by drying and the diffraction efficiency measured before exposure to humidity.

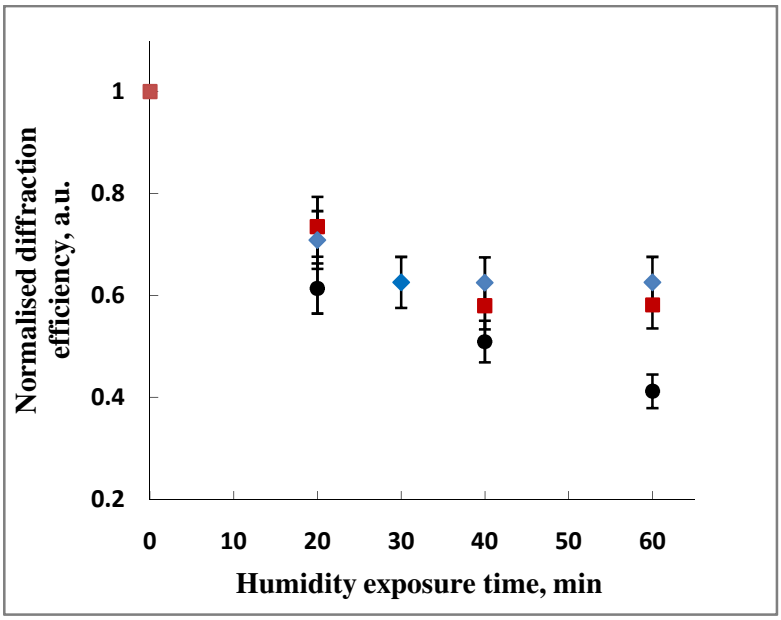

Figure 5.12. Normalised diffraction efficiency of gratings recorded in photopolymer C after exposure to the relative humidity of 70 % (♦), 80 % (■) and 90 % (●) *versus* humidity exposure time.

As can be seen from Figure 5.12, exposure to humidity of 70 %, 80 %, 90 % *RH* for 20 min causes irreversible decrease of the diffraction efficiency. No dependence of the normalised diffraction efficiency on the time of exposure to 70 % and 80 % *RH* was observed above 30 min. Maximum decrease of the diffraction efficiency and its strongest dependence on time of exposure to high humidity was detected for 90 % *RH*. One possible explanation for the observed irreversible decrease of the diffraction efficiency can be an irreversible decrease of the thickness of the grating. During

humidity exposure, expansion of the photopolymer layer in the direction parallel to the grating vector was noticed. In order to evaluate the thickness change caused by humidity exposure, normalised thickness was calculated as the ratio of the thickness measured after and before humidity exposure. The relative humidity during thickness measurements was in the range of 40 – 45 %. Figure 5.13 shows that exposure to humidity of 70, 80 and 90 % *RH* leads to irreversible decrease of grating thickness.

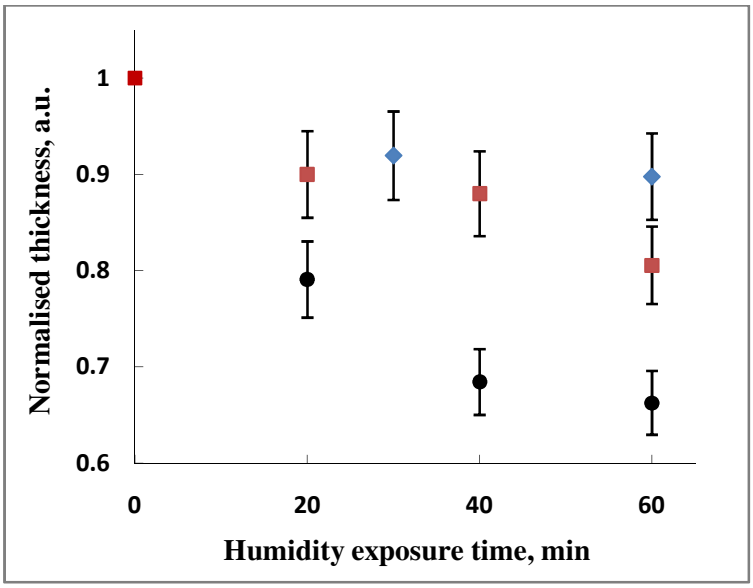

Figure 5.13. Normalised thickness after exposure to the relative humidity of 70 % (♦), 80 % (■) and 90 % (●) *versus* humidity exposure time.

Our estimations utilising Equation (5.8) reveal that the observed irreversible decrease of the diffraction efficiency (Figure 5.12) can't be explained by irreversible decrease of the thickness only. This implies that at high humidity, irreversible decrease of the refractive index modulation can also occur. To prove this assumption, the refractive index modulation before and after exposure to relative humidity of 70, 80 and 90 % for 20 min and 60 min was calculated using Equation (5.8). The calculation was based on the experimental data of the diffraction efficiency and the thickness measured

before exposure and after exposure to humidity when the samples had been dried for 24 hours. Calculated data are presented in Table 5.3 in the form of normalised refractive index modulation defined as the ratio of the refractive index modulation after the exposure followed by drying and the refractive index modulation before the exposure.

Table 5.3. Normalised refractive index modulation after exposure to humidity and drying.

Relative humidity, %	**Humidity exposure time, min**	**Normalised refractive index modulation**
70	20	0.92
	60	0.70
80	20	0.81
	60	0.70
90	20	0.80
	60	0.60

As seen from Table 5.3, the refractive index modulation after exposure to humidity decreases. One possible explanation is as follows. When the humidity is very high, the layers become close to a liquid state. The absorption of water allows for reduction in the density of the photopolymer layer and the polymer chains become less rigidly fixed and can move around, which would reduce the refractive index modulation.

Thus, photopolymer C can be utilised for the development of reversible sensors for continuous humidity monitoring in the range from 20 to 60 % *RH* and at constant temperature. The photonic structure within photopolymer C changes its optical properties irreversibly in response to changes in the level of relative humidity above 60 % *RH*, allowing for the creation of irreversible humidity holographic sensors with an operation range of $RH > 60$ % at constant temperature.

5.4.4. Temperature response of slanted transmission gratings

The temperature response of slanted transmission gratings recorded in the different photopolymers was investigated by recording Bragg selectivity curves and monitoring the position of the Bragg angle in the temperature range of 20 - 60 ^{o}C. Figure 5.14 presents the experimental data of the Bragg angle shift for photopolymer A, B and C.

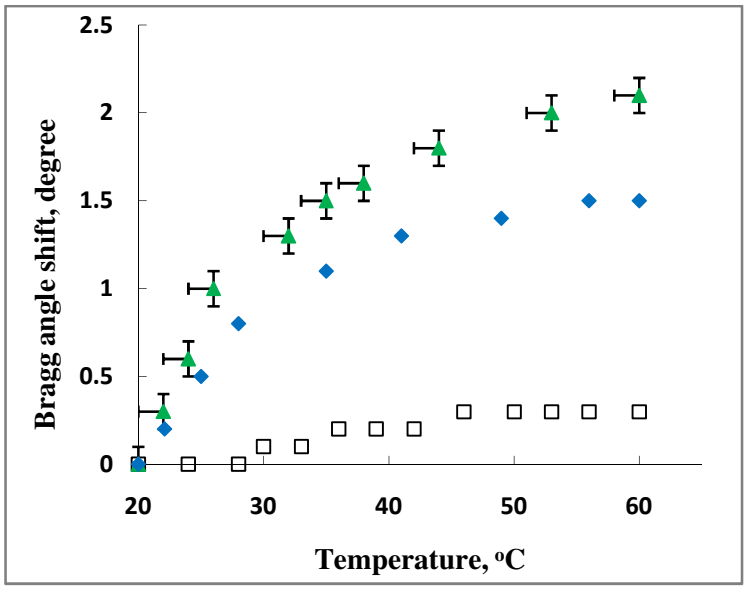

Figure 5.14. Temperature dependence of the Bragg angle shift of slanted transmission gratings recorded in photopolymer A (♦), photopolymer B (□) and photopolymer C (▲). Relative humidity was 30 ± 5 %.

It should be noted that according to the recording geometry, the Bragg angle shift to a bigger value corresponds to the shrinkage of the layer in the direction perpendicular to the grating vector.

As shown in Figure 5.14, in the case of photopolymer layers containing TEA (photopolymer A and photopolymer C) exposure to temperature causes shrinkage of the layers leading to the Bragg angle shift up to 2^{o}, whereas photopolymer B containing NPG exhibits the lower response to temperature changes and the Bragg angle shift up to

0.3° is observed. Analysis of the three types of layers carried out by DSC showed that the different behaviour of the Bragg angle shift for the different photopolymer layers can be explained by different ability of the three photopolymers to release water due to increase in temperature. DSC thermograms of photopolymers presented in Figure 5.15 reveal that photopolymer A and photopolymer C have transitions with a distinct loss of weight due to drying in the temperature range of 20 - 55 °C. Thus, drying of the layer causes its shrinkage, and, hence, the Bragg angle shift is observed (Figure 5.14). In photopolymer B, the evaporation process is not so intensive leading to a smaller Bragg angle shift in this temperature range.

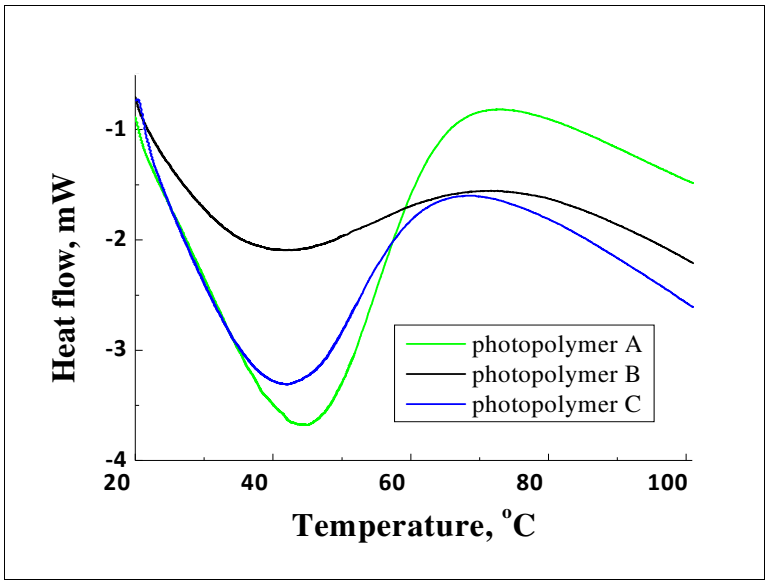

Figure 5.15. DSC thermograms of photopolymers.

As outlined in section 5.4.2, photopolymer C is a highly humidity-sensitive material suitable for humidity sensor development. In order to eliminate effects due to humidity and to analyse only the thermal effect on the properties of the holographic gratings recorded in this photopolymer, the temperature response of sealed layers was

investigated. Sealed samples were prepared by sealing the photopolymer layer on the glass substrate between two polyester films with a thickness of 50 μm. Figure 5.16 shows that the behaviour of the Bragg angle shift of sealed and unsealed samples is fully opposite, i.e. exposure to temperature causes swelling of sealed layer and shrinkage of unsealed layer. Swelling of the sealed layer can be explained by relatively large thermal expansion of photopolymer C, a property which is inherent to polymer materials with a low glass transition temperature.

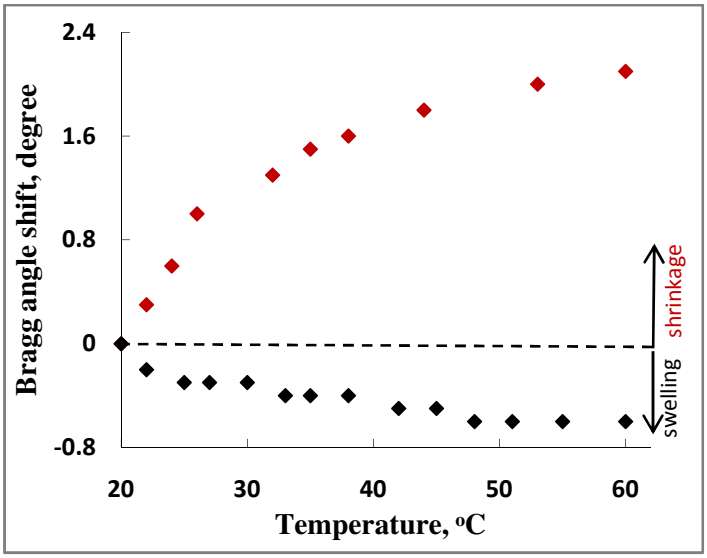

Figure 5.16. Temperature dependence of the Bragg angle shift in photopolymer C: unsealed sample (♦) and sealed sample (♦). Relative humidity during the experiment was 30 ± 5 %.

The temperature dependence of normalised diffraction efficiency of slanted transmission gratings recorded in unsealed and sealed layers for all three photopolymers is presented in Figure 5.17a and 5.17b, respectively. Normalised diffraction efficiency was calculated as the ratio of the diffraction efficiency measured at certain temperature and the diffraction efficiency measured at the start of the experiment at $T = 20\ ^{o}C$.

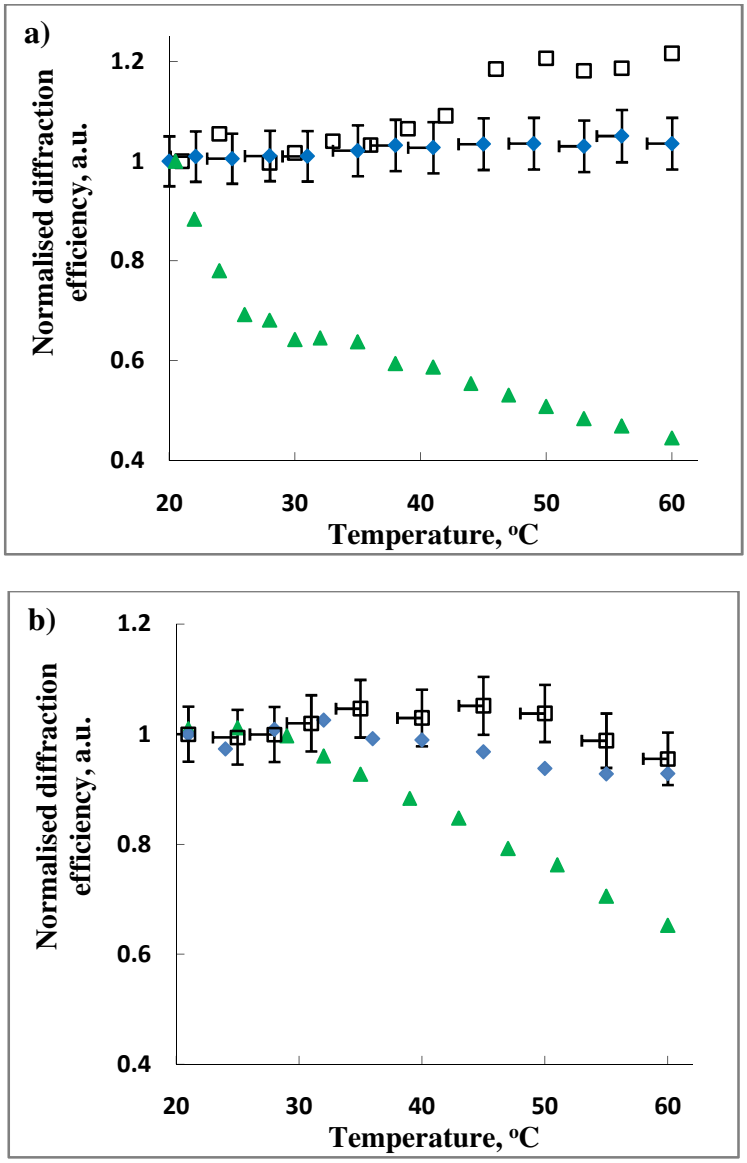

Figure 5.17. Temperature dependence of normalised diffraction efficiency of slanted transmission gratings recorded in unsealed (a) and sealed (b) photopolymer layers: (♦) – photopolymer A, (□) – photopolymer B and (▲) – photopolymer C. Relative humidity during the experiment was 30 ± 5 %.

As seen from Figure 5.17a, the diffraction efficiency of unsealed photopolymer A layers is unchanged in the temperature range from 20 to 60 °C. Photopolymer B is unresponsive to temperature change below 40 °C and shows 20 % increase in diffraction efficiency above 40 °C. Significant decrease of the diffraction efficiency of photopolymer C is observed in the range of 20 to 60 °C. Similarly to the humidity

exposure tests, the observed temperature dependence of the normalised diffraction efficiency depends greatly on changes in the grating refractive index modulation. It is expected that there are two main processes which have an effect on the refractive index modulation alterations. The first contributor is desorption of adsorbed moisture due to elevated temperature. This predominantly takes place in the dark regions as these areas are less dense and therefore absorb more water. Water desorption leads to increase of the refractive index in the dark regions and, hence, decrease of the refractive index modulation. The second contributor is thermal expansion which leads to a decrease of the polymer density. Depending on which region (i.e. the dark or bright region) expands to a greater extent, the diffraction efficiency is increased/decreased with respect to temperature change. This theory matches with the results obtained in section 5.4.2, which showed that composition C is significantly more prone to water absorption than photopolymer A and B. Therefore, a greater response to elevated temperature is expected for photopolymer C as it is more likely to experience stronger water desorption effects than either photopolymer A or B.

The reversibility of the observed decrease of the diffraction efficiency in photopolymer C (Figure 5.17a) was tested by recording the Bragg selectivity curve after exposure to temperature when the sample was recovered for 24 hours at $T = 20 \pm 1$ ^{o}C and 27 % *RH*. Figure 5.18 shows the experimental data before exposure measured at 32 % *RH* and after exposure to temperature measured at 27 % *RH*. According to our data (Figure 5.10), the diffraction efficiency is highly dependent on the relative humidity level. Decrease of the diffraction efficiency for 5 % observed in Figure 5.18 can be attributed to the different relative humidity level during the measurements. Thus, the decrease of the diffraction efficiency in photopolymer C observed during temperature exposure (Figure 5.17a) is reversible.

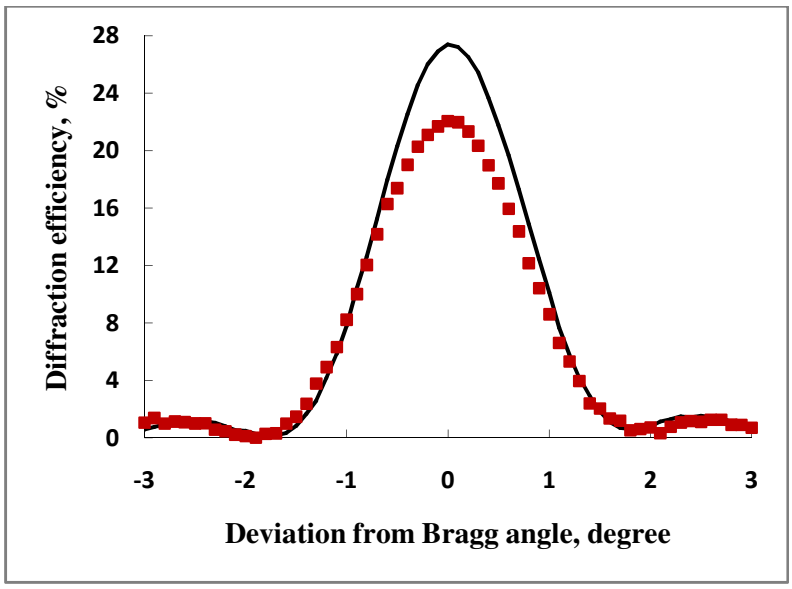

Figure 5.18. Diffraction efficiency of slanted transmission grating recorded in unsealed photopolymer layer C before (solid line) and after exposure to temperature (■).

In the case of the grating recorded in photopolymer B, the diffraction efficiency before exposure and after exposure to temperature was found to be 12.4 % and 11.9 %, respectively. The observed discrepancy in the diffraction efficiency is within the uncertainty of the measurement. Thus, the observed increase of the diffraction efficiency in photopolymer B is reversible.

Application of the sealing technique allowed for observation of changes in the diffraction efficiency caused by thermal expansion (Figure 5.17b). Photopolymer C reveals temperature sensitivity above 30 ^{o}C demonstrating its potential suitability for the development of holographic temperature sensors. Photopolymer A and photopolymer B is relatively unresponsive to temperature changes in the range of 20 – 60 ^{o}C. A photopolymer material which is stable over a large temperature range is highly desirable for many holographic applications. Changes in diffraction efficiency were found to be reversible within 0.5 % for the tree types of photopolymers.

5.5. Conclusion

The humidity and temperature sensitivity of slanted holographic gratings recorded in photopolymers containing AA and DA as monomers, and TEA and NPG as photoinitiators was investigated. It has been demonstrated that the response of the photopolymer-based holographic gratings to relative humidity and temperature can be tuned by variation of the photopolymer composition.

Characterisation of the humidity response of photopolymer-based transmission gratings was carried out in the range of 20 - 90 % *RH*. A strong humidity dependence of the diffraction efficiency of DA photopolymer-based transmission gratings was observed. Reversibility of humidity induced changes is confirmed at $RH \leq 60$ %. Thus, the response to humidity of the DA photopolymer-based transmission gratings can be utilised for the development of reversible sensors for continuous humidity monitoring in the range of 20 – 60 % *RH* and at constant temperature. Also, irreversible decrease of the diffraction efficiency caused by exposure to $RH > 60$ % is particularly useful for fabrication of irreversible humidity indicators suitable for incorporation in packaging for electronic goods, for example.

The temperature response of slanted transmission gratings recorded in photopolymers was investigated in the temperature range of 20 - 60 ^{o}C. The unsealed transmission gratings recorded in the AA-based photopolymer composition containing NPG were unresponsive to temperature changes below 30 ^{o}C and showed sensitivity to temperature above 30 ^{o}C. In the temperature range from 30 to 60 ^{o}C the diffraction efficiency changed from 12 to 14 % and the Bragg angle shift of 0.3^{o} was observed. Exposure of the transmission gratings recorded in the DA-based photopolymer composition containing TEA to elevated temperature leads to the significant decrease of the diffraction efficiency up to 2 times and the Bragg angle shift up to 2^{o} due to the

shrinkage of the unsealed layer caused by water evaporation. Temperature-induced changes are found to be reversible. Application of a sealing technique allowed for observation of swelling of the DA-based photopolymer layer due to its thermal expansion. The results demonstrate an effective approach to obtaining photopolymer-based gratings with tuneable temperature sensitivity and possibility to exploit photopolymers as a thermo-responsive material for the development of temperature holographic sensors.

References

1. Cody, D., *Low-toxicity diacetone acrylamide-based photopolymer for applications in holography*. 2014,(Doctoral Thesis). Dublin Institute of Technology: Dublin.
2. Cody, D., Naydenova, I. and Mihaylova, E. *New non-toxic holographic photopolymer material.* Journal of Optics, 2012. **14**(1): p. 015601.
3. Cody, D., Naydenova, I. and Mihaylova, E. *Effect of glycerol on a diacetone acrylamide-based holographic photopolymer material.* Applied Optics, 2013. **52**(3): p. 489-494.
4. Cody, D., Mihaylova, E., O'Neill, L. and Naydenova, I., *Determination of the polymerisation rate of a low-toxicity diacetone acrylamide-based holographic photopolymer using Raman spectroscopy.* Optical Materials, 2015. **48**: p. 12-17.
5. Mihaylova, E., Cody, D., Naydenova, I., Martin, S. and Toal, V., *Diacetone-acrylamide based pressure sensitive photopolymer*, 2014, Patent Application No. GB1411640.4.
6. Van Krevelen, D.W. and Te Nijenhuis, K., *Properties of polymers: their correlation with chemical structure; their numerical estimation and prediction from additive group contributions*. Elsevier Science 2009.
7. Dhar, L., Schnoes, M.G., Wysocki, T.L., Bair, H., Schilling, M. and Boyd C., *Temperature-induced changes in photopolymer volume holograms.* Applied Physics Letters, 1998. **73**(10): p. 1337-1339.
8. Tomita, Y., Nakamura, T. and Tago, A., *Improved thermal stability of volume holograms recorded in nanoparticle–polymer composite films.* Optics Letters, 2008. **33**(15): p. 1750-1752.

9. Naydenova, I., Jallapuram, R., Toal, V. and Martin, S., *Characterisation of the humidity and temperature responses of a reflection hologram recorded in acrylamide-based photopolymer.* Sensors and Actuators B: Chemical, 2009. **139**(1): p. 35-38.

10. Kogelnik, H., *Coupled wave theory for thick hologram gratings.* The Bell System Technical Journal, 1969. **48**(9): p. 2909-2947.

11. Martin, S., Feely, C.A. and Toal, V., *Holographic recording characteristics of an acrylamide-based photopolymer.* Applied Optics, 1997. **36**(23): p. 5757-5768.

12. Gong, Q., Wang, S., Huang, M. and Gan, F., *A humidity-resistant highly sensitive holographic photopolymerizable dry film.* Materials Letters, 2005. **59**(23): p. 2969-2972.

13. *Material Safety Data Sheet - 222348,* Retrived Decemver 10, 2014, from: http://www.sigmaaldrich.com/.

14. *Material Safety Data Sheet - G30-4,* Retrived Decemver 10, 2014, from http://www.fishersci.com/

6. DEVELOPMENT OF THE TEMPERATURE SENSITIVE PHOTOPOLYMER FOR HOLOGRAPHIC RECORDING IN TRANSMISSION AND REFLECTION MODES

6.1. Introduction

Novel functionalised photopolymer systems capable of holographic recording are of particular interest due to their potential use in the development of holographic sensors. Functionalised photopolymer systems must have both good holographic recording characteristics and the response to a specific analyte.

This chapter describes the development of a novel temperature sensitive photopolymer composition. The aim of the research was to develop a photopolymer composition capable to both achieve high diffraction efficiency during holographic recording in transmission and reflection modes and respond to temperature changes. The approach used in the present research was based on functionalisation of the photopolymer composition by incorporation of a component with sensitivity to temperature. A photopolymer system generally consists of a main monomer and, optionally, a cross-linking monomer, a photoinitiating system including a sensitising dye and an electron donor, and a polymeric binder. During the development of a novel temperature sensitive photopolymer composition the following innovations were introduced.

Firstly, a thermosensitive monomer such as *N*-isopropylacrylamide (NIPA) was used as the main monomer in order to create a temperature sensitivity of the material. Secondly, NPG was included as a photoinitiator. As shown in Chapter 4, section 4.3.1 – 4.3.2, the utilisation of NPG instead of traditionally used TEA as a photoinitiator decreased the permeability of the layer to water molecules and improved

both the humidity resistance of the holographic grating and the scratch resistance of the photopolymer layer. Thirdly, glycerol as a plasticiser was introduced into the photopolymer composition in order to achieve a better mass transport during the recording and a more stable diffraction efficiency of the grating. Fourthly, citric acid as a chain transfer agent (CTA) was incorporated. CTA along with glycerol allowed improving the spatial resolution of the material for recording in reflection mode. In addition to new components, traditionally used cross-linker as *N,N'*–methylenebisacrylamide, a binder such as polyvinyl alcohol and the light absorbing component (Erythrosine B) were utilised. Polyvinyl alcohol with the level of hydrolysis 80 % was used as it had been found to have low permeability which allowed recording in reflection mode [1]. Chemical compounds of photopolymer components are presented in Figure 6.1.

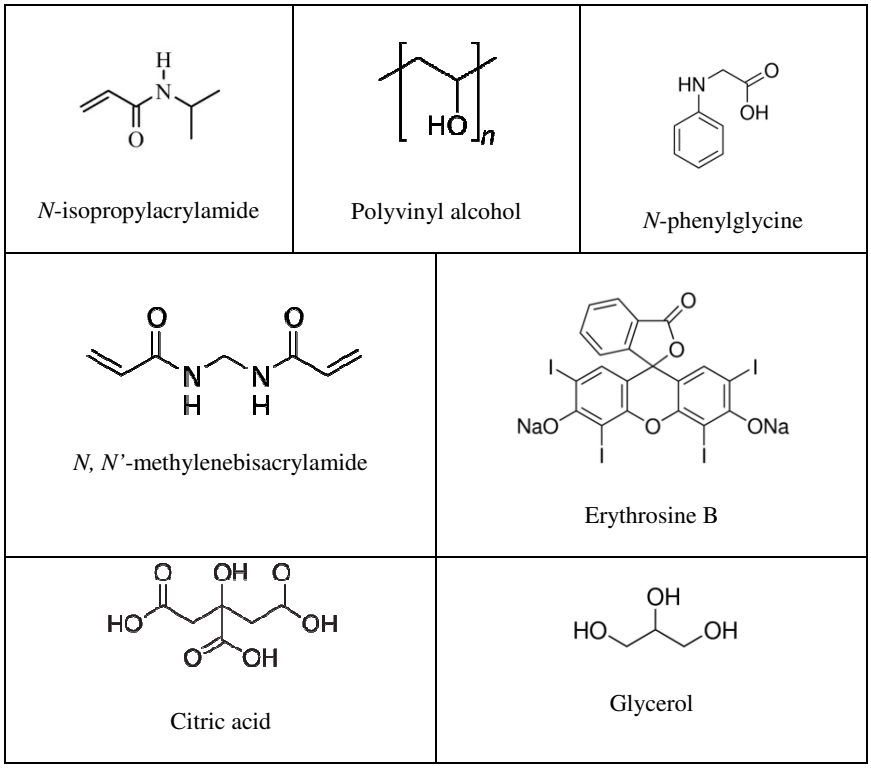

Figure 6.1. Chemical compounds of photopolymer components.

In order to create a photopolymer material with good holographic recording characteristics, optimisation of the photopolymer formulation was carried out by varying the concentration of all the constituent elements. Further details on the development and optimisation of the material are presented in section 6.4.

As the grating develops during the photopolymerisation process in the material, it is important to understand the role of the photopolymer components during the process. The following section 6.2 describes the recording mechanism in photopolymers.

6.2. Recording mechanism in photopolymers

Photopolymerisation is a polymerisation technique utilised to synthesise the polymeric structure in the photopolymer materials. The term photopolymerisation means the initiation of polymer chain growth by light exposure. The mechanism of polymerisation used in this research is free radical vinyl polymerisation which can be described as follows. During the polymerisation process the carbon-carbon double bond of the monomer is broken and replaced with a single bond. Such specie is active as it has unpaired electrons and it reacts with another monomer linking the monomers into the polymer chain.

As mentioned above, in the present research NIPA was used as a monomer and NPG along with Erythrosine B was utilised as a photoinitiating system. It was previously shown [2] that poly(*N*-isopropylacrylamide) (PNIPA) could be synthesised using free radical polymerisation. Also, it was demonstrated [3] that the photoinitiating system containing NPG and xanthene dye exhibited high initiating efficiency upon illumination with visible light. Photopolymerisation involves the following processes: initiation, propagation and termination [4, 5].

6.2.1. Initiation

According to the model proposed in [6], the following processes take place during initiation. Upon illumination, the dye molecule *D* absorbs light of a particular wavelength within its absorption band and it is excited to a singlet state $^1D^*$:

$$D + h\nu \rightarrow {}^1D^* . \tag{6.1}$$

The dye in the excited singlet state is very unstable. It may revert to the ground state by one of two possible processes: emission of a photon (fluorescence) and radiationless transfer (fluorescence quenching) to another molecule *Q*,

$$^1D^* \rightarrow D + h\nu \quad \text{(fluorescence)}, \tag{6.2}$$

$$^1D^* + Q \rightarrow D + Q \quad \text{(fluorescence quenching)}. \tag{6.3}$$

Also, it may transit from singlet state into the triplet excited state $^3D^*$ (intersystem crossing) where the life time of the excited state is longer:

$$^1D^* \rightarrow {}^3D^* \quad \text{(intersystem crossing)}. \tag{6.4}$$

In this triplet state the dye molecule is capable of reacting with the electron donor. Alternatively it may go back to the ground state by the following processes: emission of a photon (delayed fluorescence or phosphorescence), oxygen quenching and radiationless transfer (triplet quenching). In case of high dye concentration, deactivation of an excited dye molecule can happen by collision with another dye molecule.

Free radicals (*D*• and *ED*•) are generated when the exited triplet state dye molecule reacts with the electron donor. The electron donor donates an electron to the exited triplet state dye molecule and becomes a free radical:

$$^3D^* + ED \rightarrow D\bullet + ED\bullet . \tag{6.5}$$

The dye radical anion (*D*•) is not reactive enough to initiate polymerisation. The electron donor radical cation (*ED*•) in the presence of monomer (*M*) initiates the

polymerisation reaction. The initiating free radical (*ED*•) breaks the carbon-carbon double bond (the vinyl group) of the monomer (*M*) and shares the free electron with one of the electron of the carbon atom in the double bond leaving behind the other carbon bond with an unpaired electron:

$$ED\bullet + M = ED - M\bullet . \tag{6.6}$$

Produced chain initiator (*ED-M*•) is a free radical and can react with other monomers leading to the formation of polymer chains. Chain initiator *ED-M*• can also react with dye radical producing transparent form of the dye.

6.2.2. Propagation

The chain initiator (*ED-M*•) can react with another monomer molecule (*M*) by addition to the carbon-carbon double bond yielding a growing polymer radical with an active end. Thus, when the free radical reacts with a monomer, the number of molecules in the polymer chain increases:

$$ED - M\bullet + M = ED - (M)_2\bullet , \tag{6.7}$$

$$ED - (M)_n\bullet + M = ED - (M)_{n+1}\bullet . \tag{6.8}$$

This process continues until either all the monomers are consumed or a termination reaction occurs.

6.2.3. Termination

Termination in free radical polymerisation can occurs in three ways. Two of these, disproportionation and combination, are caused by interaction of two growing macroradicals [4, 5]. Combination occurs when two free radicals meet and share their free electrons forming a covalent bond resulting in a single long polymer chain:

$$ED - (M)_n\bullet + ED - (M)_m\bullet = ED - (M)_n - (M)_m - ED . \tag{6.9}$$

Disproportionation takes place when a hydrogen atom is abstracted from one of the growing polymer chains by another. This leads to a double bond on the first chain, causing the termination reaction. A carbon-carbon double bond takes the place of the missing hydrogen. Termination by disproportionation is shown below:

$$ED-(M)_n\bullet + ED-(M)_m\bullet = ED-(M)_n + ED-(M)_m . \quad (6.10)$$

Termination may also occur by a mixture of disproportionation and combination.

A third possible mechanism of termination is caused by primary radical termination [7]. A growing polymer chain reacts with the electron donor radical (*ED*•) leading to the production of inactive polymer chain:

$$ED-(M)_n\bullet + ED\bullet = ED-(M)_n - ED . \quad (6.11)$$

In the case of the NIPA-based composition described in section 6.1, the structure obtained after the finishing the process of polymerisation can be described as a hybrid polymer consisting of a crosslinked polymer network, containing PNIPA chains with interconnections formed from the *N,N'*-methylenebisacrylamide, in an inert background polymer (polyvinyl alcohol).

6.3. Experimental

6.3.1. Layer preparation

The photopolymer solution was prepared by mixing the photopolymer components such as 10 % w/v stock polyvinyl alcohol solution along with 0.11 % w/v Erythrosine B solution, *N*-isopropylacrylamide, *N,N'*-methylenebisacrylamide, glycerol, *N*–phenylglycine and citric acid (utilised in samples for reflection holography) using a magnetic stirrer. The concentration of components was varied in accordance with the aim of the experiment. In some samples for transmission mode recording glycerol was excluded. The details are presented in section 6.4. The final compositions for recording

in transmission and reflection modes are presented in section 6.4.7 and section 6.5.1, respectively.

The photopolymer layers were prepared by deposition of appropriate amount of photopolymer solution on the leveled glass slides (76 × 26 mm^2) and drying for 24 hours in a dark room at temperature of 21 ± 2 ^oC and relative humidity of 35 ± 5 %. During the development of the photopolymer composition for recording in transmission mode, photopolymer layers with the thickness of 90 μm were prepared. Photopolymer layers with the thickness of 60 μm were used for recording in reflection mode. The amount of the photopolymer solution for recording in transmission and reflection modes was 2.7 ml and 0.8 ml, respectively, in order to get 90 μm and 60 μm thick layers, accordingly. The thickness of the layers for recording in reflection mode was less in order to avoid significant difference in the intensity of incoming beams due to absorbance of light by the layer. The thickness of the dry layers was measured with a white light interferometric surface profiler MicroXAM S/N 8038.

6.3.2. Holographic recording

The recording of unslanted volume phase transmission gratings was carried out by using a setup shown in Figure 6.2a. Transmission gratings with the spatial frequency of 1000 ± 32 lines/mm were recorded. The total recording intensity and the recording time were varied in accordance with the aim of the experiment. Different total recording intensities were used in order to get different lengths of polymer chains. Different recording time allowed manipulating the concentration of unreacted monomers. Further details are presented in section 6.4. To characterise the holographic gratings, Bragg selectivity curves were recorded using a technique described in Chapter 3, section 3.3.3.

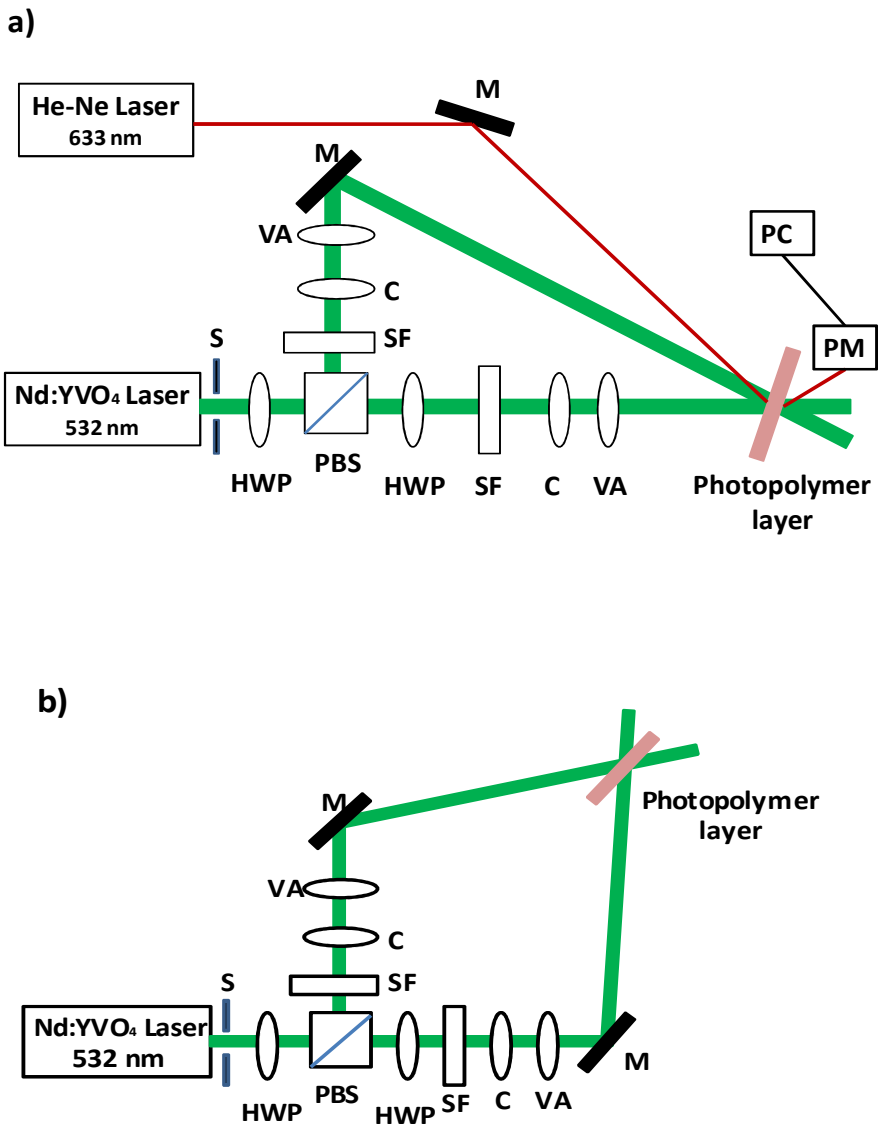

Figure 6.2. Experimental set-up for the recording of a transmission grating (a) and a reflection grating (b): S -electronic shutter; HWP – half-wave plate; PBS – polarising beam splitter; SF – spatial filter; C – collimator; VA-variable aperture; M – mirror; PM – power meter; PC - computer.

Volume phase reflection gratings with the spatial frequency of 2700 ± 44 lines/mm were recorded using a set-up shown in Figure 6.2b. Preliminary results demonstrated that the maximum diffraction efficiency can be achieved after

100 sec exposure time at the total recording intensity of 10.5 mW/cm^2. Optimisation of the recording conditions will be presented in Chapter 7.

6.3.3. Characterisation of the diffraction efficiency of reflection gratings

The diffraction efficiency of reflection gratings was monitored using a 532 nm beam from a Nd:YVO_4 laser at Bragg incidence. According to the Bragg law (Equation 2.3), in the case of the reflection grating with the spatial frequency of 2700 lines/mm, the angle of the probing beam at Bragg incidence is about 61^o with respect to the normal to the surface of the grating. This leads to losses in the intensity of the beam going through the layer due to Fresnel reflection. In order to take into account intensity losses due to Fresnel reflection, the diffraction efficiency (η) of reflection gratings was determined as follows:

$$\eta = \frac{I_d}{I_{in} - I_{refl}}, \tag{6.12}$$

where I_d is the intensity of the diffracted beam, I_{in} is the intensity of the incident beam and I_{refl} is the intensity of the reflected beam.

6.3.4. Refractive index modulation calculation

Quantitative analysis of the refractive index modulation of the material achieved during holographic recording was carried out using the coupled wave theory [8]. The applicability of the coupled wave theory was justified by calculation of Q factor using Equation (2.1). In the present research, Q factor for the transmission gratings with the spatial frequency of 1000 lines/mm and with the thickness of 90 μm was found to be about 200. For the reflection gratings with the spatial frequency of 2700 lines/mm and thickness of 60 μm, Q factor was estimated to be around 1000. This allowed applying

the coupled wave theory for the evaluation of the refractive index modulation achieved during holographic recording. Equations (6.13) and (6.14) were utilised for transmission mode and reflection mode, respectively:

$$n' = \frac{\lambda \cos\theta \sin^{-1}\left(\sqrt{\eta}\right)}{\pi d}, \tag{6.13}$$

$$n' = \frac{\lambda \cos\theta \tanh^{-1}\left(\sqrt{\eta}\right)}{\pi d}, \tag{6.14}$$

where λ is the wavelength of the reconstructing beam, θ is the Bragg angle inside the photopolymer layer for the reconstructing wavelength and d is the thickness of the grating.

6.3.5. UV-curing

In order to investigate the effect of UV-light exposure on the stability of the diffraction efficiency, the samples were UV-cured. Different UV-systems were utilised. Transmission gratings were exposed to UV-light with the intensity of 2.5 mW/cm^2 for a certain time using a UV Exposure unit (Mega Electronics, model 5503-11). Experimental data are presented in section 6.4.6. Reflection gratings were UV-cured using Dymax UV curing system (model ECE-200). It was previously demonstrated [9] that the UV-source with the high intensity was required to fix the reflection grating recorded in the DA-based photopolymer composition. Dymax UV curing system was used as it provided the intensity of exposure up to 60 mW/cm^2. Experimental data are presented in section 6.5.2.

6.4. Development and optimisation of the photopolymer composition for transmission mode recording

6.4.1. N-isopropylacrylamide monomer optimisation

PNIPA was first synthesised in 1956 [10] and its thermal properties in aqueous solutions were discovered in 1968 [11]. PNIPA can be classified as a negative temperature-sensitive system and has a lower critical solution temperature (LCST) of about 32 ^{o}C. Temperature response of PNIPA is based on temperature induced reversible conformational changes of polymer molecules and depends on the interaction between polymer molecules with water. Once the temperature reaches LCST, the polymer chains transform from water-soluble coils to water insoluble globules as the efficiency of hydrogen bonding becomes insufficient for the solubility of the polymer (Figure 6.3).

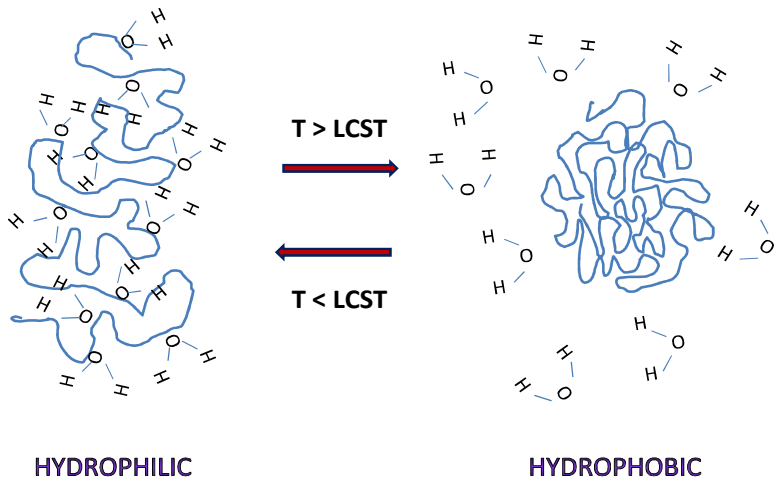

Figure 6.3. Conformational changes of Poly(*N*-isopropylacrylamide) molecules at LCST.

This phenomenon is fully reversible and it turns back to the original state when the stimulus is removed. LCST can be manipulated by copolymerisation of NIPA with other appropriate monomers [12]. In addition of temperature sensitivity, PNIPA has an

advantage such as low toxicity [13, 14]. Due to its low toxicity PNIPA is the most popular intelligent polymer used for the development of temperature responsive materials for drug delivery, tissue engineering, biosensors etc. [15-20].

For our research NIPA was bought from Sigma-Aldrich and was used as received. The concentration of NIPA monomer in the photopolymer composition was optimised by identifying the maximum monomer amount that can be dispersed in the binder. High concentration of monomers is required to get high response of the photonic structure to temperature variations. The temperature response of the holographic gratings recorded in the NIPA-based photopolymer is based on conformational changes of PNIPA molecules induced by temperature. In thick holograms, even a small change in the refractive index modulation ($< 10^{-3}$) can have a very substantial effect on the diffraction efficiency. This effect can be described as follows. During holographic recording refractive index modulation in the material is created mainly due to the spatial variation of density of PNIPA caused by spatially patterned photopolymerisation. Under illumination PNIPA is produced, resulting in higher density in illuminated areas. Temperature rise causes shrinkage of PNIPA macromolecules which increases the local density, leading to higher refractive index modulation and, hence, higher diffraction efficiency.

The maximum amount of monomers which could be accommodated by the matrix without phase separation was determined by varying the monomer concentration. The amount of NIPA in the photopolymer solution was found to be ~11 mg per ml of liquid coating solution. Introducing higher amount of NIPA leads to the deterioration of the layer quality, i.e. crystallisation of NIPA on the surface of the layer. Figure 6.4 shows the photopolymer layer prepared with the composition containing the optimum concentration of monomer.

Figure 6.4. The photograph of the photopolymer layer prepared with the composition containing the optimum concentration of monomer. The thickness of the layer is 90 μm.

Cross-linking monomer such as *N,N'*-methylenebisacrylamide was used in order to minimise the post-recording decay of the diffraction efficiency. As previously found [21], the cross-linker prevented post-recording decay of the diffraction efficiency due to its capability to keep the polymer chains together. The ratio of the main monomer and the cross-linker was important. According to the previous research [22], the best performance of the NIPA-based photopolymer was observed when the ratio of NIPA and the cross-linker such as *N,N'*-methylenebisacrylamide was 4:3. In our research the NIPA and *N,N'*-methylenebisacrylamide ratio was also kept 4:3.

The first trial of holographic recording of transmission gratings in the novel NIPA-based photopolymer composition was successful. The NIPA-based photopolymer composition contained an inert polymeric binder (polyvinyl alcohol), a monomer (NIPA), a cross-linker (*N,N'*-methylenebisacrylamide), a photo-initiator (NPG) and a light absorbing component (Erythrosin B). The diffraction efficiency of about 17 % was achieved during recording with the total intensity of 5 mW/cm^2 for 40 sec at a spatial frequency of 1000 lines/mm in layers with the thickness of 90 μm. However, the diffraction efficiency was found to decrease up to two times within few hours after the

recording. The following sections describe the behavior of the diffraction efficiency with time and approaches utilised to stabilise the photonic structure.

6.4.2. Diffraction efficiency shelf life studies

Behavior of the diffraction efficiency of transmission gratings recorded in the NIPA-based photopolymer with time was investigated. To evaluate the changes in the diffraction efficiency, normalised diffraction efficiency was used. Normalised diffraction efficiency was calculated as a ratio of the diffraction efficiency measured at certain time after the recording and the diffraction efficiency measured immediately after the recording.

Figure 6.5 presents the time dependence of normalised diffraction efficiency of transmission gratings recorded with the total intensity of 5 mW/cm^2 and exposure time 70 sec and 100 sec.

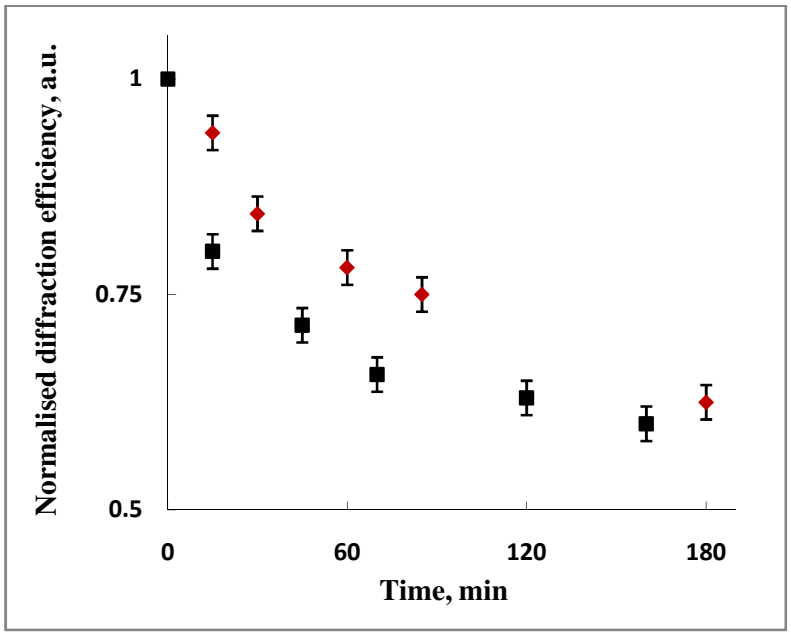

Figure 6.5. Time dependence of normalised diffraction efficiency of transmission gratings recorded with the total intensity of 5 mW/cm^2 and exposure time 70 sec (■) and 100 sec (♦).

As can be seen, significant decay of the diffraction efficiency was observed within 1 hour after recording. The samples were in dark conditions during the period of the observation. Deterioration of the diffraction efficiency was attributed to the low diffusion rate of monomers. The low diffusion rate of monomers led to the significant amount of unreacted monomers remaining in dark regions after recording. Due to the concentration gradient created during holographic recording the monomers diffused from dark to bright regions causing the refractive index modulation reduction and, as a result, the diffraction efficiency decreased. The gratings recorded at shorter exposure time (70 sec) showed bigger decrease of the diffraction efficiency due to higher amount of unreacted monomers left after recording.

Further monitoring of the diffraction efficiency for the period of 30 days after recording showed that in 4 days after recording the diffraction efficiency reached its minimum value and then was unchanged (Figure 6.6). A few different approaches were used to improve the stability of the grating. Obtained results are presented in section 6.4.3 – 6.4.5.

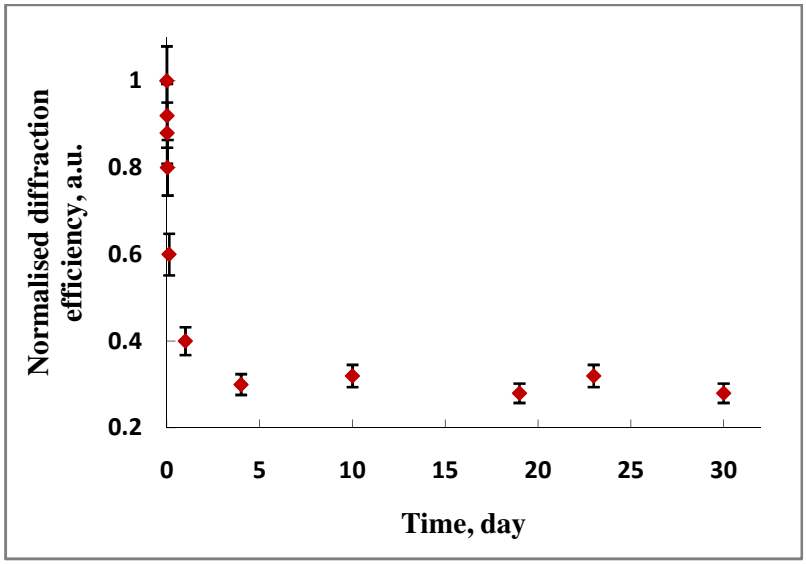

Figure 6.6. Time dependence of normalised diffraction efficiency of transmission gratings. Exposure time was 100 sec and the total recording intensity was 5 mW/cm^2.

6.4.3. Effect of recording intensity on the stability of the diffraction efficiency

The first approach was based on increasing the polymer chain length. It was previously demonstrated [23] that short polymer chains can diffuse away from bright regions. This leads to the decrease of the diffraction efficiency due to the decrease of the density profile produced during the recording. Long polymer chains are supposed to be immobile [23]. This can lead to the higher stability of the photonic structure. The length of polymer chains can be influenced by the intensity of the recording light [24]. The lower the intensity of the recording light, the lower amount of polymer chains is initiated. This allows growing the longer polymer chains and reducing the post-exposure decay of the diffraction efficiency.

In our experiment the total recording intensity was reduced from 5 to 1 mW/cm^2. The exposure time was 400 sec. However, only little improvement in the stability of the grating was observed and the diffraction efficiency decreased up to 50 % in 5 days after recording.

6.4.4. Effect of elevated recording temperature on stability of the diffraction efficiency

The second approach was based on increasing the diffusion rate of monomers by recording the gratings at an elevated temperature. It was previously demonstrated [25] that elevated temperature during recording speeded up the diffusion of monomers and improved the exposure sensitivity of the photopolymer containing TEA as a photoinitiator.

In order to investigate the effect of elevated temperature on the stability of the diffraction grating recorded in the NIPA-based photopolymer composition, transmission gratings were recorded at a temperature ranging from 21 to 60 ^{o}C. Exposure time was

100 sec and the recording intensity was 5 mW/cm^2. The diffraction efficiency of transmission gratings recorded at a temperature ranging from 21 to 60 ^{o}C is presented in Figure 6.7. Measurements were taken immediately after recording. As seen from Figure 6.7, the diffraction efficiency was improved from 12 to 31 % when the temperature during recording was increased from 21 to 60 ^{o}C.

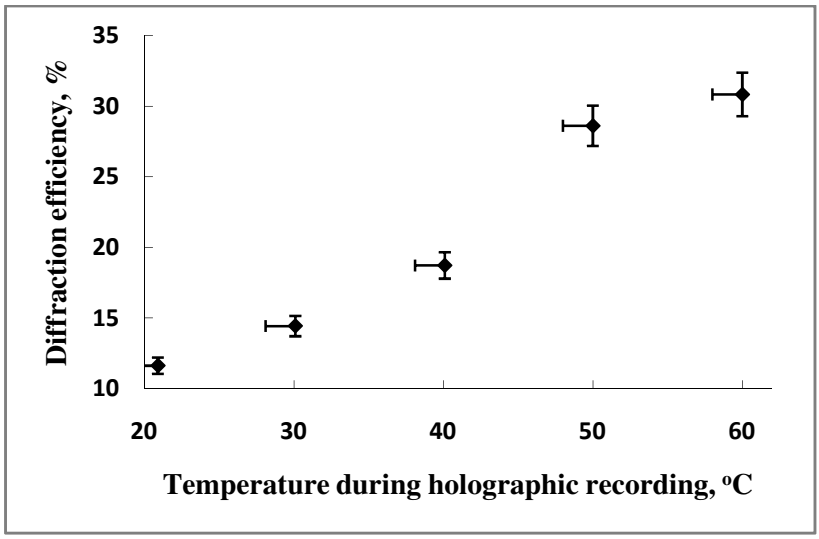

Figure 6.7. Diffraction efficiency of transmission gratings recorded at different temperatures.

The stability of the diffraction efficiency was investigated by measuring the diffraction efficiency in 1 day and 3 days after recording (Figure 6.8). Normalised diffraction efficiency was calculated as a ratio of the diffraction efficiency measured at certain time after recording (1 or 3 days) and the diffraction efficiency measured immediately after recording. As seen from Figure 6.8, the decrease of the diffraction efficiency of gratings depends on the temperature during holographic recording. The stability of the diffraction efficiency was improved at a higher temperature of recording. However, the decay of the diffraction efficiency was still observed in 3 days after recording.

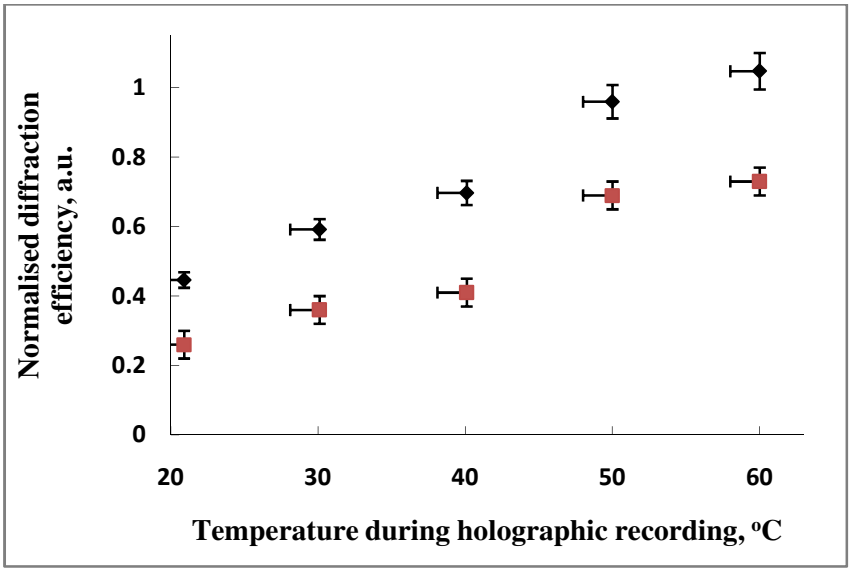

Figure 6.8. Normalised diffraction efficiency of transmission gratings recorded at different temperatures: (♦) - 1 day after recording and (■) - 3 days after recording.

The third approach was based on introducing glycerol as a plasticiser. Experimental data are presented in the following section.

6.4.5. Effect of glycerol on stability of the diffraction efficiency

In order to stabilise the diffraction efficiency, glycerol as a plasticiser was introduced into the photopolymer composition. Previously, it was shown that the addition of glycerol promoted diffusion of monomer molecules during holographic recording, improved the stability of created photonic structures and improved exposure sensitivity of the material [26].

During the development of the photopolymer composition the concentration of glycerol was optimised by finding the minimum concentration that it would still provide improvement in the stability of the diffraction efficiency. This was carried out in order to maintain the low permeability of the matrix to water molecules and avoid unwanted sensitivity to humidity changes. In composition for transmission mode of recording, the

optimum content of glycerol was determined as 0.2 ml in 18.2 ml of the photopolymer solution.

The addition of glycerol had two positive effects on the performance of the NIPA-based photopolymer. Firstly, the exposure sensitivity of the material was improved. As shown in Chapter 4, section 4.2.1, photopolymer systems containing NPG as the initiator suffered from the lower exposure sensitivity. Figure 6.9 shows the growth curve of the diffraction efficiency of transmission gratings recorded in the photopolymer layers without and with addition of glycerol. Recording intensity was 5 mW/cm^2. As can be seen from Figure 6.9, the exposure sensitivity of the photopolymer composition containing glycerol is higher. Transmission gratings with the diffraction efficiency of 37 % and 54 % can be recorded in layers without and with addition of glycerol after exposure for 70 sec, respectively.

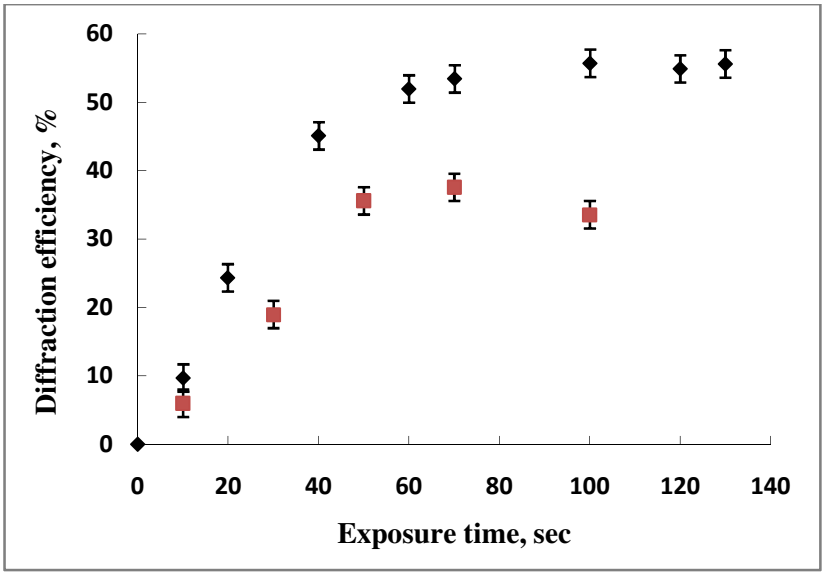

Figure 6.9. Growth of the diffraction efficiency of transmission gratings recorded in the photopolymer composition without (■) and with (♦) addition of glycerol. The thickness of the layers was 90 μm.

Secondly, the addition of glycerol improved the stability of the created photonic structures. Experimental data on stability of gratings recorded in photopolymer composition with addition of glycerol is presented in Figure 6.10.

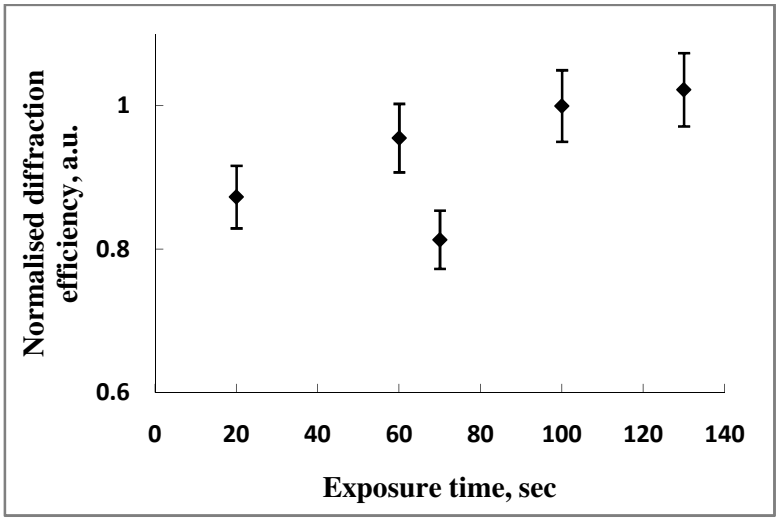

Figure 6.10. Normalised diffraction efficiency of transmission gratings recorded in the photopolymer composition containing glycerol *versus* exposure time.

Normalised diffraction efficiency was calculated as the ratio of the diffraction efficiency measured in 24 hours after recording and the diffraction efficiency measured immediately after recording. The diffraction efficiency of gratings recorded with 20, 60 and 70 sec exposure time was found to decrease up to 20 % within 24 hours after recording. The decay was 3 times less than one observed in the photopolymer composition without addition of glycerol (Figure 6.6). The gratings recorded with the exposure time of 100 sec and 130 sec had unchanged diffraction efficiency in 24 hours after recording. In two weeks after recording a few percent decrease of the diffraction efficiency of gratings recorded with the exposure time of 100 sec and 130 sec was observed. In order to prevent the decay of the diffraction efficiency of gratings recorded with relatively short exposure time less than 70 sec (Figure 6.10), the gratings were UV-

cured. Experimental data are presented in section 6.4.6.

6.4.6. Effect of UV-curing on stability of the diffraction efficiency

Effect of UV-curing on the stability of the diffraction efficiency of transmission gratings recorded using the recording intensity of 5 mW/cm^2 and different exposure times was investigated. After the recording, the gratings were exposed to UV-light with the intensity of 2.5 mW/cm^2 utilising a UV Exposure unit. Normalised diffraction efficiency of transmission gratings *versus* UV-light exposure time is presented in Figure 6.11.

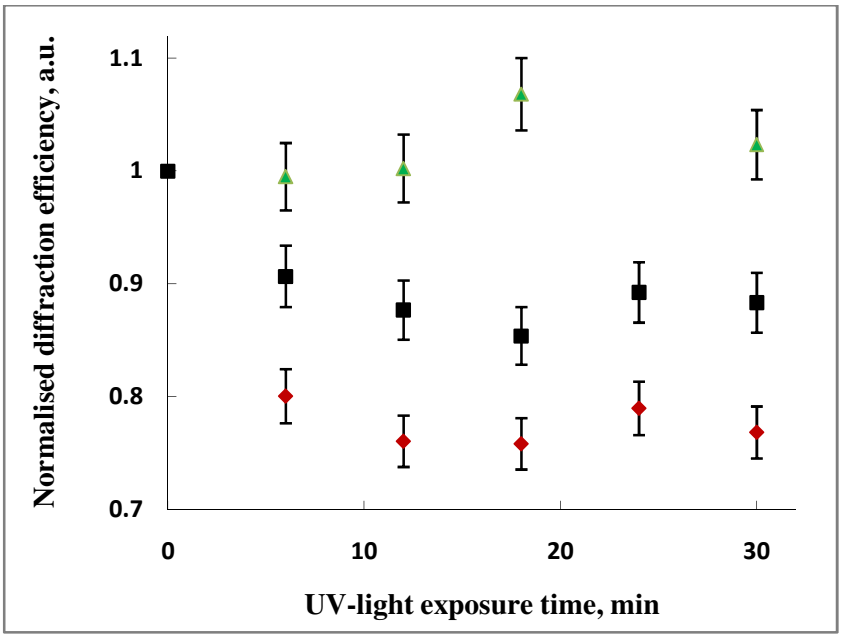

Figure 6.11. Normalised diffraction efficiency of transmission gratings recorded with 20 sec (♦), 70 sec (■) and 100 sec (▲) exposure time *versus* UV-light exposure time.

Normalised diffraction efficiency was calculated as the ratio of the diffraction efficiency measured after certain time of UV-curing and the diffraction efficiency measured immediately after recording. As can be seen, the trend of the diffraction efficiency

under exposure to UV-light was the same for samples with 20 sec and 70 sec recording times. The diffraction efficiency decreased and it reached its minimum value after 12 min of UV-exposure. The sample recorded with 20 sec exposure time showed bigger decay of the diffraction efficiency. This was attributed to the higher concentration of unreacted monomers left after recoding in dark regions. Polymerisation of monomers under uniform UV-light led to the increase of the refractive index in both bright and dark regions. However, the increase of the refractive index in dark regions was bigger than in bright regions which led to the overall decrease of the refractive index modulation and, hence, the diffraction efficiency decrease.

The diffraction efficiency of the grating recorded with 100 sec exposure time was unchanged under UV-exposure for the period of up to 12 min. This experimental data supported the discussion above. During recording for longer time most of monomers were consumed and UV-exposure did not cause any decrease of the diffraction efficiency due to uniform polymerisation of unreacted monomers.

It should be noted that a few percent increase of the diffraction efficiency recorded with 100 sec exposure time was observed for longer time of UV-exposure. This was probably due to the erasing of spatial variation of the molar refraction which led to the increase of the refractive index modulation (Figure 4.6a). Further monitoring of the diffraction efficiency of UV-cured samples for the period of 14 days after the recording showed that the diffraction efficiency was unchanged.

Thus, the addition of glycerol in the photopolymer composition and UV-curing allowed stabilising the diffraction efficiency of transmission gratings recorded in the NIPA-based photopolymer composition. Further optimisation of the photopolymer composition is presented in section 6.4.7.

6.4.7. Optimisation of the photoinitiating system

The optimisation of the photoinitiating system was carried out in order to improve the sensitivity of the material. The optimum concentrations of the light absorbing component (Erythrosin B) and NPG were obtained by determining the maximum achievable refractive index modulation during holographic recording. Refractive index modulation was calculated using Equation (6.13). Experimental data for the refractive index modulation achieved during the recording of transmission gratings in layers containing different amount of Erythrosine B are presented in Figure 6.12.

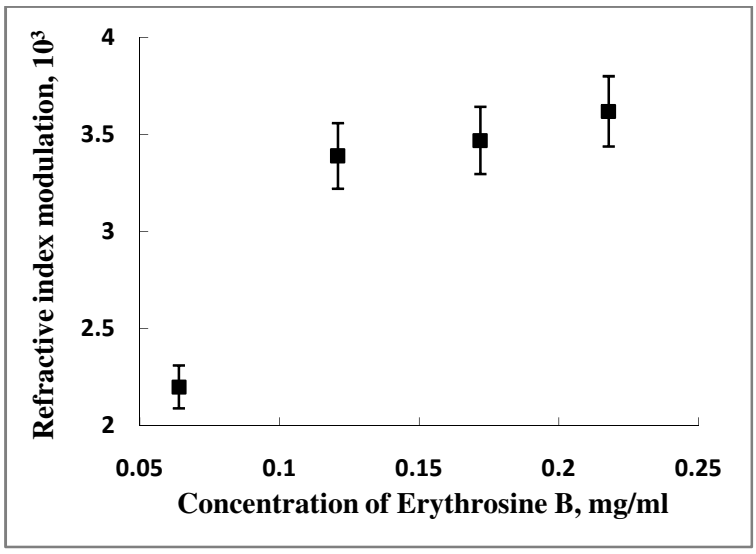

Figure 6.12. Refractive index modulation *versus* the concentration of Erythrosine B.

As can be seen, a little increase of the refractive index modulation was observed if the concentration of Erythrosine B was higher than 0.12 mg/ml in the photopolymer stock solution. The concentration of Erythrosine B of 0.12 mg/ml was found to be the optimum.

Experimental data for the refractive index modulation achieved during the recording of transmission gratings with the spatial frequency of 1000 lines/mm in layers containing different amount of NPG are presented in Figure 6.13.

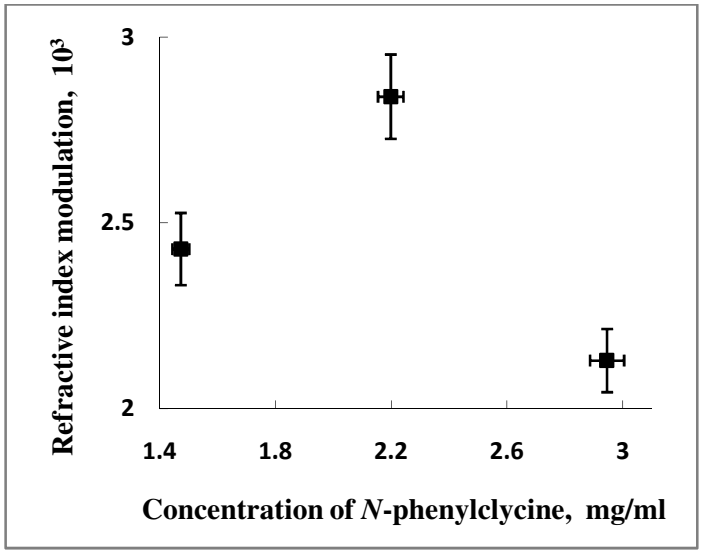

Figure 6.13. Refractive index modulation *versus* the concentration of *N*-phenylglycine.

The concentration of NPG of 2.2 mg/ml in the photopolymer stock solution was found to be the optimum. The optimised composition of the thermosensitive photopolymer for recording in transmission mode is presented in Table 6.1.

Table 6.1. Photopolymer composition for recording in transmission mode.

Chemical Reagent	**Concentration/ Molar Concentration**
Polyvinyl alcohol	8.79 % w/v
N-isopropylacrylamide	0.097 M
N, N'-methylenebisacrylamide	0.053 M
Erythrosin B	1.37×10^{-4} M
N-phenylglycine	0.0145 M
Glycerol	0.15 M

The photopolymer composition contains an inert polymeric binder (polyvinyl alcohol), a monomer (NIPA), a cross-linker (*N,N'*-methylenebisacrylamide), a photo-initiator (NPG), a plasticiser and a free radical scavenger (glycerol) and a light absorbing component (Erythrosin B). Further development of the material for holographic recording in reflection mode is presented in section 6.5.

6.5. Development of the photopolymer composition for reflection mode recording

6.5.1. Improvement of the spatial resolution

The photopolymer composition optimised for transmission mode recording (Table 6.1) was used as the starting composition during the development of the photopolymer composition for recording in reflection mode. In reflection mode, the material has to be able to achieve high spatial resolution. Spatial resolution can be manipulated by controlling the size of polymer chains during its growing and extending out/diffusing into the illuminated areas. In order to improve the spatial resolution of the material, the approach recently proposed in [27, 28] was utilised. It was observed that the combination of CTA such as citric acid with the free radical scavenger such as glycerol improved the spatial resolution of the photopolymer material and led to enhancement of the diffraction efficiency. Based on this approach, two modifications of the NIPA-based photopolymer composition were done. Firstly, citric acid was incorporated. Secondly, glycerol concentration was increased in comparison with the photopolymer composition for the transmission mode recording.

Addition of CTA to the photopolymer composition introduces the following reactions to the propagation stage during the polymerisation process. A CTA terminates the polymer chain and forms a new active radical capable of initiating the growth of a

new polymer chain [29]. The growing polymer chain $(M)_n$ reacts with CTA (XA) leading to the deactivation of the polymer chain radical:

$$(M)_n \bullet + XA = (M)_n - X + A \bullet . \quad (6.15)$$

The new radical $A\bullet$ is capable of the initiation and subsequent propagation of a new polymer chain:

$$A \bullet + M = M \bullet . \quad (6.16)$$

Thus, the addition of CTA to the photopolymer composition promotes the growth of shorter polymer chains and prevents their extending out of the bright fringe areas leading to the higher refractive index modulation and, hence, the diffraction efficiency.

In order to evaluate the effect of the addition of citric acid into the photopolymer composition on the diffraction efficiency, reflection gratings were recorded in photopolymer layers containing different concentration of citric acid (Table 6.2).

Table 6.2. Amount of citric acid in 18.2 ml of photopolymer solution for recording in reflection mode.

Citric Acid, g	**NIPA:CTA**
0.04	5
0.08	2.5
0.16	1.25
0.24	0.83

Different amounts of citric acid were added in order to manipulate the length of polymer chains. At higher concentration of citric acid, the shorter polymer chains can be formed. NIPA and citric acid ratios (NIPA:CTA) were 0.8, 1.25, 2.5 and 5 (Table 6.2). The

percentage concentration of glycerol in dry layers was same as in the photopolymer composition for transmission mode and it was found to be 11 % w/w.

Experimental data of the diffraction efficiency of gratings recorded in the photopolymer layers containing different NIPA:CTA ratios are presented in Figure 6.14.

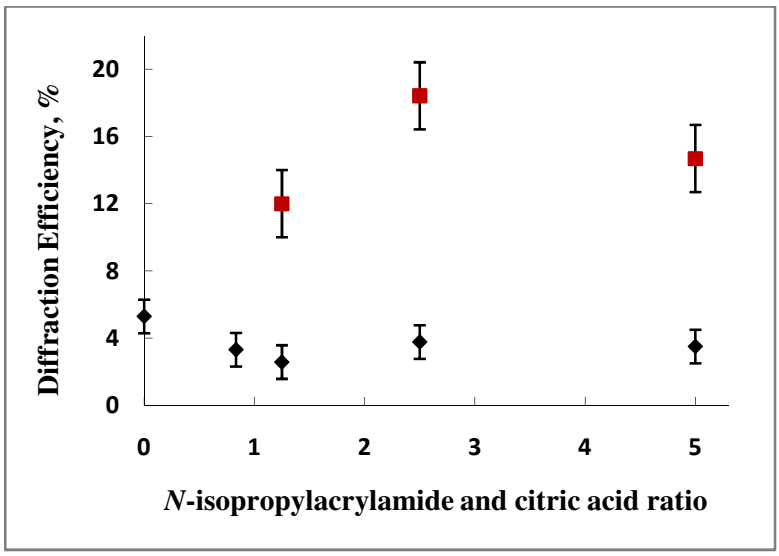

Figure 6.14. Diffraction efficiency of reflection gratings recorded in photopolymer layers with the percentage concentration of glycerol of 11 % (♦) and 38 % w/w (■) and different *N*-isopropylacrylamide and citric acid ratios.

As can be seen, no improvement of the diffraction efficiency is observed if the concentration of glycerol is 11 % w/w. The possible explanation is as follows. Addition of CTA promotes the growth of shorter polymer chains which are more mobile and can diffuse from the bright to dark regions [23, 30]. In order to limit the mobility of short chains, the permeability of the matrix must be decreased. It can be done by increasing the concentration of glycerol. Glycerol speeds up polymerisation leading to decreased permeability of the matrix and limited mobility of short chains.

In order to evaluate the effect of addition of glycerol along with citric acid into the photopolymer composition on the diffraction efficiency, reflection gratings were

recorded in the photopolymer layers contained 38 % w/w of glycerol. NIPA:CTA ratios were as shown in Table 6.2. Experimental data are presented in Figure 6.14.

As can be seen, the increase of glycerol concentration from 11 % to 38 % w/w allowed enhancing the diffraction efficiency from 6 to 19 %. Maximum diffraction efficiency of 19 % was achieved when NIPA:CTA ratio was 2.5. Thus, the improvement of the spatial resolution of the material and the diffraction efficiency can be explained by the effects of both CTA which promotes the growth of shorter chains and glycerol which restricts short polymer chain movement.

Further investigation of the effect of glycerol concentration on the performance of the photopolymer composition in the reflection mode was carried out. Reflection gratings were recorded in photopolymer layers containing different concentration of glycerol. The NIPA:CTA ratio was kept as 2.5. Refractive index modulation achieved during the recording *versus* the percentage concentration of glycerol in dry layers is presented in Figure 6.15.

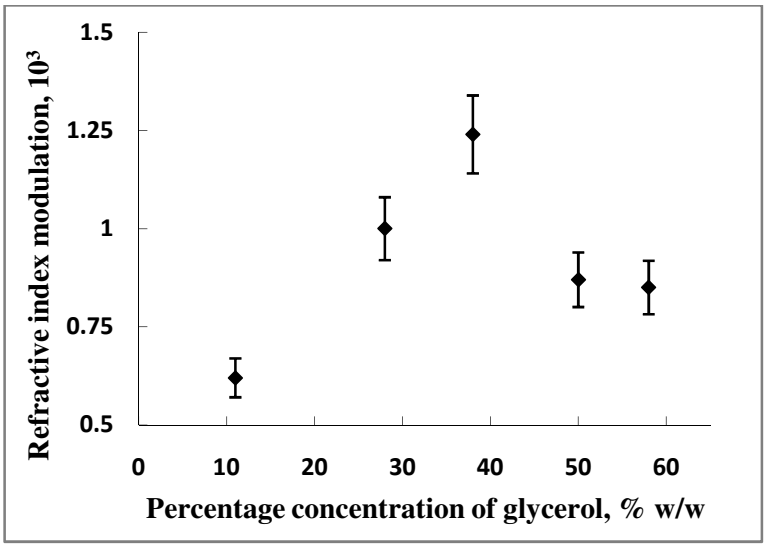

Figure 6.15. Refractive index modulation achieved during recording in reflection mode *versus* percentage concentration of glycerol in dry photopolymer layers.

Refractive index modulation was calculated using Equation (6.14). As can be seen from Figure 6.15, maximum refractive index modulation of 1.2×10^{-3} was achieve in layers containing 38 % w/w of glycerol. This concentration was found to be the optimum. The optimised photopolymer composition for recording in reflection mode is presented in Table 6.3.

Table 6.3. Photopolymer composition for recording in reflection mode.

Chemical Reagent	**Concentration/ Molar Concentration**
Polyvinyl alcohol	8.42 % w/v
N-isopropylacrylamide	0.093 M
N,N'-methylene bisacrylamide	0.051 M
Erythrosin B	1.32×10^{-4} M
N-phenylglycine	0.0139 M
Glycerol	0.72 M
Citric acid	0.022 M

The composition of the thermosensitive photopolymer for recording in reflection mode contains an inert polymeric binder (polyvinyl alcohol), a monomer (NIPA), a cross-linker (*N,N'*-methylenebisacrylamide), a photo-initiator (NPG), a plasticiser and a free radical scavenger (glycerol), a light absorbing component (Erythrosin B) and chain transfer agent such as citric acid. Investigation of the stability of the diffraction efficiency of reflection gratings is presented in section 6.5.2.

6.5.2. Diffraction efficiency of reflection gratings: dependence on time

Behavior of the diffraction efficiency of reflection gratings recorded in the NIPA-based photopolymer with time was investigated. To evaluate the changes in the diffraction efficiency, normalised diffraction efficiency was used. Normalised diffraction efficiency

was calculated as a ratio of the diffraction efficiency measured at certain time after the recording and the diffraction efficiency measured immediately after the recording. Figure 6.16 presents the time dependence of normalised diffraction efficiency of reflection gratings.

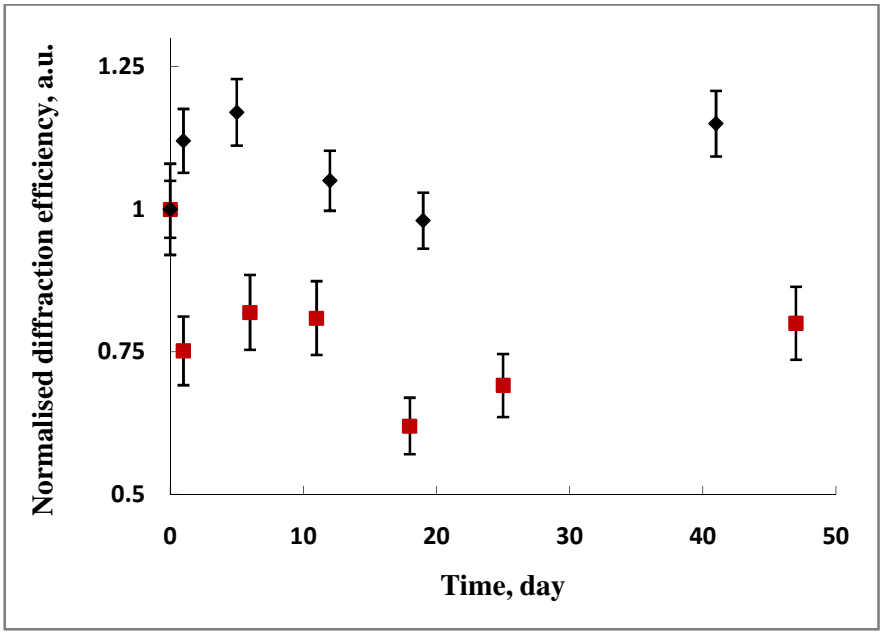

Figure 6.16. Time dependence of normalised diffraction efficiency of reflection gratings without (■) and with (♦) UV-curing.

As can be seen, the decay of the diffraction efficiency up to 35 % was observed. In order to prevent the decay of the diffraction efficiency, the reflection gratings were UV-cured for 99 sec with the total exposing intensity of 60 mW/cm^2. Experimental data are presented in Figure 6.16. The diffraction efficiency of gratings after UV-curing did not show any decay. The discrepancy can be attributed to the variations in the relative humidity during the measurements.

To investigate the effect of UV-curing on the diffraction efficiency, reflection gratings were exposed to UV-light for different exposure times. Dynamics of the

diffraction efficiency under UV-light exposure is presented in Figure 6.17.

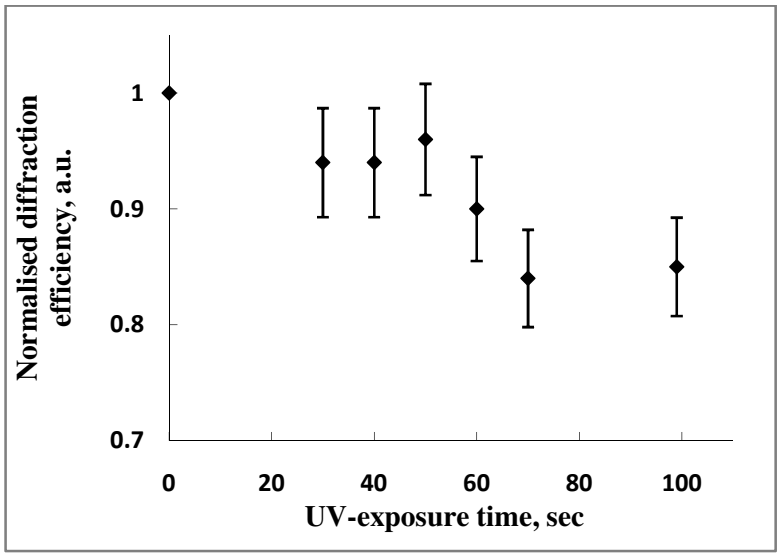

Figure 6.17. Normalised diffraction efficiency of reflection gratings *versus* UV-light exposure time.

Normalised diffraction efficiency was calculated as the ratio of the diffraction efficiency measured after certain time of UV-curing and the diffraction efficiency measured immediately after recording. As can be seen, UV-curing caused the decay of the diffraction efficiency which got it maximum value of 20 % after exposure for 70 sec. The decrease of the diffraction efficiency can be explained by uniform polymerisation of unreacted monomers.

6.6. Conclusions

A novel photopolymer composition containing *N*-isopropylacrylamide as the main monomer for holographic recording in transmission and reflection modes was developed. The novel composition has an advantage over acrylamide – based materials due to its lower toxicity. Although the new formulation did allow grating formation,

initial challenges included low diffraction efficiency and the decay of the diffraction efficiency over quite short time periods. After optimisation the composition allows the recording of stable transmission gratings. The ability of glycerol to prevent the decay of the diffraction efficiency of transmission gratings due to improved diffusion rate of monomers was demonstrated. Addition of glycerol along with citric acid was found to improve the spatial resolution of the material and enhance the diffraction efficiency of reflection gratings from 6 to 19 %. The investigation of the effect of UV-curing on the shelf life of gratings was carried out. Exposure to UV-light was found to stabilise the diffraction efficiency of the grating recorded in both reflection and transmission modes.

References

1. Raghavendra, J., *Optimisation of an acrylamides-based photopolymer for reflection holographic recording*. (Doctoral Thesis), 2005. Dublin : Dublin Institute of Tecnology.
2. Schild, H.G., *Poly(N-isopropylacrylamide): experiment, theory and application.* Progress in Polymer Science, 1992. **17**(2): p. 163-249.
3. Yamaoka, T., Zhang, Y.-C. and Koseki, K.I., *N-phenylglycine-(thio)xanthene dye photoinitiating system and application to photopolymer for visible laser exposure.* Journal of Applied Polymer Science, 1989. **38**(7): p. 1271-1285.
4. Matyjaszewski, K. and Davis, T.P., *Handbook of radical polymerisation*. John Wiley and Sons 2002.
5. Munk, P. and Aminabhavi, T.M., *Introduction to macromolecular science*. New York: John Wiley and Sons 2002.
6. Oster, G. and Adelman, A.H., *Long-lived states in photochemical reactions. I. Photoreduction of eosin.* Journal of the American Chemical Society, 1956. **78**(5): p. 913-916.
7. Gleeson, M.R., Liu, S., McLeod, R.R. and Sheridan, J.T., *Nonlocal photopolymerisation kinetics including multiple termination mechanisms and dark reactions. Part II. Experimental validation.* Journal of the Optical Society of America B, 2009. **26**(9): p. 1746-1754.
8. Kogelnik, H., *Coupled wave theory for thick hologram gratings.* The Bell System Technical Journal, 1969. **48**(9): p. 2909-2947.
9. Cody, D., *Low-toxicity diacetone acrylamide-based photopolymer for applications in holography*. 2014, Dublin Institute of Technology: Dublin.

10. Specht, E.H., Valley, H., Neuman, A., Hills, N. and Neher, H.T, *Preparation of Acrylamides*. 1956, US Patent 2773063A.

11. Heskins, M. and Guillet, J.E., *Solution properties of poly(N-isopropylacrylamide).* Journal of Macromolecular Science: Part A - Chemistry, 1968. **2**(8): p. 1441-1455.

12. Deshmukh, M.V., Vaidya, A.A, Kulkarni, M.G., Rajamohanan, P.R. and Ganapathy, S., *LCST in poly(N-isopropylacrylamide) copolymers: high resolution proton NMR investigations.* Polymer, 2000. **41**(22): p. 7951-7960.

13. Hashimoto, K., Sakamoto, J. and Tanii, H., *Neurotoxicity of acrylamide and related compounds and their effects on male gonads in mice.* Archives of Toxicology, 1981. **47**(3): p. 179-189.

14. Tanii, H. and Hashimoto, K., *Neurotoxicity of acrylamide and related compounds in rats.* Archives of Toxicology, 1983. **54**(3): p. 203-213.

15. Haraguchi, K., Takehisa, T. and Ebato, M., *Control of cell cultivation and cell sheet detachment on the surface of polymer/clay nanocomposite hydrogels.* Biomacromolecules, 2006. **7**(11): p. 3267-3275.

16. Islam, M., Ahiabu, A., Li, X. and Serpe, M., *Poly (N-isopropylacrylamide) microgel-based optical devices for sensing and biosensing.* Sensors, 2014. **14**(5): p. 8984-8995.

17. Kopeček, J., *Smart and genetically engineered biomaterials and drug delivery systems.* European Journal of Pharmaceutical Sciences, 2003. **20**(1): p. 1-16.

18. Nguyen, K.T. and West, J.L., *Photopolymerizable hydrogels for tissue engineering applications.* Biomaterials, 2002. **23**(22): p. 4307-4314.

19. Ravichandran, P., Shantha, K.L. and Rao, K.P., *Preparation, swelling characteristics and evaluation of hydrogels for stomach specific drug delivery.* International Journal of Pharmaceutics, 1997. **154**(1): p. 89-94.

20. Craciunescu, I., Nan, A., Turcu, R., Kacso, I., Bratu, I., Leostean, C. and Vekas, L., *Synthesis, characterization and drug delivery application of the temperature responsive pNIPA hydrogel.* Journal of Physics, Conference Series, 2009. **182**: p. 012060

21. Martin, S., Leclere, P., Renotte, Y., Toal, V. and Lion, Y., *Characterization of an acrylamide-based dry photopolymer holographic recording material.* Optical Engineering, 1994. **33**(12): p. 3942-3946.

22. Leite, E., *Photopolymerizable Nanocomposites for Holographic Applications.* (Doctoral Thesis), 2010. Dublin : Dublin Institute of Tecnology.

23. Babeva, T., Naydenova, I., Mackey, D., Martin, S. and Toal, V., *Two-way diffusion model for short-exposure holographic grating formation in acrylamide-based photopolymer.* Journal of the Optical Society of America B, 2010. **27**(2): p. 197-203.

24. Munk, P. and Aminabhavi, T.M., *Introduction to macromolecular science*: Wiley, Hoboken, 2002.

25. Huang, M., Yao, H., Chen, Z., Hou, L. and Gan, F., *The changes of holographic characteristics of photopolymer induced by temperature.* Chinese Optics Letters, 2003. **1**(1): p. 41-43.

26. Cody, D., Naydenova, I. and Mihaylova, E., *Effect of glycerol on a diacetone acrylamide-based holographic photopolymer material.* Applied Optics, 2013. **52**(3): p. 489-494.

27. Mihaylova, E., Cody, D., Naydenova, I., Martin, S. and Toal, V., *Diacetone-Acrylamide Based Pressure Sensitive Photopolymer*, 2014, Patent Application No. GB1411640.4.

28. Cody, D., Gribbin, S., Mihaylova, E. and Naydenova, I., *Low-toxicity photopolymer for reflection holography.* ACS Applied Materials & Interfaces, 2016. **8**(28): p. 18481-18487.

29. Furuncuoğlu, T., Uğur, İ., Değirmenci, I. and Aviyente, V., *Role of chain transfer agents in free radical polymerisation kinetics.* Macromolecules, 2010. **43**(4): p. 1823-1835.

30. Martin, S., Naydenova, I., Jallapuram, R., Howard, R.G. and Toal, V., *Two way diffusion model for the recording mechanism in a self developing dry acrylamide photopolymer*. SPIE Proceedings, 2006. **6252**: p. 625205.

7. HOLOGRAPHIC PERFORMANCE OF *N*-ISOPROPYLACRYLAMIDE-BASED PHOTOPOLYMER

7.1. Introduction

The design of the novel NIPA-based photopolymer composition has been reported in Chapter 6. Stable photopolymer layers were developed and holographic gratings with stable diffraction efficiency were recorded in both transmission and reflection modes. In order to achieve the full potential of the photopolymer composition, a characterisation of the holographic recording capabilities of the material must be carried out. Holographic recording at optimum recording conditions allows achieving the maximum refractive index modulation of the photopolymer material which provides the diffraction efficiency of the grating up to 100 % [1, 2]. Holographic gratings can operate as a diffraction grating, a spectral filter, a lens, a beam splitter and other optical components [3-6]. Depending on the application of the holographic grating, different values of the diffraction efficiency are needed. For example, if a holographic grating functions as a beam splitter, a specific value of the diffraction efficiency is required to get a certain beam ratio. This can be achieved by recording at specific conditions obtained by the characterisation of the holographic performance of the material. If a holographic grating acts as a sensor providing a visual read-out, high diffraction efficiency is essential [7].

The aim of the research presented in this chapter is to characterise the holographic performance of the NIPA-based photopolymer in both transmission and reflection modes and to identify the optimum recording conditions at the spatial frequencies of 300, 1000 and 2700 lines/mm in transmission mode and 2700 lines/mm in reflection mode. These spatial frequency values span the range of values expected to be used in sensing applications, from low spatial frequency transmission diffractive

optical elements to the typical reflection-image holograms used in colour-changing indicators.

7.2. Experimental

The photopolymer compositions used for recording in transmission and reflection modes are presented in Table 6.1 and 6.3, respectively. The photopolymer solution was prepared by mixing all the components using a magnetic stirrer in a dark room as described in Chapter 6, section 6.3.1. Photopolymer layers with the thickness varying from 20 to 115 μm were prepared by deposition of the appropriate amount of photopolymer solution on the levelled glass slides (76 × 26 mm^2) and drying for 24 hours in a dark room at temperature of 21 ± 2 ^oC and the relative humidity of 35 ± 5 %. According to our estimations, in order to get 100 μm thick layers, 3 ml and 1.5 ml of the photopolymer solution for recording in transmission and reflection modes, respectively, should be used. The thickness of the dry layers was measured with a white light interferometric surface profiler MicroXAM S/N 8038.

Transmission and reflection volume phase unslanted gratings were recorded using the set-up presented in Figure 6.2a and 6.2b, accordingly. The photopolymer layers were exposed to two beams of 532 nm wavelength obtained by splitting a Nd:YVO_4 laser beam. In order to characterise the holographic performance of the photopolymer composition and to identify the optimum recording conditions, recording time and total recording intensity were varied. The details are presented in section 7.3.

In transmission mode recording (Figure 6.2a), the angle of the recording beams (outside the layer) with respect to the normal to the layer surface was adjusted as 4.6 ± 0.5^o, 15.5 ± 0.5^o and 46 ± 0.5^o to record diffraction gratings with a spatial frequency of 300 ± 33, 1000 ± 32 and 2700 ± 22 lines/mm, respectively. To identify the

maximum achievable diffraction efficiency at different spatial frequencies, real-time diffraction efficiency growth curves were recorded using a 633 nm probe beam from He-Ne laser. The intensity of the diffracted beam was monitored by means of an optical power meter (Newport 1830-C) and the acquired data were transferred to a computer. The diffraction efficiency of the transmission gratings was calculated as the ratio of the intensity of the diffracted beam and the intensity of the incident beam.

In reflection mode recording, diffraction gratings with a spatial frequency of 2700 ± 44 lines/mm were recorded using a set-up presented in Figure 6.2b. The diffraction efficiency was monitored using a 532 nm beam from Nd:YVO_4 laser and was determined as the ratio of the intensity of the diffracted beam and the difference of the intensities of the incident beam and the reflected beam (Equation 6.12). During the measurements the intensity of the probing beam was 0.7 mW/cm^2 in order to minimise the polymerisation of unreacted monomers under uniform illumination.

Quantitative analysis of the refractive index modulation of the material achieved during holographic recording was carried out as described in Chapter 6, section 6.3.4. The applicability of the coupled wave theory was justified by calculation of Q factor using Equation (2.1). In the present research, Q factor for the gratings with a spatial frequency of 300 lines/mm and with the thickness ranging from 30 to 90 μm was found to be in the range from 6 to 18. Q factor for the gratings with a spatial frequency of 1000 lines/mm and with the thickness ranging from 30 to 90 μm was estimated to be in the range from 67 to 202. For the gratings with a spatial frequency of 2700 lines/mm and thickness ranging from 20 to 115 μm, Q factor was calculated to be in the range from 326 to 1878. This allowed applying the coupled wave theory for the evaluation of the refractive index modulation achieved during holographic recording. Equations (6.13) and (6.14) were utilised for transmission mode and reflection mode, respectively.

7.3. Characterisation of the holographic recording capabilities of the NIPA-based photopolymer

7.3.1. Diffraction efficiency

7.3.1.1. Transmission gratings with spatial frequencies of 300, 1000 and 2700 lines/mm

Holographic recording capabilities of the NIPA-based photopolymer in transmission mode were investigated by recording unslanted transmission volume phase gratings at spatial frequencies of 300 ± 33, 1000 ± 32 and 2700 ± 22 lines/mm. The spatial frequency of 300 lines/mm was found to be close to the minimum spatial frequency at which the condition for a volume grating is satisfied for 30 μm thick layer and 532 nm wavelength recording light. At the spatial frequency of 200 lines/mm the recorded holographic gratings could have properties of both volume and plain gratings as Q–factor calculated using Equation (2.1) was about 2. The spatial frequency of 2700 lines/mm was chosen as it was close to the maximum spatial frequency achievable in transmission mode recording with 532 nm wavelength light and also achievable in reflection mode recording. Holographic recordings were carried out at different total recording intensities and exposure time to identify the optimum recording conditions.

Figure 7.1 shows typical diffraction efficiency growth curves for transmission gratings with the spatial frequency of 300 lines/mm recorded using the total recording intensity of 2, 4 and 6 mW/cm^2. The thickness of the layers was 60 ± 5 μm. As seen from Figure 7.1, the photoresponse of the material is nonlinear due to complicated processes of polymerisation and diffusion resulting in the refractive index variation. The diffraction efficiency growth curve obtained by recording at 4 mW/cm^2 has lower slope probably due to losses of the diffraction efficiency caused by formation of higher orders

of diffraction because of creating non-sinusoidal profile of the refractive index modulation. At 300 lines/mm the total recording intensity of 2 mW/cm^2 was found to be the best of the three intensities that were studied as it allowed achieving maximum diffraction efficiency using minimum total exposure energy. The diffraction efficiency of 60 % was achieved in transmission gratings with a spatial frequency of 300 lines/mm after recording in 60 ± 5 μm thick layers with the total recording intensity of 2 mW/cm^2.

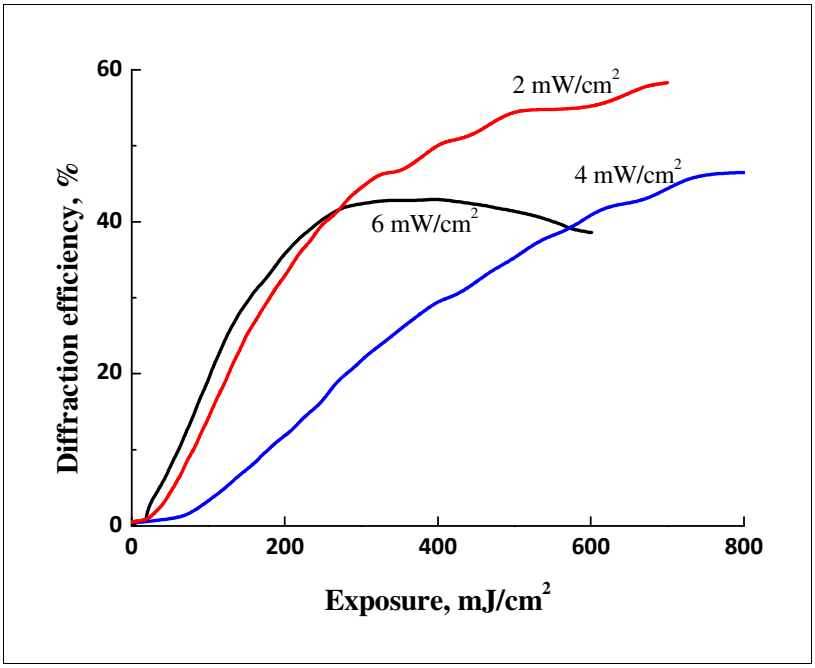

Figure 7.1. Diffraction efficiency growth curves for transmission gratings with a spatial frequency of 300 lines/mm. The total recording intensity was 2 mW/cm^2 (red line), 4 mW/cm^2 (blue line) and 6 mW/cm^2 (black line).

Figure 7.2 shows typical diffraction efficiency growth curves for transmission gratings with a spatial frequency of 1000 lines/mm recorded using the total recording intensity of 1, 2, 3 and 6 mW/cm^2. At 1000 lines/mm the total recording intensity of 2 mW/cm^2 is found to be the optimum to get maximum diffraction efficiency using minimum exposure energy. The diffraction efficiency of 80 % was achieved for

transmission gratings with a spatial frequency of 1000 lines/mm in 60 ± 5 μm thick layers. Exposure sensitivity was estimated from the linear part of the growth curve and it was found to be 0.0056 cm^2/mJ. As seen from Table 4.2, the NIPA-based photopolymer composition has better exposure sensitivity than AA-based photopolymer containing NPG as a photoinitiator (0.0047 cm^2/mJ) and it is lower than exposure sensitivity of AA-based photopolymer containing TEA as a photoinitiator (0.012 cm^2/mJ).

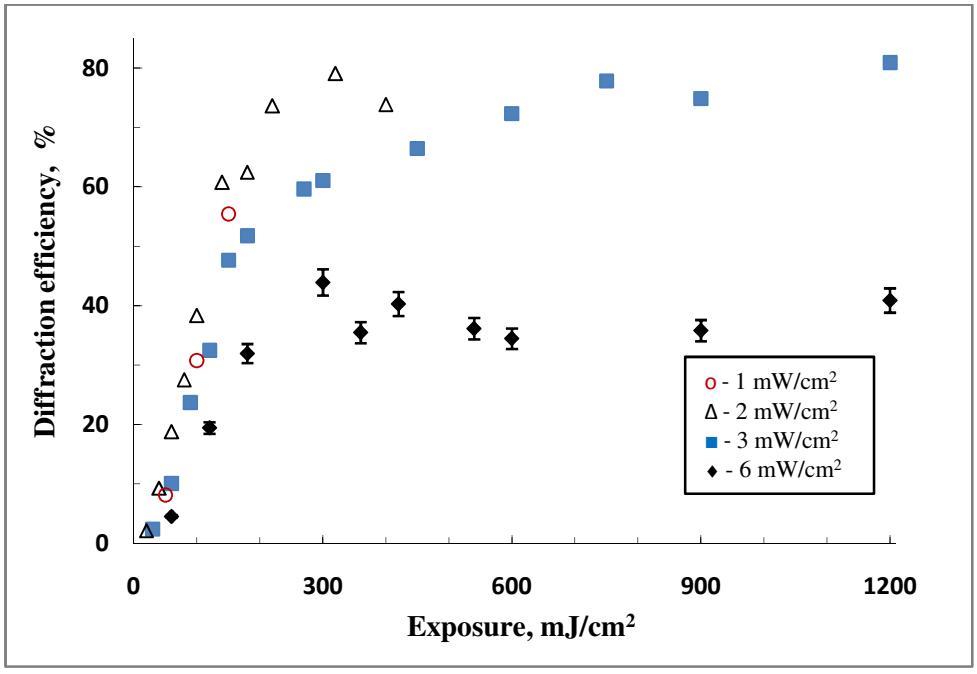

Figure 7.2. Diffraction efficiency growth curves for transmission gratings with a spatial frequency of 1000 lines/mm. The total recording intensity was 1 mW/cm^2 (o), 2 mW/cm^2 (Δ), 3 mW/cm^2 (■) and 6 mW/cm^2 (♦).

Figure 7.3 shows typical diffraction efficiency growth curves for transmission gratings with a spatial frequency of 2700 lines/mm. The total recording intensity was increased in comparison with the total recording intensity used during recordings at 300 and 1000 lines/mm in order to create shorter polymer chains and to improve the

refractive index modulation. The total recording intensity of 9.5 mW/cm^2 was found to be the optimum. At 2700 lines/mm the diffraction efficiency of 30 % was reached in 60 ± 5 μm thick layers after 63 seconds of exposure to the total recording intensity of 9.5 mW/cm^2.

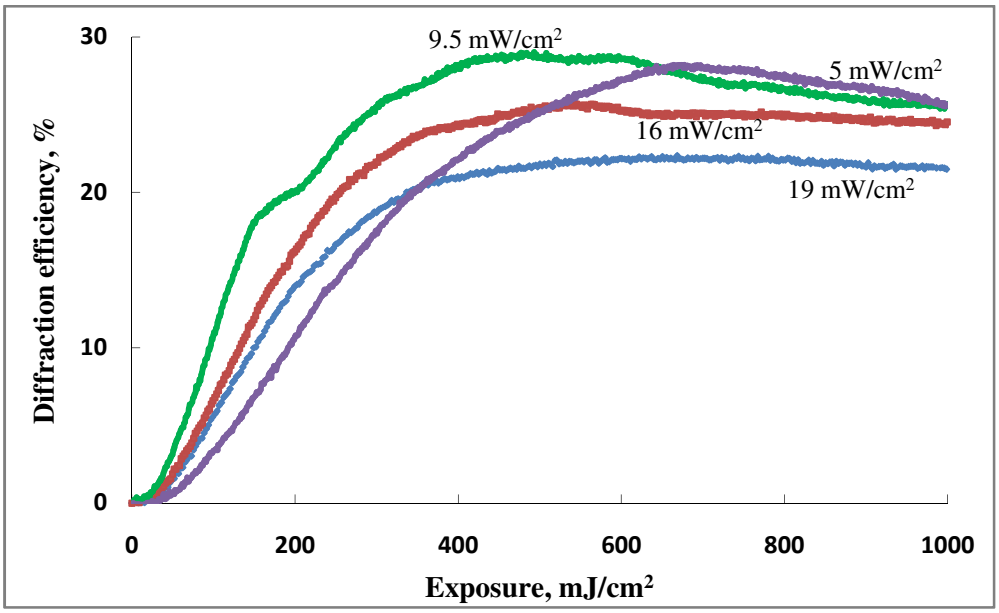

Figure 7.3. Diffraction efficiency growth curves for transmission gratings with a spatial frequency of 2700 lines/mm. The total recording intensity was 5 mW/cm^2 (purple line), 9.5 mW/cm^2 (green line), 16 mW/cm^2 (red line) and 19 mW/cm^2 (blue line).

7.3.1.2. Reflection gratings with a spatial frequency of 2700 lines/mm

The holographic recording capabilities of the NIPA-based photopolymer in reflection mode were investigated by recording reflection volume phase gratings at a spatial frequency of 2700 ± 44 lines/mm. The spatial frequency of 2700 lines/mm was used as it was close to the minimum spatial frequency available for recording in reflection mode at 532 nm wavelength light. In reflection mode, the spatial period is in the range from 0.37 μm to 0.18 μm when the spatial frequency is varying from 2700 to 5600 lines/mm.

The better performance of the material is expected at the lower spatial frequency as the higher refractive index modulation amplitude can be achieved at bigger spatial period.

Reflection gratings were recorded using the total recording intensity of 6, 8.2 and 10.5 mW/cm^2. The total recording intensity of 10.5 mW/cm^2 was the maximum achievable intensity for used recording set-up. Experimental data of the diffraction efficiency versus exposure energy are presented in Figure 7.4. The thickness of the layers was 60 ± 5 μm.

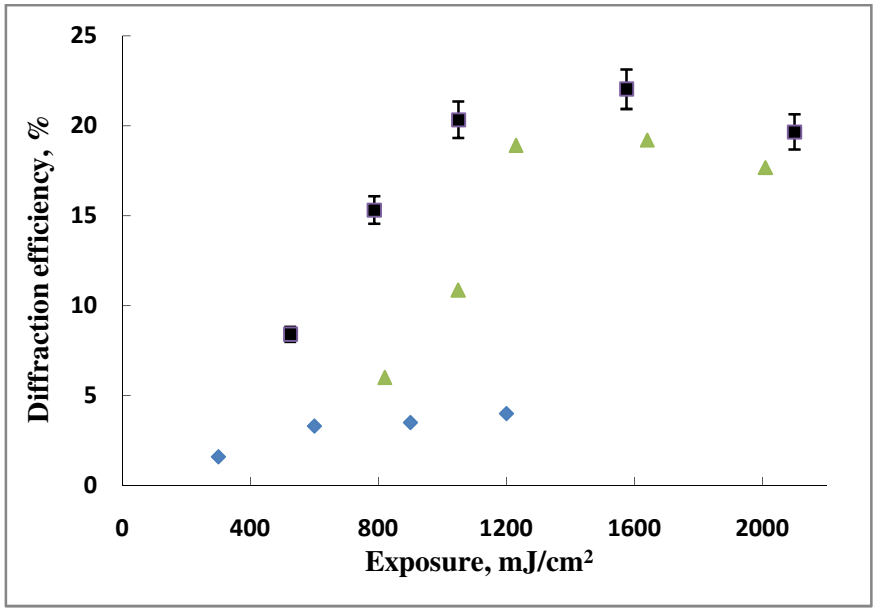

Figure 7.4. Diffraction efficiency growth curves for reflection gratings with a spatial frequency of 2700 lines/mm. The total recording intensity was 6 mW/cm^2 (♦), 8.2 mW/cm^2 (▲) and 10.5 mW/cm^2 (■).

As seen from Figure 7.4, the diffraction efficiency of 20 % was obtained for the exposure energy of 1050 mJ/cm^2 and the total recording intensity 10.5 mW/cm^2. Further increase of the exposure energy up to two times did not lead to the improvement of the diffraction efficiency. A possible explanation is that at the exposure energy of 1050 mJ/cm^2 the available dynamic range of the material has been fully used up.

Holographic recording capabilities of the NIPA-based photopolymer as a function of the recording intensity, the exposure energy and the spatial frequency have been investigated in transmission and reflection modes. The NIPA-based photopolymer is capable of recording in both transmission and reflection modes and the diffraction efficiency of 80 % and 20 % can be reached, respectively, using optimum recording conditions. Optimum conditions for recordings in transmission and reflection modes are summarised in Table 7.1.

Table 7.1. Holographic recording characteristics of the NIPA-based photopolymer

Recording Mode	**Spatial Frequency, lines/mm**	**Optimum Total Recording Intensity, mW/cm^2**	**Total Exposure, mJ/cm^2**	**Diffraction Efficiency, % (60 ± 5 μm thick layers)**
Transmission	300	2.0	700	60
Transmission	1000	2.0	320	80
Transmission	2700	9.5	600	30
Reflection	2700	10.5	1050	20

7.3.2. Refractive index modulation

Refractive index modulation is one of the most important parameters of a holographic recording material. High refractive index modulation allows high diffraction efficiency to be obtained in the holographic gratings. Characterisation of the refractive index modulation achieved during holographic recoding in the NIPA-based photopolymer was carried out in both transmission and reflection modes. Refractive index modulation as a function of the spatial frequency and the thickness of the grating was investigated. Refractive index modulation achieved during holographic recording in transmission

mode and reflection mode was calculated using Equation (6.13) and (6.14), respectively. Experimental data are presented in the following sections.

7.3.2.1. Transmission gratings with a spatial frequency of 300 lines/mm

Experimental data of the refractive index modulation for transmission gratings recorded in layers with the thickness ranging from 30 to 110 μm and at a spatial frequency of 300 ± 33 lines/mm using the total recording intensity of 2, 4, 6 mW/cm^2 are shown in Figure 7.5.

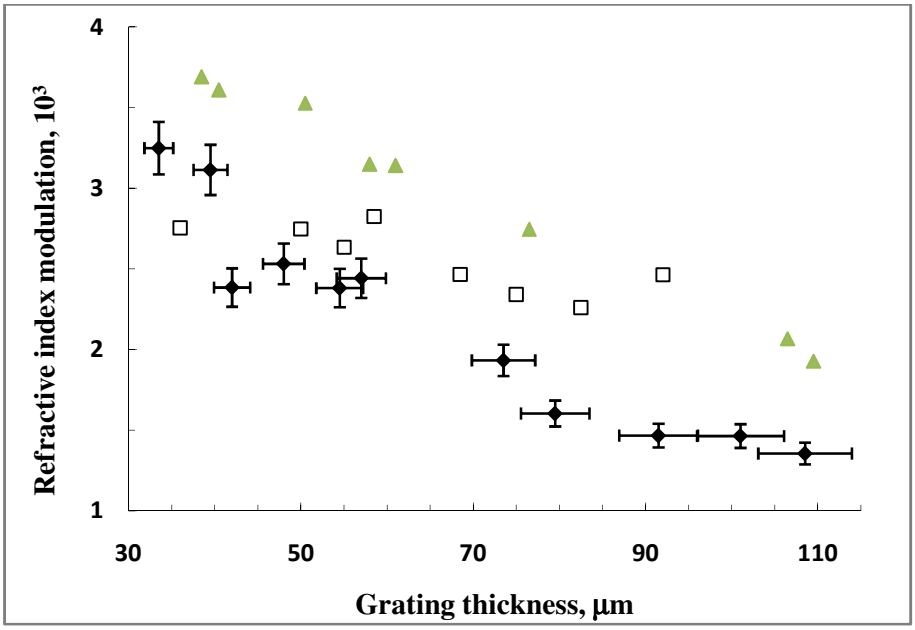

Figure 7.5. Refractive index modulation *versus* the thickness of transmission gratings recorded at a spatial frequency of 300 lines/mm. The total recording intensity was 2 mW/cm^2 (▲), 4 mW/cm^2 (□) and 6 mW/cm^2 (♦).

The photoinduced refractive index modulation was found to depend on the thickness of the grating. The decrease of the refractive index modulation with increasing thickness was observed. Possible reason is the material absorption of the incident light beams during recording process. This effect becomes more pronounced in the thick layers

leading to the incident light intensity losses and the decrease of the refractive index modulation.

Absorbance of the NIPA-based photopolymer layers at 532 nm wavelength was tested for samples with the thickness ranging from 45 to 90 μm. Absorbance at 532 (A_{532}) nm was estimated as:

$$A_{532} = -\log\left(\frac{I_{transm}}{I_{in}}\right) \quad (7.1),$$

where I_{transm} is the intensity of the beam transmitted by the photopolymer layer and I_{in} is the intensity of the beam incident on the layer. Experimental data on absorbance of the photopolymer layers with different thickness are presented in Table 7.2.

Table 7.2. Absorbance of NIPA-based photopolymer layers at 532 nm wavelength.

Thickness of the layer	45 ± 5μm	58 ± 5 μm	67 ± 5 μm	90 ± 5 μm
Absorbance	0.89	1.14	1.36	1.51

As can be seen from Table 7.2, absorbance of the photopolymer layer highly depends on the layer thickness, i.e. it increases with increasing thickness. Thus, the refractive index modulation decrease in thick gratings observed in Figure 7.5 can be explained by increasing absorbance of the material with increasing thickness of the layers. Maximum refractive index modulation of 3.7×10^{-3} was achieved in a 38 μm thick layer after exposure to the optimum total recording intensity of 2 mW/cm^2 obtained in section 7.3.1. Exposure time was 350 sec. After exposure to the optimum total recording intensity of 2 mW/cm^2 minimum refractive index modulation of 1.9×10^{-3} was obtained in a 110 μm thick layer.

As seen from Figure 7.5, refractive index modulation also depends on the total recording intensity. The refractive index modulation achieved after exposure to the total recording intensity of 2 mW/cm^2 was higher than the refractive index modulation obtained after exposure to 4 and 6 mW/cm^2. This can be attributed to the polymer chain length created during holographic recording. Lower recording intensity leads to longer polymer chains in bright fringes providing higher density and, as a result, higher refractive index modulation.

7.3.2.2. Transmission gratings with a spatial frequency of 1000 lines/mm

Experimental results of the refractive index modulation for transmission gratings recorded at a spatial frequency of 1000 ± 32 lines/mm using the total recording intensity of 2, 3, 6 mW/cm^2 in layers with thickness ranging from 45 to 98 μm are shown in Figure 7.6.

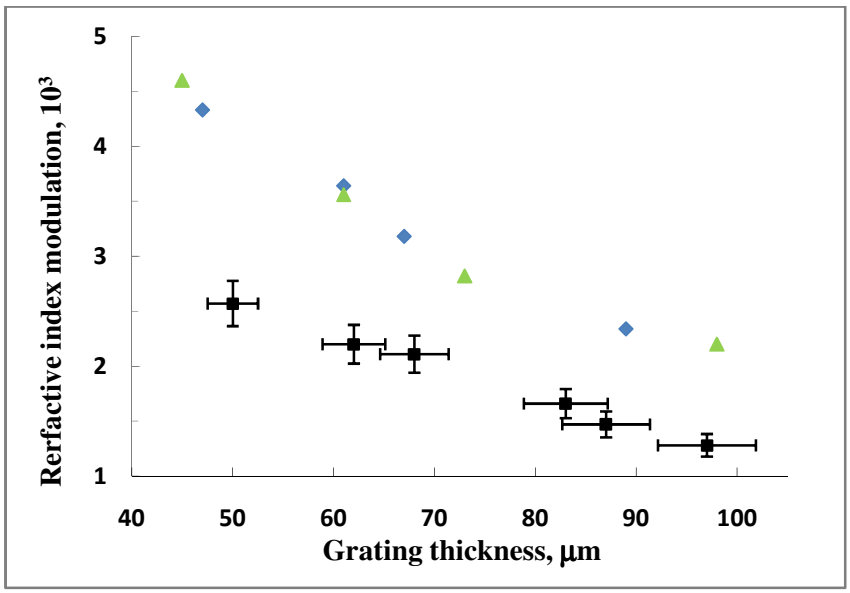

Figure 7.6. Refractive index modulation *versus* the thickness of transmission gratings recorded at a spatial frequency of 1000 lines/mm. The total recording intensity was 2 mW/cm^2 (▲), 3 mW/cm^2 (♦) and 6 mW/cm^2 (■).

As seen from Figure 7.6, the refractive index modulation depends on the thickness of the grating and the total recording intensity. Thickness dependence of the refractive index modulation can be explained by increased absorption of the material with increasing thickness as discussed in section 7.3.2.1. Intensity dependence of the refractive index modulation can be attributed to the formation of polymer chains with different length as in the case of the spatial frequency of 300 lines/mm discussed in section 7.3.2.1. Maximum refractive index modulation of 4.5×10^{-3} was achieved in a 45 μm thick layer after exposure to the optimum total recording intensity of 2 mW/cm^2 for 160 sec. After exposure to the optimum total recording intensity of 2 mW/cm^2 minimum refractive index modulation of 2.2×10^{-3} was obtained in a 98 μm thick layer.

7.3.2.3. Transmission gratings with a spatial frequency of 2700 lines/mm

Experimental results of the refractive index modulation for transmission gratings recorded in layers with thickness ranging from 30 to 85 μm and at a spatial frequency of 2700 ± 22 lines/mm using the total recording intensity ranging from 3 to 19 mW/cm^2 are shown in Figure 7.7. The total exposure energy of 600 mJ/cm^2 was used as it was identified to be optimum total exposure energy (Table 7.1).

As seen from Figure 7.7, the dependence of the refractive index modulation on the grating thickness is not as strong as observed at the spatial frequency of 300 lines/mm (Figure 7.5) and 1000 lines/mm (Figure 7.6). Holographic recordings at 2700 lines/mm were carried out using the higher total recording intensity than in the case of 300 and 1000 lines/mm in order to create shorter polymer chains and achieve better spatial resolution of the material.

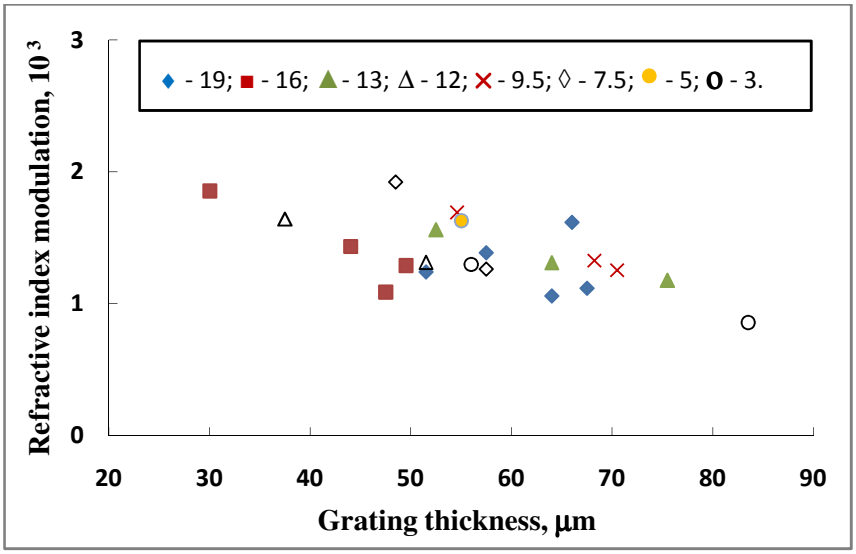

Figure 7.7. Refractive index modulation *versus* the thickness of transmission gratings recorded at a spatial frequency of 2700 lines/mm. The total recording intensity was ranging from 3 to 19 mW/cm^2.

Refractive index modulation achieved during recording of transmission gratings at a spatial frequency of 2700 lines/mm in 60 ± 5 µm thick layers as a function of the total recording intensity is presented in Figure 7.8.

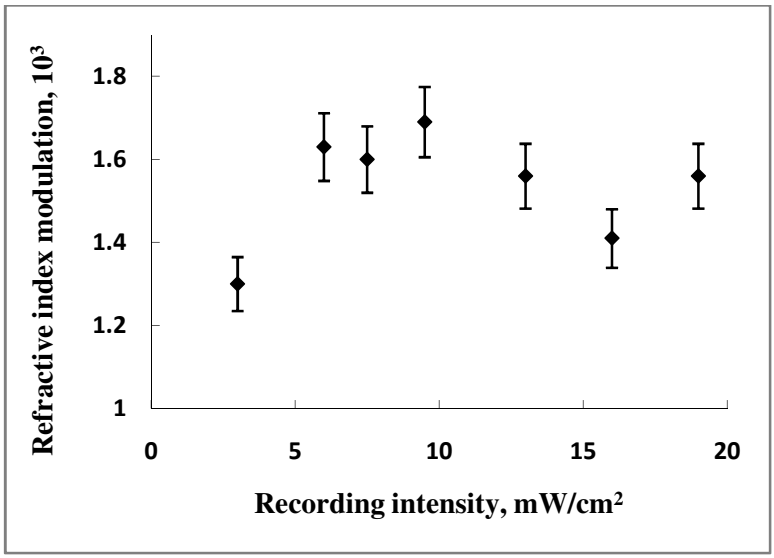

Figure 7.8. Refractive index modulation *versus* the total recording intensity for transmission gratings with a spatial frequency of 2700 lines/mm. The thickness of the layers was 60 ± 5 µm.

As can be seen, maximum refractive index modulation of 1.7×10^{-3} was achieves after exposure with the total recording intensity of 9.5 mW/cm^2.

It was found that the refractive index modulation at 2700 lines/mm was less than the refractive index modulation at 300 lines/mm (Figure 7.5) and 1000 lines/mm (Figure 7.6) probably due to limited resolution of the material. For applications where high diffraction efficiency is required at a spatial frequency of 2700 lines/mm or higher the photopolymer composition containing citric acid and increased concentration of glycerol can be used.

7.3.2.4. Reflection gratings with a spatial frequency of 2700 lines/mm

Experimental results of the refractive index modulation for reflection gratings recorded in layers with thickness ranging from 20 to 115 μm and at a spatial frequency of 2700 ± 44 lines/mm using the optimum recording conditions presented in Table 7.1 are shown in Figure 7.9.

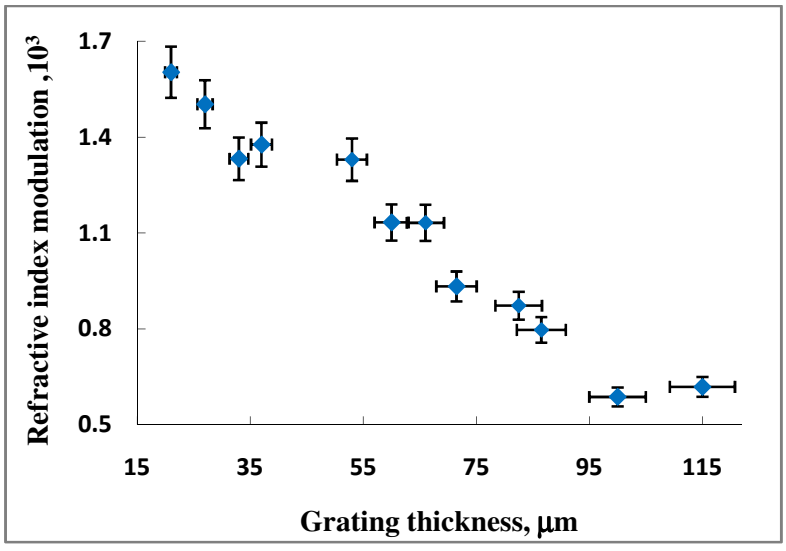

Figure 7.9. Refractive index modulation *versus* the thickness of reflection gratings recorded at a spatial frequency of 2700 lines/mm.

The decrease of the refractive index modulation with increasing thickness was observed due to light absorption in the photopolymer layer. In reflection mode, absorption has impact on the fringe visibility because the beams are incident from opposite sides of the photopolymer layer. The thicker the layer, the bigger the difference in intensity of the two recording beams. This leads to lower visibility of interference fringes during holographic recording and, hence, the lower refractive index modulation is achieved. The NIPA-based photopolymer was found to reach refractive index modulation of up to 1.6×10^{-3} in 20 ± 2 μm thick layers and up to 0.6×10^{-3} in 115 ± 5 μm thick layers. Optical thickness in 532 nm was found to be 1.8 and 3.5 for the layers with the thickness 45 and 90 μm, respectively. Thus, the refractive index modulation of the material can be tuned by the alteration of the thickness of the layer. This is beneficial for the utilisation of novel photopolymer in diffractive optics.

7.4. Conclusions

Holographic performance of the NIPA-based photopolymer as a function of the total recording intensity, the exposure energy and the spatial frequency was investigated in both transmission and reflection modes. The optimum recording conditions at spatial frequencies of 300, 1000 and 2700 lines/mm in transmission mode and 2700 lines/mm in reflection mode were identified.

The diffraction efficiency of 80 % was reached in transmission gratings recorded in 60 ± 5 μm thick layers at a spatial frequency of 1000 lines/mm with exposure of 320 mJ/cm^2. This is comparable to the diffraction efficiency achieved with acrylamide–based photopolymer [8].

The diffraction efficiency of 20 % was obtained in reflection gratings recorded in 60 ± 5 μm thick layers at a spatial frequency of 2700 lines/mm with exposure energy

of 1050 mJ/cm^2. In photopolymer materials the maximum diffraction efficiency of 38 % was previously achieved in reflection gratings with a spatial frequency of 2500 lines/mm recorded in the diacetone acrylamide-based photopolymer [9].

Refractive index modulation achieved during holographic recording in the NIPA-based photopolymer was found to depend on the grating thickness showing the decrease with increasing thickness. Thus, the refractive index modulation of the material can be tuned by the alteration of the thickness of the layer. This is beneficial for the utilisation of the novel photopolymer in diffractive optics.

In addition to fulfilling the requirements for holographic recording materials, the novel photopolymer is sensitive to temperature and has lower toxicity than the acrylamide-based photopolymer. Characterisation of the temperature response of holographic gratings recorded in the NIPA-based photopolymer is presented in Chapter 8.

References

1. Martin, S., Leclere, P., Renotte, Y., Toal, V. and Lion, Y., *Characterisation of an acrylamide-based dry photopolymer holographic recording material.* Optical Engineering, 1994. **33**(12): p. 3942-3946.
2. Marín-Sáez, J., Atencia, J., Chemisana, D. and Collados, M.-V., *Characterisation of volume holographic optical elements recorded in Bayfol HX photopolymer for solar photovoltaic applications.* Optics Express, 2016. **24**(6): p. A720-A730.
3. Battey, D.E., Slater, J.B., Wludyka, R., Owen, H., Pallister, D. M. and Morris, M.D., *Axial transmissive f/1.8 imaging Raman spectrograph with volume-phase holographic filter and grating.* Applied Spectroscopy, 1993. **47**(11): p. 1913-1919.
4. Toal, V., *Introduction to holography*. Taylors&Francis 2011.
5. Zanutta, A., Orselli, E., Fäcke, T. and Bianco, A., *Photopolymeric films with highly tunable refractive index modulation for high precision diffractive optics.* Optical Materials Express, 2016. **6**(1): p. 252-263.
6. Ye, C. and McLeod, R.R., *GRIN lens and lens array fabrication with diffusion-driven photopolymer.* Optics Letters, 2008. **33**(22): p. 2575-2577.
7. Yetisen, A.K., Naydenova, I., Vasconcellos, F.C., Blyth, J. and Lower, C.R., *Holographic sensors: Three-dimensional analyte-sensitive nanostructures and their applications.* Chemical Reviews, 2014. **114**(20): p. 10654-10696.
8. Martin, S., Feely, C.A. and Toal, V., *Holographic recording characteristics of an acrylamide-based photopolymer.* Applied Optics, 1997. **36**(23): p. 5757-5768.
9. Cody, D., *Low-toxicity diacetone acrylamide-based photopolymer for applications in holography*. (Doctoral Thesis) 2014, Dublin Institute of Technology: Dublin.

8. TEMPERATURE RESPONSE OF HOLOGRAPHIC GRATINGS RECORDED IN *N*-ISOPROPYLACRYLAMIDE-BASED PHOTOPOLYMER

8.1. Introduction

Development of a "smart" photopolymer that have ability to record holograms responsive to temperature variations was one of the main aims of the present research. In Chapter 6 newly developed *N*-isopropylacrylamide-based photopolymer composition was reported. As described in Chapter 7, the NIPA-based photopolymer is capable of holographic recording in both transmission and reflection modes and the high diffraction efficiency can be achieved. This chapter presents the characterisation of the temperature response of transmission and reflection volume phase gratings recorded in the NIPA-based photopolymer in the temperature range from 18 to 60 ^{o}C. This knowledge allows fabrication of holographic temperature sensors/indicators/actuators that can respond to temperature variations in the temperature range from 18 to 60 ^{o}C.

Recently, a holographic temperature sensor based on thermal expansion of the analyte-sensitive polymer matrix was reported [1]. The sensor was fabricated through silver halide chemistry [2] described in Chapter 2, section 2.4.2. The first stage included making of the analyte-sensitive polymer matrix by bulk polymerisation of temperature sensitive monomer combination such as *N*-isopropylacrylamide and *N,N´*–methylenebisacrylamide in a molar ratio of 24:1 under UV-light. The second stage included the recording of a hologram by silver halide photochemistry in order to create multilayer photonic structure. Developed photonic structure represented a periodic variation of the refractive index produced by periodic distribution of silver nanoparticles in the functionalised polymer matrix. The photonic structure provided the signal of the sensor such as a wavelength shift due to swelling/shrinkage of the whole hologram

matrix under exposure to temperature. Wavelength shift of over 200 nm was achieved when the temperature increased from 0 to 28 ^{o}C [1].

The mechanism of the temperature response of a holographic sensor based on a grating recorded in the NIPA-based photopolymer is different from the mechanism described above. In this case, after holographic recording the temperature responsive material such as PNIPA is primarily located in the bright fringe regions where photopolymerisation has occurred. This allows for temperature to be sensed not just through the swelling and shrinking of the hologram matrix, but also by the alteration of the physical characteristics of the bright fringes, particularly density and thickness. In thick holograms, even a small change in the refractive index modulation ($<10^{-3}$) can have a very substantial effect on their diffraction efficiency. The following sections present the temperature dependence of the diffraction efficiency and the Bragg angle shift of volume phase slanted transmission gratings and the temperature dependence of the peak wavelength of the light diffracted by volume phase reflection gratings recorded in the NIPA-based photopolymer.

8.2. Experimental

8.2.1. Layer preparation

Photopolymer compositions presented in Table 6.1 and 6.3 were used for recording in transmission and reflection mode, respectively. The photopolymer solution was prepared as described in Chapter 6, section 6.3.1. Photopolymer layers with the thickness of 60 ± 5 μm for recording in transmission and reflection mode were prepared by deposition of 1.8 ml and 0.8 ml of photopolymer solution, respectively. The thickness of the dry layers was measured with a white light interferometric surface profiler MicroXAM S/N 8038.

8.2.2. Holographic recording

Volume phase slanted transmission gratings were under investigation as they provided higher sensitivity of the sensor due to the shift in Bragg selectivity curve leading to the bigger change in the diffraction efficiency as described in Chapter 5, section 5.1. Volume phase slanted transmission gratings were recorded using a set-up presented in Figure 5.6. The incident angles of the recording beams (outside the layer), respectively to the normal to the layer surface, were adjusted as 14 ± 0.5^{o} and 46 ± 0.5^{o} in order to record gratings with a slant angle of 71.07 ± 0.04^{o} (estimated using Equation 5.1) and a spatial frequency of 948 ± 28 lines/mm (calculated using Equation 5.2).

Our preliminary results showed that exposure to temperature could lead to the increase of the diffraction efficiency of slanted transmission gratings up to two times. To exclude the possibility for transition to operation in overmodulation regime described in Chapter 5, section 5.2, slanted transmission gratings with initially low diffraction efficiency of 25 ± 2 % were recorded with exposure energy of 500 mJ/cm^2.

As shown in Chapter 6, section 6.4.6, after recording transmission gratings recorded in the NIPA-based photopolymer should be stabilised using UV-curing. In order to stabilise the gratings, they were exposed to UV-light with the intensity of 2.5 mW/cm^2 for 30 min using a UV Exposure unit (Mega Electronics, model 5503-11).

Volume phase reflection gratings with a spatial frequency of 2700 ± 44 lines/mm were recorded using a set-up presented in Figure 6.2b. Holographic recordings were carried out at the optimum recording conditions described in Chapter 7, section 7.3.1.2. Total recording intensity of 10.5 mW/cm^2 and exposure energy of 1050 mJ/cm^2 were used. As demonstrated in Chapter 6, section 6.5.2, after recording reflection gratings should be UV-cured to stabilise the diffraction efficiency. Therefore,

the gratings were stabilised by exposing to UV-light with the total exposing intensity of 60 mW/cm^2 for 99 sec using Dymax UV curing system (model ECE-200).

In order to evaluate the applicability of the reflection grating as a thermal indicator, Denisyuk holograms [3] were recorded in the NIPA-based photopolymer composition for reflection mode using the set-up presented in Figure 8.1. The recording intensity was 25 mW/cm^2 and exposure time was 100 sec. Thickness of the layer was 60 ± 5 μm.

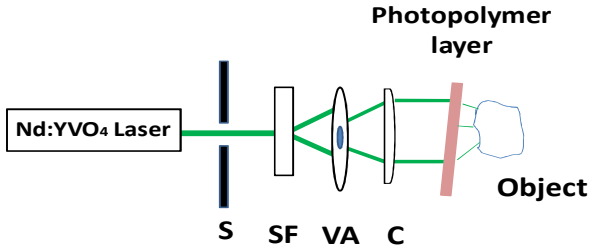

Figure 8.1. Holographic recording set-up with Denisyuk reflection geometry: S - electronic shutter; SF – spatial filter; VA-variable aperture; C – collimator.

8.2.3. Temperature response testing

The temperature response of transmission gratings was investigated by monitoring the diffraction efficiency in two ways, i.e. at Bragg incidence and at a constant angle of the probe beam. The temperature dependence of the diffraction efficiency at Bragg incidence was investigated using the set-up shown in Figure 3.3. In order to monitor the diffraction efficiency at Bragg incidence, the position of the sample at every temperature was adjusted by rotation and maximum diffraction efficiency was obtained. Different environmental conditions were created by a controlled environment chamber

with humidity and temperature control system (Electro-tech system, model 5503-11) described in Chapter 3, section 3.3.4. The chamber had no cooling system to decrease the temperature so the minimum temperature during the experiment was ambient room temperature. The chamber allowed increasing the temperature up to 47 and 50 ^{o}C at relative humidity of 60 and 50 %, respectively. During the exposure to temperature, the intensities of transmitted (I_0) and the first-order diffracted (I_d) beams were monitored by means of an optical power meter (Newport 1830-C) simultaneously (Figure 3.3). The readings were taken 15 min after exposure to a new temperature in order to allow for the samples to equilibrate with the surrounding conditions. The diffraction efficiency in this particular experiment was defined as $I_d/(I_d+I_0)$.This allowed excluding intensity losses due to Fresnel reflection at different incident angles and also losses due to scattering.

The temperature dependence of the diffraction efficiency of transmission gratings monitored at a constant angle of the probe beam was investigated using the set-up presented in Figure 5.7. The relative humidity during the measurements was 34 ± 2 %. The Bragg curve recordings were carried out 15 min after the certain temperature was reached in order to allow for the samples to equilibrate with the surrounding conditions.

The temperature response of reflection gratings was characterised by monitoring the peak wavelength of the light diffracted by the grating in the temperature range from 20 to 55 ^{o}C. During the experiment the relative humidity of 30 and 50 % was kept in order to characterise the temperature response at different relative humidity levels. The set-up is presented in Figure 8.2. The probe light from a broad band light source (AvaLight HAL-S) was guided into the chamber by a fibre optic cable (Avantes FC-UV400-2). The diffracted light from the grating was coupled through a second fibre optic cable to a spectral analyser (Avantes AvaSpec-2048). The readings were taken

15 min after exposure to the new temperature in order to allow for the samples to equilibrate with the surrounding conditions.

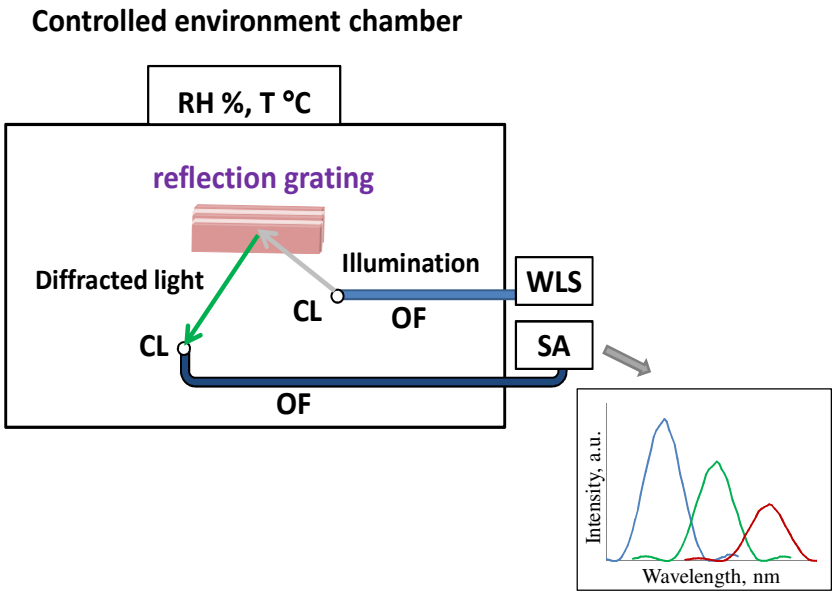

Figure 8.2. Schematic representation of the set-up for testing the temperature response of the reflection grating. CL – collimating lens; OF – optical fibre; WLS – white light source; SA – spectral analyser.

8.3. Temperature response of slanted transmission gratings recorded in the NIPA-based photopolymer

As described in Chapter 5, section 5.1, the holographic sensor based on a slanted transmission grating can operate by controlling the diffraction efficiency either at Bragg incidence or at constant angle of the probe beam. The following sections provide experimental temperature dependence of the diffraction efficiency obtained by probing the grating in these two probing regimes. Possible applications of the temperature response of slanted transmission gratings for the development of temperature sensors are also discussed.

8.3.1. Diffraction efficiency at Bragg incidence

The temperature response of slanted transmission gratings was investigated by monitoring the maximum diffraction efficiency in the temperature range from 18 to 47 ^{o}C and at relative humidity of 60 %. The dependence of normalised diffraction efficiency *versus* temperature is presented on Figure 8.3.

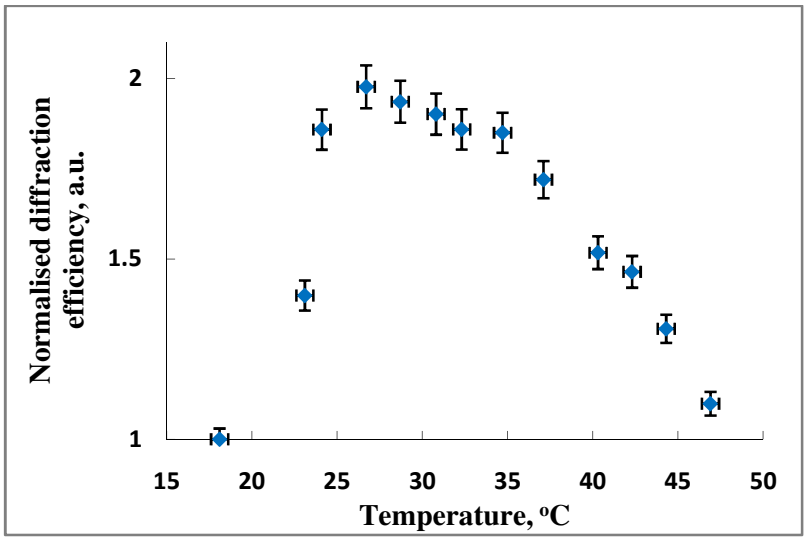

Figure 8.3. Normalised diffraction efficiency of the transmission grating monitored at Bragg incidence *versus* temperature.

Normalised diffraction efficiency was calculated as the ratio of the diffraction efficiency at certain temperature and the diffraction efficiency at the start of the experiment at 18 ^{o}C. As seen from Figure 8.3, at temperatures below 30 ^{o}C, the diffraction efficiency increases up to two times with growing temperature and it decreases above 30 ^{o}C. Such behaviour of the diffraction efficiency can be explained by means of the ability of the photopolymer layer to transit from the hydrophilic state to the hydrophobic state at a critical temperature. The temperature level at which changes in the behaviour is observed is close to the LCST of PNIPA. At temperatures below 30 ^{o}C the photopolymer layer is hydrophilic. As known the higher the temperature, the higher the

concentration of water molecules in the air at certain humidity level. The higher the temperature, the more water molecules are absorbed by the layer leading to the increase of the grating thickness and the refractive index modulation. The refractive index modulation increases as water molecules are mainly absorbed in dark fringe areas because these regions have lower density as they contain low concentration of PNIPA. This assumption has been proved by the experiment where the effect of the thickness change was excluded and only the effect of the refractive change under temperature exposure was evaluated. Further details are presented in Chapter 9, section 9.5.

At temperatures above 30 ^{o}C the photopolymer layer becomes hydrophobic and the absorbed water is expelled leading to the shrinkage of the layer and the decrease of the refractive index modulation. These cause the decrease of the diffraction efficiency. Thus, the sensing capability of the transmission grating recorded in the NIPA-based photopolymer is based on temperature induced changes in the diffraction efficiency due to alterations of both the thickness of the grating and the refractive index modulation. Temperature induced changes in the diffraction efficiency was found to be reversible within 2 %.

The temperature response of slanted transmission gratings recorded in the NIPA-based photopolymer can be used for the development of holographic temperature sensors. The operation principle of the holographic temperature sensor utilising changes in the diffraction efficiency at Bragg incidence as a signal is shown in Figure 8.4. When temperature increases from 20 to 30 ^{o}C, the diffraction efficiency (η) monitored at Bragg incidence increases, as discussed above (Figure 8.3), and provides the sensor response. In the temperature range from 30 to 47 ^{o}C, the decrease of the diffraction efficiency is observed, as previously shown in Figure 8.3.

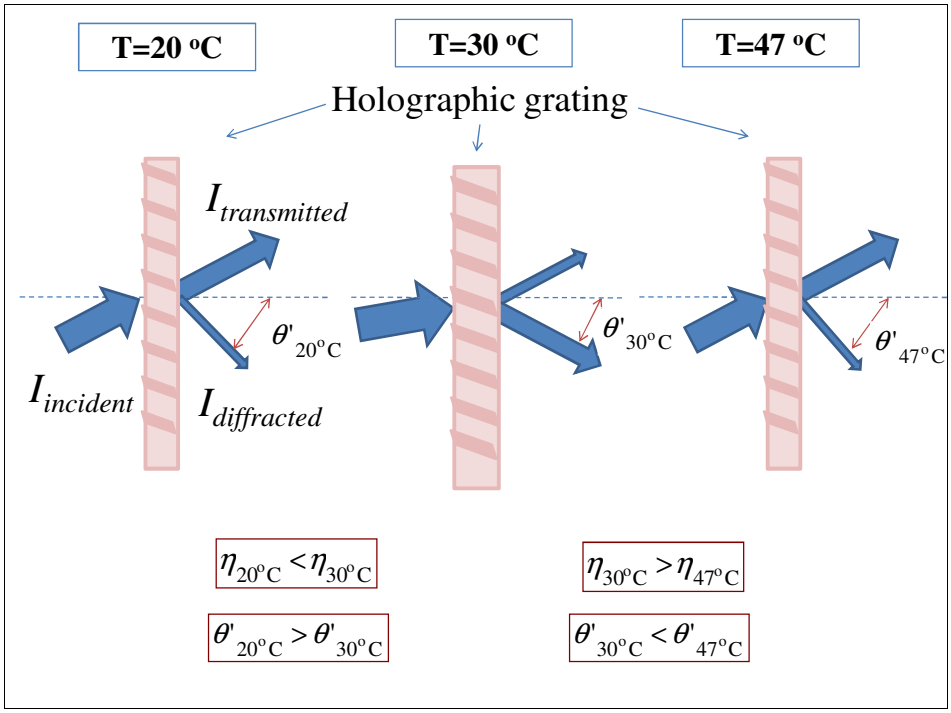

Figure 8.4. Schematic presentation of the operation principle of the temperature sensor based on a slanted transmission grating. Diffraction efficiency at Bragg incidence is used as a sensor signal.

It has been found that along with changes in the diffraction efficiency, temperature exposure causes a Bragg angle shift. Further investigation of the temperature response of slanted transmission gratings including the temperature dependence of the Bragg angle is presented in section 8.3.2.

8.3.2. Diffraction efficiency at a constant position of the probe beam

Another approach examining the temperature response of a slanted transmission grating is monitoring the diffraction efficiency at a constant position of the probe beam with respect to the sample normal. Figure 8.5 represents the temperature dependence of the diffraction efficiency measured at a constant position of the probe beam in the temperature range from 21 to 60 °C and at relative humidity of 34 ± 2 %. At the start of

the experiment (at 21 °C) the position of the probe beam was adjusted at the Bragg incidence and then was kept unchanged during the temperature exposure.

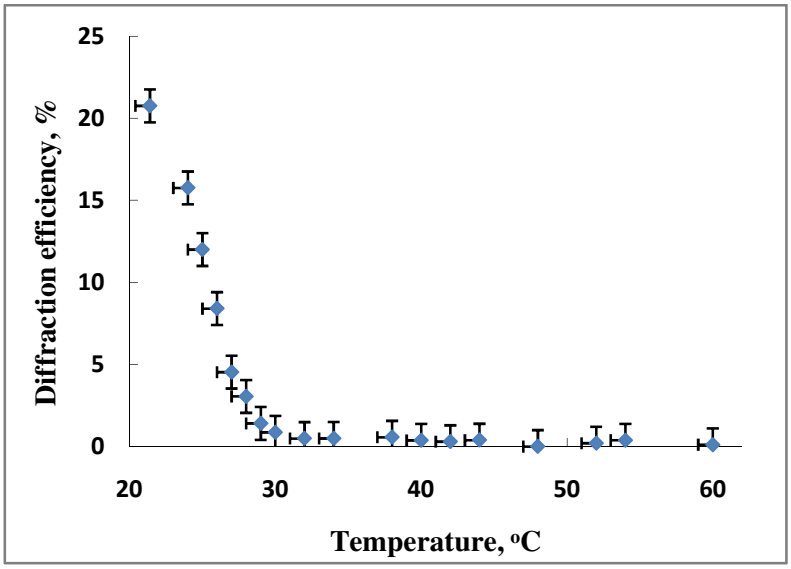

Figure 8.5. Diffraction efficiency of the slanted transmission grating measured at a constant position of the probe beam *versus* temperature.

As seen from Figure 8.5, the decrease of the diffraction efficiency was detected with increasing temperature. Such behaviour can be explained by the Bragg angle shift due to dimensional changes of the layer under exposure to elevated temperature. This is supported by the temperature dependence of the Bragg angle (Figure 8.6). As seen from Figure 8.6, the Bragg angle shift up to 3° was observed when the temperature increased from 21 to 60 °C.

In order to evaluate the reversibility of the temperature induced shift in the Bragg angle, the grating was left to recover at 21 °C and the relative humidity of 34 ± 2 % for 24 hours. The Bragg angle shift was found to be reversible within 0.1°.

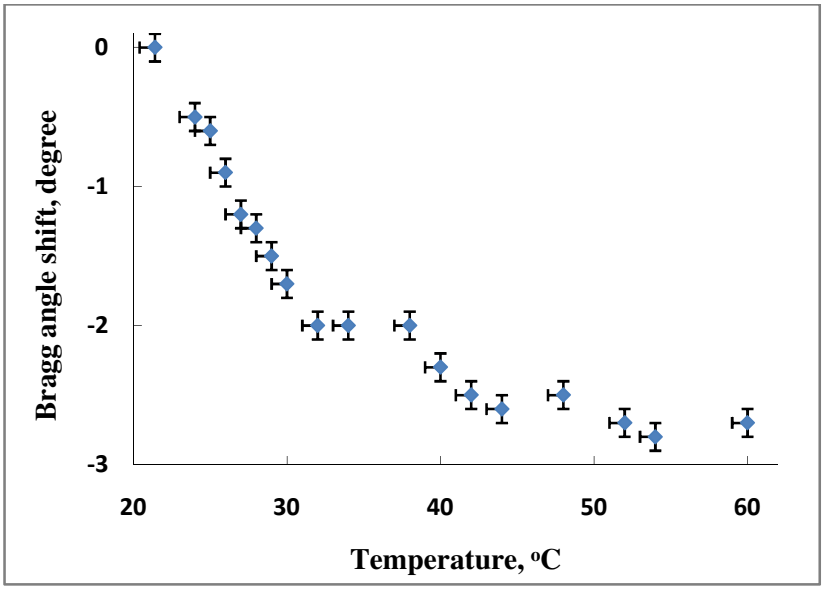

Figure 8.6. The Bragg angle shift of the slanted transmission grating *versus* temperature.

Holographic gratings with temperature response such as temperature induced shift in the Bragg angle can be implemented for the development of holographic temperature switchable actuators. When local heat is applied to the holographic grating, it will change its properties and, thus, will send a signal, i.e. intensity of the transmitted light monitored at a fixed position will alter.

The operation principle of a temperature switchable actuator based on a holographic grating recorded in the NIPA-based photopolymer is presented in Figure 8.7. During the temperature exposure the holographic grating is probed at a constant position of the probe beam (α) adjusted as the Bragg angle at 20 ^{o}C. At 20 ^{o}C the maximum diffraction efficiency is detected at a given direction. When temperature increases from 20 to 30 ^{o}C, the Bragg angle shift is induced by temperature exposure and the diffraction efficiency decreases to 0 % at a given direction (the signal disappears).

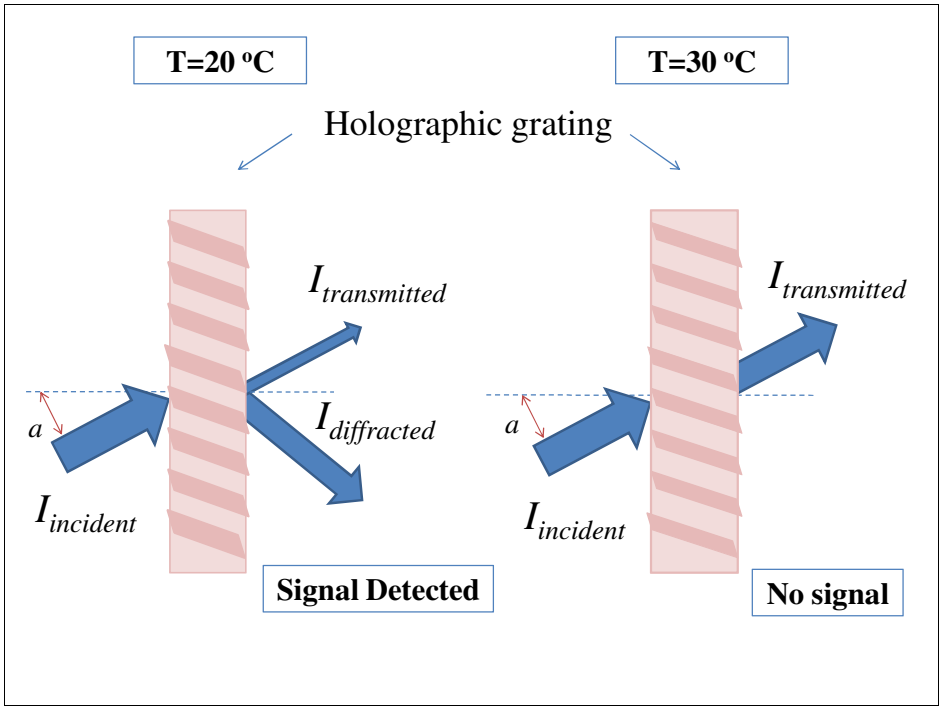

Figure 8.7. Schematic presentation of the operation principle of the temperature switchable actuator based on a slanted transmission grating.

Due to temperature induced Bragg angle shift the maximum diffraction efficiency at different temperatures is detected at different angles. This feature can be used in holographic optical elements for light beam redirection. Transmission gratings recorded in the NIPA-based photopolymer may redirect light in specific direction, depending on the environmental or locally changed temperature. One possible application for this is shading for windows or other light sources. Following section 8.3 presents the temperature response of reflection gratings and its possible applications.

8.4. Temperature response of reflection gratings recorded in the NIPA-based photopolymer

8.4.1. Temperature dependence of the peak wavelength of the light diffracted by reflection gratings

The temperature response of reflection gratings was investigated in the temperature range from 20 to 55 °C. Figure 8.8 shows the temperature dependence of the wavelength shift of the light diffracted by a reflection grating with a spatial frequency of 2700 lines/mm at relative humidity of 30 and 50 %.

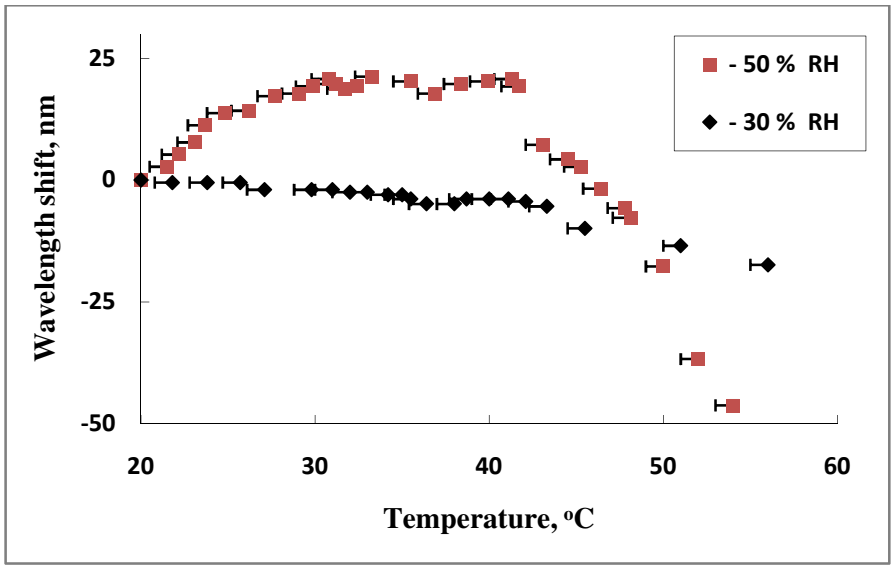

Figure 8.8. Spectral response of the reflection grating at 30 % RH (♦) and 50 % RH (■) *versus* temperature.

The wavelength shift was determined as a difference in the wavelength reconstructed by the hologram at a certain temperature and the wavelength reconstructed at the start of the experiment at 20 °C. At 30 and 50 % relative humidity the dependence of the wavelength shift *versus* temperature is different. A possible explanation is as follows.

As discussed in Chapter 2, section 2.3, under exposure to an analyte the wavelength shift of the light diffracted by the reflection grating is caused by the refractive index change, the fringe spacing alteration and the Bragg angle shift. In the present research, the angle of the probe beam was fixed and, thus, according to Equation (2.6), the wavelength shift was due to the refractive index change and the fringe spacing alteration. With increasing temperature the water concentration in the air is increased and more water molecules are absorbed by the photopolymer layer. This leads to the increase of the spatial period of the grating and, according to Equation (2.3), the wavelength shift to longer wavelengths is induced. At the same time, water (n = 1.33) absorption by the photopolymer layer (n = 1.5) causes the decrease of the average refractive index of the photopolymer layer providing the wavelength shift to shorter wavelengths. Thus, water absorption by the photopolymer layer leads to the opposite effects of the refractive index change and the fringe spacing alteration on the wavelength shift. The contribution of these two parameters is found to be different at the relative humidity of 30 and 50 %.

As seen from Figure 8.8, at the relative humidity of 30 % exposure to temperature below 30 ^{o}C causes a gradual wavelength shift up to 2 nm to shorter wavelengths. This can be explained by slightly higher impact of the refractive index change than the effect of the spatial period alteration. When temperature is above 30 ^{o}C, the photopolymer material becomes hydrophobic and absorbed water is expelled. Evaporation process induces the shrinkage of the layer and the increase of the average refractive index. Based on the experimentally observed wavelength shift up to 18 nm to shorter wavelengths, one can conclude that the spatial period alteration dominates the refractive index change.

At 50 % relative humidity the effect of the spatial period alteration dominates the refractive index change at temperature below 30 ^{o}C and above 40 ^{o}C (Figure 8.8.). In the temperature range from 30 to 40 ^{o}C contributions of the spatial period alteration and the refractive index change are equal but have opposite effect on the wavelength shift. Thus, the wavelength is unchanged in this temperature range. At temperature below 30 ^{o}C the increase of the grating period dominates the refractive index decrease and, as a result, the wavelength shift of up to 20 nm to longer wavelengths is observed. At temperature above 40 ^{o}C the shrinkage of the layer is induced due to the transition of PNIPA molecules to hydrophobic state. This leads to the decrease of the grating period and, consequently, the wavelength shifts to shorter wavelengths for up to 65 nm.

As known, the human eye is able to resolve the color with 10 nm wavelength intervals [4]. Thus, a wavelength shift of more than 10 nm can be visually detected as a color change of the hologram when reconstructed in white light. Figure 8.9 demonstrates the photographs of Denisyuk hologram recorded in the NIPA-based photopolymer at 20 ^{o}C and 50 ^{o}C.

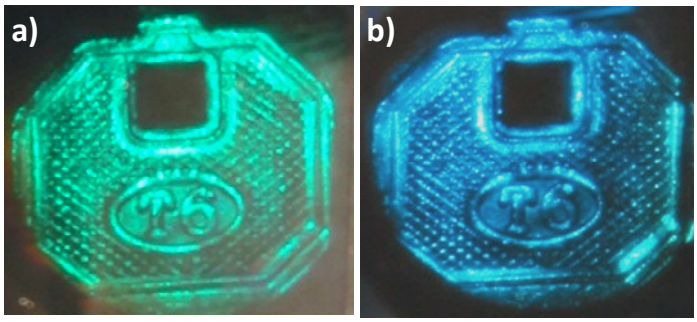

Figure 8.9. The photographs of Denisyuk hologram recorded in the NIPA-based photopolymer at 20 ^{o}C (a) and 50 ^{o}C (b).

It can be seen that the temperature increase from 20 ^{o}C to 50 ^{o}C causes a color change of the hologram. This is well suited to the application of reflection holograms as temperature visual indicators that visibly change the color under temperature exposure. One possible application is temperature sensitive labels that indicate what the current temperature of the product is and/or if it is above a temperature that is critical for protecting the quality of the goods. Such product could be useful for packaging industry where goods need to be stored at specific temperature.

8.4.2. Reversibility of the temperature induced wavelength shift

One of the main characteristics of the sensor is sensor reversibility. The reversibility of the temperature induced wavelength shift discussed in section 8.4.1 was studied by exposing the reflection grating with a spatial frequency of 2700 ± 44 lines/mm to 7 cycles of temperature changes. The measurements of the wavelength of the light diffracted by a reflection grating were carried out before temperature exposure, during exposure to temperature at 50 ^{o}C and 24 hours after exposure to temperature. During all measurements the relative humidity was kept 50 ± 1 %. Before temperature exposure, the wavelength measurements were carried at 22 ± 0.5 ^{o}C. During the temperature exposure, temperature was gradually increased from 22 to 50 ^{o}C in the period of 60 min as the environmental chamber allowed. When 50 ^{o}C was reached, the sample was kept at this temperature for 40 min and, then, the wavelength measurements were carried out. After temperature exposure the sample was left to recover at 22 ± 1 ^{o}C and at relative humidity of 50 ± 5 % for 24 hours and then the wavelength measurement was carried out again. The wavelength shift caused by temperature exposure at 50 ^{o}C for 40 min was observed to be relatively constant for 7 cycles of the temperature exposure (Figure 8.10).

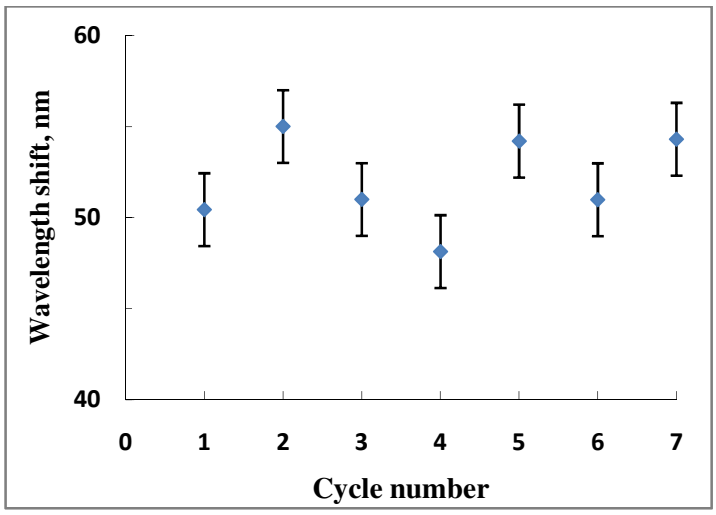

Figure 8. 10. Wavelength shift induced by temperature exposure *versus* a cycle number for the reflection grating recorded in the NIPA-based photopolymer.

The small variation of the wavelength shift can be attributed to the uncertainty of the temperature and relative humidity level during the measurements. However, the wavelength of the diffracted light was found to not recover to its initial value (Figure 8.11).

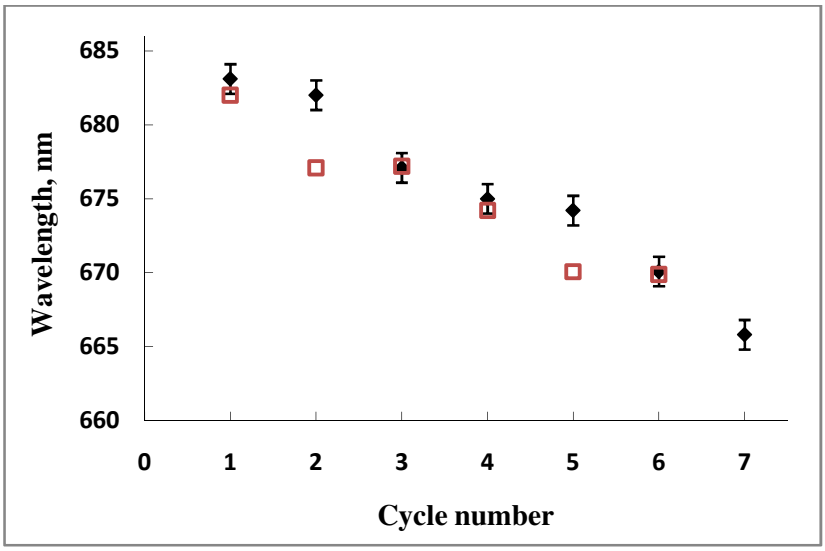

Figure 8. 11. Wavelength of the light diffracted by the reflection grating recorded in the NIPA-based photopolymer before (♦) and 24 hours after (□) the temperature exposure *versus* the cycle number of the temperature exposure.

After recovery for 24 hours at 22 ± 1 ^{o}C, the wavelength of the diffracted light shifted to the shorter wavelengths for up to 5 nm. The possible explanation can be potential inability of the matrix to recover to the original volume and/or inability of matrix to expel the water at this temperature. This leads to decreased spatial period of the grating and refractive index, according to Equation (2.3), the wavelength of the diffracted light shifts to shorter wavelengths.

8.5. Conclusions

The temperature response of volume phase slanted transmission and reflection gratings recorded in the novel NIPA-based photopolymer was investigated in the temperature range from 18 to 60 ^{o}C. The diffraction efficiency of slanted transmission gratings was found to be temperature dependent. When temperature changed from 20 to 30 ^{o}C, the diffraction efficiency increased up to two times. In the temperature range from 30 to 47 ^{o}C, the decrease of the diffraction efficiency was observed. Behaviour of the diffraction efficiency *versus* temperature was explained by the hydrophilic/hydrophobic state of PNIPA molecules mainly contained in the bright fringe areas. Temperature induced changes in the diffraction efficiency was explained by alterations of both the thickness of the grating and the refractive index modulation due to water absorption/desorption. It was found that in slanted transmission gratings temperature exposure induced a Bragg angle shift along with changes in the diffraction efficiency. When temperature increased from 20 to 30 ^{o}C, a Bragg angle shift up to 3 degrees was observed.

The temperature response of reflection gratings recorded in the novel NIPA-based photopolymer was investigated by monitoring the peak wavelength of the light diffracted by a reflection grating in the temperature range from 20 to 55 ^{o}C. The peak

wavelength was found to depend on the temperature and the following model of the temperature response was proposed. Temperature induced behaviour of the wavelength was governed by the hydrophilic/hydrophobic state of PNIPA molecules mainly contained in the bright fringe areas. The wavelength shift under temperature exposure was determined by the refractive index change and the fringe spacing alteration due to water absorption/desorption induced by conformational changes of PNIPA molecules at a critical temperature. Depending on the contribution of the refractive index change and the fringe spacing alteration, the wavelength shift to either longer or shorter wavelengths was observed. The contribution of these two parameters was found to depend on the relative humidity. At the relative humidity of 30 %, the wavelength shift up to 18 nm to shorter wavelengths was detected when the temperature increased from 30 to 55 ^{o}C. At the relative humidity of 50 %, the wavelength initially shifted up to 20 nm to longer wavelengths as the temperature increased then shifted 65 nm to shorter wavelengths when the temperature changed from 20 to 30 ^{o}C and from 40 to 55 ^{o}C, respectively.

The temperature-switchable swelling/shrinkage property of the novel NIPA-based photopolymer can be utilised for the development of holographic temperature sensors, temperature switchable actuators, temperature visual indicators and holographic optical elements with temperature controlled direction of the diffracted light and diffraction efficiency. The main drawback of the NIPA-based photopolymer is that temperature sensitivity of gratings recorded in the NIPA-based photopolymer depends on the relative humidity level.

References

1. Lowe, C.R., Blyth, J. and James, A.P., *Interrogation of a sensor*. 2006, WO Patent Application 2006008531 A1.
2. Blyth, J., Millington, R., Mayes, A. and Lowe, C., *A diffusion method for making silver bromide based holographic recording material.* The Imaging Science Journal, 1999. **47**: p. 87-91.
3. Denisyuk, Y., *On the reflection of optical properties of an object in a wave field of light scattered by it.* Doklady Akademii Nauk SSSR, 1962. **144**(6): p. 1275-1278.
4. Shevell, S.K. (Ed.), *The science of color (2nd edition).* Oxford UK: Elsevier Science 2003.

9. DEVELOPMENT OF RELATIVE HUMIDITY OPTICAL SENSOR BASED ON AZTEC GRATING

9.1. Introduction

This chapter describes the development of an alternative optical sensor responsive to changes in relative humidity. The approach is based on functionalisation of pre-recorded photonic nanostructure by coating it with analyte-sensitive layer. The optical sensor includes an embossed honeycomb pyramidal grating as a substrate (the basis for a sensor) and a coating thin polymer film as a sensing medium. The aim of using embossed honeycomb pyramidal grating is to provide the optical signal. The coating layer is utilised to functionalise the photonic nanostructure and introduce humidity response.

The embossed honeycomb pyramidal grating presents a surface-relief volume diffractive structure which comprises a hexagonal array of circular hollow nanostepped pyramids (Figure 9.1a). The diffractive structure was developed by J. Cowan [1-5]. It is called Aztec surface structure due to its profile (Figure 9.1b) which resembles Aztec temple pyramid and also because the name “Aztec” is an acronym for diazo photoresist technology used for the development of the structure. Further details on the design of the Aztec surface structure are presented in section 9.2.

The Aztec structure, or the Aztec grating, has properties of both a surface relief structure and a volume reflection grating. Upon illumination with broad band light, the Aztec structure diffracts multiple orders, as shown in Figure 9.2, which have the diffractive rainbow spectrum associated with the surface relief structure.

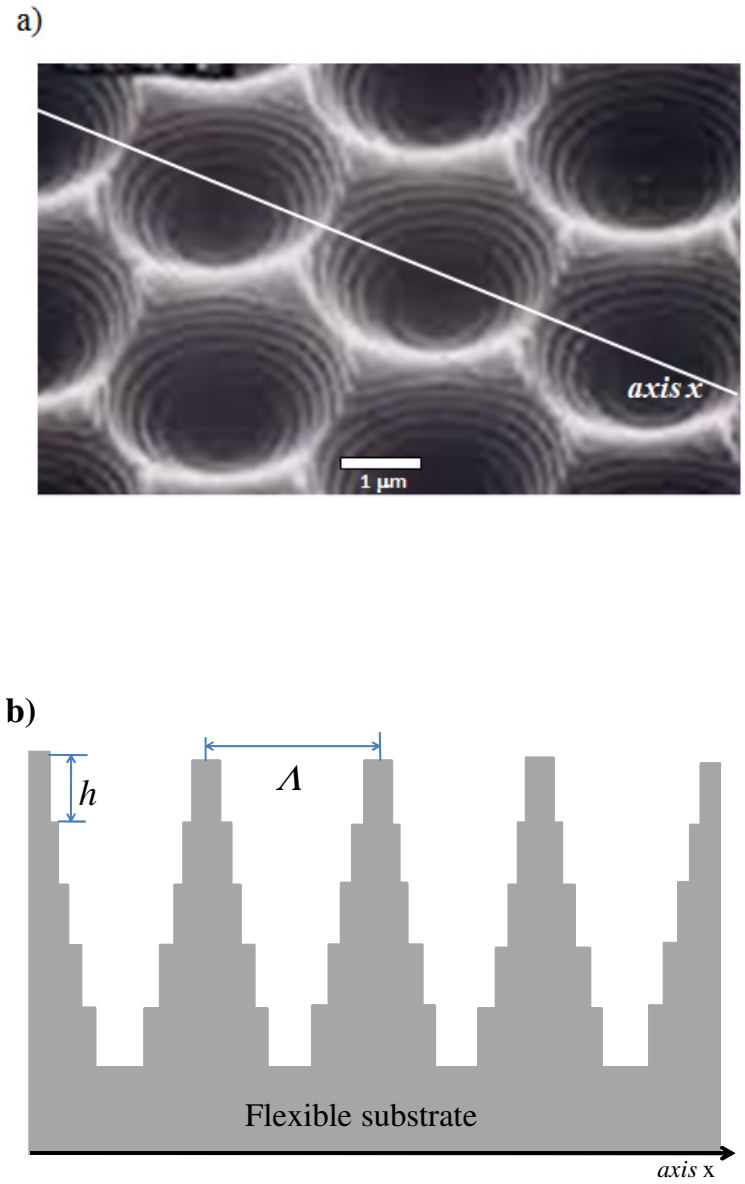

Figure 9.1. a) SEM image of the Aztec structure [6]. b) Theoretical profile of the Aztec grating: Λ is the spatial period of the surface profile structure and h is the step height of the nanostepped structure.

Also, due to the diffraction from the nanostepped structure the single order of the narrow-band light is observed (Figure 9.2). The wavelength of the light diffracted from the nanostepped structure (λ) is governed by the step height (h), playing the role of the spatial period of the reflection grating, and can be determined by the Bragg equation (Equation (2.3)) which in this case can be rewritten as follows:

$$\lambda = 2nh \sin \theta', \tag{9.1}$$

where n is the refractive index of the flexible substrate and θ' is the Bragg angle.

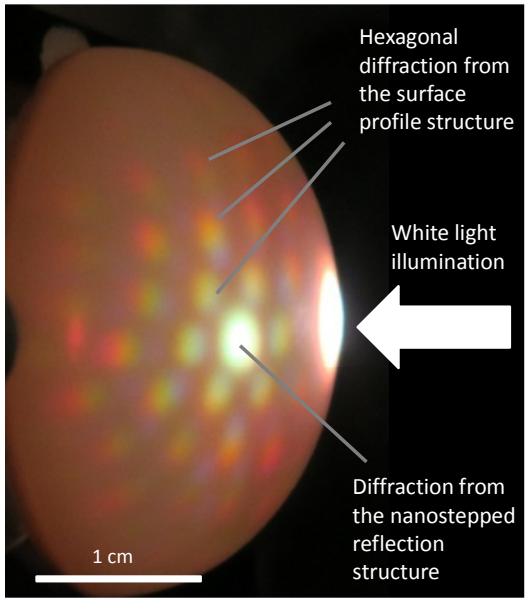

Figure 9.2. Diffraction produced by the Aztec grating under white light illumination in a hemisphere screen. Diffractive rainbow spectrum is associated with the surface profile structure and the narrow-band light is due to the 180 nm stepped reflective structure.

Aztec gratings with various step height of the nanostepped structure can be developed providing the following advantages [7]. Peak wavelength associated with a volume reflection grating shifts to longer wavelengths with increasing the step height of the nanostepped structure (Equation 9.1). This allows tuning the colour of the reflection hologram by changing the step height. The spectral bandwidth of the Bragg peak depends on the number of steps of the nanostepped structure and it is approximately equal to the reciprocal of the step number. The spectral bandwidth increases with decreasing number of steps of the nanostepped structure. This enables using the Aztec grating as an optical filter with customised bandwidth.

Also, it has been demonstrated that the Aztec structures can be utilised for the development of security labels [6, 8]. The security labels based on the Aztec structures provide multilevel authentication of a product. Firstly, the security labels can be verified by colour-selective diffraction. Secondly, the security labels can be checked by honeycomb patterns produced in the far-field projection under illumination with a laser light. Moreover, sophisticated profiles such as Aztec pyramids are in great demand from a security standpoint because manufacturing of the Aztec profile is complex which makes it extremely difficult to replicate.

Another possible application of the Aztec structures is optical sensors that can be used to identify the presence of any semi-transparent material [1, 3]. The sensing mechanism is based on the wavelength shift caused by changes in the refractive index of the material surrounding the structure. The proposed optical sensor is different from holographic sensors based on volume reflection gratings. As discussed in Chapter 2, section 2.3, the response of holographic sensors based on volume reflection gratings is mainly induced by changes of both the fringe spacing and the refractive index. It has been shown in Chapter 8, section 8.4.1 that these two effects can lead to a wavelength shift in opposite direction and this can decrease the sensitivity of the device. In the optical sensor based on the Aztec grating the step height, playing the role of fringe spacing, is fixed and does not experience any alterations in the presence of the analyte. Thus, the response of the optical sensor based on the Aztec grating is solely attributed to the change of the refractive index of the coating layer. The relationship between the peak wavelength of the light diffracted by the Aztec structure and the refractive index of the coating layer is determined by Equation (9.1) where n is the refractive index of the material surrounding the structure.

Recently, the example of the optical sensor based on the Aztec structure was reported [8]. A colorimetric refractive index sensor capable of quantifying the concentration of an analyte was developed. Glycerol was used as a model analyte. When the concentration of glycerol in the surrounding medium of the Aztec structure was changed from 0 to 100 % with 20 % step, the peak wavelength shifted from 495 to 535 nm. The colour change due to the wavelength shift was visible to the eye providing a colorimetric response of the sensor. Taking into account observed wavelength shift, a change in the refractive index of the coating layer from 1.346 to 1.472 was estimated using Equation 9.1.

The aim of the present research was the development of the optical humidity sensor based on embossed honeycomb pyramidal grating coated with a thin polymer layer. The main challenge was to identify a composition of the coating layer which was capable to provide sensitivity to humidity with reversible response in the relative humidity range from 20 to 95 %.

9.2. Experimental

9.2.1. Design of the Aztec structure

Aztec surface structures used in the present research were provided by Dr. A. K. Yetisen from Harvard Medical School and the Wellman Centre for Photomedicine, Massachusetts General Hospital, Cambridge, USA.

Aztec surface structures are fabricated by a multi-beam holographic lithography followed by printing on a poly(ethylene terephthalate) film using roll-to-roll manufacturing [3-5]. During the first step the master is produced in a positive photoresist layer (diazonaphthoquinone) with a thickness of 1.2 μm. The photoresist is

known as a material which is capable of creating a surface profile with depth proportional to the intensity of interference patterns after development.

Two separate exposures are used to create nanostepped pyramidal pattern in a thick layer of the photoresist. Firstly, multilayer pattern is created by exposing a photoresist to holographic interference pattern produced by a reference and an object beam which enter the recording medium from opposite sides (Figure 9.3a).

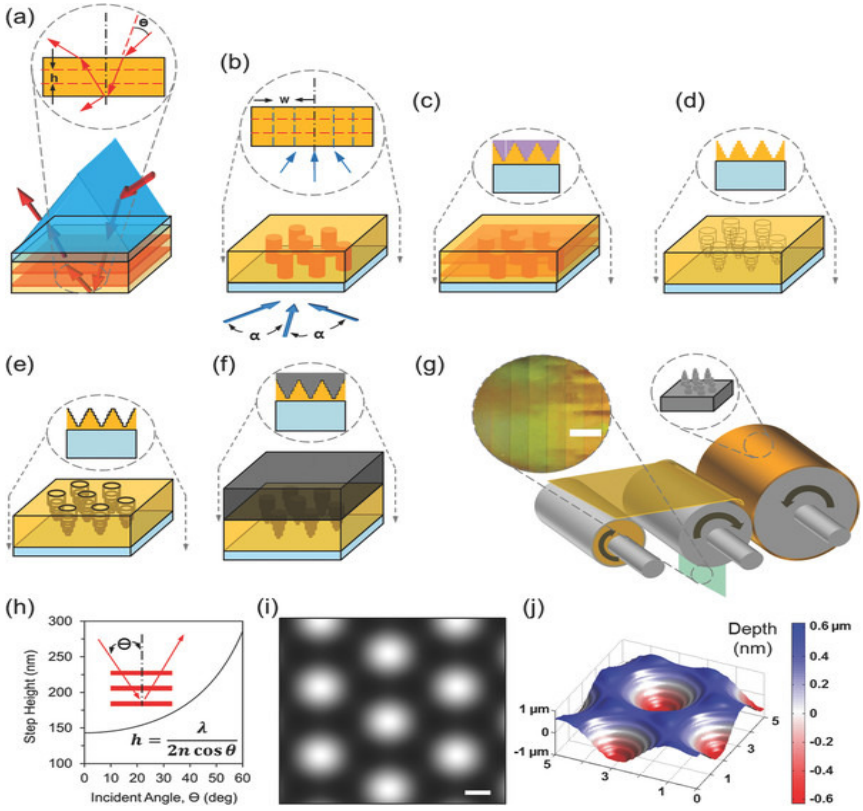

Figure 9.3. Holographic recording and printing of circular nanostepped pyramids in honeycomb arrays. (a) Prism coupling to expose a multilayer interference in a photoresist layer coated over glass; (b) Laser writing of a honeycomb pattern using three azimuthal beams (α = 120°) to create a pitch (w) of 3.3 μm; (c) Resulting interference, a superposition of the multilayer and the honeycomb pattern, shown in purple; (d) Circular nanostepped pyramids after etching with a photographic developer; (e) Evaporation of a silver layer (~300 nm) over the etched photoresist in vacuum; (f) Electroplating metallic nickel (1 mm) over the deposited silver layer to produce a master; (g) Printing the nanostepped pyramids using a nickel replica into acrylate polymer on PET film in roll-to-roll nanoimprinting. The inset shows eight different printed gratings, scale bar = 4 cm. (h) The vertical lattice step height of the multilayer as a function of incident angle (θ) in prism coupling. (i) Simulated honeycomb field intensity using three azimuthal beams (α = 120°) in the photoresist. Scale bar = 1 μm. (j) The modelled nanostepped concavities computed by superposing the multilayer and the honeycomb exposures. Figure from reference [8].

Thus, a set of fringes parallel to the photoresist surface is produced. The fringe spacing can be tuned from 160 to 200 nm by increasing the incident angle (θ) of the recording beam from 30^o to 44^o. Secondly, hexagonally packed cylindrical interference fringes are obtained by the interference of three beams with azimuthal angles 120^o apart (Figure 9.3b). The resulting pattern is a hexagonal array of circular hollow nanostepped pyramids (Figure 9.3c). The photographic development of the photoresist allows converting the resulting pattern into the surface relief stepped profile (Figure 9.3d). The second step of producing embossed holograms includes coating of the photoresist with a silver layer (300 nm thick) to make a conductive layer (Figure 9.3e). Then, the inverse nickel master (14×14 cm^2 and thickness 1 μm) is produced by electroplating of nickel metal over a hexagonal array of circular hollow nanostepped pyramids. After producing the inverse master, nanoimprinting of stepped pyramids onto a poly(ethylene terephthalate) film with 50 μm thickness is done using a roller type replication machine (Figure 9.3f). In order to improve the diffraction efficiency, the structure is coated with a thin (20 nm) aluminium layer. The resultant diffractive structure or the Aztec grating has properties of both a volume reflection grating and a surface relief structure. Upon illumination with broad band light, the Aztec structure produces the diffractive rainbow spectrum associated with the surface relief structure and the narrow-band light due to the nanostepped structure.

The approach used to design the Aztec structure provides an advantage over other fabrication techniques. The strategy to print Aztec structures on flexible polymer substrates in roll-to-roll manufacturing guarantees printing of uniform, defect-free photonic devices over 1 m^2 areas within a minute [1, 3, 8].

9.2.2. Development of the optical sensor

The optical sensor was created by coating embossed honeycomb pyramidal gratings with a thin polymer film. Embossed honeycomb pyramidal gratings with a step height of 175 nm were used as the base of the sensor to provide the optical signal. To create the sensitivity to relative humidity, the embossed honeycomb pyramidal grating was functionalised by spin coating with a thin polymer film.

Coating layers containing polyvinyl alcohol and glycerol were used as these materials were known to be hydrophilic [9, 10]. Coating polymer film solution was prepared by mixing 10 % w/v polyvinyl alcohol stock solution and glycerol using a magnetic stirrer for 30 min. Preparation of 10 % w/v polyvinyl alcohol stock solution was described in Chapter 3, section 3.3.1. Glycerol was brought from Fisher Scientific and was used as received. Three chemical compositions of the coating polymer film containing polyvinyl alcohol and glycerol with the ratio 1:0, 1:1 and 2:3 wt % were utilised. Different chemical compositions of the coating polymer film were used in order to investigate the possibility to tune the operation range of the optical sensor and its sensitivity by changing the chemical composition of the coating polymer film. 0.15 ml of the coating solution was spin coated onto the Aztec structure at spin rate 500 rpm for 15 sec using a spin coating system (Speciality Coating Systems, model G3P-8). After spin coating the samples were dried at $T = 21 \pm 2\ ^{o}C$ and $RH = 35 \pm 5$ % for 3 hours.

Figure 9.4 shows the photograph of the uncoated Aztec structure and the Aztec structure coated with the polymer film containing polyvinyl alcohol/glycerol (2:3). Under illumination with diffused white light, the uncoated Aztec grating produces both multicolour diffraction due to the surface structure with a spatial period of 3.3 μm and narrow-band diffraction due to the reflection structure with the spatial period of 175 nm.

The intensity of the light diffracted from the surface structure dominates the intensity diffracted by the nanostepped structure in the uncoated area.

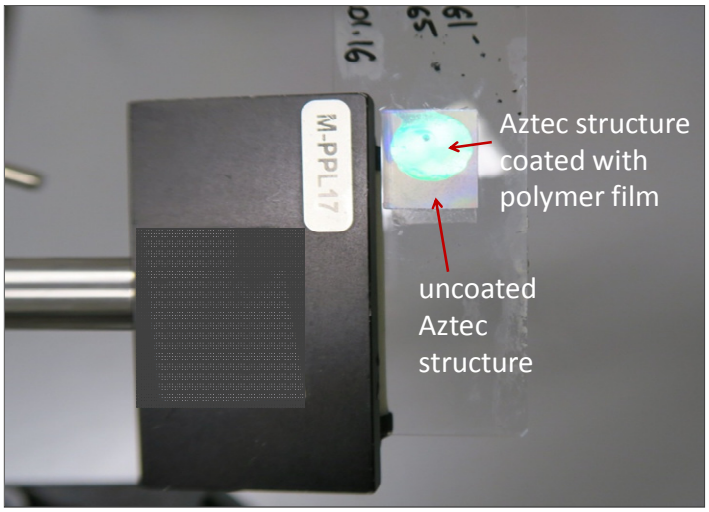

Figure 9.4. The photograph of the uncoated and coated Aztec structure with 175 nm step height under diffused light illumination.

When the Aztec structure is coated, a coating thin polymer film ($n \cong 1.5$) [10, 11] displaces the air and the surrounding refractive index is close to the refractive index of the poly(ethylene terephthalate) substrate ($n = 1.57$) [12]. Thus, the diffractive rainbow spectrum associated with a surface structure is suppressed and the diffraction from the coated Aztec structure is mainly determined by the nanostepped structure. The wavelength of the diffracted light is governed by the step height of the nanostepped structure (Equation 9.1) and it is estimated to be 520 nm for the structure with a 175 nm step.

9.2.3. Humidity response testing

The humidity response of the optical sensor was investigated by monitoring the peak wavelength of the light diffracted from the nanostepped structure at the relative humidity in the range from 8 to 97 % and at constant temperature 22 ± 1 ^{o}C. A

controlled environment chamber with humidity and temperature control system described in Chapter 3, section 3.3.4 was utilised to obtain different levels of relative humidity and maintain a constant temperature. The temperature of 22 ± 1 ^{o}C was defined as the highest temperature at which the relative humidity of 97 % can be achieved. The set up presented in Figure 8.2 was used to monitor the spectral response of the sample at different levels of relative humidity. Humidity exposure for 15 min was found to allow reaching the saturation of the wavelength shift (Figure 9.5).

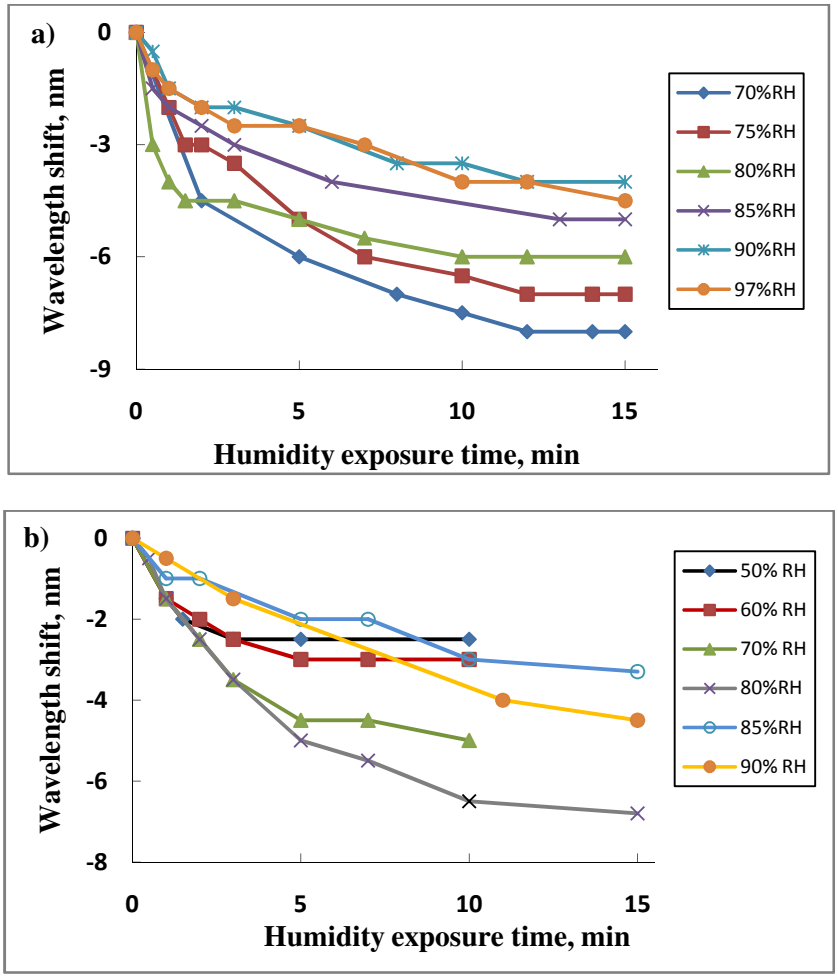

Figure 9.5. Wavelength shift of the light diffracted by the Aztec structure coated with a polymer film containing polyvinyl alcohol and glycerol with the ratio 1:1 (a) and 2:3 wt % (b) *versus* exposure time to different levels of relative humidity.

9.3. Humidity sensitivity of the optical sensor

The humidity response of the optical sensor was determined by obtaining the correlation between the peak wavelength of the light diffracted from the nanostepped structure and the relative humidity level. The peak wavelength of the diffracted light from the optical sensor at the relative humidity ranging from 8 to 97 % is shown in Figure 9.6. Polymer films containing polyvinyl alcohol and glycerol with the ratio 1:0, 1:1 and 2:3 wt % were utilised as a coating. As can be seen from Figure 9.6, at the start of the experiment (at the relative humidity of 8 %) the peak wavelength of the optical sensor system depends on the coating layer composition. The addition of glycerol (n = 1.47) to polyvinyl alcohol layer (n = 1.5) leads to the shift to shorter wavelengths due to the decrease of the average refractive index of the coating layer. With increasing concentration of glycerol the bigger shift is observed due to bigger decrease of the average refractive index.

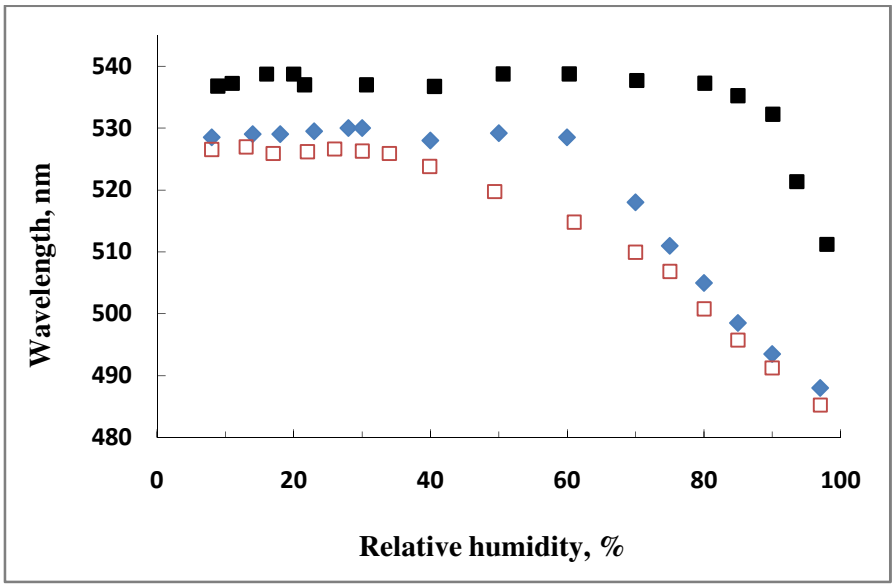

Figure 9.6. Humidity dependence of the peak wavelength of the light diffracted by the Aztec structure coated with a polymer film containing polyvinyl alcohol and glycerol with the ratio 1:0 (■), 1:1 (♦) and 2:3 wt % (□).

It is clearly seen (Figure 9.6) that the humidity sensitivity of the optical sensor depends on the concentration of glycerol in the coating layer. The probable explanation is as follows. The addition of glycerol which is a viscous liquid increases the capacity of the coating layer to absorb water by decreasing its density. This leads to the increase of the humidity sensitivity of the device.

The humidity response of the devices utilizing the coating layer containing polyvinyl alcohol and glycerol with ratio 1:0, 1:1 and 2:3 wt % was observed at the relative humidity above 85 %, 60 % and 35 %, respectively. The device coated with pure polyvinyl (alcohol/glycerol ratio 1:0) showed the wavelength shift of 26 nm in the relative humidity range from 80 to 97 %. The sensitivity of the devices was calculated to be 1.5nm/%RH. The wavelength shift of 40 nm induced by humidity change from 60 to 97 % was detected for the optical sensor coated with polyvinyl alcohol/glycerol (1:1). The sensitivity of the device was 1nm/%RH. The device coated with polyvinyl alcohol/glycerol (2:3) had sensitivity of 0.66nm/%RH and showed the wavelength shift of 41 nm when the relative humidity changed from 35 to 97 %. Thus, optical sensors with tunable sensitivity to humidity and operation range could be developed by altering the chemical composition of the coating layer. The addition of glycerol allows varying the density of the coating film and its capacity to absorb water.

The sensing mechanism of the optical sensor is based on the wavelength shift of the light diffracted from the nanostepped structure due to changes in the refractive index of the coating layer caused by its density alteration due to water absorption under exposure to humidity. Detected wavelength shifts (26, 40 and 41 nm) under humidity exposure are visible to the eye and this feature makes possible application of the Aztec structure coated with a polymer film as a visual indicator of the environmental

humidity. Following section presents data on reversibility and repeatability of the observed wavelength shift under humidity exposure.

9.4. Reversibility and repeatability of the humidity response of the optical sensor

To carry out a preliminary investigation of the reversibility and repeatability of the wavelength shift induced by humidity exposure (Figure 9.6), the optical sensor was exposed to a few cycles of the relative humidity change in the range from 20 to 97 %. The repeatability and the reversibility of the changes in devices coated with polyvinyl alcohol/glycerol with the ratio 1:0 and 1:1 was confirmed after exposure to the relative humidity of 97 % (Figure 9.7).

It was observed that the layer with the composition of polyvinyl alcohol /glycerol (2:3) became unstable after exposure to the relative humidity above 90 % and it was more suitable for operation at lower relative humidity. To investigate the reversibility of the humidity induced wavelength shift, the device coated with polyvinyl alcohol /glycerol (2:3) was exposed to the relative humidity of 70, 80 and 90 % for 90 min. Exposure time of 90 min was used in order to investigate if the long exposure time could produce any irreversible changes. Wavelength measurements were taken before exposure to humidity, during exposure and 24 hours after exposure to humidity when the sample was recovered at the relative humidity of 40 ± 3 % and temperature 22 ± 0.5 ^{o}C. Measurements before and after exposure to humidity were carried out at the relative humidity of 40 ± 3 % and temperature 22 ± 0.5 ^{o}C. Experimental data are presented in Figure 9.8. As can be seen from Figure 9.8, exposure to the relative humidity of 70, 80 and 90 % induced fully reversible wavelength shift. The wavelength shift of 17, 24 and 31 nm was observed during exposure to the relative humidity of 70,

80 and 90 %, respectively. The experimental results presented in section 9.4 and 9.5 were summarised in Table 9.1.

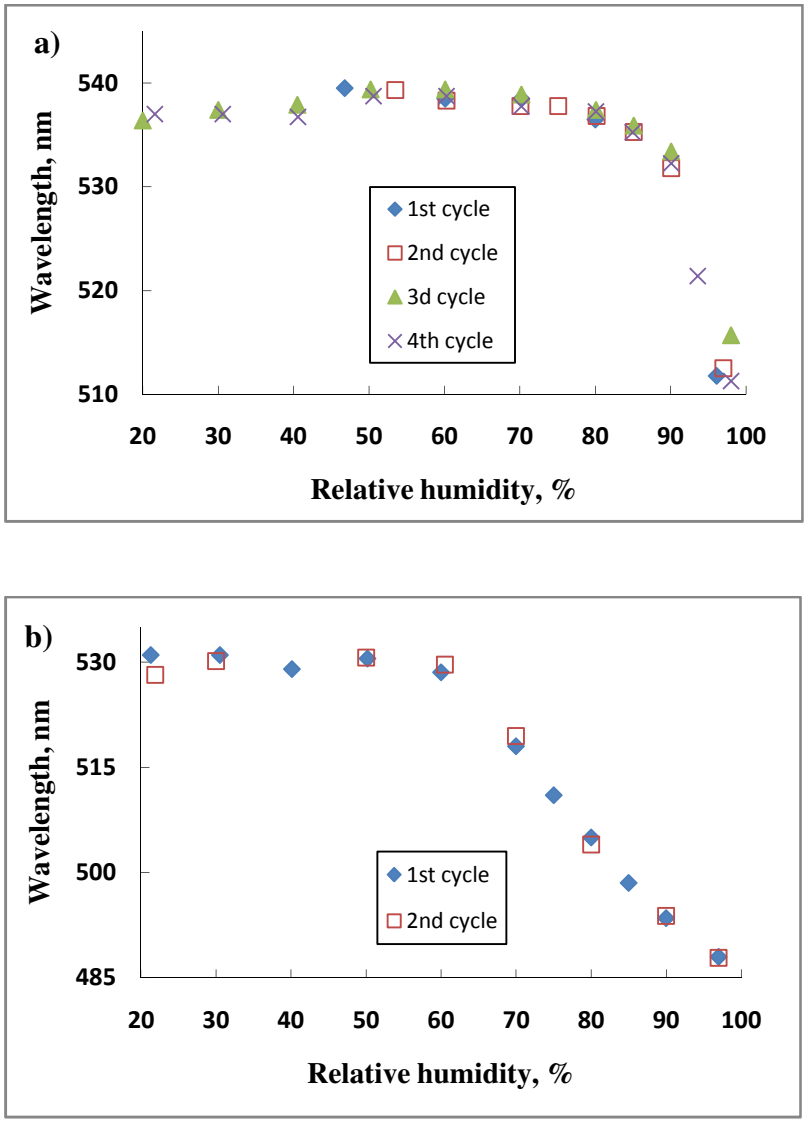

Figure 9.7. Multiple cycles of exposure to humidity of the optical sensor with respect to the repeatability and the reversibility of the sensor response. Devices coated with polyvinyl alcohol/glycerol with the ratio 1:0 (a) and 1:1 wt % (b).

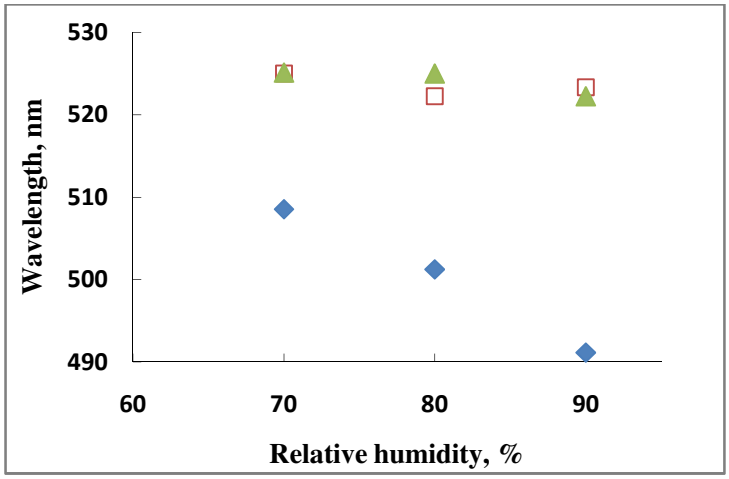

Figure 9.8. Wavelength of the light diffracted by the optical sensor coated with polyvinyl alcohol/glycerol with the ratio 2:3 wt % measured before (▲), during (♦) and 24 hours after (□) exposure to humidity.

Table 9.1. Characteristics of the optical sensors containing coating polymer film with different chemical composition

Coating polymer film	**Operation range/ relative humidity range, %**	**Wavelength shift caused by humidity exposure, nm**	**Reversibility after humidity exposure**
polyvinyl alcohol	80 - 97	26	Yes
polyvinyl alcohol/ glycerol (1:1 wt %)	60 - 97	40	Yes
polyvinyl alcohol/ glycerol (2:3 wt %)	35 - 90	33	Yes

9.5. Application of the Aztec structure for refractive index monitoring

The optical sensor based on the Aztec structure coated with an analyte-sensitive layer is potentially a very versatile sensor. It will work with any compatible layer that changes the refractive index in response to a stimulus. Selectivity to analytes will vary according to the layers used. The key factor for suitability of a certain coating material is the magnitude of the refractive index change caused by exposure to an analyte which should lead to a detectable wavelength shift of the diffracted light.

This section presents experimental results on the application of the Aztec

structure for the refractive index sensing. The aim of the present research was evaluation of the contribution of the refractive index change induced by temperature exposure to the diffraction efficiency alteration/wavelength shift observed in transmission/reflection gratings recorded in the NIPA-based photopolymer composition. This provides better understanding of the temperature response of the gratings recorded in the NIPA-based photopolymer described in Chapter 8, section 8.3.1 and 8.4.1.

As discussed in Chapter 2, section 2.3, exposure to an analyte causes changes in holographic diffraction grating parameters such as thickness, spatial period, Bragg angle and refractive index modulation. The contribution of every parameter depends on the holographic recording material and in general it is difficult to separately evaluate the effect of every parameter. The Aztec structure provides a benefit as it has a fixed spatial period of the reflection structure. This allows exclusion of the effect of the thickness/spatial period change and investigation of the contribution of the refractive index change at a fixed position of the probing beam.

In order to evaluate the effect of the refractive index alteration in the NIPA-based photopolymer layer induced by temperature (discussed in Chapter 8, section 8.3.1 and 8.4.1), the following experiment was carried out. The Aztec structure with the step height of 180 nm was spin coated with the NIPA-based photopolymer solution for recording in reflection mode presented in Table 6.3. After drying, the sample was exposed to uniform beam of light with the wavelength of 532 nm obtained from a Nd:YVO_4 laser in order to polymerise NIPA-monomers. After exposure the coating layer had a uniform distribution of PNIPA molecules in the volume. The total exposure was 500 mJ/cm^2. The wavelength of the light diffracted from the coated Aztec structure was monitored at a constant position of the probing beam in the temperature range from 20 to 56 ^{o}C and at constant relative humidity of 60 %.

The temperature dependence of the wavelength in the temperature range from 20 to 56 °C is presented in Figure 9.9.

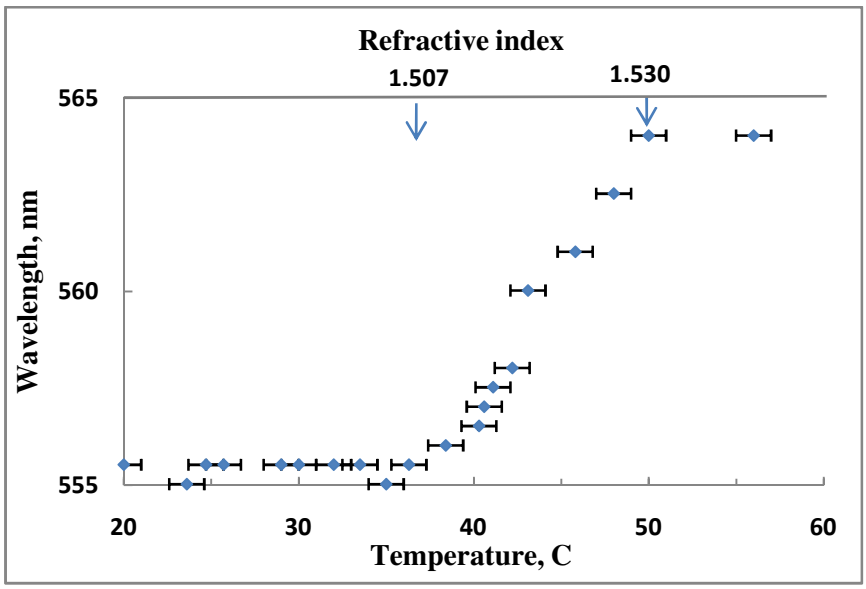

Figure 9.9. Wavelength of the light diffracted by the Aztec structure coated with the NIPA-based photopolymer *versus* temperature.

As can be seen, at temperatures up to 36 °C no wavelength shift is observed. Unchanged wavelength can be explained by unchanged refractive index of the coating layer which contains PNIPA molecules. With increasing temperature the concentration of water vapour at a certain relative humidity level increases. As the refractive index is unchanged in Figure 9.9, increased concentration of water vapour in the environment has no impact on the refractive index of the PNIPA-containing coating layer. Thus, it can be assumed that at temperatures up to 36 °C the bright fringe areas of the gratings discussed in Chapter 8, sections 8.3.1 and 8.4.1 do not absorb water vapour from the environment.

Based on the discussion presented above, the increase of the diffraction efficiency of the transmission grating up to two times at temperatures below 30 °C

(Figure 8.3) can be explained by water absorption in dark fringes. This leads to both the increase of the refractive index modulation and the thickness of the grating providing the increase of the diffraction efficiency.

As discussed in Chapter 8, section 8.4.1, the temperature induced wavelength shift of the light diffracted by the reflection grating recorded in the NIPA-based photopolymer up to 20 nm to longer wavelengths was attributed to the dominant effect of the spatial period increase due to water absorption at temperature below 30 ^{o}C and at 50 % relative humidity. Results presented in Figure 9.9, indicate that the refractive index of bright regions (containing PNIPA) is unchanged under temperature exposure and the bright fringes do not absorb water. Thus, the spatial period increase of the reflection grating is mainly induced by water absorption in dark regions. Water absorption leads to the decrease of the average refractive index of the photopolymer layer but its effect on the wavelength shift is minor.

As seen from Figure 9.9, above 36 ^{o}C the shift up to 9 nm to longer wavelengths is observed due to increasing refractive index of the coating layer. According to estimations made by using Equation (2.6), the shift up to 9 nm was caused by the refractive index increase for 0.023. The increase of the refractive index can be explained by increasing density of PNIPA molecules induced by transition of PNIPA molecules from hydrophilic to hydrophobic state. Based on this model, the decrease of the diffraction efficiency observed in Figure 8.3 at temperatures above 30 ^{o}C can be explained as follows. Temperature exposure induces two effects: 1) the increase of the refractive index modulation of the transmission grating due to the increase of the refractive index in bright fringes and 2) the thickness decrease caused by the shrinkage of the layer due to water desorption in bright regions. These two effects have opposite impact on the diffraction efficiency. The shrinkage of the layer has higher impact on the

diffraction efficiency of the transmission grating leading to its decrease.

As discussed in Chapter 8, section 8.4.1, in reflection gratings recorded in the NIPA-based photopolymer the wavelength shift up to 65 nm to shorter wavelengths (Figure 8.8) was thought to be mainly induced by the decrease of the spatial period due to water desorption at temperatures above 40 ^{o}C. Experimental data presented in Figure 9.9 show that temperature-induced refractive index change leads to the wavelength shift up to 9 nm to longer wavelengths. This confirms that in the reflection grating recorded in the NIPA-based photopolymer the spatial period decrease of the grating due to water desorption is the main contributor to observed wavelength shift up to 65 nm to shorter wavelengths (Figure 8.8).

9.6. Conclusions

A novel optical sensor with response to relative humidity changes has been developed. The optical sensor includes an embossed honeycomb pyramidal grating (the Aztec grating) as a substrate and a coating thin polymer film as a sensing medium. For the first time a solid coating layer was used in order to convert the Aztec grating into a sensor. The sensing mechanism of the optical sensor is based on the wavelength shift of the light diffracted from the nanostepped structure due to changes in the refractive index of the coating layer caused by its density alteration due to water absorption under exposure to humidity. It was demonstrated that the sensitivity to humidity and operation range of the optical sensor can be tuned by altering the chemical composition of the coating layer. Humidity induced wavelength shifts of 26, 40 and 33 nm were detected for the sensors containing the coating layer with polyvinyl alcohol/glycerol ratio 1:0, 1:1 and 2:3 wt % respectively, when the relative humidity changes from 80 to 97 %, 60 to 97 % and 35 to 90 %, correspondingly. The sensitivity of the devices was found to be

1.5nm/*%RH*, 1nm/*%RH* and 0.6nm/*%RH*. Obtained wavelength shifts are visible to the eye and this feature makes possible the application of the Aztec structure coated with a polymer film as a visual indicator of the environmental humidity.

The Aztec structure was implemented for the characterisation of the refractive index change of the NIPA-based photopolymer induced by temperature exposure. Utilisation of the Aztec structure allowed excluding the effect of the thickness/spatial period change and evaluating the contribution of the refractive index change induced by temperature exposure to the diffraction efficiency alteration/wavelength shift observed in transmission/reflection gratings recorded in the NIPA-based photopolymer composition. Obtained results are in good correlation with the proposed model of the temperature induced changes in the properties of volume phase transmission and reflection gratings recorded in the NIPA-based photopolymer composition.

References

1. Cowan, J.J., *Aztec surface-relief volume diffractive structure.* Journal of the Optical Society of America A, 1990. **7**(8): p. 1529-1544.
2. Cowan, J.J., *Holographic honeycomb microlens.* Optical Engineering, 1985. **24**(5): p. 245796-245796.
3. Cowan, J.J., *Method of replicating volume phase reflection holograms*. 1989, Patent US 4839250 A.
4. Cowan, J.J., *Surface relief volume reflective diffractive structure*. 2012, Patent US 8254029 B2.
5. Cowan, J.J., *Method of forming volume phase reflection holograms*. 1989, Patent US 4874213.
6. Cowan, J.J. *The Aztec structure: an improved replicable security device*. SPIE Proceedings 2006. **6075**: p. 60750Q-1.
7. Cowan, J.J. *Advances in holographic replication with the Aztec Structure* in *Proceeding of International Conference on Holography*. 2006. p. 1-5.
8. Yetisen, A.K., Butt, H., Mikulchyk, T., Ahmed, R., Montelongo, Y., Humar, M., Jiang, N., Naydenova, I. and Yun, S.H., *Color-Selective 2.5D Holograms on Large-Area Flexible Substrates for Sensing and Multilevel Security.* Advanced Optical Materials, 2016: DOI: 10.1002/adom.201600162.
9. *Material Safety Data Sheet-T58300*. Retrieved December 10, 2015 from: http://www.sigmaaldrich.com/.
10. *Material Safety Data Sheet-BP229-1.* Retrieved December 10, 2015 from: https://www.fishersci.com/.

11. *Refractive Index of Polymers by Index*. Retrieved December 10, 2015 from: http://scientificpolymer.com/technical-library/refractive-index-of-polymers-by-index/.

12. Speight, J.G. and Lange, N.A., *Lange's handbook of chemistry*. Maidenhead: McGraw-Hill Professional 2005.

10. CONCLUSIONS AND FUTURE WORK

10.1. The achievements of the PhD research

The main aim of this project was to develop holographic sensors with response to relative humidity changes and temperature variations. During the development of the holographic sensors two types of photonic structures was utilised as a base of the sensor: 1) a volume phase transmission/reflection grating and 2) a surface relief structure (Figure 10.1).

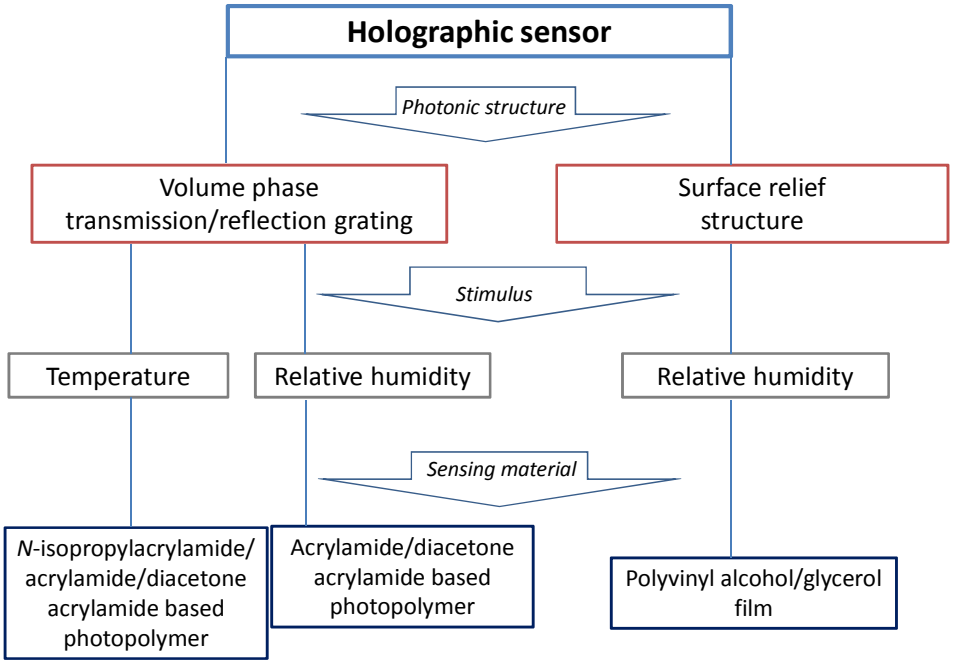

Figure 10.1. Holographic sensors developed in the project.

Photopolymer materials containing polyvinyl alcohol as a binder and different monomers with sensitivity to temperature/relative humidity were used as an analyte sensitive material in holographic sensors based on volume phase gratings. A thin polymer film containing polyvinyl alcohol and glycerol was employed as a humidity responsive material in the holographic sensor based on the surface relief structure.

Depending on the essence of the work presented in this thesis it can be divided in two main groups: 1) development of functionalised materials for holographic recording and optimisation of the conditions for fabrication of photonic structures to be used as sensors and 2) characterisation of the sensors in the presence of the analyte. The main conclusions from this research are as follows.

10.1.1. Development of the novel N-isopropylacrylamide based photopolymer for temperature sensing

- A novel photopolymer composition containing *N*-isopropylacrylamide as the main monomer for holographic recording in transmission and reflection modes was developed. The novel photopolymer is sensitive to temperature and has lower toxicity than acrylamide-based photopolymer.
- It was shown that the *N*-isopropylacrylamide based photopolymer developed performs well as a holographic recording medium and is capable of recording in both transmission and reflection modes. The diffraction efficiency of 80 % was reached in unslanted transmission gratings recorded in 60 ± 5 μm thick layers at a spatial frequency of 1000 lines/mm after exposure to the total recording intensity of 2 mW/cm^2 for 160 sec. The diffraction efficiency of 20 % was obtained in reflection gratings recorded in 60 ± 5 μm thick layers at a spatial frequency of 2700 lines/mm after exposure to the total recording intensity of 10.5 mW/cm^2 for 100 sec. The shelf life of gratings recorded in both reflection and transmission mode was improved by UV-curing for 99 sec and 1800 sec, respectively, with the total exposing intensity of 60 and 2.5 mW/cm^2, correspondingly.

- It was demonstrated that temperature induced changes of grating properties were governed by the hydrophilic/hydrophobic state of PNIPA molecules mainly contained in the bright fringe areas.

10.1.2. Mechanism of obtaining refractive index modulation in the photopolymer composition containing acrylamide as the main monomer and N-phenylglycine as a photoinitiator

- Based on the influence of UV-postexposure and exposure to the relative humidity of 90 % on the diffraction efficiency of gratings recorded in the acrylamide-based photopolymer containing *N*-phenylglycine as a photoinitiator the following model for the refractive index modulation was proposed. The photopolymer composition records in regime of slow monomer diffusion, the main contributor to the refractive index modulation is the change in molar refraction, and the refractive index modulation has its maximum in the dark regions. This will make an important contribution to the models of the recording mechanism in photopolymer formulations, by allowing us to study a version where diffusion is suppressed. It's also a robust, highly scratch-resistant and moisture-resistant photopolymer which may find application in diffractive optical devices.

10.1.3. Novel holographic humidity sensors based on transmission gratings

10.1.3.1. Holographic sensor with reversible/irreversible response to 80 and 90 % relative humidity

- For the first time it was demonstrated that volume phase unslanted transmission gratings recorded in the acrylamide-based photopolymer containing triethanolamine as a photoiniator are suitable for the development of reversible

and irreversible holographic humidity sensors with the operation range from 80 to 90 % and above 80 % relative humidity, respectively.

- Reversibility of the sensor was found to depend on the temperature. Full reversibility of humidity induced changes was confirmed for temperatures lower than 16 ^{o}C. Reversibility of the sensor response was attributed to the capacity of the photopolymer layer to recover its original dimensions fully when returned to the original conditions. Above 16 ^{o}C and at 80 and 90 % relative humidity, the layer was found to stretch beyond its capacity to recover and collapse to a lower thickness leading to the irreversible decrease of the diffraction efficiency (up to 60 %) and the Bragg angle shift (up to 1^{o}).The magnitude of the irreversible change was found to be highly dependent on humidity level, temperature during the humidity exposure and on humidity exposure time.

10.1.3.2. Holographic humidity sensors with tuneable operation range and sensitivity

- It was demonstrated that the response of the photopolymer-based gratings to humidity can be tuned by changing the photopolymer composition. Reduced humidity sensitivity was achieved by substituting the photoinitiator, i.e triethanolamine was replaced with *N*-phenylglycine.
- Diffraction efficiency of volume phase unslanted transmission gratings recorded in the acrylamide-based photopolymer containing *N*-phenylglycine as a photoinitiator was found to be constant at the relative humidity below 70 % and it decreased up to two times above 70 % relative humidity. It was shown that the decrease of the diffraction efficiency induced by exposure to high humidity (80 and 90 %) for 30 min was fully reversible. The low humidity sensitivity of the

acrylamide-based photopolymer containing *N*-phenylglycine as a photoinitiator is encouraging for applications where non-sensitive to humidity material is required.

- It was demonstrated that increased sensitivity to humidity of the holographic humidity sensor can be achieved by utilisation of the photopolymer composition containing diacetone acrylamide as the main monomer and triethanolamine as a photoinitiator.
- Humidity induced increase of the diffraction efficiency of slanted transmission gratings from 6 to 84 % was observed in the relative humidity range from 20 to 90 %. Reversibility of the observed changes was confirmed at the relative humidity below 60 %. Irreversible decrease of the diffraction efficiency up to 60 % was observed after exposure to the relative humidity above 60 %.
- Characteristics of humidity sensors based on transmission gratings recorded in photopolymers are presented in Table 10.1.

Table 10.1. Characteristics of holographic humidity sensors based on transmission gratings recorded in photopolymers

Sensor type	**Photopolymer composition (monomer/initiator)**	**Operation range: Relative humidity, %**	**Sensitivity, $(\Delta\eta/\eta)$/%RH**
Reversible humidity sensor	Acrylamide/ *N*-phenylglycine	70 – 90	-0.025
	Diacetone acrylamide/ triethanolamine	20 - 60	0.054
Irreversible humidity sensor	Acrylamide/ triethanolamine	80 - 90 ($T > 16\ ^{o}C$)	n/a
	Diacetone acrylamide/ triethanolamine	60 - 90	n/a

10.1.3.3. Modelling of the response of holographic humidity sensors

- Modelling of the humidity response of sensors based on transmission gratings recorded in the diacetone acrylamide based photopolymer was done. It was found that the main contributors to the humidity induced diffraction efficiency alteration are thickness and refractive index modulation changes. An increase of the grating thickness under humidity exposure was explained by the photopolymer layer swelling due to water absorption. The refractive index modulation increase under humidity exposure was attributed to the different ability of dark and bright regions to absorb water molecules due to its different porosity.

10.1.4. Novel holographic temperature sensors

10.1.4.1. Reversible holographic temperature sensors based on slanted transmission gratings with tuneable operation range and sensitivity

- It was demonstrated that photopolymers can be used as a temperature sensitive material for the development of holographic temperature sensors based on slanted transmission gratings. Variation of the photopolymer components such as the main monomer (acrylamide/diacetone acrylamide/*N*-isopropylacrylamie) and a photoinitiator (treithanolamine/*N*-phenylglycine) allows tuning the sensitivity and operation range of the sensor. Temperature-induced changes were found to be reversible.
- Characteristics of holographic temperature sensors based on slanted transmission gratings recorded in photopolymers are presented in Table 10.2.

Table 10.2. Characteristics of holographic temperature sensors based on transmission gratings

Photopolymer composition (monomer/initiator)	**Operation range: Temperature, ^{o}C**	**Sensitivity**	
		Diffraction efficiency, $(\Delta\eta/\eta)$/ ^{o}C	**Bragg angle shift, degree/ ^{o}C**
Acrylamide/ *N*-phenylglycine	30 - 40 (30 % RH) 40 - 50 (30 % RH)	no response 0.021	0.03 no response
Acrylamide/ triethanolamine	20 – 50 (30 % RH)	no response	0.05
Diacetone acrylamide/ triethanolamine	20 - 60 (30 % RH)	-0.017	0.05
N-isopropylacrylamide/ *N*-phenylglycine	18 - 29 (60 % RH) 30 - 47 (60 % RH) 20 - 45 (35 % RH)	0.1 -0.026 n/a	n/a n/a 0.1

10.1.4.2. Reversible holographic temperature sensors based on reflection gratings

- For the first time a holographic temperature sensor based on the reflection grating with a spatial frequency of 2700 lines/mm recorded in the novel *N*–isopropylacrylamide based photopolymer composition was developed. The wavelength shift up to 20 nm to longer wavelengths and up to 65 nm to shorter wavelengths was noticed when the temperature changed from 20 to 30 ^{o}C and from 40 to 55 ^{o}C, respectively. Characteristics of the sensor are presented in Table 10.3.

Table 10.3. Characteristics of the holographic temperature sensor based on the reflection grating recorded in the novel *N*-isopropylacrylamide based photopolymer

Operation range: Temperature, ^{o}C	**Sensitivity: Wavelength shift, nm/^{o}C**
20 - 30	2
30 - 40	0
40 - 55	-4.3

- It was shown that Denisyuk holograms recorded in the novel *N*–isopropylacrylamide based photopolymer are suited to the application as temperature visual indicators that visibly change the colour under temperature exposure.

10.1.4.3. Modelling of the response of temperature sensors utilizing novel N–isopropylacrylamide based photopolymer

- In temperature sensors based on transmission gratings, the increase of the diffraction efficiency observed at temperatures below 30 ^{o}C was found to be caused by water absorption in dark fringes. This led to both the increase of the refractive index modulation and the thickness of the grating providing the increase of the diffraction efficiency. At temperatures above 30 ^{o}C the diffraction efficiency decrease was induced by the dominant effect of the thickness decrease caused by the shrinkage of the layer due to water desorption in bright fringes.
- In temperature sensors based on reflection gratings, the wavelength shift to longer wavelengths at temperatures below 30 ^{o}C and at the relative humidity of 50 % was established to be based on the spatial period increase mainly induced by water absorption in dark fringes. At temperatures above 40 ^{o}C, the wavelength shift up to 65 nm to shorter wavelengths was found to be mainly induced by the decrease of the spatial period due to water desorption at temperatures above 40 ^{o}C.

10.1.5. Surface photonic structures with response to relative humidity

- A novel holographic sensor based on the surface photonic structure with response to relative humidity changes was developed. The holographic sensor includes an embossed honeycomb pyramidal grating as a substrate and a coating thin polymer film as a sensing medium.
- It was demonstrated that the sensitivity to humidity and operation range of the sensor can be tuned by altering the chemical composition of the coating layer. Humidity induced wavelength shifts of 26, 40 and 33 nm were detected for the sensor containing the coating layer with polyvinyl alcohol/glycerol ratio 1:0, 1:1 and 2:3 wt %, respectively, when the relative humidity changed from 80 to 97 %, 60 to 97 % and 35 to 90 %, correspondingly. The sensitivity of the devices was calculated to be 1.5nm/%RH, 1nm/%RH and 0.6nm/%RH.
- Obtained wavelength shifts are visible to the eye and this feature makes possible the application of the embossed honeycomb pyramidal grating coated with a polymer film as a visual indicator of the environmental humidity.

Key contributions:

1. Successful development of a range of new temperature sensitive volume holograms.
2. Successful development of a range of new humidity sensitive volume holograms.
3. Development of a prototype holographic colour-change indicator using Aztec structures.
4. Optimisation of a new moisture-resistant photopolymer formulation which is characterised by slow diffusion and is very robust.

10.2. Future plan

Following the preliminary research carried out in this project, future work would be beneficial in a number of areas.

- Further investigation of the irreversible changes in properties of the NIPA-based grating induced by elevated temperature should be carried out. This knowledge can assist in the development of an irreversible temperature sensor/indicator which has a great demand for monitoring temperature conditions during storage or transportation of goods.
- Capability to substitute *N,N'*-methylenebisacrylamide in the NIPA-based photopolymer with other crosslinking monomers should be investigated. It was shown [1] that copolymerisation of NIPA with other appropriate monomers enable altering the lower critical solution temperature of NIPA. This can be used for the development of temperature sensors with customised operation range. Also, swelling/shrinking capability of PNIPA depends on the crosslinking monomer utilised [2]. It is interesting to check the possibility to increase the temperature sensitivity of the transmission and reflection gratings recorded in the NIPA-based photopolymer by altering the crosslinking monomer and its concentration.
- A holographic temperature sensor based on a humidity-resistant photopolymer grating should be developed. Utilisation of the humidity resistant photopolymer as a matrix of the sensor can help to avoid unwanted sensitivity to humidity inherent to most of photopolymers. This may allow developing a holographic temperature sensor with enhanced selectivity. Proposed approach is based on functionalisation of the acrylamide-based photopolymer containing

N–phenylglycine as a photoinitiator by incorporation of nanoparticles with response to temperature. Different types of nanoparticles, such as zeolite nanocrystals, dendrimers or other nanoparticles should be tried. Effect of incorporated nanoparticles on the temperature response of holographic gratings recorded in doped photopolymer layers should be investigated. In order to find out the material with high sensitivity to temperature, the quantitative analysis of the temperature response of holographic gratings recorded in photopolymer layers containing different types of nanoparticles with different concentrations have to be done. Holographic recording ability of the doped photopolymer in transmission and reflection mode should be characterized in order to achieve the best performance of the material.

References

1. Deshmukh, M.V., Vaidya, A. A., Kulkarni, M. G., Rajamohanan, P. R. and Ganapathy, S., *LCST in poly(N-isopropylacrylamide) copolymers: high resolution proton NMR investigations.* Polymer, 2000. **41**(22): p. 7951-7960.
2. Sivaprakasam, K., Mawilmada, P., Schoess, J.N., Schaefer, L., Lee, Y.H., Ramakrishnan, L. and Mandell, M., *Rapid deswelling of Poly(N-isopropylacrylamide-co-acrylic acid) hydrogels in response to temperature changes*. World Research Journal of Biomaterials, 2012. **1**(1): p.12-15.

10.3. Dissemination of the PhD research

Journal Publications

1. Mikulchyk T, Martin S, Naydenova I 2013 Humidity and temperature effect on properties of transmission gratings recorded in PVA/AA-based photopolymer layers *Journal of Optics* **15** 105301.
2. Mikulchyk T, Martin S, Naydenova I 2014 Investigation of the sensitivity to humidity of an acrylamide-based photopolymer containing *N*-phenylglycine as a photoinitiator *Optical Materials* **37** 810-815.
3. Naydenova I, Grand J, Mikulchyk T, Martin S, Toal V, Georgieva V, Thomas S Mintova S 2015 Hybrid sensors fabricated by inkjet printing and holographic patterning *Chemistry of Materials* **27** 6097–6101.
4. Yetisen A, Butt H, Mikulchyk T, Ahmed R, Montelongo Y, Humar M, Jiang N, Martin S, Naydenova I, Yun S 2016 Color-selective 2.5 dimensional holograms on large-area flexible substrates for sensing and multilevel security. *Advanced Optical Materials* doi: 10.1002/adom.201600162.
5. Mikulchyk T, Walshe J, Cody D, Martin S, Naydenova I 2017 Humidity and temperature induced changes in the diffraction efficiency and the Bragg angle of slanted photopolymer-based holographic gratings *Sensors & Actuators B: Chemical* **239** 776-785.

Conference Proceedings

Mikulchyk T, Walshe J, Cody D, Martin S, Naydenova I 2015 Humidity and temperature response of photopolymer-based holographic gratings *Proc. SPIE* 9508, Holography: Advances and Modern Trends IV, 950809 (May 8, 2015); doi:10.1117/12.2183782.

Book chapter

Zawadzka M, Mikulchyk T, Cody D, Martin S, Yetisen A, Martinez-Hurtado J, Butt H, Mihaylova E, Awala H, Mintova S, Yun S, Naydenova I, Ed. Serpe M, Kang Y, Zhang Q 2016 Photonic Materials for Holographic Sensing in: Photonic Materials for Sensing, Biosensing, and Display Devices *Springer International Publishing*.

Patent Application

1. Patent application no. 1522739.0 filed in Great Britain on 23 December 2015 Thermosensitive photopolymer and method for making same, to protect the use of *N*-isopropylacrylamide photopolymer composition as a holographic recording material and its application in holographic sensors.
2. Patent application no. 1608987.2 filled in Great Britain on 23 May 2016 Optical Devices for Authentication and Methods of Making same, to protect a method based on using visible wavelength light and a fully transparent photopolymerizable material to make diffractive optical elements that produce a variable two- or three- dimensional diffraction pattern.

Oral presentations

1. Mikulchyk T, Cody D, Martin S, Naydenova I 2016 Application of photonic structures holographically recorded in acrylamide derivative photopolymers for temperature and relative humidity sensing *Photonics North 23-26 May, Quebec, Canada.*
2. Mikulchyk T, Walshe J, Cody D, Martin S, Naydenova I 2015 Humidity and temperature response of photopolymer-based holographic gratings *SPIE Optics+Optoelectronics 13-16 April, Prague, Czech Republic.*

3. Mikulchyk T, Martin S, Naydenova I 2014 Investigation of the humidity sensitivity of acrylamide-based photopolymer containing *N*-phenylglycine as a photoinitiator *II International Conference on Applications of Optics and Photonics 26-30 May, Aveiro, Portugal.*
4. Mikulchyk T, Martin S, Naydenova I 2014 Exploitation of photopolymer's response to humidity for fabrication of disposable holographic humidity sensor *5th Annual Postgraduate Research Symposium, Dublin Institute of Technology, 25 November, Dublin, Ireland.*
5. Naydenova I, Grand J, Mikulchyk T, Martin S, Toal V, Georgieva V, Thomas S, Mintova S 2014 Ink-jet printing for fabrication of nanozeolite based holographic sensors *6th FEZA Conference, Leipzig, 8-11 September 2014*.

Poster presentations

1. Mikulchyk T, Martin S, Naydenova I 2013 High humidity induced irreversible changes in properties of transmission gratings recorded in acrylamide-based photopolymer layers *Photonics Ireland 2013*, *Belfast, United Kingdom.*
2. Mikulchyk T, Martin S, Naydenova I 2013 Humidity and temperature indicators developed in photopolymer *Irish Research Council Annual Symposium 2013, Dublin, Ireland*.
3. Mikulchyk T, Martin S, Naydenova I 2013 Humidity response of transmission gratings recorded in acrylamide-based photopolymer layers *4th DIT Annual Postgraduate Research Symposium, Dublin Institute of Technology, 22 November, Dublin, Ireland.*
4. Mikulchyk T, Martin S, Naydenova I 2014 Humidity response of transmission gratings recorded in PVA/AA-based photopolymer containing N-phenylglycine

as a photoinitiator *COST Action MP 1205 Advances in Optofluidics: Integration of Optical Control and Photonics with Microfluidics, Dublin, Ireland.*

5. Connell D, Browne C, Mikulchyk T, Naydenova I and Martin S 2015 Effect of elevated temperature on the dynamics of holographic recording in photopolymer materials *COST Action MP 1205 Advances in Optofluidics: Integration of Optical Control and Photonics with Microfluidics, 07-08 May, Porto, Portugal.*
6. Zawadzka M, Cody D, O'Hara C, Mikulchyk T, Toal V, Martin S, Naydenova I 2015 Photosensitive Materials for Fabrication of Diffractive Optical Devices using a Spatial Light Modulator *6th International Symposium of Advanced Micro- and Mesoporous Materials, 6-9 September, Bulgaria.*
7. Naydenova I, Grand J, Mikulchyk T, Martin S, Mintova S 2016 Nanozeolites-photopolymer hybrid sensors for environmental monitoring *18th International Zeolite Conference 19-24 June, Rio de Janeiro, Brazil.*

Courses attended as a part of the structured PhD programme

1. Holography: Techniques and Applications.
2. Photonic Materials and Devices.
3. Special Topics in Nanoscience.
4. Polymer Materials.